Universidad de Valladolid

Escuela de Doctorado Universidad de Valladolid

PROGRAMA DE DOCTORADO EN INVESTIGACIÓN BIOMÉDICA

TESIS DOCTORAL:

ENGINEERING RESPONSIVE AND BIOMIMETIC MATERIAL BASED ON ELASTIN-LIKE RECOMBINAMERS FOR BIOMEDICAL APPLICATION

Presentada por Filippo Cipriani para optar al grado de Doctor/a por la Universidad de Valladolid

Dirigida por:

José Carlos Rodríguez Cabello

Israel González de Torre

Gracias a la vida que me ha dado tanto

Me ha dado la marcha de mis pies cansados

Con ellos anduve ciudades y charcos

Playas y desiertos, montañas y llanos.

Gracias a la vida – Violeta Parra (1966)

ACKNOWLEDGMENTS - AGRADECIMIENTOS - RINGRAZIAMENTI

Muchos años después, sobre un avión que conducía desde Florencia a Madrid, el suscrito había de recordar aquella tarde remota en que abrió Google Maps y busco donde estaba Valladolid.

Me encuentro sobre el vuelo que va desde Florencia a Madrid y me acuerdo de la primera vez que vine a Valladolid; no sabía dónde estaba y nunca hubiera pensado de vivir casi 4 años en esta ciudad. Pero, si lo pienso bien, tengo que confesar que siempre he tenido un débil por España. No sé, será el Mediterráneo que nos acomuna y nos acerca; también será por el idioma tan sencillo de aprender que seguramente en estos agradecimiento estarán muchos errores. Poco importa, alguien demostró que el 90% de las comunicación nos es verbal y creo que con esto escrito el mensaje llegará aunque haya muchos errores gramaticales. Quiero empezar diciendo que haber tenido la oportunidad de vivir en este país ha sido una gran fortuna y tengo que agradecer muchas persona que han permitido que mi recorrido pasase por aquí. Habría muchos que agradecer, pero intentaré ser los más conciso posible para no aburrir demasiado.

En primer lugar quiero agradecer mis directores Carlos y Israel. Muchas gracias por haberme dado esta oportunidad y por haberme guiado a lo largo del camino hasta conseguir el título de Doctor en Investigación Biomédica. Muchas gracias Carlos por tus preciosos consejos, tu enorme conocimiento sobre la ciencia, por tu generosidad y para haberme dado la libertad necesaria para desarrollar recursos que si no nunca habría descubierto. Muchas gracias Israel por tu inmenso ayudo, tu capacidad de aclararme las idea, de animarme en los momentos bajos y por haberme reconducido a las cosas prácticas cuando me estabas perdiendo en mil vueltas mentales. Muchas gracias a Matilde por tu ayuda tanto científica cuando humana, toda las veces que he entrado en tu despacho en momentos críticos, siempre he salido con más fe en mi camino y en mí mismo. Muchas gracias a Javier por tu preciosos consejos sobre el mágico mondo de la Biología Molecular; gracias a Alessandra por tu consejos sobre los experimentos de células y también para los buenos ratos pasados a hablar de la nuestra Italia y de las orígenes Etruscas que tenemos. Gracias a Luis y Menchu porque trabajar con vosotros es un auténtico lujo, donde se aprende lo que es ser científico y trabar con profesionalidad. Gracias a Merche y Irene, que me han dado mucho cariño y sencillamente verlas con esa sonrisa me animaban el corazón. Gracias a Leander y Soraya, mi inseparable compañeros del despacho. Madre mía cuantas horas pasadas untos confrontándonos sobre los problemas y ayudándose para solucionarlos. Nos hemos animado muchísimo, tanto dentro como fuera del laboratorio. Muchas Gracias a Juan y Sofía por todas las risas que nos hemos hechos, por todas las frases épicas que nos han ayudado a tener un ánimo alegre también cuando buscábamos cazar gnomos y no encontrábamos ninguno. Gracias a Tatiana y Sergio por los buenos momentos pasados en muchos congresos; gracias a Ito para sus consejos sobre que canción escuchar para motivarse y sobre los rinconcitos más bonitos de Valladolid; gracias a Arturo y Doriana porque nunca olvidaré mi primer congreso con vosotros en Oporto. Gracias a Fer, Miguel y Marcos porque MAAACCHHOOO este es un cachondeo! (y otros mil dichos que nos han hechos reír mucho). Gracias a Rocío

y a Sandra por vuestra ayuda. Rocío eres una crack (como se dice aquí). Siempre lista para ayudar, tanto profesionalmente como humanamente, te mereces lo mejor. Gracias a los nuevos como Diana y Sara, que por mala suerte no hemos tenido la oportunidad de pasar mucho tiempo untos, pero estoy convencido que estaremos en contacto y nos volveremos a ver. Gracias a Sandra por haberla ayudada con su proyecto, te deseo lo mejor por tu trayectoria científica. Gracias también a lo que se han marchados antes que yo: Mohammed, Lorena, Elena, Leticia, Esther, Alicia, Teresa y Dasha, gracias por los buenos momentos pasados untos. También quiero agradecer a Gastón y sus historias sobre Cuba, al final consiguió convencerme a visitarla. Gracias también a todos los colaboradores externos, como los colegas conocidos en las estancias, los médicos de Valladolid y todos los coautores de los artículos. Gracias mis fantásticos compañeros del BIOGEL, tanto los estudiantes cuanto los Seniors, compartir con vosotros este camino profesional ha sido una oportunidad estupenda: agradezco el día que decidí aplicar por este proyecto.

He aprendido muchísimo desde cada uno de vosotros, en un sentido común he aprendido lo que significa hacer ciencia y ser científico. A todos vosotros os deseo lo mejor.

Terminados los agradecimientos profesionales, quiero agradecer también mi mundo fuera del Doctorado, un mundo donde conseguías recargar las pilas para volver a dar lo mejor. Gracias a todos los amigos conocidos en Valladolid; amigos inolvidable con los cuales hemos creado una conexión especial; nombrarlos todos sería demasiado, por esto me limito a decir un GRACIAS general y que llegue a todos, desde los chicos de la cafetería, pasado por los compañeros de balonmano hasta a quien me cogió en Valladolid como en una Familia. Gracias también a todos los amigos fuera de Valladolid: a lo de España, de Holanda, de Alemania, a mi amigos históricos de Italia, a los nuevos que conocí en los congresos y a lo que conocí en otros rincones del mundo.

Gracias a mi Familia, porque no obstante la distancia su ayudo me ha llegado intacto y poderoso. Gracias por todas las veces que habéis venido a visitarnos recordándonos cuanto nos queréis. Que cuando estaba por el mundo conociendo gente de cultura diferente, llevaba conmigo mi mundo y mi raíces y me sentía como si vosotros estuvierais conmigo.

4 años inolvidables! Hechos principalmente de momentos buenos, pero también de momentos difíciles… como el clima de Valladolid. Niebla donde no se ve nada y solo se puede proceder a tentones. Un sol que pega tan fuerte encima de la cara que solo hay que cerrar los ojos y no permitir a las gotas de sudor de entrar. Un frio que penetra los pies porque anden más rápido, de manera de calentarse y alcanzar una meta más lejana.

4 años y mucho más pasado untos! Donde cuando había niebla andabas tu delante de mí; que cuando teníamos el sol en la cara que no se veía nada, estabas tú mirando el camino; y que cuando hacia frio para pararse, me abrazabas y me decías que la meta estaba cerca. Sin ti este reto no hubiera sido posible. Gracias a ti, Sara por todos los momentos que hemos vivido… y que tenemos que vivir.

Filippo

INDEX

ABSTRACT

Regenerative Medicine is a well-established field of science that aims to replace, engineer and regenerate human cells, damaged tissues or organs to restore their normal function. This branch of translational research finds a deep interest in the *Science of Biomaterials*; indeed, the knowledge acquired in that field goes proportionally with the development of novel biomaterials. There is a great need in developing advanced biomaterials capable to fulfil the requirements of stability and bioactivity for their application in biomedicine. Moreover, considering the complexity of the human body, this system needs a certain rate of versatility in order to be tailored to a specific area of application. For all these reasons, recombinant proteins are an interesting approach, in which, elastin-like recombinamers (ELRs) represent one of the most promising biomaterials. ELRs are obtained through DNA recombinant technology, which allows the precise control at the genetic level, affording exquisite control over final protein functionality. ELRs are protein-based polypeptides that comprise repetitive units of the Val−Pro−Gly−X−Gly $(VPGXG)_n$ pentapeptide, in which X (guest residue) could be any amino acid except L-proline. In terms of biomaterial design, ELRs show several outstanding properties. ELRs are inspired by elastin, which is a component of natural extracellular matrix (ECM), showing excellent biocompatibility. One of the most important features of ELRs is that they exhibit thermo-responsiveness; this is due to the change of protein conformation above the so-called transition temperature (T_t), which depends on the amino acid composition of the polymer. Moreover, according to the ELRs design, they can be processed as several supramolecular structures, such as micelles, nanoparticles, films, and hydrogels. The large variety of ELRs, both in terms of structures and bioactivity, permits the application of these protein-based biomaterials to diverse biomedical applications.

This Thesis represents a sort of journey towards the exploration of the evolution of ELRs as a powerful tool with great potential in the biomedical field. The first part of this Thesis is dedicated to the description of the history of ELRs from their ancient chemical origin as ELPs (Elastin-like Polypeptides) to the most cutting-edge bioproduction techniques becoming into ELRs. Moreover, it is reported an exhaustive explanation of how ELRs can be processed in many forms (aggregates, fibers, layers, nanoparticles, or hydrogels),

giving examples of their great potential in many fields, including drug delivery, tissue engineering, protein purification, anticancer gene therapies, and nanovaccines. Moreover, considering their large interest, one chapter of this Thesis is dedicated to the ELRs as biomaterial forming hydrogels for tissue regeneration and repair. The different mechanisms of gelation are reported, and it is given an overview of the possible applications in tissue engineering, such as osteochondral application, (cardio-)vascular tissue regeneration, and ocular prostheses.

The first experimental work of this Thesis is dedicated to the development of novel ELRs-based hydrogel for cartilage repair. Tissue engineering for cartilage repair requires biomaterials that show rapid gelation and adequate mechanical properties. Although the use of hydrogel is the most promising biomaterial, it often lacks in rigidity and anchorage of cells when they are surrounded by synovial fluid while they are subjected to heavy loads. In this work, it has been developed and produced the Silk Elastin-Like co-Recombinamer (SELR), which contains both the physical interaction from elastin motifs and from silk motifs. In the first part of this study, it was set up and optimized a pre-annealing treatment based on the evolution of silk motifs into β-sheet structures in order to fulfil the required mechanical properties of hydrogels for cartilage repair. The new pre-annealed SELRs ($pA(EIS)_2$-$(I_5R)_6$) were characterized with the combination of several experimental techniques (CD, TEM, SEM, and rheology) to provide a deep insight into the material features. Finally, the regeneration properties of the $pA(EIS)_2$-$(I_5R)_6$ hydrogel embedded with chondrocytes were evaluated. After 4 weeks of culturing in a standardized and representative *ex vivo* model, the biochemical and histological analysis revealed the production of glycosaminoglycans and collagen. Finally, the immunohistochemistry showed the absence of fibro-cartilage and the presence of hyaline cartilage, which leads to the successful regeneration of hyaline cartilage in an *ex vivo* model.

Not only the physically cross-linked hydrogels have been investigated; indeed, an *in situ* chemically cross-linked hydrogels have been developed for osteochondral repair. Moreover, another bioactive composition of this biomaterial has been tested; this ELRs-based hydrogel has been designed containing bioactive sequences, such as the well knows adhesion sequences RGD and REDV, and the elastase target domain VGVAPG that

provides proteolytic sensitivity to the biomaterial. Compared to the previous study reported in this Thesis, where the *ex vivo* platform was used, the regeneration properties of the chemically cross-linked ELRs hydrogel were evaluated with an *in vivo* study. Furthermore, it has been made a comparison between the usage of that biomaterial itself, and the biomaterial embedded with cells (*tissue engineering*). Both the ELR-based hydrogel alone and the ELR-based hydrogel embedded with rabbit Mesenchymal Stem Cells (rMSCs) were tested for the regeneration of critical subchondral defects in 10 New Zealand rabbits. Thus, cylindrical osteochondral defects were filled with an aqueous solution of ELRs. The animals were sacrificed at 4 months for histological and gross evaluation of features of biomaterial performance, including integration, cellular infiltration, surrounding matrix quality and evaluation of the new matrix in the defects. Although both groups helped cartilage regeneration, the results suggest that the specific composition of the rMSCs-containing hydrogel permitted adequate bone regeneration, whereas the ELR-based hydrogel alone led to an excellent regeneration of hyaline cartilage. In conclusion, the ELR cross-linker solution can be easily delivered and forms a stable, well-integrated hydrogel that supports infiltration and *de novo* matrix synthesis.

As it has been reported above, the aim of this Thesis is to explore the possibilities of ELRs as a powerful tool capable of containing various bioactivities with great potential in the biomedical field. As a further step in the evolutional process towards advanced bioactive ELRs, one objective of this Thesis is to combine these two diametrically opposed approaches in a new hybrid biomaterial. Biomaterial design in tissue engineering aims to identify appropriate cellular microenvironments in which cells can grow and guide new tissue formation. Despite the large diversity of synthetic polymers available for regenerative medicine, most of them fail to fully match the functional properties of their native counterparts. In this work, we have combined the strategy of synthetic peptides with the DNA recombinant techniques generating a new hybrid biomaterial. Human umbilical vein endothelial cells (HUVECs) adhesion and proliferation were studied over the ELRs covalently functionalized with each three high-affinity and selectivity $\alpha_v\beta_3$- and $\alpha_5\beta_1$-binding bicyclic RGD peptides. Next, to the bicycles, ELRs were also functionalized with various integrin-binding benchmark peptides, i.e. knottin-RGD, cyclo-[KRGDf] and GRGDS, allowing for better classification of the obtained results. Covalent

functionalization with the RGD peptides, as validated by MALDI-TOF analysis, guarantees flexibility and a minimal steric hindrance for interactions with cellular integrins. In addition to the covalently modified RGD-ELRs, it was also synthesized another benchmark ELR comprising RGD as part of the backbone. HUVECs adhesion and proliferation analysis using the PicoGreen® assay revealed a higher short-term adhesion and proliferative capacity of cells on ELR surfaces functionalized with high affinity, integrin-binding bicyclic RGD-peptides compared with the ELRs containing RGD in the backbone.

Finally, in order to move forward the evolution of ELRs as advanced biomaterial showing multiple modular behaviours, it has been developed a new smart ELRs with the aim of targeting complex biomedical system. Taking advantages by the recombinant DNA techniques, it has been developed a smart biomaterial based on Elastin-like Recombinamers with allosteric control of RNase A activity. The ELRs design comprised bioactive sequences sensible to external stimuli; It was designed containing ten consensus sequence phosphorylation sites regularly distributed along the ELR, and by the Ribonuclease A active sequence (RNase A). According to the position of RNase A relative to the ELR backbone, several variants of the smart-ELR have been produced. The smart-ELRs were further characterized by several experimental techniques (SDS-PAGE, FTIR and HPLC-HR-MS), showing the capacity to be fully phosphorylated and further de-phosphorylated. This reversible system was then investigated by turbidity analysis, demonstrating an evident shift in Temperature transition (T_t) value due to the (de-)phosphorylation. Finally, the allosteric control of the RNase A catalytic activity was evaluated for all the different variants of the smart-ELR. The allosteric control of RNase A activity by the selective phosphorylation was demonstrated. Moreover, the different designs of the smart-ELRs exhibited different catalytic activity, showing the importance of the RNase A position according to the ELR backbone.

In summary, the works reported in this Thesis provides an overview of the ELRs as engineering responsive and biomimetic material for the biomedical application. Specifically, it describes in the first part the base knowledge of this class of recombinant protein, focussing on the different structures that can be formed and their great potential in many biomedical fields. Furthermore, special interest has been dedicated to the potential of ELRs as biomaterial forming hydrogels for tissue regeneration and repair.

Following this trend, for osteochondral repair application, two types of ELRs based hydrogel showing different bioactivities and gelation mechanisms have been developed and tested with an *ex vivo* and an *in vivo* study. Finally, taking advantages from the DNA recombinant technology which allows the precise control at the genetic level, news advanced ELRs have been developed. A new class of hybrid ELRs combining the synthetic synthesis of peptides with the DNA recombinant techniques has been designed, and a new generation of smart-ELRs with allosteric control has been obtained.

INTRODUCTION

The worship for the "universe" that surrounds the human body, both spiritual and physical found manifest (in ancient times) in religions and cultural myths and more recently in Medicine and Science. Since the beginning of time, Mankind has used his intelligence to find solutions to all the different diseases and aging effects that affect the human body. The knowledge and possibilities to "repair" the ultra-complex human-body machine has increased with technology. This branch of translational research is called *Regenerative Medicine*. It seeks to repair or replace tissues and organs that have been damaged; one approach considers an external substance implanted in the area affected by disease or trauma (1). Many different types of materials have been used along with the history of humanity, from wood to ceramics passing through scaffolds based on metals (2). As the competences of intervention on the human body have improved, also the materials have evolved towards various approaches with the aim of imitating the complex system for which they are though (*Biomaterials*). The science of biomaterials has evolved along the years exploring several types of solutions from natural sources, such as alginate (3) and collagen (4) to synthetic polymers such as polyethylene glycol (PEG) (5) and Poly(N-isopropylacrylamide) (PNIPAAm) (6,7) among others. The indispensable feature of a biomaterial is the *biocompatibility*, namely the ability of a material to perform with an appropriate host response in a specific application (8). Indeed, it is necessary that the material used in surgical implants does not show cause any harmful or toxic reaction to living tissue. Moreover, simultaneously to the knowledge gained over the complexity of the different tissues of the human body, advanced biomaterials with different compositions have been developed for the different areas of application. In that sense, recombinant proteins represent a powerful tool in the field of biomaterials. Among all the advantages of this class of proteins, the biggest one is the precise control over the design and the composition of the biomaterial. Indeed, this capacity allows to obtain tailored biomaterials, targeting the different tissue applications.

Elastin-like recombinamers (ELRs)

Over the last decades, recombinant DNA techniques have proven to be very powerful tools for the development of novel protein-based biomaterials. This class includes elastin-

like recombinamers (ELRs), which are protein-based polypeptides that comprise repetitive units of the Val−Pro−Gly−X−Gly $(VPGXG)_n$ pentapeptide, in which X (guest residue) could be any amino acid except L-proline (9). ELRs shows several advantages of designing biomaterials. They are inspired by elastin, which is a component of natural extracellular matrix (ECM), showing excellent biocompatibility (10,11). One of the most important features of ELRs, is that they exhibit thermo-responsiveness in acqueous media; this is due to the change of protein conformation above the so-called transition temperature (T_t), which itself depends on the amino acid composition of the polymer (12). Moreover, according to the ELRs design, it can be obtained several supramolecular structures, such as micelles, nanoparticles, films and hydrogels (13). Furthermore, as it will be described ahead, due to the DNA recombinant technology it is possible to include bioactive sequences in the final composition of the protein (14). An extended explanation about the thermo-sensitiveness property of ELRs and their capacity to self-assembly in several supramolecular structures can be found in Chapter 1.

Hydrogel-based on ELRs

As it has been extensively studied, hydrogels have become a popular option for regenerative medicine applications (15). The use of hydrogels as a scaffold to regenerate damaged tissues could provide both basic support, in case of hydrogel itself, and could promote an added repopulation contribution when embedded with cells. ELRs allows to obtain several types of biomaterial for a broad variety of applications. According to the amino acid composition, several structures can be formed, such as particles, micelles or hydrogels (13). Regarding the hydrogel structure, in this Thesis, two different gelation mechanisms have been explored: chemically & physically cross-linked hydrogels. Following the evolution of biomaterials, this is a clear example of how it is necessary to find out new solutions to more precise requests. In the case of chemically cross-linked hydrogels, the ELR sequence comprises amino acids having a functional group on the side chain, which, could be modified in order to confer a sort of reactivity; such as lysine that contains ε-amino. This ε-amino group from lysine can be chemically functionalized to provide a concrete reactivity to the ELRs molecule. In our case, we will take advantage of the 1-3 Huisgen cycloaddition to perform a crosslinking between ELRs molecules. The chemical cross-link can occur by catalyst-free click chemistry, allowing immediate gelation

of the hydrogel even at a small concentration (16). On the other hand, according to the amino acid composition of the polymer, ELRs exhibit thermo-responsiveness, indeed, above the T_t the protein conformation is translated into a hydrophobically driven self-assembly of the molecules toward supramolecular hydrogels (17). Moreover, it has been already demonstrated that the amino acid sequences GAGAGS hexapeptide (G: Glycine, A: Alanine, S: Serine) found in *Bombyx mori* silk fibroin, can be included in the ELR sequence by DNA recombinant technique. It has been found that this silk domain is responsible for the supramolecular rearrangement into β-sheets, giving stability to the hydrogel (18). In the light of the definition of *Tissue Engineering*, as the combination of cells with engineered materials to improve or replace biological functions, these two different mechanisms of gelation represent two different approaches for the tissue repair application. As it is reported above, ELR-based hydrogels are one of the most promising solutions for Tissue Engineering, along the last decades they have gained interest in the most challenging fields of tissue regeneration (19). Chapter 2 of this Thesis is an exhaustive overview of the possible applications of the ELRs in Tissue Engineering field. Both approaches reported above (chemically & physically cross-linked hydrogels) have been investigated in this Thesis; two comprehensive examples of physically and chemically cross-linked hydrogels for osteochondral repair can be found in Chapter 3 and Chapter 4.

Advanced ELRs with gained bioactivity

The evolution of ELRs as a versatile solution for biomedical application passes through the ability to form different supramolecular structures according to the designed composition of the polymer. The capacity of comprehending any sort of bioactivity represents another important milestone towards advanced materials that can be tailored for certain applications. The capacity to confer bioactivity is possible thanks to the DNA recombinant technology that allows the fusion of the desired sequences with the ELR counterpart (20). As it is reported in the literature, many ELRs containing diverse bioactive sequences have been investigated (21,22). In terms of adhesion capacities of the biomaterial, one of the most extensively used bioactive sequences is the triple peptide Arginine - Glycine - Aspartic acid (RGD), which supports cell adhesion via integrins (23). Another bioactive sequence that provides cell adhesion is the CS5 human fibronectin REDV (Arginine -

Glutamic acid – Aspartic acid - Valine) which improve the selectivity for endothelial cells (24). At the same time, the design of ELRs comprising the elastase target domain (human leukocyte elastase I) VGVAPG (L-Valine – Glycine - L-Valine - L-Alanine - L-Proline - Glycine) provides proteolytic sensitivity to the biomaterial (25). In this Thesis is reported the development of novel biomaterials based on ELRs containing the listed sequence in order to evaluate their effectiveness in the most emerging fields. Moreover, generally speaking, it has to be taken into consideration that combining opposite approaches may compensate the drawbacks shown by each one if taken individually. For example, the recombinant synthesis has limitations on the incorporation of non-canonical amino acids and does not allow the formation of cyclized peptides (26). In that sense, the recombinant technique of ELR can be combined with the strategy of designing novel and efficient peptides (27). As a further step in the evolutional process towards advanced bioactive ELRs, one objective of this Thesis is to combine these two diametrically opposed approaches in a new hybrid biomaterial. In Chapter 5 is reported the combination of synthetic peptides with the ELR backbone that can be obtained using copper-free click chemistry (15).

A new frontier of ELRs

Target complex systems require new approaches capable to combine modular features in multi-capable material. Due to its potentiality, smart materials have gained widespread interest in material science (28). Smart (or stimuli-responsive material) derived from the development of materials that show large conformational changes in response to small environmental stimuli such as temperature, ionic strength, solvent polarity, electric/magnetic field, or light (29). In that sense, ELRs represent a promising tool for the generation of a new frontier of biomaterials. As it has been reported above, the ELRs exhibit several advantages as biomaterials, such as their compatibility, and their thermo-sensitivity; however, the most important remains the precise control at the genetic level, affording exquisite control over final protein functionality. There are many examples of smart biomaterials based on ELR (smart-ELR); for biomedical and biomimetic applications (30-34). Moreover, recent works have explored a new type of ELRs, which are not only enzyme-responsive but also contain their own activity due to the fusion of selected catalytic domains at the genetic level (35,36). Following this strategy, another aim of the

Thesis was to explore a new generation of ELRs. In Chapter 6 is reported the experimental work regarding the design of a new smart ELR containing consensus sequences for enzymatic responsiveness and a catalytic domain for allosteric control.

The common ground of this Thesis is the ELRs technology with its outstanding properties; the leitmotiv is represented by the development of engineering material in a sort of journey towards the exploration of new possibilities, mashing approaches and crossing boundaries.

References

1. Mason, C. and P. Dunnill, A brief definition of regenerative medicine. Regenerative Medicine, 2008. 3(1): p. 1-5.

2. Migonney V. History of Biomaterials. Biomaterials: John Wiley & Sons, Inc.; 2014. P. 1-10.

3. Sun, J. and H. Tan, Alginate-Based Biomaterials for Regenerative Medicine Applications. Materials (Basel), 2013. 6(4): p. 1285-1309.

4. Ramshaw, J.A., Biomedical applications of collagens. J Biomed Mater Res B Appl Biomater, 2016. 104(4): p. 665-75.

5. Chaudhari, A.A., et al., Future Prospects for Scaffolding Methods and Biomaterials in Skin Tissue Engineering: A Review. Int J Mol Sci, 2016. 17(12).

6. Alexander, A., et al., Polyethylene glycol (PEG)-Poly(N-isopropylacrylamide) (PNIPAAm) based thermosensitive injectable hydrogels for biomedical applications. Eur J Pharm Biopharm, 2014. 88(3): p. 575-85.

7. Nagase, K., et al., Poly(N-isopropylacrylamide)-based thermoresponsive surfaces provide new types of biomedical applications. Biomaterials, 2018. 153: p. 27-48.

8. Eloy, R., Challenges in biocompatibility and failure of biomaterials. 2012. p. 18-29.

9. Meyer, D.E. and A. Chilkoti, Genetically Encoded Synthesis of Protein-Based Polymers with Precisely Specified Molecular Weight and Sequence by Recursive Directional Ligation: Examples from the Elastin-like Polypeptide System. Biomacromolecules, 2002. 3(2): p. 357-367.

10. Ibáñez-Fonseca, A., et al., Biocompatibility of two model elastin-like recombinamer-based hydrogels formed through physical or chemical cross-linking for various applications in tissue engineering and regenerative medicine. Journal of Tissue Engineering and Regenerative Medicine, 2018. Volume12(Issue3): p. e1450-e1460.

11. Meyer, D.E. and A. Chilkoti, Purification of recombinant proteins by fusion with thermally-responsive polypeptides. Nat Biotechnol, 1999. 17(11): p. 1112-5.

12. Urry, D.W., Molecular Machines: How Motion and Other Functions of Living Organisms Can Result from Reversible Chemical Changes. Angewandte Chemie International Edition in English, 1993. 32(6): p. 819-841.

13. J. Carlos Rodriguez-Cabello, A.I.F., Matilde Alonso, Leander Poocza, Filippo Cipriani, Israel González de Torre., Elastin-Like Polymers: Properties, Synthesis, and Applications, in Encyclopedia of Polymer Science and Technology, Wiley, Editor. 2017. p. 1-36.

14. Girotti, A., et al., Design and bioproduction of a recombinant multi(bio)functional elastin-like protein polymer containing cell adhesion sequences for tissue engineering purposes. Journal of Materials Science: Materials in Medicine, 2004. 15(4): p. 479-484.

15. Park, K.M. and K.D. Park, In Situ Cross-Linkable Hydrogels as a Dynamic Matrix for Tissue Regenerative Medicine. Tissue Eng Regen Med, 2018. 15(5): p. 547-557.

16. González de Torre, I., et al., Elastin-like recombinamer catalyst-free click gels: Characterization of poroelastic and intrinsic viscoelastic properties. Acta Biomaterialia, 2014. 10(6): p. 2495-2505.

17. Martín, L., et al., Synthesis and Characterization of Macroporous Thermosensitive Hydrogels from Recombinant Elastin-Like Polymers. Biomacromolecules, 2009. 10(11): p. 3015-3022.

18. Fernández-Colino, A., et al., Self-Organized ECM-Mimetic Model Based on an Amphiphilic Multiblock Silk-Elastin-Like Corecombinamer with a Concomitant Dual Physical Gelation Process. Biomacromolecules, 2014. 15(10): p. 3781-3793.

19. Rodríguez Cabello, J.C., et al., 12 - Elastin-like materials for tissue regeneration and repair A2 - Barbosa, Mário A, in Peptides and Proteins as Biomaterials for Tissue Regeneration and Repair, M.C.L. Martins, Editor. 2018, Woodhead Publishing. p. 309-327.

20. Rodríguez-Cabello, J.C., et al., Synthesis of Genetically Engineered Protein Polymers (Recombinamers) as an Example of Advanced Self-Assembled Smart Materials, in Nanotechnology in Regenerative Medicine: Methods and Protocols, M. Navarro and J.A. Planell, Editors. 2012, Humana Press: Totowa, NJ. p. 17-38.

21. Nettles, D.L., A. Chilkoti, and L.A. Setton, Applications of elastin-like polypeptides in tissue engineering. Adv Drug Deliv Rev, 2010. 62(15): p. 1479-85.

22. Santos, M., et al., Genetically Engineered Elastin-based Biomaterials for Biomedical Applications. Curr Med Chem, 2018.

23. Ruoslahti, E. and M.D. Pierschbacher, Arg-Gly-Asp: A versatile cell recognition signal. Cell, 1986. 44(4): p. 517-518.

24. Ji, Y., et al., Zwitterionic polycarboxybetaine coating functionalized with REDV peptide to improve selectivity for endothelial cells. J Biomed Mater Res A, 2012. 100(6): p. 1387-97.

25. Lombard, C., et al., Human leukocyte elastase hydrolysis of peptides derived from human elastin exon 24. Biochimie, 2006. 88(12): p. 1915-21.

26. Link, A.J., M.L. Mock, and D.A. Tirrell, Non-canonical amino acids in protein engineering. Current Opinion in Biotechnology, 2003. 14(6): p. 603-609.

27. Cai, L., C.B. Dinh, and S.C. Heilshorn, One-pot Synthesis of Elastin-like Polypeptide Hydrogels with Grafted VEGF-Mimetic Peptides. Biomaterials science, 2014. 2(5): p. 757-765.

28. Furth, M.E., A. Atala, and M.E. Van Dyke, Smart biomaterials design for tissue engineering and regenerative medicine. Biomaterials, 2007. 28(34): p. 5068-5073.

29. Galaev, I.Y. and B. Mattiasson, 'Smart' polymers and what they could do in biotechnology and medicine. Trends in Biotechnology, 1999. 17(8): p. 335-340.

30. Alvarez-Rodríguez, R., et al., Gold Tailored Photosensitive Elastin-like Polymer: Synthesis of Temperature, pH and UV-vis Sensitive Probes. Vol. 31. 2010. 568-73.

31. Herrero-Vanrell, R., et al., Self-assembled particles of an elastin-like polymer as vehicles for controlled drug release. Journal of Controlled Release, 2005. 102(1): p. 113-122.

32. Nawroth, J.F., et al., Maleimide-Functionalized Poly(2-Oxazoline)s and Their Conjugation to Elastin-Like Polypeptides. Macromolecular Bioscience, 2016. 16(3): p. 322-333.

33. Kinikoglu, B., et al., A smart bilayer scaffold of elastin-like recombinamer and collagen for soft tissue engineering. Journal of Materials Science: Materials in Medicine, 2011. 22(6): p. 1541-1554.

34. Cipriani, F., et al., Bicyclic RGD peptides with high integrin $\alpha_v\beta_3$ and $\alpha_5\beta_1$ affinity promote cell adhesion on elastin-like recombinamers. Biomed Mater, 2019.

35. Du, K., et al., Enhancement of the solubility and stability of d-amino acid oxidase by fusion to an elastin like polypeptide. Journal of Biotechnology, 2015. 212: p. 50-55.

36. Gao, Q., et al., Genetically-modified R-ω-transaminase: purification and self-assembly facilitating interaction with substrate droplets. Biotechnology letters., 2016. 38(3): p. 489-494.

PROBLEM STATEMENT AND HYPOTHESIS

The Biomaterial field is a branch of translational research that evolves with technology. Many types of technology have a crucial impact in this scientific field, both for the development of biomaterials and for the application of those biomaterials in the biomedical field. Along the last decades, the scientific community came up with several types of biomaterials from natural sources to synthetic polymers. Despite the large variety of biomaterials, only a few of them are able to show adequate properties of bioactivity and versatility for being applied to different biomedical applications. Nowadays, a partial wrong approach is the tendency to use a "one-type" biomaterial to address diverse biomedical issues. The strategy of developing one type of biomaterial for a large variety of biomedical applications may results successful for some, but unsuccessful for the others. Every issue in the biomedical field needs to be targeted with tailored therapies. One of the biggest challenges of today is to develop tailored biomaterials for specific applications. In this Thesis, we propose to explore the potential of Elastin-like Recombinamers (ELRs) as an engineering responsive and biomimetic material, towards the development and the optimization of tailored solutions for specific biomedical applications.

The following points represent the hypothesis of the research planning of this Thesis:

- Considering that the DNA recombinant technique allows an exquisite control at the genetic level, we hypothesize to generate several ELRs comprising diverse combinations of bioactive domains. Furthermore, we aim to bio-produced the designed ELRs in *Escherichia coli* taking advantage of their thermo-responsiveness whereby depending on the composition of the ELRs several structures could be formed.

- It is well known that hydrogels based on specifically designed ELRs can be formed by different gelation mechanisms and that these mechanisms influence the mechanical properties of the hydrogels. We hypothesize that the different gelation mechanism (chemical or physical cross-linking) has a crucial influence for

the generation of a 3D hydrogel embedded with cells as a successful scaffold for osteochondral repair.

- It is well described in the literature that ELR can be modified in order to be reactive for click chemistry reaction. We hypothesized that the strategy of copper-free click chemistry allows the incorporation of non-canonical amino acids and the formation of cyclized peptides, (which represents a limitation shown by the recombinant synthesis) in order to generate a new class of hybrid biomaterials.

- The consensus sequence sensible for the kinase/phosphorylase can be included in the ELR composition in combination with the RNAse A catalytic domain in order to verify the allosteric domain regulation. Indeed, new combinations of ELR with bioactive sequences can be explored.

OBJECTIVES

- The main purpose of this Thesis is to develop engineered responsive materials capable to overcome some limitations shown by the existing solutions for biomedical applications. Our research focuses on the potentiality of using elastin-like recombinamers (ELRs) as the common ground for the development of different biomimetic materials. Different aspects will be touched within this Thesis, lining up a sort of evolution in the complexity of the ELR-based biomaterials.

- The first concrete scope of the Thesis is to design and produce bioactive hydrogels for Tissue Engineering (TE) application. Specifically, the goal is to develop bioactive hydrogels for osteochondral repair. The need to include bioactive domains in the ELR's composition will be investigated focussing on different bioactive domains such as adhesion sequence and proteases sensitiveness, we aim to find the right ratio of bioactive sequences in order to permit the replacement of the scaffold for the regenerated tissue. ELRs containing tailored bioactive motifs will be obtained through recombinant DNA technology. Moreover, two different gelation mechanisms of hydrogels by chemical (covalent bonds) or by physical cross-linking will be investigated and characterized by different methods such as rheology and Scanning Electronic Microscopy (SEM).

- Secondly, the cyto-compatibility of the designed hydrogels will be assessed by *in vitro* analysis. Moreover, the effective regeneration enhancement of the designed ELR-based hydrogels for osteochondral application will be evaluated by *ex vivo* and *in vivo* studies. In the first case, the study will be carried forward in collaboration with LifeTec Group, using an *ex vivo* platform for cartilage repair. On the other hand, we intend to assess the osteochondral regeneration of a critical defect with animal study trials. In both cases, the regeneration rate will be evaluated with different techniques, such as histology and immunohistochemistry (IHC).

- Furthermore, a new hybrid ELRs containing bioactive sequences will be generated combining the recombinant technique of the elastin-like recombinamers with the strategy of designing novel and more efficient synthetic peptides (in collaboration with PepScan). The potentiality of combining these two diametrically opposed approaches in a new hybrid biomaterial for broad biomedical application will be explored. Indeed, the adhesion capacity of the new material will be evaluated by different techniques such as DNA quantification and Morphological analysis for HUVECs. Thereby, we intend to discover the enhanced adhesion capacity of the hybrid material at short-term or long term, and that may be used as a new tool for biomedical applications.

- Finally, a new class of smart-ELRs with an allosteric domain will be investigated. We will take advantages from the recombinant technique of ELRs to include bioactive consensus sequences and enzymatic activity. A new smart-ELR containing the Kinase/Phosphatase consensus sequence will be produced, and the thermo-sensitiveness modulation will be evaluated according to the phosphorylation/de-phosphorylation of the smart-ELRs. Moreover, in order to aim the allosteric control of the smart-ELR, different variants of smart-ELR having fused the RNase A catalytic domain will be produced. Then, the smart-ELRs will be characterized by several techniques such as mass analysis and turbidity; furthermore, the allosteric control of the RNase A catalytic will be assessed by RNA quantification analysis.

STATE OF THE ART

CHAPTER 1

ELASTIN-LIKE POLYMERS: PROPERTIES, SYNTHESIS AND APPLICATIONS

José Carlos Rodríguez-Cabello,[1] Arturo Ibáñez-Fonseca,[1] Filippo Cipriani,[2] Leander Poocza,[1] Israel González de Torre,[1,2] Matilde Alonso[1]

[1] Universidad de Valladolid, BIOFORGE, CIBER-BBN, Valladolid, Spain

[2] Technical Proteins NanoBioTechnology (TPNBT) S.L., Valladolid, Spain

J.C. Rodríguez-Cabello, A. Ibáñez-Fonseca, F. Cipriani, L. Poocza, I. González de Torre, M. Alonso. Elastin-like Polymers: Properties, Synthesis and Applications. *Encyclopedia of Polymer Science and Technology* (2017). doi: 10.1002/0471440264.pst656

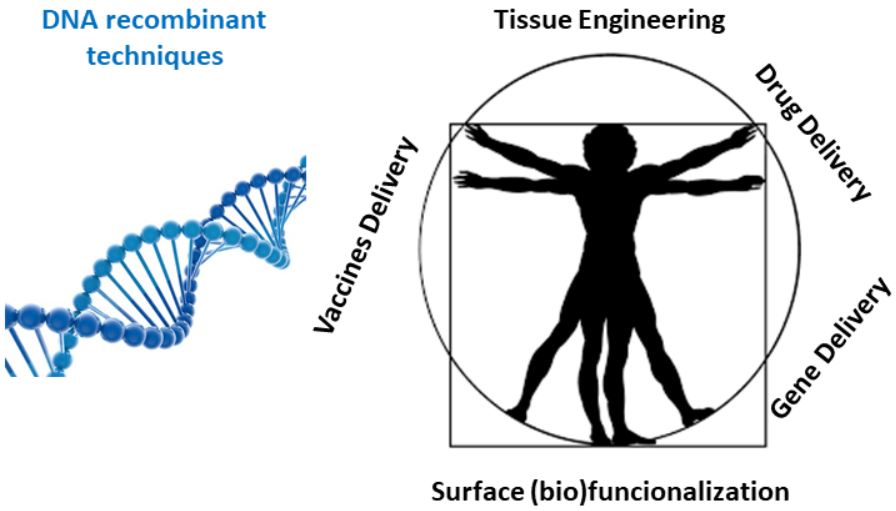

1. INTRODUCTION

Etymologically, the term protein comes from the Greek *proteios*, which means “holding first place”, or could come from the god *Proteus* which name suggests “primal”, “firstborn” and it is associated to the facility of this God to change his form and opinion. The name itself indicates the crucial role that proteins have in the living beings and the diverse forms in which we can find them in nature. If the importance of water is well known in the composition of the human beings, around 60% in adult males (1), proteins are not less important. In fact, more than 50% of the dry weight of our bodies is formed by proteins. They may have very different functionalities in the living systems, and some of them are large molecules that help to form the structure of our tissues irrespective of their location. In this way, we can find them forming really hard structures like bones, nails, horns or scales but they are also present in softer tissues like liver, muscles or connective tissue. Furthermore, proteins are not only involved in these structural tasks but they play a paramount role in the activation or deactivation of gene expression, or having regulatory functions helping to organize several processes or regulating metabolism or even taking part in muscle contractions.

Among these proteins, elastin is one of the most important proteins that can be found composing the extracellular matrix (ECM) which provides structural integrity to the organs and tissues in the living beings. Elastin is not only an important protein within the composition of the ECM, but it also possesses certain features that make it unique. For instance, it is extremely durable and with a very low turnover in healthy tissues, the estimated half-life of this protein is around 70 years (2). Elastin confers elasticity and resilience to many tissues like ligaments, tendons, arteries or lungs among others (3). This elasticity is given by the presence of hydrophobic regions within the structure of the monomers of elastin that tend to aggregate and self-assemble contributing to the polymeric organization of the elastin (4). Along the last decades of the 20th century not few researchers were interested in this self-assemble property and started to explore the synthesis and production of artificial polypeptides based on these hydrophobic domains that conferred such properties to the elastin molecule (5-8). They found that the most frequent fragment of pentapeptides in the structure of the natural elastin was the sequence VPGVG, appearing up to 50 times in a single elastin molecule. It was discovered

that synthetic polymers of $(VPGVG)_n$ ($n \leq 150$) were soluble in water below 25°C but they aggregated suffering a phase transition above this temperature (8). This change in the conformation of the protein leads to a viscoelastic state in which the amount of polymer is around 50% and the other 50% is water. This process is common to all the elastin-like polymers (ELPs) and it is accompanied by a halving of the length of the polymer and a release of a great amount of energy (9). All this process is driven by a change in the structure of the ELP, from an extended conformation below the transition temperature (T_t), to a β-spiral with three units of the basic pentamer VPGVG, forming a type II β-turn per turn of the spiral, above the T_t (5) (Figure 1). The T_t can be tuned by changing the fourth amino acid of the pentamer VPGXG, where X could be any amino acid except proline, because its structure destabilizes the β-turn impeding the correct packing of the chains of the polymer. The T_t of an ELP is clearly influenced by the nature of the guest amino acid on the X position in the sequence $(VPGXG)_n$ (apolar residues decrease the T_t, while polar ones increase the value of the T_t) and by the overall polymer length (n). The effect of these two parameters has been deeply investigated and described by Urry and coworkers (10). Moreover, the T_t is sensitive to other external factors as for instance ionic strength, pH, pressure, light or chemical modifications (9).

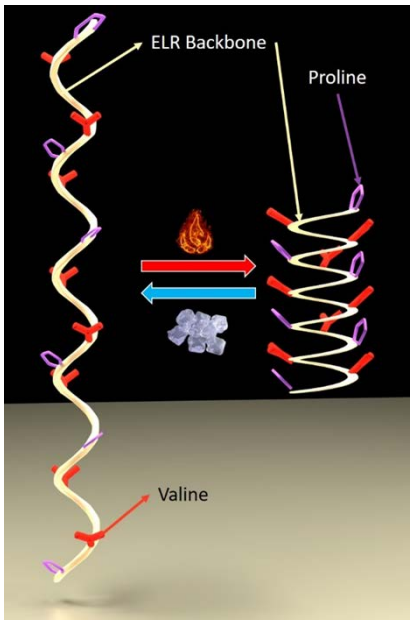

Figure 1. Schematic representation of the conformational change of the ELP and ELR backbone depending on the temperature.

Chemical synthesis of various polypeptides based on elastin were successfully obtained by using standard chemical processes as demonstrated by Urry, Prasad and others (11,12), but some problems arise when more complex structures or simply larger polymers want to be synthetized, like problems in purification and polydispersity and, even if these amounts of mixture of products are obtained in small quantities, they can drastically affect the physical properties of the final product (13). The arrival of the recombinant DNA technology opened a new way to design and produce synthetic proteins. The old nomenclature of ELPs was changed to ELRs (elastin-like recombinamers) pointing out the recombinant origin of this new family of elastin-based polymers. With this new approach, some of the problems derived from the old chemical synthesis, like polydispersity, need for organic solvents and the further elimination of their residues, were overcome while a higher control over the amino acid sequence was obtained. Moreover, the purification process changed from classical chemical purification pathways to one based exclusively on the thermal behavior of the ELRs. After some inverse transition cycles (ITC), which imply heating and cooling of the suspension containing ELRs above and below their inverse temperature transition (ITT), they can be easily purified without the need of the addition of chemical agents or solvents that should be removed afterwards. During the last decade, a better control over the recombinant techniques and the use of more specific and accurate enzymes has led to the precise biotechnological processes that are nowadays applied in the production of the ELRs.

ELRs are biological polymers that due to their flexibility in the design, their self-assembly properties, easy chemical modification allowing the introduction of many interesting functionalities, versatility to be processed in many forms (aggregates, fibers, layers, nano-particles or hydrogels) and excellent cyto- and biocompatibility, have a high potential in many fields, from drug-delivery to tissue engineering, including others such as protein purification, anti-cancer gene therapies or nano-vaccines.

In the next pages, we will explore the evolution of ELRs from their ancient chemical origin to the most cutting-edge bioproduction techniques, exploring the several hosts that can be used to bioproduce them and their versatility in the design. We will also immerse in the several structures that ELRs can form and their possibilities in the numerous medical fields where they can be applied.

2. ELASTIN-LIKE RECOMBINAMERs ENGINEERING, BIOPRODUCTION AND DESIGN

2.1. History and evolution of the synthesis of elastin-like recombinamers

1.3.1. Ancient times (the "chemistry ages")

The finding of repetitive sequences in porcine elastin by Gray *et al*., in 1973 (14), led to the chemical synthesis of different versions of some of these oligopeptides, being one of them the pentapeptide Val-Pro-Gly-Val-Gly (VPGVG in single-letter amino acid code). There was a lot of enthusiasm to study the conformational properties of these peptides in an attempt to shed light into the features of natural elastin, a polymeric protein that gathered a lot of attention due to its relationship with several diseases (15,16). Hence, Urry's laboratory began synthetizing elastin-derived peptides and soon became one of the leading research groups in this field. However, the synthetic strategies required complex methods including the use of diverse precursors and solvents, while the overall yield and the length of the polypeptide were very limited (17). Despite the limitations, these synthetic approaches allowed the attaining of VPGVG (poly)pentapeptides to perform conformational studies (17,18), even by covalent cross-linking of these peptides, which also led to morphological studies by scanning electron microscopy (SEM) and to the determination of stress-strain curves (19). Finally, all these early studies resulted in the development of molecular dynamics calculations which gave more information about the secondary structure of the protein and about the backbone torsion angles ψ and ϕ of the amino acid residues in the polypeptide, both in its relaxed and extended state (20).

2.1.2. Modern times (the "recombinant ages")

By that time, the last years of the 80´s, recombinant DNA technology had arisen as a very promising tool for the biotechnological synthesis of proteins in heterologous hosts, mainly *Escherichia coli*. Therefore, researchers started to use this technology for the expression of polymeric proteins to overcome the disadvantages of both chemical synthesis and extraction from natural sources. The first biosynthetic strategy for the production of ELRs,

in this case fused to silk-like sequences (repetitions of the GAGAGS hexapeptide), was reported by Cappello *et al*. in 1990 (21). Nevertheless, the molecular biology methods that led to the obtaining of the elastin-like gene were described two years before in a patent by Ferrari *et al.* (22). This document explains the head-to-tail concatemerization of the elastin-like gene by self-ligation of cohesive DNA ends leading to a final gene encoding the amino acid sequence $(VPGVG)_{160}$. Hence, this self-ligation method allowed the synthesis of ELR genes with different lengths, although in an uncontrolled manner and without the guarantee of achieving a gene with the desired length. This process was further explained by Tirrell *et al.* for the genetic engineering and expression of protein polymers in general, also discussing the potential issues derived from the use of the recombinant DNA technology (23).

2.1.3. Contemporary times (the "seamless recursive ages")

After these first steps towards genetic engineering of ELRs, new methods were developed to overcome some disadvantages, like the low number of endonucleases recognizing non-palindromic cleavage sites needed for the self-ligation in a correct head-to-tail orientation. Hence, some procedures described for general cloning were used in the context of ELRs. This is the case of the "seamless cloning" technique that allowed the cleavage of DNA outside the recognition sequence by the use of the type IIs restriction endonuclease *Eam1104I* and, therefore, avoided the introduction of extraneous nucleotides (nts) in the cloned sequence (23). This method was first used successfully by Conticello and co-workers for the synthesis of ELR genes, suggesting that it could be a more rapid and efficient system for the bioproduction of protein polymers (25). Nonetheless, they still relied in concatemerization to achieve the desired length of the gene. To overcome this limitation, Meyer and Chilkoti proposed a new method termed "recursive directional ligation" (RDL) (26). In their work, they described the use of two different restriction endonucleases with well-defined features, namely *PflMI* and *BglI*, to synthetize ELR genes. These two restriction enzymes leave single-stranded DNA ends upon cleavage that are cohesive one with the other, so one of them can be used to extract the ELR insert, while the other one is used to linearize the cloning vector. Both molecules were then mixed together for ligation to achieve the final construction. The plasmid vector was designed so the restriction sites were maintained after each cloning step, allowing

subsequent insertions of ELR-coding genes. As an evolution of this method, Chilkoti and co-workers described a new RDL strategy termed plasmid reconstruction (PRe)-RDL (27). In this case, they introduced type IIs restriction endonucleases to RDL for a more efficient seamless cloning. Moreover, it avoided self-ligation of the vector and nonproductive circularization of the insert by cutting both the insert-donor plasmid and the receptor vector in halves with two different type IIs endonucleases that leave non-complementary overhangs. Therefore, a circular plasmid is only achieved when both insert and vector have been ligated.

Despite the great improvement in the genetic engineering of ELRs reached so far, there were still some limitations that should be overcome, like complexity in plasmid design. In this regard, Rodríguez-Cabello *et al.* described a new method for the easy and rapid generation of ELR gene constructs and their expression in heterologous hosts (28). For this purpose, they relied on the seamless cloning approach through two type IIs endonucleases, namely the aforementioned *Eam1104I* and *SapI*. The only difference between them is that SapI recognizes a 7-nt sequence, while *Eam1104I* recognizes a 6-nt one (GCTCTTC and CTCTTC, respectively), being the latter included in the *SapI* one. With this strategy, it is possible to engineer a plasmid so it can include two *Eam1104I* restriction sites, being one of them also a *SapI* recognition sequence. For this purpose, two commercially available plasmids, one being the pDrive cloning vector and the other one the pET-25b(+) expression vector, were modified by site-directed mutagenesis to exclude inherent *Eam1104I* and *SapI* restriction sites and only include the desired ones. On the other hand, it allows controlled concatemerization following the previous guidelines for RDL. Furthermore, it avoids self-ligation in a very simple way by treating the receptor plasmid with a shrimp alkaline phosphatase, hence eluding the need of cutting plasmids in halves as described above. This procedure, named iterative-recursive method, is a good example of how molecular biology methods can be fine-tuned to achieve well-defined repetitive genes coding for protein polymer sequences very efficiently.

A schematic representation of the multiple options in ELR design and genetic engineering can be observed in Figure 2.

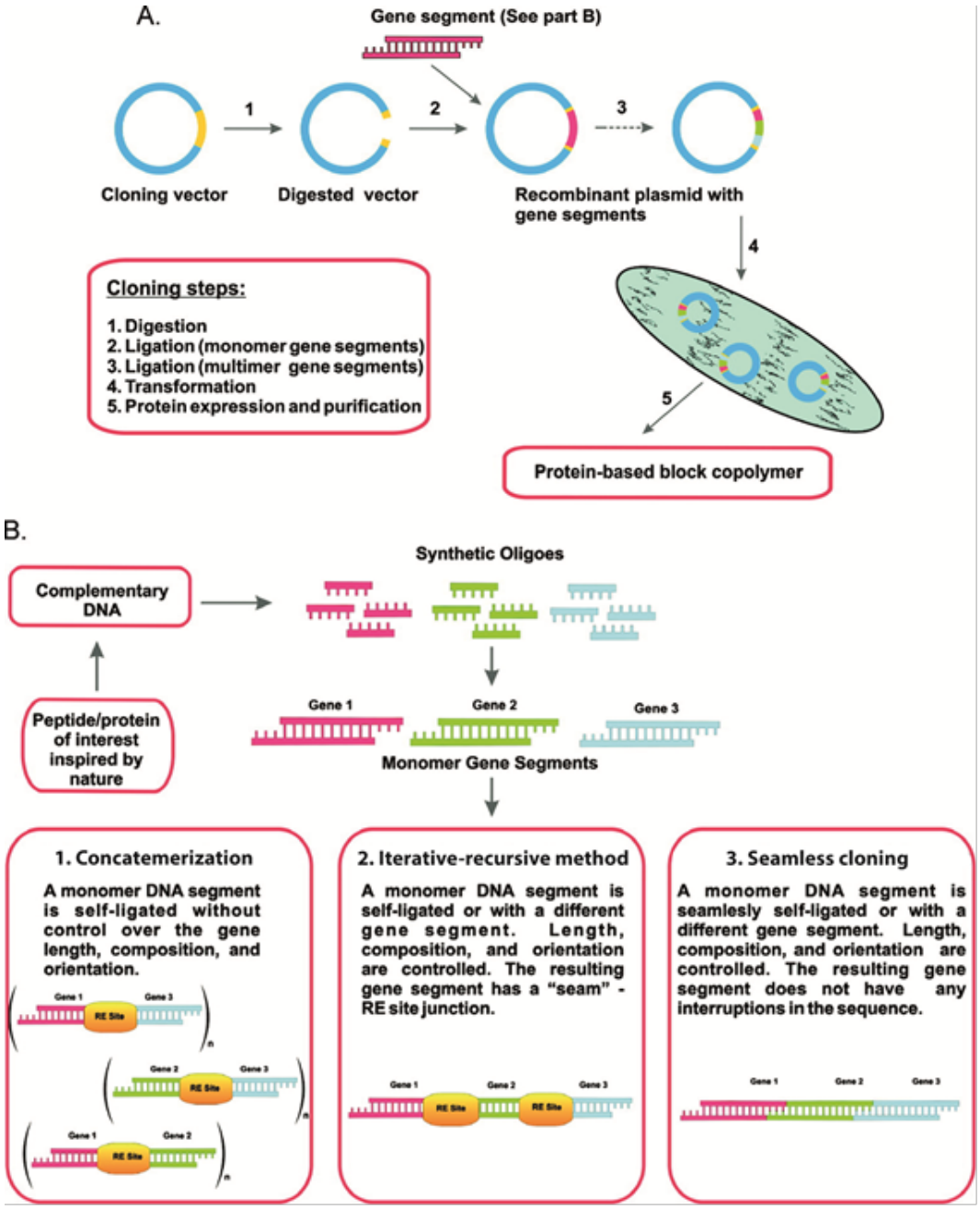

Figure 2. Schematic representation of the different approaches for the design and genetic engineering of protein polymers in general and ELRs in particular. Adapted with permission from (29).

2.2. Hosts for the expression of elastin-like recombinamers

2.2.1. Prokaryotic hosts

2.2.2.1 *The gold standard: Escherichia coli*

Like in the case of many other proteins produced by recombinant DNA technology, *E. coli* was used for the heterologous expression of ELRs in the first place, as is the case for all the works commented above. This is mainly due to the well-studied metabolism and culture conditions of this *Enterobacteriaceae.* Furthermore, ELRs do not undergo post-translational modifications and their folding is correctly achieved without the mediation of eukaryotic chaperones or any similar system. Hence, *E. coli* arose from the beginning as a good host to achieve an optimal expression and yield of ELR biosynthesis. However, although expression was easily achieved for short (30) and long ELRs (31), there was still plenty of room for optimization. First, Guda *et al.* compared the expression of the gene coding for G-(VPGVG)119-VPGV in Luria Broth (LB) culture medium following induction with isopropylthio-β-D-galactoside (IPTG) and Terrific Broth (TB) without induction (32), and they found that the expression was very much higher in the case of TB culture after 24 hours. This TB medium had shown before a favorable effect on plasmid stability, while the use of lactose in TB made it a good auto-induction medium (33).

Other approaches regarding the optimization of ELR bioproduction explored the supplementation of *E. coli* culture medium with amino acids that are highly repeated in the ELR sequence: glycine, valine, proline, and alanine. In this way, depletion of intracellular amino acid pools in E. coli could be avoided. Therefore, Chow *et al.* studied the expression of ELR and the final yield in terms of grams of ELR per liter of culture, both with LB culture medium followed by IPTG induction, and with TB medium (34). In this work, the authors showed that the use of glycerol, phosphate buffer and proline as supplements of TB medium enhanced 6-fold the ELR yield compared to the basal TB, from an initial 0.27 g/L to 1.6 g/L, with the subsequent reduction in cost. Furthermore, their results suggest that, surprisingly, supplementation of amino acids other than those abundant in ELRs (asparagine, aspartic acid, glutamine and glutamic acid) also enhanced

protein yields, indicating that regulatory mechanisms in the control of intracellular amino acid pools that are more complicated than it could be expected in the first place may exist.

Other works have reported a high-level expression of ELRs fused to silk-like domains, hence making silk-elastin-like recombinamers (SELRs). Machado *et al.* showed a volumetric yield of 150 mg/L, being 6-fold higher than previously reported productivities, just by using auto-induction TB medium supplemented with lactose and controlling the temperature at 37°C (35). However, cell densities were too low compared with lactose supplemented TB at the same conditions, so the process could still be optimized. Furthermore, it was a low-scale batch production and some parameters influencing bacterial culture were uncontrolled. Henceforth, a comprehensive and detailed study was carried out by Collins *et al.*, even though it was performed again in low-scale fermentation systems (shake flasks) (35). Cultures were performed at different conditions by changing medium and medium composition, initial pH, incubation temperature, flask volume to culture volume ratio, agitation rate, IPTG induction concentration, elapsed fermentation time at induction and induction period. Though the chosen approach was 'one-factor-at-a-time' and therefore the study had some limitations. Despite these limitations, it was found that the best yield of 500 mg/L is achieved at 37°C with TB at pH 6-7.5, a 10:1 flask volume: culture volume ratio, agitation speed of 200 rpm and induction at the beginning of the stationary phase with 0.5 mM IPTG for 4 hours. Further studies were performed by the same group, in this case using a fed-batch approach and a 3 L bioreactor, allowing a more powerful and deeper experimental design (36). Then, they evaluated the effect of the pre-induction and post-induction growth rates, dissolved oxygen concentration, dry cell weight at induction, and IPTG concentration for induction. Furthermore, they could control pH, O2 concentration and feeding of a glucose solution during all the fermentation process. With this experimental setting, they showed that they obtained a yield of 4.3 g/L of SELR in the best conditions. This is 9-fold higher than the data previously reported by them.

2.2.2. Eukaryotic hosts

2.2.2.1 *Aspergillus nidulans fungus*

One of the first attempts to produce ELRs in eukaryotic hosts was made by Herzog *et al.* in *Aspergillus nidulans (A. nidulans)* fungus (37). They inserted the gene encoding for G-(VPGVG)$_{119}$-VPGV mentioned above into an expression vector designed for *A. nidulans* under the control of a constitutive promoter. Their results showed that they were able to isolate different fungus colonies that integrated the plasmid with varying copies into their own genome. However, the translational efficiency was low, and they suggest that this effect could be due to some codons found in the ELR gene (cloned from an *E. coli*-optimized plasmid) that are rarely used in A. nidulans. Despite the proposal made by the authors towards the optimization of ELR bioproduction through *A. nidulans*, no other examples have been found in the literature.

2.2.2.2 *Yeast*

On the other hand, the well-studied *Pichia pastoris (P. pastoris)* yeast has become a model eukaryotic organism for recombinant protein expression and there are some examples in the literature in which it has been chosen for the biosynthesis of ELRs. In the first case reported, Schipperus *et al.* produced secreted ELRs in *P. pastoris* with a yield of 255 mg of ELR per liter of culture medium (38). They suggest that this low-scale system is completely scalable, easily purifying ELRs without the need of cell disruption, even though times for culturing and inducing expression in yeast are substantially longer than in the case of *E. coli.* Furthermore, this expression host allows glycosylation and/or formation of disulfide bonds, so it is proposed as a good system for the expression of ELR fusion proteins that may undergo any of these post-translational modifications. Almost at the same time, Sallach *et al.* described the expression in *P. pastoris* of non-repetitive ELR genes with identical amino acid sequences, taking advantage of the degenerate genetic code (39). They propose the same advantages than the previous work, but they also emphasize that in a yeast expression system there is no need to remove bacterial lipopolysaccharide, achieving an endotoxin-free product after simple ITC purification. In another study by Schipperus *et al.* comparing the secretion of ELRs with different transition temperatures (T_t) by *P. pastoris,* they found that higher yields are obtained for shorter and more hydrophilic ELRs (39). Therefore, they suggest that below T_t the ELRs are soluble and more

easily secreted. However, the conclusion to this work seems too ambitious since only three ELRs were designed and produced for the comparison, and none of them was strongly hydrophilic.

2.2.2.3 *Plants*

As regards other expression systems, recombinant protein production in plants has been widely developed since the beginning of the recombinant DNA era and, hence, ELRs have been produced in this system too. In the first work describing ELR production in plant cells, Zhang *et al.* transformed tobacco cells physically by particle bombardment (biolistics) for the expression of the gene encoding $(GVGVP)_{121}$ (41). They showed the integration of the ELR gene in the genome of the cells (2-5 copies) and expression of the elastomeric protein, although at very low quantities. As a next step, the following article by this group showed the feasibility to express the same ELR in transgenic tobacco *(Nicotiana tabacum)* plants (42). Nonetheless, only 0.5 to 5 μg per g of fresh weight of leaf tissues were obtained, being approximately 0.003 to 0.03% of total soluble proteins, while 0.01 to 0.05% was observed by Western blot prior to purification. Even though there are many other examples of expression of ELRs in transgenic plants, they mostly use them as fusion tags to improve the stability of the expression and the purification efficiency of different recombinant proteins, which will be briefly described below. However, there is a very recent work by Heppner *et al.* that describes the bioproduction of a fusion protein comprising spider silk and ELR sequences in tobacco leaves (43). The spider silk block is not excised from the whole protein after purification, so it can be taken as an example of ELR expression in plants. Authors showed a yield of 400 mg per 6 kg of leaves (66.7 mg/kg or μg/g) which is more than a 13-fold increase when compared to the results commented above, although the comparison is limited because in this last case ELR is fused to spider silk. The expression of ELRs in all the heterologous hosts described in this section is summarized in Table 1.

Host		$(VPGXG)_n$ composition	Main achievements	Refs.
Prokaryotic	*Escherichia coli*	$(VPGVG)_{160}$	First recombinant production of an ELR combined with silk-like sequences	(22)
		$(VPGVG)_{20}$	First biotechnological production of an ELR by itself	(30)
		$(VPGVG)_{251}$	First reported expression of extremely long ELRs	(31)
		$(VPGVG)_{120}$	Comparison between culture media of different composition	(32)
		$[(VPGVG)_2$-VPGGG-VPGAG-$(VPGVG)_3$-VPGGG-VPGAG-$VPGGG]_9$ (also called ELP-90)	Supplementation of medium with amino acids highly repeated in ELRs to avoid depletion	(34)
		$(VPAVG)_{20}$ and $(VPAVG)_9$	SELR with high yield by using auto-induction medium	(35)
		$(VPAVG)_9$	'One-factor-at-a-time' optimization of the bioproduction of a SELR in shake flask cultures (low scale)	(36)
		$(VPAVG)_9$	Optimization of the bioproduction of a SELR in fed-batch culture in a bioreactor obtaining the highest yield reported to date	(37)
Eukaryotic	*Aspergillus nidulan*s fungus	$(VPGVG)_{120}$	Unique example of ELR expression in fungal hosts	(38)

	Pichia pastoris yeast	ELP-90	First reported expression of secreted ELRs in yeasts	(39)
		$[(VPGVG)_{2}$-VPGEG-$(VPGVG)_{2}]_{21}$	Suggestion of avoidance of LPS removal	(40)
		ELP-90 ELP-40 $[(VPGVG)_{2}$-VPGGG-VPGLG-$(VPGVG)_{3}$-VPGGG-VPGLG-$VPGGG]_{4}$	Higher yields for shorter and more hydrophilic ELRs	(41)
	Nicotiana tabacum cells and plants	$(VPGVG)_{121}$	First work describing ELR production in plant cells	(42)
		$(VPGVG)_{121}$	First expression of an ELR in plants	(43)
		ELP-100	ELR fused to a spider silk protein produced through a simple and scalable method	(44)

Table 1. Table describing the heterologous hosts used for the bioproduction of ELRs to date.

2.3. Novel design of elastin-like recombinamers with different features

Taking advantage of the genetic engineering, which may allow the inclusion of changes in the amino acid sequence of ELRs or even the fusion of different proteins, the features of ELRs can be tuned and/or improved, increasing the complexity of these protein polymers (44).

2.3.1. Substitution of the guest amino acid

One of the first choices regarding the modification of the ELR sequences is the amino acid in the fourth position (guest residue) of the elastin-derived pentapeptide, or the X in VPGXG, as described above. Since this choice may change completely the physicochemical

properties of the ELR, the T_t above all, it is a common way to differently design ELRs and has been extensively evaluated (45). Moreover, the molecular biology methods used in the synthesis of ELR genes permit the construction of elastin-like block corecombinamers (ELbcR) that arise as a result of the combination of elastin-like sequences with different substitutions in the guest residue. This approach may confer different properties to a single ELR molecule (46), and also leads to more complex self-assemblies above the T_t as evaluated in different works (47,48). In addition, Meyer *et al*. studied the effect of the length and concentration on the T_t for different ELRs, showing that there is a higher decrease of T_t for ELRs with lower molecular weight (MW) when the concentration is increased, while this effect is lower for ELRs with higher MW (49). Furthermore, they proposed equations that may allow the prediction of the T_t for other ELRs. Some years later, the same group further evaluated the changes of T_t depending on alanine content as the guest residue, and on MW of the ELR and concentration, developing a model to predict T_t by changing these conditions (50). Through the combination of two different factors affecting T_t, i.e. the arrangement of blocks with different guest residues and the length of these blocks, Ribeiro *et al.* showed that it is not only the mean polarity what influences variations in T_t and enthalpy (ΔH) of the transition, but also the distribution and length of the polar/apolar blocks within the ELbcR molecule (51).

2.3.2. Fusion of other protein polymers

Many studies have explored the possibility of using ELRs in combination to other protein polymers like silk, collagen or resilin to improve or change their properties in different applications, most of them within the field of tissue engineering (52).

The first examples of this section have already been shown above in relation to SELRs. Silk-like domains derive from the repetition of the GAGAGS hexapeptide found in *Bombyx mori* silk fibroin, which is known to self-assemble into β-sheet secondary structures, conferring high strength, toughness and ductile elongation to materials (21). They have been widely fused to elastin-like blocks by different groups. For example, Nagarsekar *et al.* described the design and production of different silk-elastin-like block co-recombinamers (SELbcRs) that showed sensitiveness to diverse stimuli like pH and temperature (53). In another study, Wang *et al.* developed a high-throughput for the screening of SELRs matching specific material functions (54). For this purpose, they

expressed a library of different SELRs in *E. coli* cultured in 96-well plates and purified the recombinamers *in situ*. Then, they performed a physicochemical and mechanical characterization on those SELRs without taking them out of the plates, suggesting that it could be a rapid and powerful tool to elucidate the properties of recombinant materials.

In another work, Bracalello *et al.* designed and produced a chimeric resilin-elastin-collagen-like recombinamer that showed a different self-assembling pattern than any of each protein polymer had shown separately, with great tendency to form higher order fibrillar structures (55).

2.3.3. Fusion of bioactive domains

In order to generate extracellular matrix-like materials, cell adhesion motifs have been fused to ELR sequences by genetic engineering as described by different groups. In a first example, Panitch *et al.* combined a VPGIG repeated sequence with the REDV peptide found in the CS5 region of fibronectin that promotes endothelial cell attachment and spreading, but not smooth muscle cells or platelets (56). In their work, they showed a successful attachment of cells on surfaces coated with the ELR, compared to the control surfaces. Similarly, Girotti *et al.* fused the REDV sequence to an ELR including lysine-containing blocks that could be cross-linked to form artificial matrices, as demonstrated (57).

Regarding other cell-adhesion sequences, Urry and co-workers used the RGD tripeptide (58) for the first time to successfully enhance cell attachment on ELR-based matrices cross-linked by γ-irradiation (59). However, this first case of RGD modification was performed with chemically synthetized polypeptides. On the other hand, the first example found in the literature of a recombinantly produced ELR including RGD sequences was reported by Liu *et al.* who compared the cell response between RGD and REDV sequences (60). In their study, they found that RGD promoted a faster attachment while being stronger than in the case of REDV. Most probably because of that finding, many other groups have included RGD domains within ELR molecules since then to improve cell adhesion.

In addition to these works regarding cell-adhesion sequences, other motifs have been fused to ELRs to undergo dimerization, therefore modifying the structural properties of

their supramolecular assembling. This is described in the work by Fernández-Colino *et al*., where they showed the fusion of a leucine zipper domain, containing a cysteine residue, to an ELbcR (61). This domain was shown to be able to form dimers stabilized by a disulfide bond, hence allowing the cross-linking of hydrogels based on this zipper-containing ELbcR in a reversible manner, depending on the redox conditions of the system. On the other hand, Zhang *et al.* designed and bioproduced ELRs including either a SpyTag short polypeptide or a SpyCatcher protein (62). This protein is able to recognize the SpyTag polypeptide undergoing an autocatalytic bond formation between them. The combination of ELRs comprising these Spy sequences resulted in different supramolecular structures that were further characterized.

As can be deduced from the above paragraphs, many different sequences can be recombinantly introduced within the backbone of the ELRs depending on the physical, chemical and biological requirements of the final protein and the subsequent application.

2.3.4. Fusion of full-length proteins

In order to anticipate the properties of ELRs when fused to different proteins, Chilkoti and co-workers studied the effect of the arrangement of four proteins in the final fusion product, i.e. C-terminus or N-terminus, on the expression levels and yields of purified protein (63). By their results, they could conclude that the yield was higher when the proteins were placed at the C-terminus, and that the specific activity of the fused proteins was higher in that case for three out of four proteins. However, as they comment themselves in the manuscript, these results are applicable only to an ELR with a specific sequence, and to four particular proteins. Additionally, the same group was able to develop a model to predict the effect of hydrophilic proteins on the thermal behavior of ELR fusion proteins, showing that the presence of charged residues is the most important parameter affecting the T_t of the ELR when compared to the ELR itself (64).

Many other proteins have been fused to ELRs to date. Some of them used ELRs as tags, taking advantage of their facile purification by ITC (31) to produce recombinant proteins (65) that are finally excised from the ELRs by different methods, namely intein self-cleavage (66), protease-mediated cleavage (67), or by including the self-processing module from *Neisseria meningitides* FrpC (68). There are many examples in which this

approach has been employed in the expression of recombinant proteins in *Nicotiana tabacum* plants (69), like an anti-human TNF antibody (70), and in tobacco cell suspensions to produce human IL-10 (71). Furthermore, this strategy has been also shown to be successful to produce antimicrobial peptides in *E. coli* efficiently (72,73).

3. STRUCTURES AND PHYSICAL CHARACTERISTICS OF ELASTIN-LIKE RECOMBINAMERs

Materials based on ELRs underlie a high potential, characterized by the extraordinary biocompatibility, tunable mechanical properties and the variety of structures that can be generated (i.e. micelles, nanoparticles, hydrogels, films, and nanofibers). Besides the introduction of bioactive sequences into the ELR-based structures, ELRs can be designed to self-assemble into either micelles, physical hydrogels, nanoparticles, or solvent casted films (Figure 3). Furthermore, reactive cues can be introduced in the sequence to allow chemical modification.

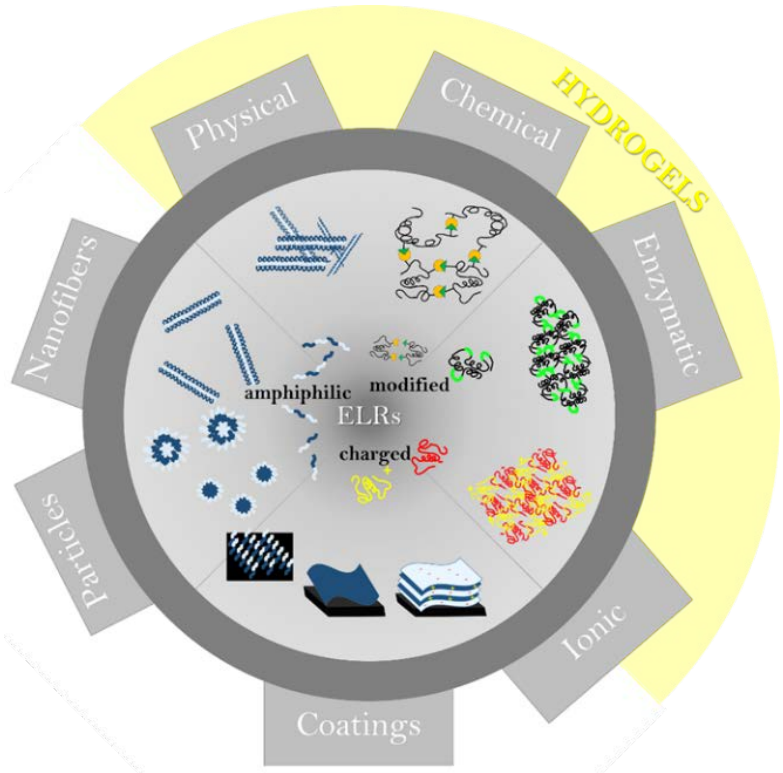

Figure 3. The diversity of ELR structures and their sequential origin.

3.1. Micelles and nanoparticles

The first self-assembling ELRs were achieved with polymers containing blocks of different polarity, inspired by block-copolymers and their related properties, like phase separation, micelle formation, etc. The difference between block-copolymers and amphiphilic ELRs, is that in amphiphilic ELRs the blocks of different polarity retain the ELR pentapeptide sequence (VPGXG), and the changes in polarity are introduced through the X amino acid. The influence of the X amino acid, has been methodically described by Urry (74). As well as block-copolymers, elastin-like block co-recombinamers (ELbcRs) showed the ability to form micelles in solution. The hydrophobic block tends to be embedded in the core, hidden from the water solution, while the hydrophilic block(s) forms the corona exposed to the outer part of the structure. It has been shown that the formation of stable nanoparticles requires a relatively high molecular weight of at least 48 pentapeptides. Furthermore, the particle size and the molecular weight of the ELR are directly related (75). The ITT of the ELRs, depending on the characteristics of the micelles, can either lead to coalescence of micelles into lyotropic gels (76), through polydisperse microparticles (77), or to a simple swelling and deswelling of the micelles, accompanied by size changes. Typical sizes of ELR nanoparticles reported are usually in the range of 10 to 100 nm (78-83), but due to the temperature sensitivity and related agglomeration, also micro sized particles have been reported (77, 84). The ability to trigger the formation of nanoparticles by the swelling and shrinking kinetics, intensified the research on the tuning of the micelle sizes and the T_t related changes. Several methods have been explored to either stabilize ELR-based micelles. For instance, the concentration of the ELR solution, which has been found to have a clear effect in the particle size (76); another method is the addition of surfactants that can stabilize or destabilize the ELR particles (85); salt concentration is crucial, higher compensation of the charges of the hydrophilic blocks through counter ions can lead to stronger agglomeration of particles (80, 81, 83); and last but not least, the pH affects the stability and size, depending on the chemical properties of the guest amino acid in the fourth position of the basic pentamer (VPGXG) of the hydrophilic block. In the case of cationic amino acids the charge is reduced at high pH, on the other hand, anionic amino acids show the same behavior at low pH (80). Moreover, more specific sensors for changes in salt concentrations have been designed. For instance, the introduction of a

calcium selective sequence amplified the influence of calcium concentration, by reducing the transition temperature of the corresponding ELR from 70°C to 35°C (86). Even when the general shape of homogenous micelles is round, it can be tuned to more anisotropic cylindrical shapes by varying the architecture of the ELRs introducing amphiphilic blocks of different sizes in the protein sequence (87). In principle, each ELR has one clear transition temperature, but in the case of amphiphilic ELRs with different blocks, long enough to develop an own intrinsic transition, the effect of temperature on the particles shows two temperature-induced changes. First, the rearrangement of the hydrophobic core, driven by a change in the secondary structure from random coil and β-sheets to type-II β-turns. This change as well corresponds with the exhibition of a cylindrical shape of the particles. This effect is also known as critical micelle temperature (CMT). The second and more prominent change is due to the collapse of the hydrophilic part, which is responsible for the coalescence, agglomeration and precipitation of the micelles (75). Other reported rearrangements describe the change from micelles to vesicles by reorganizations of the hydrophobic blocks. Here, vesicles could be obtained either by an increase of the length of the hydrophilic block, or by addition of another hydrophilic block to a triblock copolymer of the structure hydrophilic-hydrophobic-hydrophilic (48).

3.2. ELR-coatings and films

The generation of ELR coatings has a great interest for the creation of either antimicrobial, anti-fibrotic coatings, or for the deposition of a bioinductive layer that allows cellular interaction driving to a good implant integration within the surrounding tissues. In theory, there are two ways to accomplish a coating: physisorption by intermolecular interactions (hydrophobic and/or electrostatic interactions), or a grafting approach by covalent binding (Figure 3). For completion, a third possibility could be possible, which is the creation of elastin-like brushes by a grafting approach, but due to the relatively high molecular weight of ELRs, and the related cost to generate such proteins in a synthetic way, this approach is still a hypothetical option. Additionally, these proteins would not be ELRs since they are not obtained by recombinant techniques so they should be classified as ELPs (8, 19, 88, 89).

Physisorption of ELRs has been deeply studied and applied in different works. It was described by Srokowski *et al.* that longer ELRs formed more stable coatings by physisorption than ELRs with lower MWs (90). Another approach targets on the endothelialization of CoCr alloys, that could be enhanced by physically adsorbed or covalently bond ELRs that bear a REDV sequence (91). ELR coatings also proved to reduce platelet activation and smoothening of surface topographies when coated PTFE substrates by a layer-by-layer approach (92). This was corroborated by other studies that showed that longer ELR sequences not only have a better deposition, but also decrease platelet activation more than short ELRs (90). In an earlier study, the patency time of non-thrombogenic ELR coatings could be more than doubled (93), and thrombus formation reduced (94).

Further micelle solutions have been used to adsorb ELRs to surfaces under retention of their nano- and microtopography. For the generation of surfaces that induce bone mineralization nanotopographies, it was performed a coating with an ELR containing a human salivary statherin sequence (95). The coating of previously generated orientated electrospun fibers with ELRs led to a conserved orientation in the scaffold, which guided human vocal fold fibroblasts (96). The transition temperature of the ELRs was also used to enhance the physisorption by thermally induced deposition. Here, surfaces with a low RGD concentration were formed, high enough to allow cell adhesion, but too little to form a cellular monolayer. Thus cells were forced to cluster and semi-functional pseudoislets could be formed (97). The good mechanical performance of SELR hybrids further led to the development of coatings for osteochondral applications (98). Besides the deposition of ELRs in order to induce or avoid attachment of cells or proteins, the ability of the ELRs themselves to influence the microenvironment by temperature changes is of great interest, for example for biosensors, or drug delivery systems. By changing the temperature, features like the wettening of the surface (77), the release kinetics of drugs embedded in the coating (84), or the accessibility of active groups inside the ELR sequence in swelling and deswelling ELR/RGD brushes (99), can be controlled.

3.3. ELR-based hydrogels

In tissue engineering, hydrogels have been the predominant matrices for application in the human body in the last 40 years (100). A high water content leads to convenient mechanical properties and stimuli-responsiveness, which in many cases chimes with the properties of natural tissues (101,102). ELRs, inspired in a natural protein such as elastin, are excellent candidates for many researchers focused on the generation of artificial matrices that can be used as scaffolds for biomedical applications. The ECM is a very complex system in which the physical properties (elasticity, stiffness), the nano-topography, the presence of signaling molecules, protease-sensitive sites and adhesion domains are of great importance, and gathering as many of these properties as possible is a major requirement that have to be demanded to any material that might be used in tissue engineering. The generation of hydrogels from linear ELRs requires paying special attention to the mechanism that will drive the cross-linking of different ELRs molecules. These cross-linking methods can be either of covalent or physical nature and the position of cross-linking points along the ELR backbone can be fully controlled through genetic engineering to get a precise tuning of the mechanical properties. Polypeptide-based block-copolypeptides, for example, manage to self-assemble into stable hydrogels (103), which can be further stabilized when flanked by protein segments with coiled-coil secondary structure (104, 105). Another approach is the use of recombinant segments of elastin, silk and collagen (106-108). In contrast to general methods for the formation of hydrogels by radically or photo-polymerized acrylate cross-links, ELR hydrogels can be thoroughly controlled (e.g. chain and segment length, number of cross-links per chain). This leads to more homogeneous matrices, and to the reduction of artifacts, which could impair the mechanical properties of the resulting hydrogels (109).

Cross-linking mechanisms for ELRs can be as versatile as ELRs themselves: ionic or hydrophobic interactions, reaction of complementary groups, or enzymatically induced cross-links (Figure 4) (110, 111). All these strategies can provide a very tight control over the length and the molecular weight of the proteins by the selection of the cross-linking sites, which usually correspond to lysine groups (112, 113). Besides the control of the cross-linking, aforementioned bioactivities can be introduced into ELRs, so that the matrix is able to interact with the organism, improving the good integration of the generated

tissue. The basic ELR sequence (VPGXG) is biocompatible, but lacks cellular adhesion sites. Nevertheless, the possibility of a tailored genetic design permits changes in the transition temperature, integration of protease-sensitive sites (114, 115), cellular adhesion motifs (59, 116), or biological triggers (117-119).

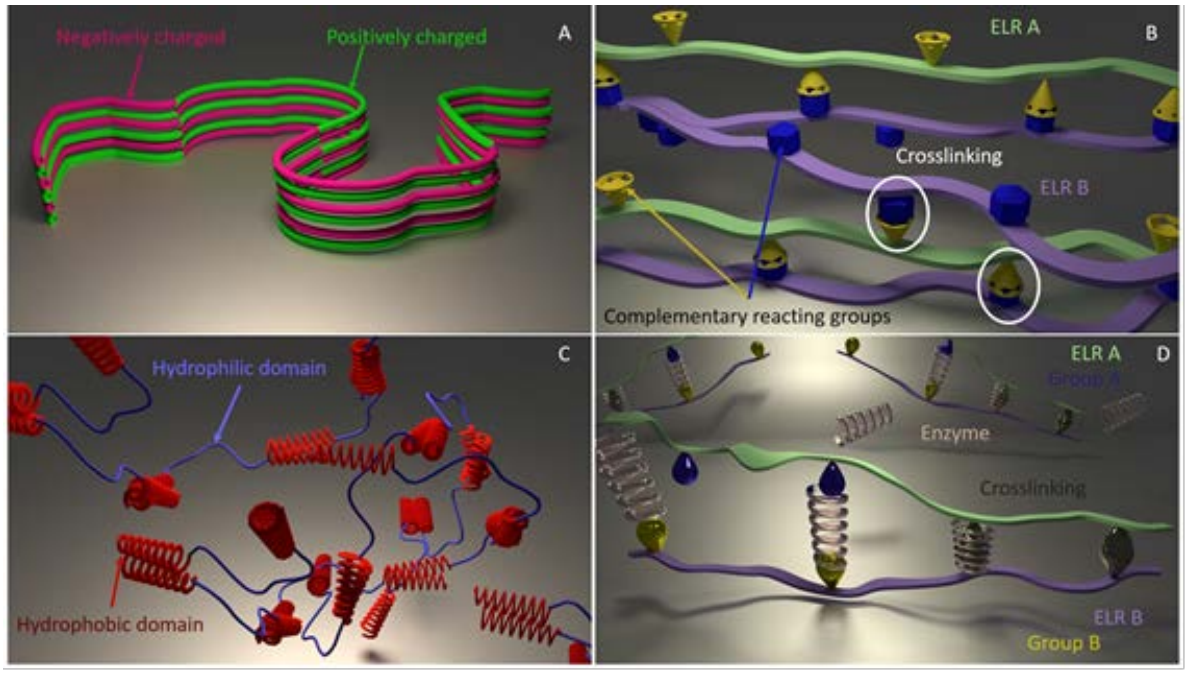

Figure 4. Common ELR crosslinking strategies: A) ionic interaction, B) chemical crosslinking, C) hydrophobic interactions, D) enzyme triggered crosslinking.

Physical cross-linking of ELRs can be obtained by several strategies. One approach is a cross-linking based on ionic interactions by segments of opposite charge (e.g. cationic and anionic amino acids in the X position of the ELR). Even though ionic interactions are relatively weak, a specific design of complementary charged strands (120, 121) helps to a better strengthening of these interactions which leads to obtain stable ELR hydrogels at room temperature and physiological pH (122). Potentially, the presence of ions could trigger the formation of hydrogels, since some ELRs are sensible to salts concentration changes, especially to chelating ions like calcium (121). More advanced approaches including ELR/chitosan blends, could be stabilized by sodium ions (123), and modification with monosaccharide side chains allowed a complexation with potassium (124). A second way of physical cross-linking is obtained by the introduction of self-assembling motifs, i.e. amphiphilic blocks, or interaction of protein secondary structures (β-sheets, leucine zippers). The self-organization is basically driven by aggregation of different segments. In

the case of amphiphilic block ELRs this self-assembling is due to the aggregation process of the hydrophobic segments. On the other hand, the interaction of secondary structures is triggered by the aggregation of β-sheets or pairing of leucine zippers.

Hydrophobic blocks are generated when the ELR sequence has several hydrophobic amino acids (like alanine (Ala), leucine (Leu), isoleucine (Ile), valine (Val), phenylalanine (Phe), tryptophan (Trp), tyrosine (Tyr) or methionine (Met)) on the X position. This results in segments of distinct polarity within the same protein chain and leads to mutual repulsion between the different blocks, that tend to segregate. The segregation is locally constrained by the "forced cohabitation" of the blocks within the same ELR chain, resulting in a separation into different domains, which as a consequence, self-assemble into periodic nanostructures (125). Amphiphilic blocks can be designed to form stable hydrogels that even persist *in vivo.* One way to enhance stability is to create longer sequences with several blocks of alternating polarity (108, 126, 127).

The interaction of intermolecular secondary structures, on the other hand, follows the key-lock-principle with the assembly of matching structures of similar polarity. From the tailor perspective, almost any protein secondary structure that is able to form a stable link with itself or contrary groups could be implemented. It has to be considered that in one component systems gelation can occur easily, and solvation is limited. Furthermore, the effect on the ELRs T_t has to be considered.

The recent approaches to include physical cross-linking cues into ELRs are inspired by natural silk sequences that enable crystalline-like β-sheets formation with unique mechanical properties (128-132). The repetitive sequence responsible for the β-sheet formation and for the intrinsic strength is the GAGAGS hexapeptide (*Bombyx mori* silkworm) (133). In this silkworm, the blocks are stabilized by hydrophilic compartments within the protein and a complex mixture of stabilizing agents (134). The integration into ELRs needs to consider the stability of the resulting bonds and the amount of silk domains govern the manipulation of the material. Silk-ELR (SELR) hybrid materials reveal a two-step gelation process when heated above the T_t. The ELR transition occurs first, enabling the thermodynamically driven annealing of silk sequences, hence forming stable physically cross-linked hydrogels *in situ* (108). SELRs are biocompatible and performed well in *in vivo* studies (135-137). Moreover, they have been forged into a variety of

structures like hydrogels, films, 3D porous matrices and submicron to macroscale fibers (138).

Lately, ELRs physically cross-linked by leucine zipper domains (139-145) gained interest. The leucine zippers are capable to dimerize with other leucine zipper domains driven by hydrophobic interactions (139,146-148), and ionic interactions (149-151). On account of its novelty, ELRs with leucine zipper motifs have been less explored than SELRs, and the complete potential remains to be discovered. Nevertheless, the human origin of the domain and the conserved nature of the structure alleviate concerns regarding the biocompatibility. First studies on ELR-Zippers support the biocompatibility and showed enhanced stability when compared to pure amphiphilic block ELRs (61). Furthermore, a recent *in vivo* study regarding zipper-based scaffolds revealed no foreign body reaction (152).

The introduction of amino acids bearing functional groups in the X position can be used for subsequent reactions without losing the pH and temperature sensitivity of the ELRs. The majority of published works used the free ε-amine of lysine residues within the ELR chain for chemical modification due to its reactivity. (153, 154) Regarding the cross-linking process, the MW, concentration and the number of cross-links are important to form stable hydrogels (155). ELRs with high molecular weight have a higher entanglement and are more prone to establish a sufficient number of cross-links to stabilize the hydrogel network. Due to the tailored design of the ELR sequence, the number of cross-linking sites and the segment length between cross-links can be precisely controlled, enabling the tuning of relevant features such as pore size, gelation time, stiffness and degradability. Functionalization of ELRs aims to introduce bioactive sequences, adhesion sites, inhibitors, antibodies or anchor and signaling molecules (156). Degradation can be further controlled through the introduction of protease-sensitive sequences, or through the introduction of labile chemical linkages (157).

One drawback of common chemical linkages is that they are reactive under conditions that require organic solvents or other chemical reagents to avoid hydrolysis. To elude removal of this undesired components, the typical cross-linking of hydrogels is based on the reaction of complementary groups (158), enzymatic cross-linking (159-161), condensation reactions (162), or high-energy irradiation (163). The classical cross-linking

reactions of ELRs are solvent dependent, in organic solvents, due to the absence of a lower critical solution temperature (LCST). The obtained hydrogels are very homogenous, whereas in water the diffusion of active sites is limited above the LCST (112). The fusion of several ELR strands by cross-linking results in stable hydrogels, which remain stable when cooled below the ELRs T_t. Using enzymatic cross-links, hybrid protein hydrogels of ELR and other functional proteins can be obtained. Mild covalent cross-linking strategies without organic solvents and cytotoxic reactants have some important advantages, such as that the gelation can be performed in the implantation site, without further purification *in situ*, without the diffusion out of the injection site. Ravi *et al.* showed that an ELR/fibronectin gel cross-linked by genipin performed well *in vitro.* (164) Moreover, the Huisgen reaction has been introduced in the past years to form ELR networks in water (165, 166). The reaction of complementary groups can be used further to fuse ELRs of different bioactivity together (167), and to generate hybrid materials. This method has been used for the creation of non-thrombogenic stents (165).

4. ELASTIN-LIKE RECOMBINAMERS: APPLICATIONS

4.1. ELRs for gene delivery applications

Gene therapy provides a unique approach to deliver a therapeutic gene into specific human tissues or cells; the modification of patient's altered gene expression can be performed by gene addition, gene correction, gene knockdown or their combination (168, 169). The concept of gene therapy is based on nucleic acids being used as pharmaceutical products to obtain *in vivo* production or silencing of therapeutic proteins (170, 171); the therapeutic material can be integrated into the host chromosome or remained as an episomal plasmid with transient expression (168, 172). The successful expression of the deficient gene product at physiological levels (168, 173) is based on an appropriate delivery system (174). The most important properties that a delivery vector must have are the biocompatibility and the ability to release the cargo into a specific target.

Gene delivery systems can be divided into two categories: viral and non-viral vectors. Despite approximately 65% of clinical trials use a viral vector for DNA delivery (175), non-viral vectors have been widely studied over the past few years and constitute the most promising alternative for overcoming the immunogenicity problems inherent to viral

vectors; moreover, they are easier to produce on a large scale (176, 177). Cationic polymers can form a complex with DNA by electrostatic interactions with the negatively charged phosphates from nucleic acids. The formed polyplex is able to protect the genetic material from degradation by nucleases (178). PEI (polyethylenimine), PEG (polyethyleneglycol), PLL (poly-L-lysine), chitosan, PLGA (polylactic-coglycolic acid), and PDMAEMA (polydimethylaminoethyl methacrylate) are some of the most widely used non-viral gene delivery vehicles (169, 179-181). The cytocompatible nature of the biomaterial forming the polyplexes and their ability to be internalized into the cell determine the success of the system (177, 179, 182-184). Nevertheless, most of the cationic polymers mentioned above are not ideal for drug delivery application. For instance, the main problem of PEI is its cytotoxicity, causing cell apoptosis in a wide number of human cell lines (185). Regarding PEG, not only hypersensitivity reactions occur when it is injected intravenously, but also cutaneous application can cause allergic reactions, such as contact dermatitis (186).

Thus, it is required a new design of gene delivery vectors able to address the individual rate-limiting steps along the gene delivery process (187). ELRs have grown in popularity in the field of protein-inspired biomimetic materials, and they are becoming increasingly important in different fields of biomedicine (165, 188-190). ELRs are non-immunogenic, and according to with their biodegradability and biocompatibility for human tissue, blood, and other fluids, they can play a key role as carriers in delivery systems (189, 191, 192). ELRs have been previously used as oligo-lysine carriers by Furgerson's group to deliver an EGFP−plasmid inside cells in *in vitro* assays (193). The use of specifically designed ELRs joined to functional peptides as agents shows promising results for delivering genes *in vitro* (190). Moreover, cellular transfection can be improved through the formation of charged polyplexes and their further interaction with the negatively charged components on the cell membrane, such as proteoglycans and cell-surface receptors (194, 195). In this study, taking advantage of the recombinant DNA technology to design and produce ELRs, functional motifs were incorporated into a basic ELR sequence. Then, imidazole groups were covalently bound, obtaining stable polyplexes composed of plasmid DNA and ELRs (190). Several studies have demonstrated the use of ELRs fused to a cell penetrating peptide (CPP) as a drug delivery vector for solid tumors (182, 196, 197). In this sense, a

similar combination of ELRs fused to CPPs was utilized to deliver therapeutic peptides into target tumor cells (198). Finally, Piña *et al.*, specifically designed a lysine-enriched ELR in order to complex and protect the therapeutic DNA, forming stable polyplexes. In this work, for the first time, cancer-specific aptamers were incorporated into ELR polyplexes with potential application in the treatment of breast cancer (199).

4.2. ELRs as vaccine delivery systems

In the past recent years, due to the increasing knowledge about the mechanisms of protective immune responses, and about new biotechnology techniques, newer vaccine designs have been considered. For instance, a novel approach based on genetic engineering in order to obtain non-pathogenic vaccine strains, naked plasmid DNA vaccines, or for the preparation of relevant recombinant proteins that may lead to adequate immunity (199). Certainly, the ability to isolate and produce pure proteins and peptide antigens that are safer than traditional vaccines has enhanced the vaccine efficacy (201-203). However, a limiting factor with antigens made by recombinant DNA technology is that they are often weakly immunogenic on their own, thus it is often required the inclusion of immune adjuvants to enhance the resultant immune responses (204, 205). Adjuvants have the ability to activate antigen-presenting cells (APCs), and despite their clear relevance and essential role, only adjuvants that induce minimal adverse effects are acceptable for standard prophylactic immunization in healthy individuals.

Certainly, the relative lack of antigenic carriers approved for the usage in humans suggests that better materials and new strategies are needed to generate successful nanovaccines. As it has been already described, biomaterials play a key role in the therapeutic field regarding vaccine development. The engineering of materials that can modulate the immune system, known as immunobioengineering, is playing an increasingly important part for the development of new particulate vaccines and adjuvants carrying the desired epitopes for immunization (201, 206, 207). Therefore, because of one of the most powerful strategies to form very small particles is based on self-assembled di-block co-polymers, many different materials displaying stimuli-responsiveness with different molecular architectures have been investigated (207).

Several factors such as particle size, surface properties, particle shape, and hydrophobicity (201, 208, 209), affect the nature of the immune response caused by biomaterial-based nano-objects. It has been shown that the particles themselves are intrinsically recognized as a sign of danger (210), and considering that the particle size is the primary control parameter, a particulate vaccine can target several pathways depending on its size. Biomaterial particles can include specific functional domains such as targeting ligands that are able to bind specific receptors for endocytosis, promoting an increase of specific cellular uptake (204, 211). In addition, another important parameter is the hydrophilicity in the nanoformulation, that can modulate the amount of proteins adsorbed onto the surface of nanoparticles after the administration, increasing their residence time in circulating blood (212).

ELRs play a key role in several biomedical applications due to the ability to control and manipulate the interface between them and the biological components. In this sense, the American Society for Testing and Materials (ASTM) has demonstrated their extraordinary biocompatibility, while the feasibility of tuning and controlling the shape and topology of ELRs has been previously explored (213, 214). In addition, elastin-like block co-recombinamers (ELbcRs) are able to form multimeric nanoparticles by self-assembling, and considering the ability to control their hydrophobicity, molecular weight and block rearrangement, ELRs are exceptional candidates as carriers in vaccine-delivery approaches (191, 215). The recombinant production of ELRs allows obtaining a highly monodisperse, multivalent and biocompatible properties of the resulting constructions by a simple, affordable, reproducible and easy to scale up the process of bioproduction (216, 217). Furthermore, ELbcRs can be subjected to secondary processes such as sterilization, drying, packaging, and reconstitution of the resulting dried powder (126, 218).

Another advantage of the ELRs about the vaccine formulation regards the possibility to develop a single-gene product that self-assembles into a nanoparticle with the desired antigenic sequence. Therefore, thanks to the fusion strategy to produce ELR-based constructions, it is not required the use of bioconjugate chemistry to fuse other proteins to the nanoparticles. It has been already described the potential use of this strategy for

many biomedical applications such as protein purification (219) or as drug and gene delivery systems (216).

Previous works (48, 51, 216) describe the nanoparticle structure of an ELbcR obtained by recombinant process, having the antigenic sequence(s) at the hydrophilic terminus gene(s); the genetically encoded synthesis does not affect the assembly of the nanoparticles, in fact, the elastin contribution serves as hidden support, whereas the antigen molecule(s) is oriented towards the outside of the particle. García-Areválo *et al.,* developed a new ELbcR-based vaccine carrier that self-assembles into highly monodisperse and stable nanovesicles that can be used to present low antigenic peptides, for example, from the bacterium *M. tuberculosis* (189). In another work, it was described the expression and immunogenicity of a construct produced by combining plant-based production and the ELR fusion strategy in order to produce a potential vaccine candidate containing two major antigens from *M. tuberculosis* (220).

4.3. ELR-based hydrogels for tissue engineering applications

Widely defined, tissue engineering is the process of restoring, maintaining, or enhancing living, physiological, three-dimensional tissues and organs utilizing specific combinations of cells, scaffolds, and/or signals, both chemical and physical. The process involves mainly four components: a material scaffold, functional cells, biomolecules (e.g. growth factors, extracellular matrix (ECM) molecules, and other biological), and dynamic forces (221). Thanks to the recombinant DNA technology, ELRs allow the tailoring at the genetic level of the mechanical and biological properties to satisfy end-user application, thus offering numerous choices for the development of cell culture matrices for a specific tissue (222). Several studies have shown how different types of ELRs can be addressed over the most challenging fields in tissue regeneration, such as cardiovascular, ocular prosthesis and osteochondral applications, among others.

Biofunctional materials require advanced design and preparation with the purpose of matching the sophisticated recognition ability of biological systems. The biocompatibility of any biomaterial has a critical importance and must be assessed prior to any clinical trial.

As regards the purity of the biomaterial, any contamination with (globular) proteins entails one of the greater risks, namely the development of immunological responses that preclude their application in regenerative medicine and tissue engineering. Thus, the biomaterial is required to pass the toxicological test that takes into account the duration and the type of tissue in contact with the tested one.

As it has previously mentioned, ELRs have been used for the development of novel protein peptide biomaterials obtained through recombinant DNA technology that are playing an increasingly important role in a diverse range of applications such as drug delivery, tissue engineering, biosensors and a wide variety of 'smart' systems. Sallach *et al.* have described the production of a recombinant elastin-mimetic triblock copolymer and the further application *in vivo* for more than 1 year. During this time, the ELR-based hydrogel showed a minimal inflammatory response, confirming its high and extraordinary biocompatibility (127).

Considering the ability of the ELRs to self-assemble into different structures such as hydrogels, and taking into account that ELRs completely fulfill the prerequisites of biocompatibility and bioactivity, ELRs play a key role for the development of scaffolds and advanced systems for application in the fields of regenerative medicine and tissue engineering. In this sense, specific requirements of ELRs, such as topographic, chemical configuration and viscoelastic patterns, determine the hydrogel properties. Hence, they can be tuned specifically to match proteins at the nanometer scale and cells at the micrometer scale. In the light of this, numerous reports have largely demonstrated requests from in vitro experiments (192, 223, 224).

In vascular tissue, elastin is an essential extracellular matrix protein that plays an important biomechanical and biological signaling role. Elastin-like recombinamers are able to mimic the structure and function of native elastin, representing a practical alternative to the native elastic fiber (which is difficult to extract from tissues) for vascular applications. Several studies have demonstrated that stent surface endothelialization is a well-known methodology to inhibit restenosis and thrombosis (91, 225-227). The use of active ELR coatings with endothelial cell adhesion sequences onto stents surfaces is a great strategy to recover a healthy endothelium. *In vivo* studies have demonstrated how ELR scaffolds support the neovascularization in the total absence of an immune response

(91). In this sense, González de Torre *et al.* have shown the applicability of recently developed ELRs as a coating for vascular stents with the ultimate goal of producing a new endovascular device (165). The ELR applied on the stent gain a full endothelialization in a short time (2 weeks), showing high biocompatibility and a reduced response of the immune system. Finally, another approach by Weber *et al.* was to generate tissue-engineered heart valves (TEHVs) by multi-step injection molding using ELR as a hybrid system with fibrin (228).

In 2015, Mata's group demonstrated the supramolecular interaction between peptides and ELRs to generate complex 3D architectures through a dynamic self-assembly system, forming a stable multilayer membrane. This membrane can be spatiotemporally controlled and can be used to form bioactive tubular scaffolds which may support and lead the growth of different cell lines (229). This tubular morphogenesis could play an important role in tissue engineering applications that requires the formation of tubular structures that usually are complex to obtain in the milli- and micro scale.

According to the elastin-like nature of the hydrogel and the high percentage of elastin present in the native chondral matrix, ELR-based hydrogels are likely to simulate the properties of hyaline cartilage (230, 231). The hyaline articular cartilage is a highly specialized tissue characterized by its unique mechanical features and it is formed by a matrix that embeds chondrocytes. Considering that the articular hyaline cartilage does not repair itself and that the generally regenerated fibrocartilage is unable to maintain the biomechanical characteristics of articular cartilage (232, 233), ELR hydrogels could be used as scaffolds for osteochondral tissue engineering. As it has been previously described above, ELRs show thermo-sensitivity, on that regard is possible to form hydrogels stable at body temperature, whenever the transition temperature (T_t) of the ELR is lower than the body temperature. Moreover, ELRs containing bioactive sequences, such as the well-known RGD cell-adhesion sequence found in fibronectin, which promotes specific cell attachment via integrins (162), are able to form a bioactive scaffold that improves the regenerative potential of the implanted hydrogel.

Vila *et al.* showed how ELR coatings are able to improve the well-known biocompatible and bone regeneration properties of calcium phosphate-based materials (234).

Due to the development of novel tissue-engineering methods (52, 235), it has been considered the use of mesenchymal stromal cell (MSC) therapy (236, 237) for the treatment of musculoskeletal lesions (238, 239). For articular defect applications, the use of a hydrogel serves as a vehicle for the MSCs to acquire a 3D structure that could mimic the properties of the ECM providing a cell-friendly environment in order to increase the persistence of the implanted cells at the site of injury. According to ELRs properties, a homogeneous embedding of MSCs in the ELR solution can be achieved at a temperature below T_t, and further applied as a cell-scaffold system for injectable therapies (Figure 5).

Figure 5. ELR-based injectable hydrogel for osteochondral applications.

Moreover, ELRs might also have beneficial applications in the field of ocular tissue engineering. Cornea wound healing requires cell adhesion and proliferation on a substrate with ligands such as fibronectin, secreted by corneal epithelial cells and stromal fibroblasts during the first steps of corneal wound healing (240). Nevertheless, the ocular surface, unwounded cornea and conjunctiva do not express elastin. Therefore, several metalloproteinases (MMPs) have been described in pathological ocular processes such as dry eye (241) or conjunctivochalasis (242), while some other MMP present at the ocular surface are able to degrade elastin fibers (241). Thus, ELRs are a potential candidate for Bruch´s membrane prosthesis. Martínez-Osorio *et al.* showed how a blend of ELRs was able to promote epithelial cell adhesion from human conjunctiva-derived primary cells (192). Finally, ELRs application as ocular implants was studied by Srivastasa *et al.,* which confirmed ELRs as a suitable carrier for the transplantation of autologous RPE cells for the treatment of age-related macular degeneration (AMD) (243).

4.4. ELRs for surface bio-functionalization

The ELRs properties of elasticity and self-assembling allow the formation of a wide range of biomaterial-based constructs such as aggregates (51), films (77), fibers (224), micelles (48, 244), nanoparticles (245), and hydrogels (246). Another advantage of this recombinant biomaterial is the capacity to form hybrid systems with materials having different origins, in order to obtain several morphologies and functional possibilities for a diverse range of applications such as functionalized surfaces, fibers, and drug delivery. Therefore, the recombinant technologies by which ELRs are obtained, allow a perfect control of their sequence, length and stereochemistry; moreover, for functionalized surfaces even a nanometric control of their position displayed by these systems is possible.

Chilkoti's group has created what they refer to as the "Thermodynamically Reversible Addressing of Proteins" (TRAP) (247), where an ELR is covalently micropatterned onto a glass surface obtaining a spatial-temporal system for protein binding that can be applied as a microsensor for detecting single biomolecules in bioanalytical applications. Additionally, different approaches based on controllable properties (stimuli-responsive) of the biofunctionalized surfaces have been studied in order to obtain a cell sheet harvesting system from a culture dish. In this sense Okano *et al.,* have developed a smart surface with PIPAAm polymer (and its derivates) that can switch between a cell-adherent and non-adherent state as a result of a change in temperature (248). Despite this approach led a significant progress in this field (249-251), PIPAAm polymer lacks specific bioactivity, meaning that cellular membrane proteins, such as integrins, are not able to directly bind to the surface. To address this issue, Pierna *et al.* developed a smart surface system by covalent coupling of tailored ELRs onto glass surfaces by click chemistry methods. This cell sheet harvesting system leads to the exposition of the bioactive RGD motif to the water interface at physiological temperature, producing a cell adherent surface (252) (Figure 6). Na *et al.* also took advantage of the rapid response to external stimuli of a smart material surface created by adsorption of ELRs for use in cell-based biochips. The smart transition of ELR-based micropatterns between a hydrophilic and a hydrophobic surface glass at T_t allows to revert cell adhesion by way of the incubation temperature (253).

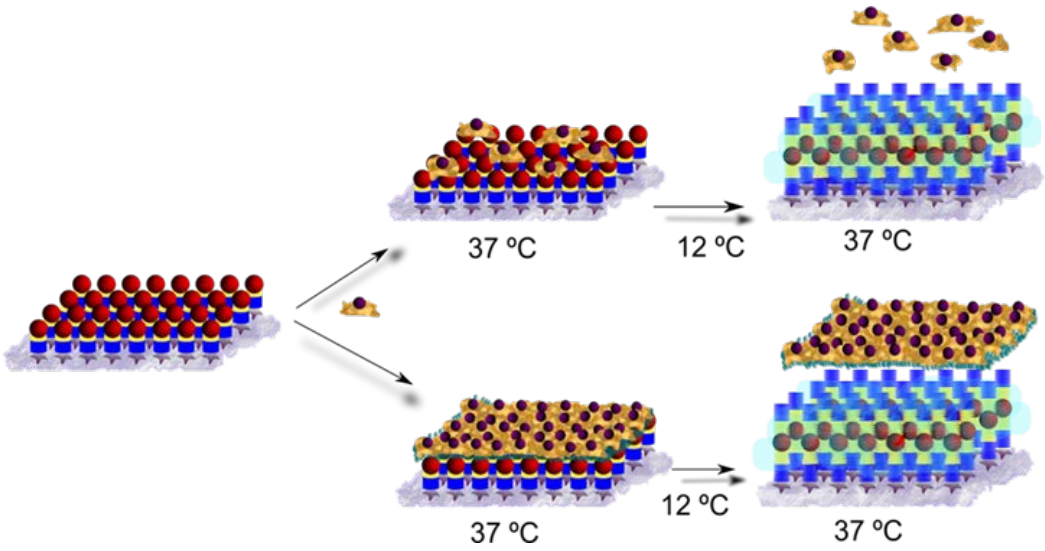

Figure 6. Schematic representation of a system based on ELRs for cell sheet harvesting.

Layer-by-layer (LbL) techniques are one of the most versatile and easy-to-apply of the numerous surface-modification tools. They are based on the spontaneous adsorption of materials onto a substrate, generally a polymer, biomolecule, or inorganic particle, and allow the sequential formation of a nanostructured film, hence having a great interest in tissue-engineering applications (254-257). Layer-by-layer deposition of alternating ELR-polyelectrolytes generated bioactive surfaces (258). In this work, it was developed a thermoresponsive thin coating by electrostatic self-assembly (ESA); the deposition of an ELR containing the bioactive RGD motif can be exploited for tunable cell adhesion and controlled protein adsorption by nanoscale surface tailoring (77). Another example of biomimetic surface-modification regards the chemical functionalization of ELRs in order to obtain metallic (Commercial pure titanium, Cp Ti) dental implants with osteostimulative capabilities by the covalent immobilization of biomolecules on the Cp Ti (259). Finally, Costa *et al.* demonstrated the feasibility of LbL synthesis using natural marine-based polysaccharides (chitosan and alginate) and ELRs (260) for possible application in wound dressings and drug-delivery systems (261, 262). Furthermore, ELR molecules can be used for the functionalization of surfaces in order to obtain stronger and faster cell responses on the tissue–biomaterial interface, thus promoting better implant integration than short peptides functionalization; for instance, ELRs have been used to enhance the properties of poly-methylmethacrylate (PMMA) surfaces. Although PMMA has a great usage in several biomedical applications (263-269), this study showed that

ELR-functionalized PMMA surfaces can enhance the cellular attachment efficiency and the cell anchorage strength (270). Finally, ELRs were thoroughly investigated as biocompatible vasculogenic surface coatings and smooth muscle cells (SMC) showed enhanced attachment under retention of their contractile phenotype on similar ELR-coated electrospun fibers (271).

Abbreviations

A	Alanine
Ala	Alanine
AMD	Age-related macular degeneration
APCs	Antigen-presenting cells
ASTM	American Society for Analysis of Materials
C	Cysteine
CMT	critical micelle temperature
CPPs	Cell penetrating peptides
D	Aspartic Acid
DNA	Deoxyribonucleic acid
E	Glutamic Acid
E. coli	*Escherichia coli*
ECM	Extracellular matrix
EGFP	Enhanced green fluorescent protein
ELbcR	Elastin-like block co-recombinamer
ELP	Elastin-like polymer
ELR	Elastin-like recombinamer
ESA	Electrostatic self-assembly
G	Glycine
Gly	Glycine
IL	Interleukin
Ile	Isoleucine
IPTG	Isopropylthio-β-D-galactoside
ITC	Inverse transition cycle
ITT	Inverse temperature transition
LB	Luria Broth
LbL	Layer by layer
LCST	Lower critical solution temperature
Leu	Leucine
M. tuberculosis	*Mycobacterium tuberculosis*
Met	Methionine
MMPs	Matrix metalloproteinases
MSCs	Mesenchymal stromal cells
Mw	Molecular weight
nts	Nucleotides

P	Proline
P. pastoris	*Pichia pastoris*
PDMAEMA	Poly(2-dimethylamino-ethylmethacrylate)
PEG	Polyethylenglycol
PEI	Polyethylenimine
Phe	Phenylalanine
PIPAAm	poly(N-isopropylacrylamide)
PLGA	Poly(Lactide-co-Glycolide)
PLGA	Polylactic-coglycolic acid
PLL	Polylysine
PMMA	Polymethyl methacrylate
Pre-RDL	Plasmid reconstruction-recursive directional ligation
Pro	Proline
PTFE	Polytetrafluoroethylene
R	Arginine
RDL	Recursive directional ligation
RPE	Retinal pigment epithelium
SELR	Silk Elastin like recombinamer
SEM	Scanning electron microscopy
SMCs	Smooth muscle cells
T	Threonine
TB	Terrific Broth
TEHVs	Tissue engineering heart valves
TNF	Tumor necrosis factor
TRAP	Thermodynamically Reversible Addressing of Proteins
Trp	Tryptophan
T_t	Transition temperature
Tyr	Tyrosine
V	Valine
Val	Valine

References

1. P. E. Watson, I. D. Watson and R. D. Batt. The American Journal of Clinical Nutrition 33, 27-39 (1980).

2. E. Petersen, F. WÃ¥gberg and K. A. A. Angquist. European journal of vascular and endovascular surgery : the official journal of the European Society for Vascular Surgery 24, 440-444 (2002).

3. S. M. Mithieux and A. S. Weiss. Elastin. In: David ADP, John MS, editors. Advances in Protein Chemistry: Academic Press; 2005. p. 437-461.

4. F. W. Keeley, C. M. Bellingham and K. A. Woodhouse. Philosophical Transactions of the Royal Society B: Biological Sciences 357, 185-189 (2002).

5. D. W. Urry. J Protein Chem 7, 1-34 (1988).

6. A. M. Tamburro, V. Guantieri, A. Scopa and J. M. Drabble. Chirality 3, 318-323 (1991).

7. M. A. Morelli, M. DeBiasi, A. DeStradis and A. M. Tamburro. J Biomol Struct Dyn 11, 181-90 (1993).

8. H. Reiersen, A. R. Clarke and A. R. Rees. Journal of molecular biology 283, 255-64 (1998).

9. D. W. Urry. Angewandte Chemie-International Edition in English 32, 819-841 (1993).

10. D. W. Urry. What sustains life? Consilient mechanisms for protein-based machines and materials. Springer-Verlag, New York, 2006.

11. D. W. Urry. J Protein Chem 7, 81-114 (1988).

12. D. Urry and K. P. D. Williams. Syntheses, Characterizations and Medical Uses of the Polypentapeptide of Elastin and its Analogs. In: Williams DF, editor. Biocompatibility of Tissue Analogues: CRC Press, Inc; 1985. p. 27.

13. D. T. McPherson, C. Morrow, D. S. Minehan, J. Wu, E. Hunter and D. W. Urry. Biotechnol Prog 8, 347-52 (1992).

14. W. R. Gray, L. B. Sandberg and J. A. Foster. Nature 246, 461-466 (1973).

15. L. D. Muiznieks, A. S. Weiss and F. W. Keeley. Biochemistry and Cell Biology 88, 239-250 (2010).

16. B. Vrhovski and A. S. Weiss. European Journal of Biochemistry 258, 1-18 (1998).

17. D. W. Urry, W. D. Cunningham and T. Ohnishi. Biochemistry 13, 609-16 (1974).

18. V. Renugopalakrishnan, M. A. Khaled, R. S. Rapaka and D. W. Urry. Biochim Biophys Acta 536, 421-8 (1978).

19. D. W. Urry, K. Okamoto, R. D. Harris, C. F. Hendrix and M. M. Long. Biochemistry 15, 4083-9 (1976).

20. D. K. Chang and D. W. Urry. Chemical Physics Letters 147, 395-400 (1988).

21. J. Cappello, J. Crissman, M. Dorman, M. Mikolajczak, G. Textor, M. Marquet and F. Ferrari. Biotechnology Progress 6, 198-202 (1990).

22. U.S. Pat. WO/1988/003533 (1988), F. A. Ferrari, C. Richardson, J. Chambers, S. C. Causey and T. J. Pollock (to Google Patents).

23. D. A. Tirrell, M. J. Fournier and T. L. Mason. MRS Bulletin 16, 23-28 (1991).

24. K. A. Padgett and J. A. Sorge. Gene 168, 31-5 (1996).

25. R. A. McMillan, T. A. T. Lee and V. P. Conticello. Macromolecules 32, 3643-3648 (1999).

26. D. E. Meyer and A. Chilkoti. Biomacromolecules 3, 357-367 (2002).

27. J. R. McDaniel, J. A. Mackay, F. G. Quiroz and A. Chilkoti. Biomacromolecules 11, 944-52 (2010).

28. J. C. Rodriguez-Cabello, A. Girotti, A. Ribeiro and F. J. Arias. Methods in molecular biology 811, 17-38 (2012).

29. O. S. Rabotyagova, P. Cebe and D. L. Kaplan. Biomacromolecules 12, 269-289 (2011).

30. D. T. McPherson, C. Morrow, D. S. Minehan, J. Wu, E. Hunter and D. W. Urry. Biotechnology Progress 8, 347-52 (1992).

31. D. T. McPherson, J. Xu and D. W. Urry. Protein expression and purification 7, 51-7 (1996).

32. C. Guda, X. Zhang, D. T. McPherson, J. Xu, J. H. Cherry, D. W. Urry and H. Daniell. Biotechnology Letters 17, 745-750 (1995).

33. K. D. Tartof and C. A. Hobbs. Bethesda Res. Lab. Focus 9, 12-16 (1987).

34. D. C. Chow, M. R. Dreher, K. Trabbic-Carlson and A. Chilkoti. Biotechnology Progress 22, 638-46 (2006).

35. R. Machado, J. Azevedo-Silva, C. Correia, T. Collins, F. J. Arias, J. C. Rodriguez-Cabello and M. Casal. AMB Express 3, 11 (2013).

36. T. Collins, M. Barroca, F. Branca, J. Padrao, R. Machado and M. Casal. Biomacromolecules 15, 2701-8 (2014).

37. R. W. Herzog, N. K. Singh, D. W. Urry and H. Daniell. Applied microbiology and biotechnology 47, 368-72 (1997).

38. R. Schipperus, R. L. M. Teeuwen, M. W. T. Werten, G. Eggink and F. A. de Wolf. Applied Microbiology and Biotechnology 85, 293 (2009).

39. R. E. Sallach, V. P. Conticello and E. L. Chaikof. Biotechnology Progress 25, 1810-1818 (2009).

40. R. Schipperus, G. Eggink and F. A. de Wolf. Biotechnology Progress 28, 242-247 (2012).

41. X. Zhang, C. Guda, R. Datta, R. Dute, D. W. Urry and H. Daniell. Biotechnology Letters 17, 1279-1284 (1995).

42. X. Zhang, D. W. Urry and H. Daniell. Plant Cell Reports 16, 174-179 (1996).

43. R. Heppner, N. Weichert, A. Schierhorn, U. Conrad and M. Pietzsch. International Journal of Molecular Sciences 17, 1687 (2016).

44. J. C. Rodriguez-Cabello, S. Prieto, J. Reguera, F. J. Arias and A. Ribeiro. Journal of biomaterials science. Polymer edition 18, 269-86 (2007).

45. D. W. Urry. The Journal of Physical Chemistry B 101, 11007-11028 (1997).

46. E. R. Wright and V. P. Conticello. Advanced Drug Delivery Reviews 54, 1057-1073 (2002).

47. T. A. T. Lee, A. Cooper, R. P. Apkarian and V. P. Conticello. Advanced Materials 12, 1105-1110 (2000).

48. L. Martín, E. Castro, A. Ribeiro, M. Alonso and J. C. Rodríguez-Cabello. Biomacromolecules 13, 293-298 (2012).

49. D. E. Meyer and A. Chilkoti. Biomacromolecules 5, 846-851 (2004).

50. J. R. McDaniel, D. C. Radford and A. Chilkoti. Biomacromolecules 14, 2866-72 (2013).

51. A. Ribeiro, F. J. Arias, J. Reguera, M. Alonso and J. C. Rodríguez-Cabello. Biophysical Journal 97, 312-320 (2009).

52. A. Girotti, D. Orbanic, A. Ibáñez-Fonseca, C. Gonzalez-Obeso and J. C. Rodríguez-Cabello. Advanced Healthcare Materials 4, 2423-2455 (2015).

53. A. Nagarsekar, J. Crissman, M. Crissman, F. Ferrari, J. Cappello and H. Ghandehari. Biomacromolecules 4, 602-607 (2003).

54. Q. Wang, X. Xia, W. Huang, Y. Lin, Q. Xu and D. L. Kaplan. Advanced Functional Materials 24, 4303-4310 (2014).

55. A. Bracalello, V. Santopietro, M. Vassalli, G. Marletta, R. Del Gaudio, B. Bochicchio and A. Pepe. Biomacromolecules 12, 2957-2965 (2011).

56. A. Panitch, T. Yamaoka, M. J. Fournier, T. L. Mason and D. A. Tirrell. Macromolecules 32, 1701-1703 (1999).

57. A. Girotti, J. Reguera, J. C. Rodríguez-Cabello, F. J. Arias, M. Alonso and A. M. Testera. Journal of Materials Science: Materials in Medicine 15, 479-484 (2004).

58. M. D. Pierschbacher and E. Ruoslahti. Nature 309, 30-33 (1984).

59. A. Nicol, D. Channe Gowda and D. W. Urry. Journal of Biomedical Materials Research 26, 393-413 (1992).

60. J. C. Liu, S. C. Heilshorn and D. A. Tirrell. Biomacromolecules 5, 497-504 (2004).

61. A. Fernández-Colino, F. J. Arias, M. Alonso and J. C. Rodríguez-Cabello. Biomacromolecules 16, 3389-3398 (2015).

62. W.-B. Zhang, F. Sun, D. A. Tirrell and F. H. Arnold. Journal of the American Chemical Society 135, 13988-13997 (2013).

63. T. Christensen, M. Amiram, S. Dagher, K. Trabbic-Carlson, M. F. Shamji, L. A. Setton and A. Chilkoti. Protein Science 18, 1377-1387 (2009).

64. T. Christensen, W. Hassouneh, K. Trabbic-Carlson and A. Chilkoti. Biomacromolecules 14, 1514-1519 (2013).

65. D. E. Meyer and A. Chilkoti. Nat Biotech 17, 1112-1115 (1999).

66. M. R. Banki, L. Feng and D. W. Wood. Nat Meth 2, 659-662 (2005).

67. W. Hassouneh, T. Christensen and A. Chilkoti. Elastin-Like Polypeptides as a Purification Tag for Recombinant Proteins. Current Protocols in Protein Science: John Wiley & Sons, Inc.; 2001.

68. W.-J. Liu, Q. Wu, B. Xu, X.-Y. Zhang, X.-L. Xia and H.-C. Sun. Protein Expression and Purification 98, 18-24 (2014).

69. J. Patel, H. Zhu, R. Menassa, L. Gyenis, A. Richman and J. Brandle. Transgenic Research 16, 239-249 (2007).

70. U. Conrad, I. Plagmann, S. Malchow, M. Sack, D. M. Floss, A. A. Kruglov, S. A. Nedospasov, S. Rose-John and J. Scheller. Plant Biotechnology Journal 9, 22-31 (2011).

71. A. Kaldis, A. Ahmad, A. Reid, B. McGarvey, J. Brandle, S. Ma, A. Jevnikar, S. E. Kohalmi and R. Menassa. Plant Biotechnology Journal 11, 535-545 (2013).

72. F. Hu, T. Ke, X. Li, P. H. Mao, X. Jin, F. L. Hui, X. D. Ma and L. X. Ma. Applied Biochemistry and Biotechnology 160, 2377-2387 (2010).

73. D. A. Sousa, K. C. L. Mulder, K. S. Nobre, N. S. Parachin and O. L. Franco. Journal of Biotechnology 234, 83-89 (2016).

74. D. W. Urry. Methods Enzymol 82 Pt A, 673-716 (1982).

75. S. M. Janib, M. Pastuszka, S. Aluri, Z. Folchman-Wagner, P.-Y. Hsueh, P. Shi, Yi-An, H. Cui and J. A. Mackay. Polymer chemistry 5, 1614-1625 (2014).

76. M. H. Misbah, L. Quintanilla, M. Alonso and J. C. Rodríguez-cabello. Polymer 81, 37-44 (2015).

77. R. R. Costa, C. A. Custodio, A. M. Testero, F. J. Arias, J. C. Rodriguez-Cabello, N. M. Alves and J. F. Mano. Advanced Functional Materials 19, 3210-3218 (2009).

78. X. X. Xia, M. Wang, Y. Lin, Q. Xu and D. L. Kaplan. Biomacromolecules 15, 908-914 (2014).

79. M. R. Dreher, A. J. Simnick, K. Fischer, R. J. Smith, A. Patel, M. Schmidt and A. Chilkoti. Journal of the American Chemical Society 130, 687-694 (2008).

80. A. Ghoorchian, K. Vandemark, K. Freeman, S. Kambow, N. B. Holland and K. A. Streletzky. Journal of Physical Chemistry B 117, 8865-8874 (2013).

81. G. Pinedo-martín, M. Santos, A. M. Testera, M. Alonso and J. C. Rodríguez-cabello. Polymer 55, 5314-5321 (2014).

82. R. E. Sallach, M. Wei, N. Biswas, V. P. Conticello, S. Lecommandoux, R. A. Dluhy and E. L. Chaikof. Journal of the American Chemical Society 128, 12014-12019 (2006).

83. A. Ghoorchian, J. T. Cole and N. B. Holland. Macromolecules 43, 4340-4345 (2010).

84. N. U. Patel, C. A. Purser, R. C. Baker and A. V. Janorkar. Biomacromolecules 14, 2891-2899 (2013).

85. G. Pinedo-martin, E. Castro, L. Martin, M. Alonso and J. C. Rodr. Langmuir 30, 8 (2014).

86. W. Hassouneh, M. L. Nunalee, M. C. Shelton and A. Chilkoti. Biomacromolecules 14, 2347-2353 (2013).

87. J. R. McDaniel, I. Weitzhandler, S. Prevost, K. B. Vargo, M. S. Appavou, D. A. Hammer, M. Gradzielski and A. Chilkoti. Nano Letters 14, 6590-6598 (2014).

88. R. M. Senior, G. L. Griffin, R. P. Mecham, D. S. Wrenn, K. U. Prasad and D. W. Urry. The Journal of Cell Biology 99, 870-874 (1984).

89. M. R. Banki and D. W. Wood. Microbial Cell Factories 4, 32 (2005).

90. E. M. Srokowski and K. A. Woodhouse. Journal of Biomedical Materials Research - Part A 102, 540-551 (2014).

91. M. I. Castellanos, A.-S. Zenses, A. Grau, J. C. Rodríguez-Cabello, F. J. Gil, J. M. Manero and M. Pegueroles. Colloids and Surfaces B: Biointerfaces 127, 22-32 (2015).

92. S. W. Jordan, C. A. Haller, R. E. Sallach, R. P. Apkarian, S. R. Hanson and E. L. Chaikof. Biomaterials 28, 1191-1197 (2007).

93. K. A. Woodhouse, P. Klement, V. Chen, M. B. Gorbet, F. W. Keeley, R. Stahl, J. D. Fromstein and C. M. Bellingham. Biomaterials 25, 4543-4553 (2004).

94. A. Waterhouse, S. G. Wise, M. K. Ng and A. S. Weiss. Tissue engineering. Part b 17, 93-99 (2011).

95. Y. Li, X. Chen, A. J. Ribeiro, E. D. Jensen, K. V. Holmberg, J. C. Rodriguez-cabello and C. Aparicio. advanced Healthcare Materials 3, 1638-1647 (2014).

96. L. A. Hughes, J. Gaston, K. McAlindon, K. A. Woodhouse and S. L. Thibeault. Acta Biomaterialia 13, 111-120 (2015).

97. K. M. Lee, G. S. Jung, J. K. Park, S. K. Choi and W. B. Jeon. Acta Biomaterialia 9, 5600-5608 (2013).

98. J. Scheller, D. Henggeler, A. Viviani and U. Conrad. Transgenic Research 13, 51-57 (2004).

99. M. Pierna, M. Santos, F. J. Arias, M. Alonso and J. C. Rodríguez-Cabello. Biomacromolecules 14, 1893-1903 (2013).

100. J. Kopeček. Biomaterials 28, 5185-5192 (2007).

101. N. A. Peppas. Journal of Controlled Release 68, 135 (2000).

102. A. S. Hoffman. Advanced Drug Delivery Reviews 54, 3-12 (2002).

103. A. P. Nowak, V. Breedveld, L. Pakstis, B. Ozbas, D. J. Pine, D. Pochan and T. J. Deming. Nature 417, 424-428 (2002).

104. C. Xu, V. Breedveld and J. Kopecek. Biomacromolecules 6, 1739-1749 (2005).

105. W. A. Petka, J. L. Harden, K. P. Mcgrath, D. Wirtz and D. A. Tirrell. Science 281, 389-392 (1998).

106. D. W. Urry. The Journal of Physical Chemistry B 101, 11007-11028 (1997).

107. J. T. Prince, K. P. McGrath, C. M. DiGirolamo and D. L. Kaplan. Biochemistry 34, 10879-10885 (1995).

108. A. Fernandez-Colino, F. J. Arias, M. Alonso and J. Carlos Rodriguez-Cabello. Biomacromolecules 15, 3781-3793 (2014).

109. J. Kopeček and J. Yang. Polymer International 56, 1078-1098 (2007).

110. D. Campoccia, P. Doherty, M. Radice, P. Brun, G. Abatangelo and D. F. Williams. Biomaterials 19, 2101-2127 (1998).

111. G. D. Prestwich, D. M. Marecak, J. F. Marecek, K. P. Vercruysse and M. R. Ziebell. Journal of Controlled Release 53, 93-103 (1998).

112. R. A. McMillan and V. P. Conticello. Macromolecules 33, 4809-4821 (2000).

113. R. A. McMillan, K. L. Caran, R. P. Apkarian and V. P. Conticello. Macromolecules 32, 9067-9070 (1999).

114. A. J. Alix. Journal de la Société de biologie 195, 181-93 (2001).

115. A. Girotti, J. Reguera, J. C. Rodríguez-Cabello, F. J. Arias, M. Alonso and A. M. Testera. Journal of Materials Science: Materials in Medicine 15, 479-484 (2004).

116. D. W. Urry, A. Pattanaik, J. Xu, T. C. Woods, D. T. McPherson and T. M. Parker. Journal of biomaterials science. Polymer edition 9, 1015-48 (1998).

117. T. Miyata, N. Asami and T. Uragami. Nature 399, 766-9 (1999).

118. C. Wang, J. Kopecek and R. J. Stewart. Biomacromolecules 2, 912-20 (2001).

119. K. Ulbrich, J. Strohalm and J. Kopecek. Biomaterials 3, 150-154 (1982).

120. T. C. Holmes, S. de Lacalle, X. Su, G. Liu, A. Rich and S. Zhang. Proceedings of the National Academy of Sciences 97, 6728-6733 (2000).

121. S. Zhang. Nature Biotechnology 21, 1171-1178 (2003).

122. B. Ozbas, J. Kretsinger, K. Rajagopal, J. P. Schneider and D. J. Pochan. Macromolecules, (2004).

123. R. R. Costa, C. A. Custódio, F. J. Arias, J. C. Rodríguez-Cabello and J. F. Mano. Small 7, 2640-2649 (2011).

124. G. C. Yeo, F. W. Keeley and A. S. Weiss. Advances in Colloid and Interface Science 167, 94-103 (2011).

125. M. Li and C. K. Ober. Materials Today 9, 30-39 (2006).

126. J. C. Rodríguez-Cabello, L. Martín, A. Girotti, C. García-Arévalo, F. J. Arias and M. Alonso. Nanomedicine (London, England) 6, 111-122 (2011).

127. R. E. Sallach, W. Cui, F. Balderrama, A. W. Martinez, J. Wen, C. A. Haller, J. V. Taylor, E. R. Wright, R. C. Long Jr and E. L. Chaikof. Biomaterials 31, 779-791 (2010).

128. T. Asakura, J. Yao, T. Yamane, K. Umemura and A. S. Ulrich. (2002).

129. Y. Takahashi, M. Gehoh and K. Yuzuriha. Journal of Polymer Science Part B: Polymer Physics 29, 889-891 (1991).

130. Y. Takahashi, M. Gehoh and K. Yuzuriha. International Journal of Biological Macromolecules 24, 127-138 (1999).

131. K. Shimura, A. Kikuchi, K. Ohtomo, Y. Katagata and A. Hyodo. Journal of biochemistry 80, 693-702 (1976).

132. F. G. Omenetto and D. L. Kaplan. Science (New York, N.Y.) 329, 528-31 (2010).

133. K. Tanaka, S. Inoue and S. Mizuno. Insect Biochemistry and Molecular Biology 29, 269-276 (1999).

134. J. G. Hardy, L. M. Römer and T. R. Scheibel. Polymer 49, 4309-4327 (2008).

135. J. Zhou, C. Cao, X. Ma, L. Hu, L. Chen and C. Wang. Polymer Degradation and Stability 95, 1679-1685 (2010).

136. B. Panilaitis, G. H. Altman, J. Chen, H.-J. Jin, V. Karageorgiou and D. L. Kaplan. Biomaterials 24, 3079-3085 (2003).

137. H. Fan, H. Liu, S. L. Toh and J. C. H. Goh. Biomaterials 30, 4967-4977 (2009).

138. B. Kundu, R. Rajkhowa, S. C. Kundu and X. Wang. Advanced Drug Delivery Reviews 65, 457-470 (2013).

139. P. B. Harbury, T. Zhang, P. S. Kim and T. Alber. Science (New York, N.Y.) 262, 1401-7 (1993).

140. J. R. Litowski and R. S. Hodges. The Journal of Peptide Research 58, 477-492 (2001).

141. G. De Crescenzo, J. R. Litowski, R. S. Hodges and M. D. O'Connor-McCourt. Biochemistry 42, 1754 (2003).

142. C. Vinson, M. Myakishev, A. Acharya, A. A. Mir, J. R. Moll and M. Bonovich. Molecular and cellular biology 22, 6321-35 (2002).

143. C. R. Vinson, P. B. Sigler and S. L. McKnight. Science (New York, N.Y.) 246, 911-6 (1989).

144. T. Abel and T. Maniatis. Nature 341, 24-25 (1989).

145. D. N. Woolfson. Advances in Protein Chemistry 70, 79-112 (2005).

146. J. Yang, C. Xu, P. Kopečková and J. Kopeček. Macromolecular Bioscience 6, 201-209 (2006).

147. J. Moitra, L. Szilak, D. Krylov and C. Vinson. Biochemistry 36, 12567-12573 (1997).

148. B. Tripet, K. Wagschal, P. Lavigne, C. T. Mant and R. S. Hodges. Journal of Molecular Biology 300, 377-402 (2000).

149. D. Krylov, I. Mikhailenko and C. Vinson. The EMBO journal 13, 2849-61 (1994).

150. T. Alber. Current opinion in genetics & development 2, 205-10 (1992).

151. D. Krylov, J. Barchi and C. Vinson. Journal of Molecular Biology 279, 959-972 (1998).

152. C.-C. Huang, S. Ravindran, Z. Yin and A. George. Biomaterials 35, 5316-5326 (2014).

153. J. C. Rodríguez-Cabello, J. Reguera, A. Girotti, M. Alonso and A. M. Testera. Progress in Polymer Science 30, 1119-1145 (2005).

154. J. C. Rodríguez-Cabello, M. Alonso, L. Guiscardo, V. Reboto and A. Girotti. Advanced Materials 14, 1151-1154 (2002).

155. K. Trabbic-Carlson, L. A. Setton and A. Chilkoti. Biomacromolecules 4, 572-580 (2003).

156. E. Ruoslahti and M. D. Pierschbacher. Cell 44, 517-518 (1986).

157. W. E. Hennink and C. F. van Nostrum. Advanced Drug Delivery Reviews 54, 13-36 (2002).

158. T. R. Hoare and D. S. Kohane. Polymer 49, 1993-2007 (2008).

159. Y. Garcia, N. Hemantkumar, R. Collighan, M. Griffin, J. C. Rodriguez-Cabello and A. Pandit. Tissue engineering. Part A 15, 887-899 (2009).

160. E. Westhaus and P. B. Messersmith. Biomaterials 22, 453-462 (2001).

161. Y. Garcia, R. Collighan, M. Griffin and A. Pandit. Journal of Materials Science: Materials in Medicine 18, 1991-2001 (2007).

162. A. E. J. de Nooy, G. Masci and V. Crescenzi. Macromolecules 32, 1318-1320 (1999).

163. M. R. Huglin. British Polymer Journal 21, 184-184 (1989).

164. S. Ravi, J. M. Caves, A. W. Martinez, C. A. Haller and E. L. Chaikof. Journal of Biomedical Materials Research Part A 101A, 1915-1925 (2013).

165. A. M. Testera, A. Girotti, I. G. de Torre, L. Quintanilla, M. Santos, M. Alonso and J. C. Rodríguez-Cabello. Journal of Materials Science: Materials in Medicine 26, 105 (2015).

166. J. Patterson, M. M. Martino and J. A. Hubbell. Materials Today 13, 14-22 (2010).

167. I. G. de Torre, M. Santos, L. Quintanilla, A. Testera, M. Alonso and J. C. Rodríguez Cabello. Acta Biomaterialia 10, 2495-2505 (2014).

168. D. J. Glover, H. J. Lipps and D. A. Jans. Nature Reviews Genetics 6, 299-310 (2005).

169. M. Ramamoorth and A. Narvekar. Journal of Clinical and Diagnostic Research : JCDR 9, GE01-GE06 (2015).

170. M. D. Brown, A. G. Schätzlein and I. F. Uchegbu. International Journal of Pharmaceutics 229, 1-21 (2001).

171. J. M. Bergen, I.-K. Park, P. J. Horner and S. H. Pun. Pharmaceutical Research 25, 983-998 (2008).

172. K. Van Craenenbroeck, P. Vanhoenacker and G. Haegeman. European Journal of Biochemistry 267, 5665-5678 (2000).

173. M. A. Kay. Nat Rev Genet 12, 316-328 (2011).

174. Z. Liu, Z. Zhang, C. Zhou and Y. Jiao. Progress in Polymer Science 35, 1144-1162 (2010).

175. D. Putnam. Nat Mater 5, 439-451 (2006).

176. H. Yin, R. L. Kanasty, A. A. Eltoukhy, A. J. Vegas, J. R. Dorkin and D. G. Anderson. Nat Rev Genet 15, 541-555 (2014).

177. P. Midoux, C. Pichon, J.-J. Yaouanc and P.-A. Jaffrès. British Journal of Pharmacology 157, 166-178 (2009).

178. M. A. Mintzer and E. E. Simanek. Chemical Reviews 109, 259-302 (2009).

179. M. S. Al-Dosari and X. Gao. The AAPS Journal 11, 671 (2009).

180. X. Gao, K.-S. Kim and D. Liu. The AAPS Journal 9, E92-E104 (2007).

181. M. W. Konstan, P. B. Davis, J. S. Wagener, K. A. Hilliard, R. C. Stern, L. J. H. Milgram, T. H. Kowalczyk, S. L. Hyatt, T. L. Fink, C. R. Gedeon, S. M. Oette, J. M. Payne, O. Muhammad, A. G. Ziady, R. C. Moen and M. J. Cooper. Human Gene Therapy 15, 1255-1269 (2004).

182. J. J. Thomas, M. R. Rekha and C. P. Sharma. Molecular Pharmaceutics 9, 121-134 (2012).

183. M. R. Rekha and C. P. Sharma. Acta Biomaterialia 7, 370-379 (2011).

184. C. L. Grigsby and K. W. Leong. Journal of The Royal Society Interface 7, S67 (2009).

185. A. C. Hunter. Advanced Drug Delivery Reviews 58, 1523-1531 (2006).

186. K. Knop, R. Hoogenboom, D. Fischer and U. S. Schubert. Angewandte Chemie International Edition 49, 6288-6308 (2010).

187. N. L. Goeden-Wood, V. P. Conticello, S. J. Muller and J. D. Keasling. Biomacromolecules 3, 874-879 (2002).

188. J. R. McDaniel, S. R. MacEwan, M. Dewhirst and A. Chilkoti. Journal of Controlled Release 159, 362-367 (2012).

189. C. García-Arévalo, J. F. Bermejo-Martín, L. Rico, V. Iglesias, L. Martín, J. C. Rodríguez-Cabello and F. J. Arias. Molecular Pharmaceutics 10, 586-597 (2013).

190. J. C. Rodríguez-Cabello, M. J. Piña, A. Ibáñez-Fonseca, A. Fernández-Colino and F. J. Arias. Bioconjugate Chemistry 26, 1252-1265 (2015).

191. S. R. Ong, K. A. Trabbic-Carlson, D. L. Nettles, D. W. Lim, A. Chilkoti and L. A. Setton. Biomaterials 27, 1930-1935 (2006).

192. H. Martínez-Osorio, M. Juárez-Campo, Y. Diebold, A. Girotti, M. Alonso, F. J. Arias, J. C. Rodríguez-Cabello, C. García-Vázquez and M. Calonge. Current Eye Research 34, 48-56 (2009).

193. T.-H. H. Chen, Y. Bae and D. Y. Furgeson. Pharmaceutical Research 25, 683-691 (2008).

194. W. Shen, M. A. van Dongen, Y. Han, M. Yu, Y. Li, G. Liu, M. M. Banaszak Holl and R. Qi. European Journal of Pharmaceutics and Biopharmaceutics 88, 658-663 (2014).

195. S. Blau, T. T. Jubeh, S. M. Haupt and A. Rubinstein. Critical Reviews in Therapeutic Drug Carrier Systems 17, 41 (2000).

196. H. Lee, J. H. Jeong and T. G. Park. Journal of Controlled Release 79, 283-291 (2002).

197. L. Walker, E. Perkins, F. Kratz and D. Raucher. International Journal of Pharmaceutics 436, 825-832 (2012).

198. G. L. Bidwell and D. Raucher. Advanced drug delivery reviews 62, 1486-1496 (2010).

199. M. J. Piña, A. Girotti, M. Santos, J. C. Rodríguez-Cabello and F. J. Arias. Molecular Pharmaceutics 13, 795-808 (2016).

200. M. T. Dertzbaugh. Plasmid 39, 100-113 (1998).

201. J. A. Hubbell, S. N. Thomas and M. A. Swartz. Nature 462, 449-460 (2009).

202. K. S. Jones. Biotechnology Progress 24, 807-814 (2008).

203. O. A. Ali, N. Huebsch, L. Cao, G. Dranoff and D. J. Mooney. Nat Mater 8, 151-158 (2009).

204. S. T. Reddy, M. A. Swartz and J. A. Hubbell. Trends in Immunology 27, 573-579 (2006).

205. M. O. Oyewumi, A. Kumar and Z. Cui. Expert Review of Vaccines 9, 1095-1107 (2010).

206. A. Travesset. Science 334, 183-184 (2011).

207. M. A. C. Stuart, W. T. S. Huck, J. Genzer, M. Muller, C. Ober, M. Stamm, G. B. Sukhorukov, I. Szleifer, V. V. Tsukruk, M. Urban, F. Winnik, S. Zauscher, I. Luzinov and S. Minko. Nat Mater 9, 101-113 (2010).

208. P. L. Mottram, D. Leong, B. Crimeen-Irwin, S. Gloster, S. D. Xiang, J. Meanger, R. Ghildyal, N. Vardaxis and M. Plebanski. Molecular Pharmaceutics 4, 73-84 (2007).

209. A. Verma, O. Uzun, Y. Hu, Y. Hu, H.-S. Han, N. Watson, S. Chen, D. J. Irvine and F. Stellacci. Nat Mater 7, 588-595 (2008).

210. F. A. Sharp, D. Ruane, B. Claass, E. Creagh, J. Harris, P. Malyala, M. Singh, D. T. O'Hagan, V. Petrilli, J. Tschopp, L. A. O'Neill and E. C. Lavelle. Proc Natl Acad Sci U S A 106, 870-5 (2009).

211. S. D. Xiang, A. Scholzen, G. Minigo, C. David, V. Apostolopoulos, P. L. Mottram and M. Plebanski. Methods 40, 1-9 (2006).

212. D. J. Bharali, V. Pradhan, G. Elkin, W. Qi, A. Hutson, S. A. Mousa and Y. Thanavala. Nanomedicine: Nanotechnology, Biology and Medicine 4, 311-317 (2008).

213. L. Martin, M. Alonso, M. Moller, J. C. Rodriguez-Cabello and P. Mela. Soft Matter 5, 1591-1593 (2009).

214. R. Sivakumar. Bulletin of Materials Science 22, 647-655 (1999).

215. D. W. Urry, T. M. Parker, M. C. Reid and D. C. Gowda. Journal of Bioactive and Compatible Polymers 6, 263-282 (1991).

216. G. Sun, P.-Y. Hsueh, S. M. Janib, S. Hamm-Alvarez and J. Andrew MacKay. Journal of Controlled Release 155, 218-226 (2011).

217. J. C. Rodríguez-Cabello, S. Prieto, F. J. Arias, J. Reguera and A. Ribeiro. Nanomedicine 1, 267-280 (2006).

218. A. Chilkoti, M. R. Dreher and D. E. Meyer. Advanced Drug Delivery Reviews 54, 1093-1111 (2002).

219. D. E. Meyer, K. Trabbic-Carlson and A. Chilkoti. Biotechnology Progress 17, 720-728 (2001).

220. D. M. Floss. Journal of Biomedicine and Biotechnology Volume 2010 (2010), 14 pages (2010).

221. D. S. W. Benoit, M. P. Schwartz, A. R. Durney and K. S. Anseth. Nat Mater 7, 816-823 (2008).

222. T. Johnson and P. Koria. BioDrugs 30, 117-127 (2016).

223. J. Andrew MacKay, M. Chen, J. R. McDaniel, W. Liu, A. J. Simnick and A. Chilkoti. Nat Mater 8, 993-999 (2009).

224. C. Garcia-Arevalo, M. Pierna, A. Girotti, F. J. Arias and J. C. Rodriguez-Cabello. Soft Matter 8, 3239-3249 (2012).

225. Y. Wei, Y. Ji, L.-L. Xiao, Q.-k. Lin, J.-p. Xu, K.-f. Ren and J. Ji. Biomaterials 34, 2588-2599 (2013).

226. L. G. Melo, M. Gnecchi, A. S. Pachori, D. Kong, K. Wang, X. Liu, R. E. Pratt and V. J. Dzau. Arteriosclerosis, Thrombosis, and Vascular Biology 24, 1761-1774 (2004).

227. T. Inoue, K. Croce, T. Morooka, M. Sakuma, K. Node and D. I. Simon. JACC: Cardiovascular Interventions 4, 1057-1066 (2011).

228. M. Weber, I. Gonzalez de Torre, R. Moreira, J. Frese, C. Oedekoven, M. Alonso, C. J. Rodriguez Cabello, S. Jockenhoevel and P. Mela. Tissue Engineering Part C: Methods 21, 832-840 (2015).

229. K. E. Inostroza-Brito, E. Collin, O. Siton-Mendelson, K. H. Smith, A. Monge-Marcet, D. S. Ferreira, R. P. Rodríguez, M. Alonso, J. C. Rodríguez-Cabello, R. L. Reis, F. Sagués, L. Botto, R. Bitton, H. S. Azevedo and A. Mata. Nat Chem 7, 897-904 (2015).

230. B. Kinikoglu, J. C. Rodriguez-Cabello, O. Damour and V. Hasirci. J Mater Sci Mater Med 22, 1541-54 (2011).

231. B. Kinikoglu, J. C. Rodriguez-Cabello, O. Damour and V. Hasirci. Biomaterials 32, 5756-64 (2011).

232. J. A. Vega Álvarez, O. García-Suárez, D. Fernández Monjil and M. E. del Valle Soto Revista Española de Cirugía Ortopédica y Traumatología 46, 391-400 (2002).

233. T. Minas and L. Peterson. Operative Techniques in Orthopaedics 7, 323-333 (1997).

234. M. Vila, A. García, A. Girotti, M. Alonso, J. C. Rodríguez-Cabello, A. González-Vázquez, J. A. Planell, E. Engel, J. Buján, N. García-Honduvilla and M. Vallet-Regí. Acta Biomaterialia 45, 349-356 (2016).

235. J. T. Kerker, A. J. Leo and N. A. Sgaglione. Sports Medicine and Arthroscopy Review 16, 208-216 (2008).

236. J. Vaquero and F. Forriol. Injury 43, 694-705 (2012).

237. S. Vijayan, W. Bartlett, G. Bentley, R. W. J. Carrington, J. A. Skinner, R. C. Pollock, M. Alorjani and T. W. R. Briggs. a two- to eight-year follow-up study 94-B, 488-492 (2012).

238. S. Trattnig, A. Ba-Ssalamah, K. Pinker, C. Plank, V. Vecsei and S. Marlovits. Magnetic Resonance Imaging 23, 779-787 (2005).

239. M. W. Kessler, G. Ackerman, J. S. Dines and D. Grande. Sports Medicine and Arthroscopy Review 16, 246-254 (2008).

240. L. S. Fujikawa, C. S. Foster, T. J. Harrist, J. M. Lanigan and R. B. Colvin. Lab Invest 45, 120-9 (1981).

241. F. Bian, F. S. A. Pelegrino, S. C. Pflugfelder, E. A. Volpe, D.-Q. Li and C. S. de Paiva. Investigative Ophthalmology & Visual Science 56, 4908-4918 (2015).

242. D. Meller, D. Q. Li and S. C. G. Tseng. Investigative Ophthalmology & Visual Science 41, 2922-2929 (2000).

243. G. K. Srivastava, L. Martín, A. K. Singh, I. Fernandez-Bueno, M. J. Gayoso, M. T. Garcia-Gutierrez, A. Girotti, M. Alonso, J. C. Rodríguez-Cabello and J. C. Pastor. Journal of Biomedical Materials Research Part A 97A, 243-250 (2011).

244. M. R. Dreher, A. J. Simnick, K. Fischer, R. J. Smith, A. Patel, M. Schmidt and A. Chilkoti. Journal of the American Chemical Society 130, 687-694 (2008).

245. S. Roberts, M. Dzuricky and A. Chilkoti. FEBS Letters 589, 2477-2486 (2015).

246. A. M. Testera, A. Girotti, I. G. de Torre, L. Quintanilla, M. Santos, M. Alonso and J. C. Rodríguez-Cabello. Journal of Materials Science: Materials in Medicine 26, 105 (2015).

247. N. Nath and A. Chilkoti. Analytical Chemistry 74, 504-509 (2002).

248. T. Okano, N. Yamada, M. Okuhara, H. Sakai and Y. Sakurai. Biomaterials 16, 297-303 (1995).

249. H. Imen Elloumi, Y. Masayuki and O. Teruo. Biofabrication 1, 022002 (2009).

250. M. Hirose, M. Yamato, O. H. Kwon, M. Harimoto, A. Kushida, T. Shimizu, A. Kikuchi and T. Okano. Yonsei Med J 41, 803-813 (2000).

251. J. Yang, M. Yamato, T. Shimizu, H. Sekine, K. Ohashi, M. Kanzaki, T. Ohki, K. Nishida and T. Okano. Biomaterials 28, 5033-5043 (2007).

252. M. Pierna, M. Santos, F. J. Arias, M. Alonso and J. C. Rodríguez-Cabello. Biomacromolecules 14, 1893-1903 (2013).

253. K. Na, J. Jung, O. Kim, J. Lee, T. G. Lee, Y. H. Park and J. Hyun. Langmuir 24, 4917-4923 (2008).

254. T. Boudou, T. Crouzier, K. Ren, G. Blin and C. Picart. Advanced Materials 22, 441-467 (2010).

255. V. Gribova, R. Auzely-Velty and C. Picart. Chemistry of materials : a publication of the American Chemical Society 24, 854-869 (2012).

256. H. S. Silva and P. B. Miranda. The Journal of Physical Chemistry B 113, 10068-10071 (2009).

257. Z. Tang, Y. Wang, P. Podsiadlo and N. A. Kotov. Advanced Materials 18, 3203-3224 (2006).

258. M. Swierczewska, C. S. Hajicharalambous, A. V. Janorkar, Z. Megeed, M. L. Yarmush and P. Rajagopalan. Acta Biomaterialia 4, 827-837 (2008).

259. C. Aparicio, E. Salvagni, M. Werner, E. Engel, M. Pegueroles, C. Rodriguez-Cabello, F. Munoz, J. A. Planell and J. Gil. Journal of Medical Devices 3, 027555-027555 (2009).

260. R. R. Costa, A. M. Testera, F. J. Arias, J. C. Rodríguez-Cabello and J. F. Mano. The Journal of Physical Chemistry B 117, 6839-6848 (2013).

261. J. S. Boateng, K. H. Matthews, H. N. E. Stevens and G. M. Eccleston. Journal of Pharmaceutical Sciences 97, 2892-2923 (2008).

262. M. George and T. E. Abraham. Journal of Controlled Release 114, 1-14 (2006).

263. R. Q. Frazer, R. T. Byron, P. B. Osborne and K. P. West. Journal of Long-Term Effects of Medical Implants 15, 629-639 (2005).

264. B. Wang, Q. Lin, C. Shen, J. Tang, Y. Han and H. Chen. Journal of Colloid and Interface Science 431, 1-7 (2014).

265. B.-S. Yu, Z.-K. Yang, Z.-M. Li, L.-W. Zeng, L.-B. Wang and W. W. Lu. Clinical Spine Surgery 24, E49-E56 (2011).

266. J. Jaberi, K. Gambrell, P. Tiwana, C. Madden and R. Finn. Journal of Oral and Maxillofacial Surgery 71, e81-e88 (2013).

267. K. Sawakami, A. Yamazaki, S. Ishikawa, T. Ito, K. Watanabe and N. Endo. Clinical Spine Surgery 25, E28-E35 (2012).

268. G. Lemperle, H. Ott, U. Charrier, J. Hecker and M. Lemperle. Annals of Plastic Surgery 26, 57-63 (1991).

269. N. M. Goodger, J. Wang, G. W. Smagalski and B. Hepworth. Journal of Oral and Maxillofacial Surgery 63, 1048-1051 (2005).

270. X. Punet, R. Mauchauffé, J. C. Rodríguez-Cabello, M. Alonso, E. Engel and M. A. Mateos-Timoneda. Regenerative Biomaterials, (2015).

271. P. H. Blit, K. G. Battiston, M. Yang, J. Paul Santerre and K. A. Woodhouse. Acta Biomaterialia 8, 2493-2503 (2012).

CHAPTER 2

ELASTIN-LIKE MATERIALS FOR TISSUE REGENERATION AND REPAIR

José Carlos Rodríguez-Cabello,[1,2] Israel González de Torre,[1,2] Filippo Cipriani,[2] Leander Poocza,[1]

[1] Universidad de Valladolid, BIOFORGE, CIBER-BBN, Valladolid, Spain

[2] Technical Proteins NanoBioTechnology (TPNBT) S.L., Valladolid, Spain

J.C. Rodríguez-Cabello, I. G. de Torre, F. Cipriani, L. Poocza. Elastin-like materials for tissue regeneration and repair. *Peptides and Proteins as Biomaterials for Tissue Regeneration and Repair* (2018). doi: 10.1016/B978-0-08-100803-4.00012-7

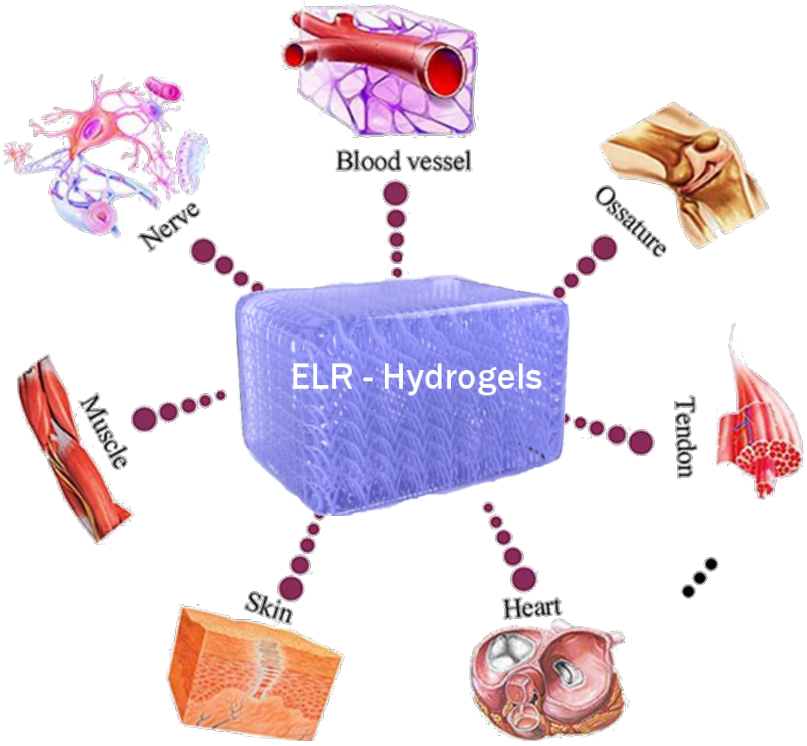

1. INTRODUCTION

1.1. Elastin-like recombinamers

The prerequisites for the use of materials in tissue regeneration include biocompatibility and bioactivity. As such, elastin-like recombinamers (ELRs), which are novel biomaterials inspired by elastin, a component of the natural extracellular matrix (ECM), meet both these requirements (1). Elastin is a fibrous and insoluble protein that constitutes one of the most important structural and functional components of the ECM, allowing for high deformations without damage (2). It is abundant in the lungs (3-7%), skin (2-3%), blood vessels (28-32%) and elastic ligaments (50%) (3), where its elastic properties are essential. Elastin, the main function of which is to provide elasticity to organs and tissues, is an excellent example of how all the properties displayed by biological materials and systems are determined exclusively by the physicochemical properties of the monomers and their sequence (4, 5). Indeed, a single repeated pentapeptide sequence has been shown to be responsible for the elastic behavior in elastin and, as such, forms the basis of all ELRs (6, 12).

The most widely studied pentapeptide is (VPGXaaG), namely poly(Val-Pro-Gly-Val-Gly), where Xaa is any natural amino acid except proline. All functional ELRs present a reversible lower critical solution temperature (LCST) in aqueous solution with sharp responsiveness (13). According to Urry's model, the polymer chains fold hydrophobically and undergo a conformational transition that leads to phase separation above this temperature (14, 15). It has been proven that the amino acid sequence has a significant influence on the LCST of ELRs (16). Thus, substitutions of the amino acid at the fourth position (Xaa) of the pentamer modify the LCST to an extent that depends on the polarity of the amino acid side-chain. The transition temperature of an ELR sequence based on $(VPGXG)_n$ can be controlled and adjusted to the desired applications by varying Xaa (hydrophobic AAs decrease T_t and hydrophilic AAs increase it) (16), the segment length *n* (longer ELR sequences have a lower T_t) (17, 18), concentration (higher ELR concentrations decrease T_t) (17), pH (19) and salt concentration in the selected solvent (20-22).

Biotechnology provides us with a powerful set of tools, such as recombinant DNA design (23), that can be used to successfully control the physicochemical features of the amino

acid side-chains and their association (24, 25), or to include any protein-based functionality, such as protease active sites, which become important when degradation of the scaffold has to be adjusted to the growth rate of new tissue (26).

1.2. Mechanisms to form ELR matrices for tissue-engineering applications

The predominant matrices for tissue regeneration, which were also the first to be applied in humans (27), are hydrogels. Indeed, due to their high water content, resemblance to natural tissue, biocompatibility and stimuli-responsiveness, these compounds have attracted increasing interest in the last 40 years (28, 29). However, as traditional methods of hydrogel synthesis lack an exact control over cross-linking points, chain length and sequence, the resulting three-dimensional structure may contain defects that can impair the mechanical properties of the material (30). These problems have been addressed by the development of novel polypeptide-based responsive hydrogels, including block-copolypeptides (31), or recombinant co-polypeptides flanked by two coiled-coil blocks (32, 33) and recombinant segments of elastin, silk and collagen (34-36).

The integration of crosslinking motifs that lead to a stable hydrogel is a prerequisite for the formation of ECM-like matrices from ELRs. This crosslinking can be of either a physical or a covalent nature, with the possible cross-linking mechanisms being as versatile as the ELRs themselves, ranging from ionic and hydrophobic interactions and the reaction of complementary groups to bioinspired protein crosslinks (37, 38).

ELRs have the potential to form a material that is both biocompatible and has specific mechanical properties, and can also interact with the body to improve the natural regeneration of tissue. Although the repetitive ELR pentapeptide (VPGXG) itself does not facilitate adhesion, its extraordinary design means that adhesive (RGD) (39, 40) and degradation sequences (41, 42), as well as sequences that allow the inclusion of temperature-related or biological triggers, can readily be integrated (43-45). All these strategies can provide very close control over the length and molecular weight of the proteins by careful selection of the crosslinking sites, which usually correspond to the lysine groups (46, 47).

1.3. Physically Cross-linked ELR Hydrogels

Several strategies can be applied to prepare physically crosslinked ELR hydrogels. Some of the most popular are described below.

1.3.1. Crosslinking via ionic interactions

Ionic crosslinking motifs are based on ELR segments of opposite charge, or the introduction of groups that can chelate multivalent cations into the ELR backbone, which can be further controlled by varying the salt concentration.

Peptide sequences with alternating charges and with complementary ionic sites have been shown to perform well in physical crosslinking. Such sequences are classified into different moduli, depending on the size of the equally charged ionic blocks (1-4 amino acids): modulus I, – + – + – + –+; modulus II, – – + + – – + +; modulus III – – – + + +; and modulus IV – – – – + + + +. A modulus I sequence reported by Holmes *et al.* (48) exhibited salt-induced in situ gelation (49). Ion complexation is obtained by including glutamic and aspartic acid residues in the ELR sequence accompanied by the addition of Ca^{2+} ions. The resulting hydrogels can be stabilized at room temperature and at physiological pH (50) and are sensitive to chelating agents, which reduces the number of accessible Ca^{2+} ions. Another approach by Yeo *et al.* (51) involved the addition of monosaccharides to the side chains of the ELRs, thus allowing them to form stable complexes with potassium. Furthermore, ELR/chitosan blends have been shown to form stable films in the presence of sodium ions (52).

1.3.2. Self-assembly of amphiphilic blocks and graft copolymers

Hydrogels can be obtained by aggregation between the hydrophobic segments of multi-block ELR copolymers. The hydrophobic functionalities are provided by alkyl-rich amino acids such as alanine (Ala), leucine (Leu), isoleucine (Ile), valine (Val), phenylalanine (Phe), tryptophan (Thp), tyrosine (Tyr) or methionine (Met). The resulting amphiphilic blocks have been shown to be stable *in vivo* (36, 53, 54). Furthermore, it is common to find protein polymers characterized by alternating blocks of essentially hydrophilic and essentially hydrophobic amino acids. The presence of chemically distinct segments within the same protein chain causes a mutual repulsion between the different blocks, which

tend to segregate. However, this segregation is constrained by the “forced cohabitation” of these blocks within the same molecule. As a result, they simply separate into different domains, thereby forming periodic nanostructures (55).

1.3.3. Intermolecular interaction of secondary protein structures

Structure design offers the possibility to include almost any sequence that is able to form intramolecular interactions via secondary structures into the ELR backbone using a recombinant approach. The limiting factors in this approach are the need to retain the ELR temperature transition and the fact that complex folding might not occur.

One bioinspired approach involved the inclusion of natural silk sequences that are known to form intramolecular beta-sheets which self-assemble into crystalline regions and have unique mechanical properties (56-60). These silk-based materials can be used to form a variety of structures, such as hydrogels, films, 3D porous matrices and submicron to macroscale fibers (61). Furthermore, silk scaffolds have been proven to be biocompatible and to perform well in vivo (62-64). As regards the silkworm (*Bombyx mori*), the repetitive hydrophobic sequence GAGAGS has been shown to be responsible for the strength of silk fibers (65). These blocks are stabilized by hydrophilic compartments in the protein and a complex mixture of stabilizing proteins (66). Fernandéz-Colino *et al.* have shown that the GAGAGS sequence can be successfully integrated into an ELR, thereby facilitating in situ gelation of the material and its use as an injectable system (36).

A more complex crosslinking has been achieved by using coiled-coil induced oligomerization via leucine zipper motifs, which include sequences that are known to form well-defined secondary structures (67-69). Leucine zippers are characterized by heptad repeating peptide units that form a distorted α-helix, designated as “abcdefg”, where the “a” and “d” positions are occupied by hydrophobic residues such as leucine and “b”, “c”, “e”, “f” and “g” are usually of a hydrophilic nature (see Figure 1) (70). The oligomerization

of different α-helices is primarily driven by hydrophobic interactions (71-74), and partly by electrostatic interactions (75-77) and the number of heptad repeats (72, 78, 79).

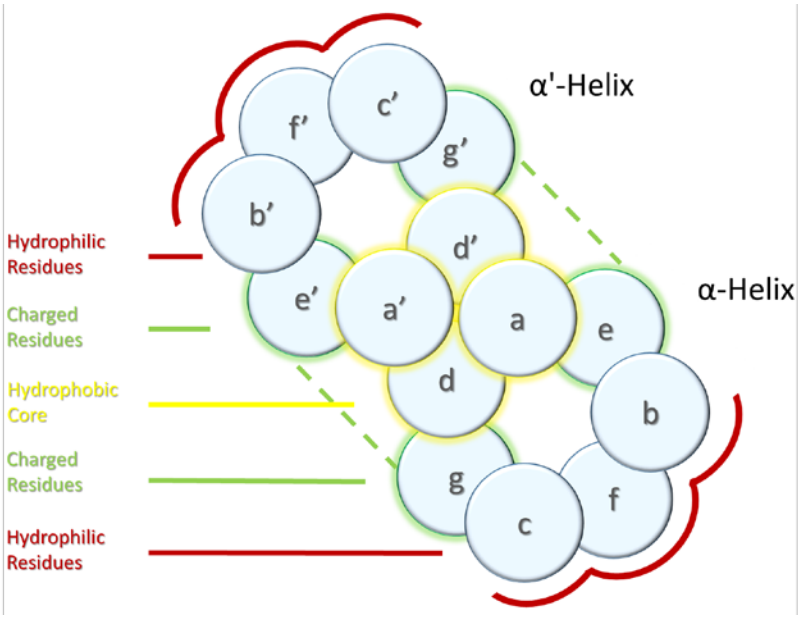

Figure 1. Hydrophobic interaction of two leucine zipper heptad units.

The potential extrapolation of these domains to the creation of bioinspired domains has been explored to a much lesser extent than in the case of their elastin or silk counterparts, thus meaning that fewer studies available concerning their biocompatibility are available. However, their human origin and the conserved nature of the sequence of these domains alleviate any concerns regarding their biocompatibility. To further support this notion, *in vivo* implantation of the leucine zipper based scaffolds in a mouse model was recently reported and no foreign body reaction to the scaffold was detected (80).

Protein-based physical crosslinks are ubiquitous in nature, therefore it can be assumed that those reported to date are merely the tip of the iceberg.

1.4. Functionalization of ELRs and covalent cross-linked ELR hydrogels

Post-translational modification of ELRs is obtained by reaction of the functional groups in the protein backbone. In ELRs, this can be facilitated by including active amino acids into the X position of the (VPGXG) sequence, thus maintaining the pH- and temperature-

sensitivity of the resulting ELRs (81, 82). These active amino acids facilitate both crosslinking reactions and chemical modifications. The concentration, molecular weight and lysine content of ELRs are key parameters in the hydrogel formation. Thus, below a critical concentration (83), the hydrogel network is not formed due to the lack of sufficient intermolecular contacts to allow a continuous entanglement of the ELR chains. Under these low concentration conditions, it is possible to form stable nanogels that already possess the thermal sensitivity found in the macroscopic ELR-based hydrogels (84). ELRs with a high number of potential crosslinking points are more prone to establishing a high number of intermolecular contacts that promote network formation. ELRs with a high lysine content are the most widely used in the preparation of hydrogel networks given the ability of the amino group on lysine to form covalent bonds between ELR chains. Furthermore, relevant features of the hydrogel, such as gelation time, network pore size, stiffness and degradability, can be closely controlled by varying the nature and concentration of the crosslinking agent. Labile chemical linkages that can be broken either enzymatically or chemically under physiological conditions can also be formed (85). Chemical crosslinking strategies have some important advantages. For instance, the covalent bonds avoid hydrogel network dilution and prevent components diffusing out from the site where the hydrogel is implanted. As a drawback, chemical crosslinking usually requires organic solvents and reagents that have to be exhaustively removed after synthesis of the network. To overcome this problem, click chemistry has been of growing interest for the formation of ELR-based networks in the past five years as this technique avoids the need for organic solvents (86, 87). In addition, it can be used to fuse ELRs with different bioactivities (88) or even to form hybrid ELR systems in an in situ gelation manner. This method has also been used to create non-thrombogenic stents (89).

Chemical crosslinking can be achieved using the following techniques: 1) radical polymerization (acrylates), 2) coupling of complementary groups (click reaction, Michael addition (90), condensation (91)), 3) high-energy irradiation (92), or 4) enzymatic crosslinking (transglutaminase) (93-95). Typical functionalization motifs include bioactive sequences with adhesion sites (such as RGD (96)), inhibitors, antibodies and anchor or signalling molecules.

Permanent or chemical hydrogels are covalently cross-linked networks that may contain clusters dispersed within regions of low crosslinking density and high water swelling. Free chain ends also cause defects in the gel and do not contribute to the elasticity of the networks. Both aqueous and organic media can be used to form ELR networks, with crosslinking in an organic solvent resulting in hydrogels with a more uniform structure due to the absence of transitions. Conversely, the behavior of ELR molecules in water is governed by the LCST (47). Some organic solvents, such as tris-succinimidyl aminotriacetate, can react with the lysine residues of different ELR chains to form a network. Crosslinking confers structural stability on the hydrogel, which is insoluble in water even upon cooling. Intermolecular crosslinks between proteins can also be obtained using genipin, as shown for an ELR/fibronectin hybrid (97).

2. IN VITRO CYTO- AND BIOCOMPATIBILITY OF ELRs

Biofunctional materials require advanced design and preparation in order to match the sophisticated recognition capabilities of biological systems. Moreover, in order to ensure the safety and effectiveness of devices containing these materials, it is fundamental to clearly understand their effects on surrounding tissues. Thus, materials are required to pass a toxicological test, known as a biocompatibility test, that takes into account the duration and type of tissue that it may come into contact with, along with all the functional requirements of the corresponding host response (98).

Any material proposed for use in biomedical applications must be biocompatible and highly pure as the contamination thereof with (globular) proteins that may provoke an immunological response is one of the most common factors precluding the use of biomaterials in such applications. However, it is also important to note that peptide-based materials are often touted as biocompatible in the absence of hard experimental evidence. Indeed, as noted by Chow *et al.* (5), there is no intrinsic reason for peptide-based materials to be biocompatible other than the somewhat naive notion that they must be, simply because they are composed of building blocks that are native to all organisms. As an important counterexample, it should be noted that many peptides and protein drugs are immunogenic, so the potential immunogenicity of all peptide-based materials must be considered, especially peptides that are “non-self”. In contrast to

classical materials, biocompatibility studies, especially innate immunity induction, cytotoxicity and fibrosis, are often lacking for many novel biomaterials, including recombinant protein-based materials, as has been extensively explored in the scientific literature.

ELRs have grown in popularity in the field of protein-inspired biomimetic materials and have found widespread uses in biomedical applications. These materials are playing an increasingly important role in a diverse range of applications such as drug delivery, tissue engineering, biosensors and a wide variety of "smart" systems. The great potential of ELRs in several biomedical applications is due to their ability to control and manipulate the interface between themselves and biological components, thus maintaining their biocompatibility.

Given their recombinant production in *Escherichia coli* bacteria, ELRs could be affected by a potential source of risks in terms of biocompatibility. In this regard, the standard analysis recommended by the American Society for Analysis of Materials for materials in contact with tissues and fluids has demonstrated the extraordinary biocompatibility of ELRs (99). As has already been described, ELRs don't provoke a. immunogenic response. In addition, given their biodegradability and biocompatibility for human tissue, tissue fluids, and blood, these polymers play a key role as carriers in delivery systems (99-101). ELRs used for tissue engineering have specific requirements in terms of biocompatibility that must be combined with topographic, chemical and viscoelastic patterns on materials to match proteins at the nanometer scale and cells at the micrometer scale. In this regard, numerous studies have clearly demonstrated both these requirements in *in vitro* experiments (102-104).

Additional findings corroborating the *in vivo* biocompatibility of ELRs have come from studies published by Rincon *et al*., who evaluated the cytotoxic effects of microparticles prepared from poly(VPAVG) and showed that the particles did not induce any cytotoxicity or inflammatory response after subcutaneous injection in rats. These authors also demonstrated intraocular tolerance after intravitreal injection into pigmented rabbits (105). Herrero-Vanrell *et al.* also observed a poor inflammatory response when they used poly(VPAVG) as a vehicle for intraocular drug-delivery systems (1). Other studies by Sallach *et al*., who developed a recombinant elastin-mimetic triblock copolymer in the

absence of either chemical or ionic crosslinking, showed a minimal inflammatory response and robust *in vivo* stability for periods exceeding one year, thereby further highlighting the high and extraordinary biocompatibility of ELRs (53). Similarly, Gonzalez *et al.* have shown the applicability of recently developed ELRs as a coating for vascular stents with the ultimate goal of producing a new endovascular device (89). The ELRs used to cover the stent supported full endothelialization in less than two weeks *in vitro* and showed high biocompatibility, physiological hemo-compatibility and a reduced response of the immune system. Other medium- and long-term viability studies have revealed a good cyto-compatibility with respect to several human primary cell types in both surface and 3D cultures (86). Furthermore, ELR molecules can be used to functionalize surfaces in order to obtain stronger and faster cell responses at the tissue–biomaterial interface, thus promoting better implant integration than functionalization with short peptides (106). For instance, functionalization of CoCr metallic surfaces with ELRs for cardiovascular applications may offer an efficient alternative to enhance rapid endothelialisation (107).

As noted above, the biocompatibility of these materials is of vital importance given their wide-ranging potential applications in biomedical fields such as regenerative medicine and tissue engineering. The cyto- and biocompatibility of ELRs, along with their interesting possibilities in terms of functionalization via recombinant DNA technology, make them ideal candidates for the development of scaffolds and advanced systems for applications in the biomedical field.

3. ELASTIN-LIKE RECOMBINAMERS FOR TISSUE-ENGINEERING APPLICATIONS

3.1. Osteochondral applications

Musculoskeletal disorders include more than 150 different diseases and syndromes, the majority of which are progressive and painful. Such disorders can be classified as joint diseases, physical disabilities, vertebral disorders and trauma-related conditions. The most affected joint is the knee, followed by the hip, ankle and shoulder, all of which, but especially the knee, are liable to suffer cartilage degeneration. Chondral and osteochondral injuries, both traumatic and non-traumatic, produced in the articular

cartilage of the knee and in other joints progress with time to degenerative osteoarthritis, which is usually treated by total replacement of the joint by a prosthesis (110). These incurable injuries entail disability, and all treatments applied to date to restore the articular surface are unsatisfactory.

The articular cartilage is formed by a matrix in which chondrocytes are embedded. This matrix is fundamentally made of various types of collagen (mainly type II) and proteoglycans (109). Articular hyaline cartilage, which covers the articular surfaces, is one of several types of cartilage (110). This cartilage is a highly specialized tissue characterized by its unique mechanical properties. It is a smooth layer, pearly bluish in colour, with a width of 2-4 mm, that is located between the bone and articular surface and has an extremely low friction coefficient due to its endurance to compression forces and elasticity. Articular hyaline cartilage has two main roles, namely to absorb the pressure overload at the articular surface and to allow the friction-less sliding of this surface (110-114). Mature articular hyaline cartilage has no vascular or lymphatic vessels or nerves, therefore (115) renewal of this matrix is very slow and the chondrocytes are usually dormant, with few mitoses. Furthermore, articular hyaline cartilage does not repair itself and regenerated cartilage is generally rich in type I collagen (fibro cartilage) instead of the type II collagen essential for the articular hyaline functional properties. This fibro cartilage is therefore unable to maintain the biomechanical characteristics of normal articular cartilage (116, 117).

Biomaterials play a fundamental role in the field of tissue engineering. There are several methods for obtaining biomaterials, the most common being by chemical reaction or purification from natural sources. In addition to these, recombinant DNA techniques have proven to be very powerful tools for the development of protein-based biomaterials, such as ELRs, over the last few decades (54). As mentioned previously, ELRs are able to self-assemble into different structures, such as hydrogels, and may find uses in biomedical applications (23, 118).

From another biological viewpoint, the development of novel tissue-engineering methods (119, 121) involving mesenchymal stromal cells (MSCs) (121, 122), which are pluripotent cells that can differentiate into diverse cell types (including chondrocytes and osteocytes)

and exert immunomodulatory properties, means that such methods are good candidates for the treatment of musculoskeletal lesions (123, 124).

For articular defect applications, the suspension of MSCs needs a scaffold as a cell-carrier in order to acquire a 3D structure that could be re-populated by these cells and to increase the persistence of the implanted cells at the injury site. Moreover, the hydrogels used as vehicles for MSCs should closely mimic the properties of the ECM and provide a cell-friendly environment that supports their regenerative potential.

As described previously, elastin-like recombinamers are based on a repetition of the VPGXG pentapeptide found in natural elastin, in which X can be any amino acid except proline. Given the elastin-like nature of the hydrogel and the high percentage of elastin present in the native chondral matrix, ELR-based hydrogels are likely to be similar to hyaline cartilage (125, 126). Furthermore, ELRs show thermo-sensitivity, thus meaning that it should be possible to form hydrogels that are stable at body temperature provided the transition temperature (T_t) of the ELR is lower than body temperature. In addition, as they are soluble at low temperatures, ELRs can be injected at low temperature and rapidly form a gel at physiological temperature, thereby representing a good candidate for use in arthroscopy to reduce the invasiveness of the treatment (Figure 2).

This remarkable property permits MSCs to be homogeneously embedded in the ELR solution at a temperature below T_t and to self-assemble into hydrogels above T_t, thus allowing the use of the cell-scaffold system in injectable therapies. Finally, in addition to the significant advantages of ELRs described in this chapter, they can also be designed to contain bioactive sequences, such as the well-known RGD cell-adhesion sequence from fibronectin, which promotes specific cell attachment via integrins (96), in order to achieve a bioactive scaffold that provides a cell-friendly environment, thereby improving the regenerative potential of hydrogel implantation.

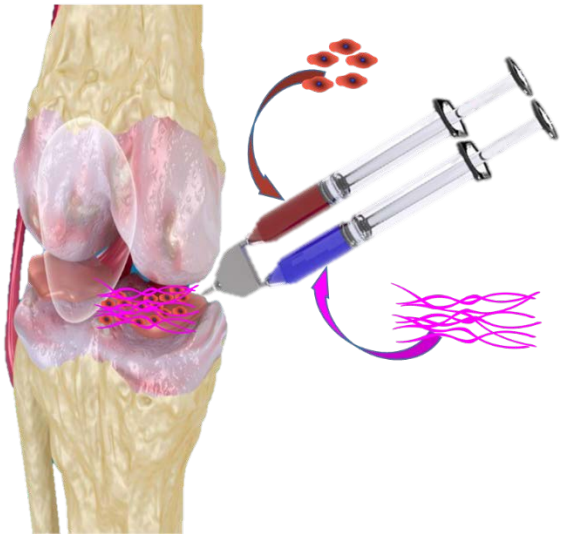

Figure 2. ELR-based injectable hydrogel for osteochondral applications

3.2. ELRs for (cardio-)vascular tissue regeneration

Elastin is an essential extracellular matrix protein in vascular tissue that plays an important biomechanical and biological signaling role. However, as native elastin is insoluble and is difficult to extract from tissues, its use for the manufacture of vascular tissue engineering scaffolds remains relatively rare. ELRs that mimic the structure and function of native tropoelastin represent a practical alternative to the native elastic fiber for vascular applications, especially in cardiovascular implants, where metal-based stents are known to cause in-stent restenosis (ISR) and late thrombosis diseases (107). The most common surgeries in cardiovascular disease are coronary angioplasty and stent insertion (127,128), with stent thrombosis (ST) and ISR being the main reasons for the failure of bare metal stents after implantation. This effect is decreased to less than 10% with the use of drug-eluting stents (DES), but remains critical (129), thus emphasizing the need for more efficient coatings. The coating of active ELRs containing adhesion sequences onto stent surfaces is one strategy for recovering a healthy endothelium. However, the bioactive sequences required to selectively promote endothelial growth remain unclear.

ELRs have been thoroughly investigated as biocompatible vasculogenic surface coatings (53), with smooth muscle cells (SMC) showing enhanced attachment and retention of their contractile phenotype on similar ELR-coated electrospun fibers (130). It has also been shown that ELR coatings are able to reduce blood platelet activation on synthetic

scaffolds (131), which delays the formation of healthy endothelium due to the need for anti-proliferative drugs and leads to late ST, thereby increasing the time patients are required to take anti-platelet therapy (132), thus addressing a negative side-effect of DES. Several studies have also demonstrated that stent surface endothelialization is suitable for inhibiting restenosis and thrombosis (107, 132-134). In addition, ELRs including endothelial adhesion sequences (REDV) have been shown to facilitate endothelialization of CoCr alloys by an early HUVEC cell-adhesion response (107). These findings indicate an involvement of elastin-laminin in the initial SMC/ELR contact (130).

de Torre *et al*. recently used catalyst-free click chemistry to cover stents by injection molding with an in situ gelating ELR system. Full endothelialization was obtained in a flow-controlled bioreactor and enabled by REDV and RGD sequences in less than two weeks. Minimal platelet adhesion and fibrin adsorption were detected and the ELR-coated stents exhibited mechanical stability even under high flow conditions (89). A more heterogeneous approach by Weber *et al*. involved generating tissue-engineered heart valves (TEHVs) by multi-step injection molding using an ELR as a hybrid system with fibrin (135). Conditioning of TEHVs in bioreactor systems is necessary to achieve an adequate ECM to withstand the mechanical loads in bodily circulation, with 3D printing (136) and orientated electrospinning (137) also being used in TEHVs to address the stress differences. Since heart valves are elaborate and highly complex structures in the circulatory system, the spatial diversity of this hybrid system was considered to meet the challenges raised by the structural and mechanical anisotropy and optimal function of such valves. Thus, different materials were used for the wall (fibrin) and leaflets (fibrin/ELR) to maintain the functionality of the TEHVs and to address the problems of poor elastogenesis in tissue-engineered constructs (135, 138), which is of particular importance for their long term durability (139).

In vivo studies of ELR-based scaffolds with leucine zipper motifs and RGD adhesion sites showed that they were able to support neovascularization without further growth factor treatment and an absence of immune responses, thereby underlining the potential of elastin-like materials for vascular tissue regeneration (80).

3.3. ELRs for ocular prostheses

Corneal wound healing requires cell adhesion and proliferation, both of which are mediated by the binding of epithelial membrane-bound integrins to substrate ligands, such as fibronectin. The secretion of fibronectin by corneal epithelial cells and stromal fibroblasts increases exponentially in the first steps of corneal wound healing (140).

However, the ocular surface, undamaged cornea and conjunctiva do not express elastin. Instead, a "diffusible factor" (141) secreted by the corneal epithelium has been implicated in maintaining the cellular and physiological homeostasis of the ocular surface. Several metalloproteinases (MMP) have been reported to be involved in pathological ocular processes such as dry eye (142) or conjunctivochalasis (143). As such, MMP-3 (Stromelysin 1), MMP-7 (Matrilysin 1), and MMP-9 (Gelatinase B), which are present at the ocular surface and are able to degrade elastin fibers (142), are potential candidates for Bruch's membrane prostheses. In this regard, Martínez-Osorio *et al*. (102) showed that an ELR blend containing four different types of building blocks was able to achieve an adequate balance of properties and to foster epithelial cell adhesion from human conjunctiva-derived primary cells. This ELR consisted of VPGIG, which has outstanding biocompatibility (99) and appropriate mechanical behaviour (144), a lysine-containing block (VPGKG) for crosslinking purposes, a CS5 human fibronectin REDV domain for efficient cell attachment (145) and an elastase target domain to enhance bioprocessing by naturally occurring enzymes. The resulting biomaterial maintained the growth, phenotype and functional characteristics of the primary cell line and did not exhibit any cytotoxicity. The performance of ELRs as ocular implants was further confirmed by Srivastasa *et al*. (146), who retained the efficiency of retinal pigment epithelial (RPE) cells and demonstrated that ELRs could be suitable carriers for the transplantation of autologous RPE cells for the treatment of age-related macular degeneration (AMD).

3.4. Other applications of ELRs

Even though the excellent and tunable mechanical properties and very low thrombogenicity of these materials make them excellent candidates for applications related to traumatology or cardiovascular diseases, ELRs also have a wide range of possibilities in the wider field of tissue engineering. As noted above, elastin-like

recombinamers are a novel peptide-based biomaterial, therefore their full potential remains to be explored. For instance, very few studies have been performed concerning the application of ELRs in neural injuries such as spinal cord injuries, traumatic brain injuries, or nerve transection. As an example, two studies have shown how surface-adsorbed recombinant protein can be used to modulate the behavior and differentiation of neuronal cells *in vitro* (147) and the biological activity of neurotrophin-ELR fusion proteins via *in vitro* culture models (148). As such, the potential applications of ELRs could be many and diverse. Indeed, they are currently being investigated for use in fields as disparate as diabetes treatment or *in vitro* fertilization.

4. CONCLUSIONS

This chapter has described elastin-like recombinamers, a family of novel protein peptide biomaterials obtained using recombinant DNA techniques. Moreover, ELRs meet all the prerequisites of biocompatibility and bioactivity for use in the field of tissue regeneration. Given that the predominant matrices for tissue regeneration are hydrogels, and that ELRs are able to self-assemble into different structures, including hydrogels, these biomaterials play a key role in the development of scaffolds and advanced systems for applications in the biomedical field.

As noted previously in this chapter, numerous techniques can be used to form different ELR matrices via physical or covalent crosslinking or by functionalization. Furthermore, the range of tissue-engineering applications for ELRs is very extensive, with recent studies having shown how different types of ELRs can be applied in the most challenging areas of tissue regeneration, such as cardiovascular, ocular prosthesis and osteochondral applications or even in nerve regeneration, diabetes and *in vitro* fertilization.

Finally, one of the greatest advantages of elastin-like recombinamers is that their biological and mechanical properties can be readily tailored at the genetic level to satisfy end-user applications, thus offering numerous choices for the development of cell-culture matrices for tissue engineering (149).

References

1. Herrero-Vanrell R, et al. Self-assembled particles of an elastin-like polymer as vehicles for controlled drug release. J Control Release 2005;102:113–22.

2. Debelle L, et al. The secondary structure and architecture of human elastin. Eur J Biochem 1998;258:533–9.

3. Uitto J. Biochemistry of the elastic fibers in normal connective tissues and its alterations in diseases. J Investig Dermatol 1979;72:1–10.

4. Nair LS, Laurencin CT. Biodegradable polymers as biomaterials. Prog Polym Sci 2007;32:762–98.

5. Chow D, Nunalee ML, Lim DW, Simnick AJ, Chilkoti A. Peptide-based biopolymers in biomedicine and biotechnology. Mater Sci Eng R Rep 2008;62:125–55.

6. Urry DW. Protein elasticity based on conformations of sequential polypeptides: the biological elastic fiber. J Protein Chem 1984;36.

7. Debelle L, Tamburro AM. Elastin: molecular description and function. Int J Biochem Cell Biol 1999;31:261–72.

8. Urry DW. Characterization of soluble peptides of elastin by physical techniques. Methods Enzymol 1982;82:673–716.

9. Khaled MA, Prasad KU, Venkatachalam CM, Urry DW. Nuclear magnetic resonance and conformational energy characterization of repeat peptides of elastin: the cyclohexadecapeptide, cycZo-(L-Val 1- ~ -Pro2-G1y3-G1y4)4. J Am Chem Soc 1985;107:7139–45.

10. Urry DW, Long MM, Harris RD, Prasad KU. Temperature-correlated force and structure development in elastomeric polypeptides: the Ile1 analog of the polypentapeptide of elastin. Biopolymers 1986;25:1939–53.

11. Tamburro AM, Guantieri V, Scopa A, Drabble JM. Polypeptide models of elastin: CD and NMR studies on synthetic poly(X-Gly-Gly). Chirality 1991;3:318–23.

12. Guantieri V, Tamburro AM, Cabrol D, Broch H, Vasilescu D. Conformational studies on models of collagen. Poly(Gly-Pro-Val), poly(Gly-Pro-Met), poly(Gly-Val-Pro) and poly(Gly-Met-Pro). Int J Pept Protein Res 2009;29:216–30.

13. Urry DW. Molecular machines: how motion and other functions of living organisms can result from reversible chemical changes. Angew Chem Int Ed 1993;32:819–41.

14. Urry DW, Trapane TL, Prasad KU. Phase-structure transitions of the elastin polypentapeptide-water system within the framework of composition-temperature studies. Biopolymers 1985;24:2345–56.

15. Manno M, et al. Interaction of processes on different length scales in a bioelastomer capable of performing energy conversion. Biopolymers 2001;59:51–64.

16. Ribeiro A, Arias FJ, Reguera J, Alonso M, Rodriguez-Cabello JC. Influence of the amino-acid sequence on the inverse temperature transition of elastin-like polymers. Biophys J 2009;97:312–20.

17. Meyer DE, Chilkoti A. Quantification of the effects of chain length and concentration on the thermal behavior of elastin-like polypeptides. Biomacromolecules 2004;5:846–51.

18. Girotti A, et al. Influence of the molecular weight on the inverse temperature transition of a model genetically engineered elastin-like pH-responsive polymer. Macromolecules 2004;37:3396–400.

19. Reguera J, Fahmi A, Moriarty P, Girotti A, Rodriguez-Cabello JC. Nanopore formation by self-assembly of the model genetically engineered elastin-like polymer $[(VPGVG)_2(VPGEG)(VPGVG)_2]_{15}$. J Am Chem Soc 2004;126:13212–3.

20. Cho Y, et al. Effects of hofmeister anions on the phase transition temperature of elastin-like polypeptides. J Phys Chem B 2008;112:13765–71.

21. Pinedo-martin G, Santos M, Testera AM, Alonso M, Rodriguez-cabello JC. The effect of NaCl on the self-assembly of elastin-like block co-recombinamers: tuning the size of micelles and vesicles. Polymer (Guildf) 2014;55:5314–21.

22. Luan C-H, Parker TM, Prasad KU, Urry DW. Differential scanning calorimetry studies of NaCl effect on the inverse temperature transition of some elastin-based polytetra-, polypenta-, and polynonapeptides. Biopolymers 1991;31:465–75.

23. Rodriguez-Cabello JC, Girotti A, Ribeiro A, Arias FJ. Synthesis of genetically engineered protein polymers (recombinamers) as an example of advanced self-assembled smart materials. In: Navarro M, Planell JA, editors. Nanotechnology in regenerative medicine: methods and protocols. Totowa, NJ: Humana Press; 2012. p. 17–38. https://doi.org/10.1007/978-1-61779-388-2_2.

24. Altunbas A, Pochan DJ. Peptide-based and polypeptide-based hydrogels for drug delivery and tissue engineering. Top Curr Chem 2012;310:135–67.

25. Hyde S. The language of shape: the role of curvature in condensed matter-physics, chemistry and biology. Amsterdam, Netherlands, New York: Elsevier; 1997. p. 87–140.

26. Liu X, Ma PX. Polymeric scaffolds for bone tissue engineering. Ann Biomed Eng 2004;32:477–86.

27. Kopecěk J. Hydrogel biomaterials: a smart future? Biomaterials 2007;28:5185–92.

28. Bonassar LJ, Vacanti CA. Tissue engineering: the first decade and beyond. J Cell Biochem 1998;72:297–303.

29. Hoffman AS. Hydrogels for biomedical applications. Adv Drug Deliv Rev 2002;54:3–12.

30. Kopeček J, Yang J. Hydrogels as smart biomaterials. Polym Int 2007;56:1078–98.

31. Nowak AP, et al. Rapidly recovering hydrogel scaffolds from self-assembling diblock copolypeptide amphiphiles. Nature 2002;417:424–8.

32. Xu C, Breedveld V, Kopecek J. Reversible hydrogels from self-assembling genetically engineered protein block copolymers. Biomacromolecules 2005;6:1739–49.

33. Petka WA, Harden JL, McGrath KP, Wirtz D, Tirrell DA. Reversible hydrogels from self-assembling artificial proteins. Science 1998;281:389–92.

34. Urry D, Physical W. Chemistry of biological free energy transduction as demonstrated by elastic protein-based polymers. J Phys Chem B 1997;101:11007–28.

35. Prince JT, McGrath KP, Carla DiGirolamo JM, Kaplana DL. Construction, cloning, and expression of synthetic genes encoding spider dragline silk. Biochemistry 1995;34:10879–85.

36. Fernadez-Colino A, Arias FJ, Alonso M, Rodriguez-Cabello JC, Bioforge GIR. Selforganized ECM-mimetic model based on an amphiphilic multiblock silk-elastin-like corecombinamer with a concomitant dual physical gelation process. Biomacromolecules 2014;15:3781–93.

37. Campoccia D, et al. Semisynthetic resorbable materials from hyaluronan esterification. Biomaterials 1998;19:2101–27.

38. Prestwich GD, Marecak DM, Marecek JF, Vercruysse KP, Ziebell MR. Controlled chemical modification of hyaluronic acid: synthesis, applications, and biodegradation of hydrazide derivatives. J Control Release 1998;53:93–103.

39. Urry DW, et al. Elastic protein-based polymers in soft tissue augmentation and generation. J Biomater Sci Polym Ed 1998;9:1015–48.

40. Nicol A, Channe Gowda D, Urry DW. Cell adhesion and growth on synthetic elastomeric matrices containing ARG-GLY-ASP-SER-3. J Biomed Mater Res 1992;26:393–413.

41. Alix AJ. A turning point in the knowledge of the structure-function-activity relations of elastin. J Soc Biol 2001;195:181–93.

42. Girotti A, et al. Design and bioproduction of a recombinant multi(bio)functional elastin-like protein polymer containing cell adhesion sequences for tissue engineering purposes. J Mater Sci Mater Med 2004;15:479–84.

43. Miyata T, Asami N, Uragami T. A reversibly antigen-responsive hydrogel. Nature 1999;399:766–9.

44. Wang C, Kopecek J, Stewart RJ. Hybrid hydrogels cross-linked by genetically engineered coiled-coil block proteins. Biomacromolecules 2001;2:912–20.

45. Ulbrich K, Strohalm J, Kopecek J. Polymers containing enzymatically degradable bonds. VI hydrophilic gels cleavable by chymotrypsin. Biomaterials 1982;3:150–4.

46. McMillan RA, Conticello VP. Synthesis and characterization of elastin-mimetic protein gels derived from a well-defined polypeptide precursor. Macromolecules 2000;33:4809–21.

47. McMillan RA, Caran KL, Apkarian RP, Conticello VP. High-resolution topographic imaging of environmentally responsive, elastin-mimetic hydrogels. Macromolecules 1999;32:9067–70.

48. Holmes TC, de Lacalle S, Su X, Liu GS, Rich A, Zhang SG. Extensive neurite outgrowth and active synapse formation on self-assembling peptide scaffolds. Proc Natl Acad Sci USA 2000;97:6728–33.

49. Zhang S. Fabrication of novel biomaterials through molecular self-assembly. Nat Biotechnol 2003;21:1171–8.

50. Ozbas B, Kretsinger J, Rajagopal K, Schneider JP, Pochan DJ. Salt-triggered peptide folding and consequent self-assembly into hydrogels with tunable modulus. Macromolecules 2004;37:7331–7.

51. Yeo GC, Keeley FW, Weiss AS. Coacervation of tropoelastin. Adv Colloid Interface Sci 2011;167:94–103.

52. Costa RR, Custodio CA, Arias FJ, Rodriguez-Cabello JC, Mano JF. Layer-by-layer assembly of chitosan and recombinant biopolymers into biomimetic coatings with multiple stimuli-responsive properties. Small 2011;7:2640–9.

53. Sallach RE, et al. Long-term biostability of self-assembling protein polymers in the absence of covalent crosslinking. Biomaterials 2010;31:779–91.

54. Rodriguez-Cabello JC, et al. Emerging applications of multifunctional elastin-like recombinamers. Nanomedicine 2011;6:111–22.

55. Li M, Ober CK. Block copolymer patterns and templates. Mater Today 2006;9:30–9.

56. Asakura T, Yao J, Yamane T, Umemura K, Ulrich AS. Heterogeneous structure of silk fibers from Bombyx mori resolved by 13C solid-state NMR spectroscopy. J Am Chem Soc 2002;124:8794–5.

57. Takahashi Y, Gehoh M, Yuzuriha K. Structure refinement and diffuse streak scattering of silk (Bombyx mori). Int J Biol Macromol 1999;24:127–38.

58. Takahashi Y, Gehoh M, Yuzuriha K. Crystal structure of silk (Bombyx mori). J Polym Sci B Polym Phys 1991;29:889–91.

59. Shimura K, Kikuchi A, Ohtomo K, Katagata Y, Hyodo A. Studies on silk fibroin of Bombyx mori. I fractionation of fibroin prepared from the posterior silk gland. J Biochem 1976;80:693–702.

60. Omenetto FG, Kaplan DL. New opportunities for an ancient material. Science 2010;329:528–31.

61. Kundu B, Rajkhowa R, Kundu SC, Wang X. Silk fibroin biomaterials for tissue regenerations. Adv Drug Deliv Rev 2013;65:457–70.

62. Zhou J, et al. In vitro and in vivo degradation behavior of aqueous-derived electrospun silk fibroin scaffolds. Polym Degrad Stab 2010;95:1679–85.

63. Panilaitis B, et al. Macrophage responses to silk. Biomaterials 2003;24:3079–85.

64. Fan H, Liu H, Toh SL, Goh JCH. Anterior cruciate ligament regeneration using mesenchymal stem cells and silk scaffold in large animal model. Biomaterials 2009;30:4967–77.

65. Tanaka K, Inoue S, Mizuno S. Hydrophobic interaction of P25, containing Asn-linked oligosaccharide chains, with the H-L complex of silk fibroin produced by Bombyx mori. Insect Biochem Mol Biol 1999;29:269–76.

66. Hardy JG, Romer LM, Scheibel TR. Polymeric materials based on silk proteins. Polymer (Guildf) 2008;49:4309–27.

67. Vinson C, et al. Classification of human B-ZIP proteins based on dimerization properties. Mol Cell Biol 2002;22:6321–35.

68. Vinson CR, Sigler PB, McKnight SL. Scissors-grip model for DNA recognition by a family of leucine zipper proteins. Science 1989;246:911–6.

69. Abel T, Maniatis T. Action of leucine zippers. Nature 1989;341:24–5.

70. Woolfson D, The N. Design of coiled-coil structures and assemblies. Adv Protein Chem 2005;70:79–112.

71. Yang J, Xu C, Kopečkova P, Kopeček J. Hybrid hydrogels self-assembled from HPMA copolymers containing peptide grafts. Macromol Biosci 2006;6:201–9.

72. Harbury PB, Zhang T, Kim PS, Alber T. A switch between two-, three-, and four-stranded coiled coils in GCN4 leucine zipper mutants. Science 1993;262:1401–7.

73. Moitra J, Szilak L, Krylov D, Vinson C. Leucine is the most stabilizing aliphatic amino acid in the d position of a dimeric leucine zipper coiled coil. Biochemistry 1997;36:12567–73.

74. Tripet B, Wagschal K, Lavigne P, Mant CT, Hodges RS. Effects of side-chain characteristics on stability and oligomerization state of a de Novo-designed model coiled-coil: 20 amino acid substitutions in position ‘d’. J Mol Biol 2000;300:377–402.

75. Krylov D, Mikhailenko I, Vinson C. A thermodynamic scale for leucine zipper stability and dimerization specificity: e and g interhelical interactions. EMBO J 1994;13:2849–61.

76. Alber T. Structure of the leucine zipper. Curr Opin Genet Dev 1992;2:205–10.

77. Krylov D, Barchi J, Vinson C. Inter-helical interactions in the leucine zipper coiled coil dimer: ph and salt dependence of coupling energy between charged amino acids. J Mol Biol 1998;279:959–72.

78. Litowski JR, Hodges RS. Designing heterodimeric two-stranded α-helical coiledcoils: the effect of chain length on protein folding, stability and specificity. J Pept Res 2001;58:477–92.

79. De Crescenzo G, Litowski JR, Hodges RS, O'Connor-McCourt MD. Real-time monitoring of the interactions of two-stranded de novo designed coiled-coils: effect of chain length on the kinetic and thermodynamic constants of binding. Biochemistry 2003;42:1754.

80. Huang C-C, Ravindran S, Yin Z, George A. 3-D self-assembling leucine zipper hydrogel with tunable properties for tissue engineering. Biomaterials 2014;35:5316–26.

81. Rodriguez-Cabello JC, Reguera J, Girotti A, Alonso M, Testera AM. Developing functionality in elastin-like polymers by increasing their molecular complexity: the power of the genetic engineering approach. Prog Polym Sci 2005;30:1119–45.

82. Rodriguez-Cabello JC, Alonso A, Guiscardo L, Reboto V, Girotti A. Amplified photoresponse of ap-phenylazobenzene derivative of an elastin-like polymerbya-cyclodextrin: the amplified DTt mechanism. Adv Mater 2002;14:1151–4.

83. Trabbic-Carlson K, Setton LA, Chilkoti A. Swelling and mechanical behaviors of chemically cross-linked hydrogels of elastin-like polypeptides. Biomacromolecules 2003;4:572–80.

84. Gonzalez de Torre I, Quintanilla L, Pinedo-Martin G, Alonso M, Rodriguez-Cabello JC. Nanogel formation from dilute solutions of clickable elastin-like recombinamers and its dependence on temperature: two fractal gelation modes. ACS Appl Mater Interfaces 2014;6:14509–15.

85. Hennink W, van Nostrum C. Novel crosslinking methods to design hydrogels. Adv Drug Deliv Rev 2002;54:13–36.

86. Testera AM, et al. Biocompatible elastin-like click gels: design, synthesis and characterization. J Mater Sci Mater Med 2015;26:105.

87. Patterson J, Martino MM, Hubbell JA. Biomimetic materials in tissue engineering. Mater Today 2010;13:14–22.

88. Gonzalez de Torre I, et al. Elastin-like recombinamer catalyst-free click gels: characterization of poroelastic and intrinsic viscoelastic properties. Acta Biomater 2014;10:2495–505.

89. de Torre IG, et al. Elastin-like recombinamer-covered stents: towards a fully biocompatible and non-thrombogenic device for cardiovascular diseases. Acta Biomater 2015;12:146–55.

90. Hoare TR, Kohane DS. Hydrogels in drug delivery: progress and challenges. Polymer (Guildf) 2008;49:1993–2007.

91. De Nooy AEJ, Masci G, Crescenzi V. Versatile synthesis of polysaccharide hydrogels using the passerini and Ugi multicomponent condensations. Macromolecules 1999;32:1318–20.

92. Huglin MR. Hydrogels in medicine and pharmacy. Br Polym J 1989;21:184.

93. Garcia Y, et al. In vitro characterization of a collagen scaffold enzymatically cross-linked with a tailored elastin-like polymer. Tissue Eng A 2009;15:887–99.

94. Westhaus E, Messersmith PB. Triggered release of calcium from lipid vesicles: a bioinspired strategy for rapid gelation of polysaccharide and protein hydrogels. Biomaterials 2001;22:453–62.

95. Garcia Y, Collighan R, Griffin M, Pandit A. Assessment of cell viability in a three-dimensional enzymatically cross-linked collagen scaffold. J Mater Sci Mater Med 2007;18:1991–2001.

96. Ruoslahti E, Pierschbacher MD. Arg-Gly-Asp: a versatile cell recognition signal. Cell 1986;44:517–8.

97. Ravi S, Caves JM, Martinez AW, Haller CA, Chaikof EL. Incorporation of fibronectin to enhance cytocompatibility in multilayer elastin-like protein scaffolds for tissue engineering. J Biomed Mater Res A 2013;101A:1915–25.

98. Sivakumar R. On the relevance and requirements of biomaterials. Bull Mater Sci 1999;22:647–55.

99.Urry DW, Parker TM, Reid MC, Gowda DC. Biocompatibility of the bioelastic materials, poly(GVGVP) and its -irradiation cross-linked matrix: summary of generic biological test results. J Bioact Compat Polym 1991;6:263–82.

100. Ong SR, Trabbic-Carlson KA, Nettles DL, Lim DW, Chilkoti A, Setton LA. Epitope tagging for tracking elastin-like polypeptides. Biomaterials 2006;27:1930–5.

101. Garcia-Arevalo C, et al. Immunomodulatory nanoparticles from elastin-like recombinamers: single-molecules for tuberculosis vaccine development. Mol Pharm 2013;10:586–97.

102. Martinez-Osorio H, et al. Genetically engineered elastin-like polymer as a substratum to culture cells from the ocular surface. Curr Eye Res 2009;34:48–56.

103. Andrew MacKay J, et al. Self-assembling chimeric polypeptide–doxorubicin conjugate nanoparticles that abolish tumours after a single injection. Nat Mater 2009;8:993–9.

104. Garcia-Arevalo C, Pierna P, Girotti A, Arias FJ, Rodriguez-Cabello JC. A comparative study of cell behavior on different energetic and bioactive polymeric surfaces made from elastin-like recombinamers. Soft Matter 2012;8:3239.

105. Rincon AC, et al. Biocompatibility of elastin-like polymer poly(VPAVG) microparticles: *in vitro* and *in vivo* studies. J Biomed Mater Res A 2006;78A:343–51.

106. Punet X, et al. Biomolecular functionalization for enhanced cell-material interactions of poly(methyl methacrylate) surfaces. Regen Biomater 2015;2:167–75.

107. Castellanos MI, et al. Biofunctionalization of REDV elastin-like recombinamers improves endothelialization on CoCr alloy surfaces for cardiovascular applications. Colloids Surf B: Biointerfaces 2015;127:22–32.

108. Guillen P. El condrocito, una oportunidad terapeutica en traumatologia y cirugia ortopedica, Edt, clinica CEMTRO; 2013.

109. Mankin HJ. The response of articular cartilage to mechanical injury. J Bone Joint Surg Am 1982;64:460–6.

110. Jimenez Collado J, Guillen Garcia P, Sobrado Perez J. Rodilla: morfogenesis, anatomía aplicada vias de acceso the knee: morphogenesis, applied anatomy, approach routes. Ed MAPFRE. 1994. p. 1–416. ISBN: 9788471009623.

111. Altman RD, Lozada CJ. Practice guidelines in the management of osteoarthritis. Osteoarthr Cartil 1998;6:22–4.

112. Chevalier X, Richette P. Cartilago articular normal: anatomia, fisiologia, metabolismo y envejecimiento. EMC—Apar Locomot 2005;38:1–13.

113. Sharma A, Wood LD, Richardson JB, Roberts S, Kuiper NJ. Glycosaminoglycan profiles of repair tissue formed following autologous chondrocyte implantation differ from control cartilage. Arthritis Res Ther 2007;9:R79.

114. Miller MD, Thompson SR, Hart J. In: Review of orthopaedics. 7th ed. Elsevier; 2015. p. 904. ISBN 9780323355179.

115. Vega Alvarez JA, Garcia-Suarez O, Fernandez Monjil D, del Valle Soto ME. Bioquimica y biologia del cartilago articular. Rev Esp Cir Ortop Traumatol 2002;46:391–400.

116. Guielen Garcia P. Medicina Celular en las lesiones del sistema muscolo esquelético (Deporte). (Celulas para curar). An R Acad Nac Med (Madr) 2010;CXXVII:171–83.

117. Peterson L. Articular cartilage regeneration: chondrocyte transplantation and other technologies. In: Annual meeting of the American Academy of Orthopaedic Surgeons; 1997.

118. Girotti A, Orbanic D, Ibanez-Fonseca A, Gonzalez-Obeso C, Rodriguez-Cabello JC. Recombinant technology in the development of materials and systems for soft-tissue repair. Adv Healthc Mater 2015;4:2423–55.

119. Kerker JT, Leo AJ, Sgaglione NA. Cartilage repair: synthetics and scaffolds. Sports Med Arthrosc Rev 2008;16:208–16.

120. Vaquero J, Forriol F. Knee chondral injuries: clinical treatment strategies and experimental models. Injury 2012;43:694–705.

121. Vijayan S, et al. Autologous chondrocyte implantation for osteochondral lesions in the knee using a bilayer collagen membrane and bone graft: a two- to eight-year follow-up study. J Bone Joint Surg (Br) 2012;94:488–92.

122. Trattnig S, et al. Matrix-based autologous chondrocyte implantation for cartilage repair: noninvasive monitoring by high-resolution magnetic resonance imaging. Magn Reson Imaging 2005;23:779–87.

123. Kessler MW, Ackerman G, Dines JS, Grande D. Emerging technologies and fourth generation issues in cartilage repair. Sports Med Arthrosc Rev 2008;16:246–54.

124. Chen FH, Rousche KT, Tuan RS. Technology insight: adult stem cells in cartilage regeneration and tissue engineering. Nat Clin Pract Rheumatol 2006;2:373–82.

125. Kinikoglu B, Rodriguez-Cabello JC, Damour O, Hasirci V. A smart bilayer scaffold of elastin-like recombinamer and collagen for soft tissue engineering. J Mater Sci Mater Med 2011;22:1541–54.

126. Kinikoglu B, Rodriguez-Cabello JC, Damour O, Hasirci V. The influence of elastin-like recombinant polymer on the self-renewing potential of a 3D tissue equivalent derived from human lamina propria fibroblasts and oral epithelial cells. Biomaterials 2011;32:5756–64.

127. Palmaz JC. Intravascular stents in the last and the next 10 years. J Endovasc Ther 2004;11(Suppl. 2):II200–6.

128. Tan A, et al. Inception to actualization: next generation coronary stent coatings incorporating nanotechnology. J Biotechnol 2013;164:151–70.

129. Busch R, et al. New stent surface materials: the impact of polymer-dependent interactions of human endothelial cells, smooth muscle cells, and platelets. Acta Biomater 2014;10:688–700.

130. Blit PH, Battiston KG, Yang M, Paul Santerre J, Woodhouse KA. Electrospun elastin-like polypeptide enriched polyurethanes and their interactions with vascular smooth muscle cells. Acta Biomater 2012;8:2493–503.

131. Blit PH, McClung WG, Brash JL, Woodhouse KA, Santerre JP. Platelet inhibition and endothelial cell adhesion on elastin-like polypeptide surface modified materials. Biomaterials 2011;32:5790–800.

132. Wei Y, et al. Surface engineering of cardiovascular stent with endothelial cell selectivity for in vivo re-endothelialisation. Biomaterials 2013;34:2588–99.

133. Melo LG, et al. Endothelium-targeted gene and cell-based therapies for cardiovascular disease. Arterioscler Thromb Vasc Biol 1761; 2004.

134. Inoue T, et al. Vascular inflammation and repair: implications for re-endothelialization, restenosis, and stent thrombosis. JACC Cardiovasc Interv 2011;4:1057–66.

135. Weber M, et al. Multiple-step injection molding for fibrin-based tissue-engineered heart valves. Tissue Eng Part C Methods 2015;21:832–40.

136. Hockaday LA, et al. Rapid 3D printing of anatomically accurate and mechanically heterogeneous aortic valve hydrogel scaffolds. Biofabrication 2012;4:035005.

137. Courtney T, Sacks MS, Stankus J, Guan J, Wagner WR. Design and analysis of tissue engineering scaffolds that mimic soft tissue mechanical anisotropy. Biomaterials 2006;27:3631–8.

138. Patel A, et al. Elastin biosynthesis: the missing link in tissue-engineered blood vessels. Cardiovasc Res 2006;71:40–9.

139. Vesely I. The role of elastin in aortic valve mechanics. J Biomech 1997;31:115–23.

140. Fujikawa LS, Foster CS, Harrist TJ, Lanigan JM, Colvin RB. Fibronectin in healing rabbit corneal wounds. Lab Invest 1981;45:120–9.

141. Isnard N, Thevenin D, Robert L, Renard G. Tropoelastin biosynthesis by corneal cells. Ophthalmologica 2003;218:36–42.

142. Bian F, et al. Desiccating stress-induced MMP production and activity worsens wound healing in alkali-burned corneas. Invest Ophthalmol Vis Sci 2015;56:4908–18.

143. Meller D, Li D, Tseng SCG. Regulation of collagenase, stromelysin, and gelatinase B in human conjunctival and conjunctivochalasis fibroblasts by interleukin-1β and tumor necrosis factor-α. Invest Ophthalmol Vis Sci 2000;41:225–2929.

144. Di Zio K, Tirrell DA. Mechanical properties of artificial protein matrices engineered for control of cell and tissue behavior. Macromolecules 2003;36:1553–8.

145. Panitch A, Yamaoka T, Fournier MJ, Mason TL, Tirrell DA. Design and biosynthesis of elastin-like artificial extracellular matrix proteins containing periodically spaced fibronectin CS5 domains. Macromolecules 1999;32:1701–3.

146. Srivastava GK, et al. Elastin-like recombinamers as substrates for retinal pigment epithelial cell growth. J Biomed Mater Res A 2011;97A:243–50.

147. Jeon W, et al. Functional enhancement of neuronal cell behaviors and differentiation by elastin-mimetic recombinant protein presenting Arg-Gly-Asp peptides. BMC Biotechnol 2012;12:61.

148. Johnson T, Koria P. Expression and purification of neurotrophin-elastin-like peptide fusion proteins for neural regeneration. BioDrugs 2016;30:117–27.

149. Mie M, Mizushima Y, Kobatake E. Novel extracellular matrix for cell sheet recovery using genetically engineered elastin-like protein. J Biomed Mater Res B Appl Biomater 2008;86B:283–90.

PLANNING OF RESEARCH

In order to address the objectives of this Thesis, several ELRs have been designed and produced. In Table 1 it is reported the amino acid sequence of each ELR, which has a specific composition comprising bioactive sequences. Moreover, in Figure 1 it is reported a scheme of all the ELRs, where the coloured blocks represent the disposition of the bioactive domains of each ELR.

Code	Name	Sequence	MW (Da)
A	$(EIS)_2$-$(I_5R)_6$	MESLLP-{[$(VPGVG)_2$-VPGEG-$(VPGVG)_2$]$_{10}$-$(VGIPG)_{60}$-[V$(GAGAGSG)_5$]$_2$G}-[$(VPGIG)_5$-AVTGRGDSPASS]$_6$V	121012
B	VKVx24	MESLLP-VGVPGVG [VPGKG$(VPGVG)_5$]$_{23}$VPGKGVPGVGVPGVGVPGVGVPGV	60451
C	$HRGD_6$	MGSSHHHHHHSSGLVPRGSHMESLLP-{[$(VPGIG)_2$-(VPGKG)-$(VPGIG)_2$]$_2$-AVTGRGDSPASS-[$(VPGIG)_2$-(VPGKG)-$(VPGIG)_2$]$_2$}$_6$V	60660
D	REDV	MESLLP-[$(VPGIG)_2$VPGKG$(VPGIG)_2$EEIQIGHIPREDVDYHLYP$(VPGIG)_2$VPGKG$(VPGIG)_2$$(VGVAPG)_3$]$_{10}$V	80813
E	TI	MESLLP-[(VDLDVPIPGRFDRRVSVAAE$(VGIPG)_{10}$]$_{10}$V	65075
F	TR	MESLLP-[(VDLDVPIPGRFDRRVSVAAE$(VGIPG)_{10}$]$_{10}$VETAAAKFERQHMDSSTSAASSSNYCNQMMKSRNLTKDRCKPVNTFVHESLADVQAVCSQKNVACKNGQTNCYQSYSTMSITDCRETGSSKYPNCAYKTTQANKHIIVACEGNPYVPVHFDASV	78618

G	RT	MESLLP- VETAAAKFERQHMDSSTSAASSSNYCNQMMKSRNLTKDRCKPV NTFVHESLADVQAVCSQKNVACKNGQTNCYQSYSTMSITDCRET GSSKYPNCAYKTTQANKHIIVACEGNPYVPVHFDAS- [(VDLDVPIPGRFDRRVSVAAE(VGIPG)$_{10}$]$_{10}$V	78618
H	TRT	MESLLP- [(VDLDVPIPGRFDRRVSVAAE(VGIPG)$_{10}$]$_5$VETAAAKFERQHMDS STSAASSSNYCNQMMKSRNLTKDRCKPVNTFVHESLADVQAVCS QKNVACKNGQTNCYQSYSTMSITDCRETGSSKYPNCAYKTTQAN KHIIVACEGNPYVPVHFDAS- [(VDLDVPIPGRFDRRVSVAAE(VGIPG)$_{10}$]$_5$V	78618

Table 1. ELRs used during the Thesis. Coloured sequences correspond to bioactive sequences as represented in Figure 1.

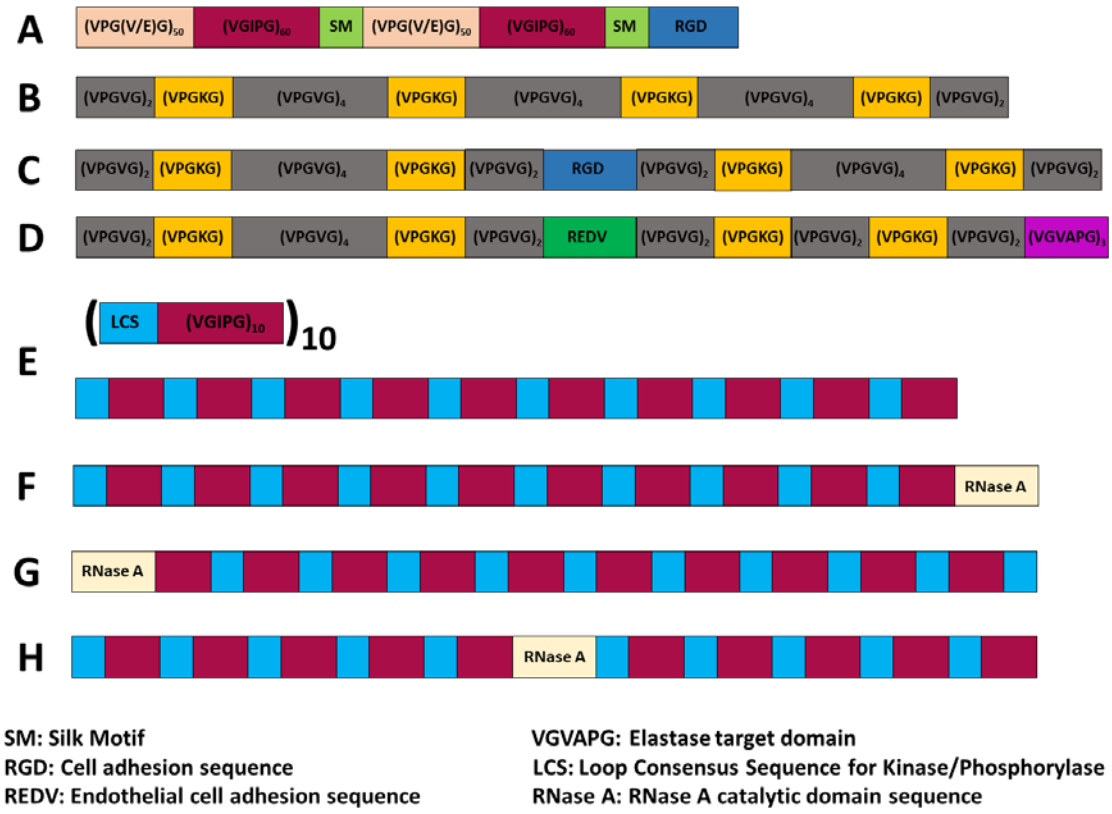

Figure 1. Scheme of all the ELRs used during the Thesis.

ELR **A** has been used in Chapter 3; ELR **B** has been used in Chapter 4 and Chapter 5; ELRs **C** and **D** have been used in Chapter 4; ELRs **E, F, G** and **H** have been used in Chapter 6. All the ELRs have been produced and characterized according to the following methods.

ELR biosynthesis and purification

The gene construction was performed by molecular biology and recombinant DNA technique following standard methods previously described (1, 2). Briefly, the genes encoding the different polypeptides, both ELR and bioactive sequences are synthesized by an external service (NZYTech), and cloned in the pDriveAll plasmid. For the molecular cloning steps, they were used two restriction enzymes without interruptions ("seamless cloning"): EarI and SapI (Thermo Scientific). These two restriction enzymes are type IIS that have endonuclease activity on a sequence contiguous to the recognition, so they are optimal for this type of cloning. Once the final gene construct was obtained, it was extracted from the cloning plasmid and a subcloning was carried out in the expression plasmid pET7, resulting from different modifications on the commercial vector pET-25b

(+) (Novagen). Subsequently, this plasmid was used to transform expression strains of *Escherichia coli*, in particular BLR (DE3) (Novagen). BLR strain was cultured in a 15 L bioreactor (Applikon Biotechnology) under controlled conditions of pH, temperature, agitation and O_2 concentration, in order to guarantee a correct bioproduction of the different ELRs. Subsequently, the bacterial cells were disrupted by a mechanical process (disruption model: TS 0.75KW, Constant Systems). Moreover, the ELRs were purified from the rest of cellular content taking advantage of their thermo-sensitivity; the purification process was carried out by several centrifugations preceded by inverse transition cycling (3). The pure ELRs were finally obtained, they were dialyzed and filtered through 0.22 µm filters (Nalgene) to achieve sterile ELR solutions which were then lyophilized (FreeZone 1, LABCONCO) for a better long term preservation.

Physical - Chemical characterization of ELRs

Analysis of the level of endotoxins

The level of endotoxins was determined for all the ELRs used *in vivo* by the Limulus amebocyte lysate assay (LAL) with the Endosafe-PTS system (Charles River Laboratories). The Endosafe® cartridge technology is a fast and high sensitivity method to perform the analysis of the level of endotoxins (4). The cartridge technology eliminates a significant amount of the raw material and accessories required for traditional LAL methods. The cartridges are pre-loaded with all of the reagents required to perform a LAL test, eliminating the preparation of multiple reagents; thus only the ELRs solution was loaded for the endotoxins analysis. The endotoxin levels of the ELRs used for the *in vivo* experiments were measured, resulting in a maximum of 2 endotoxin units/mg ELR for the ELRs used at a lower concentration. ELRs used at higher concentrations (up to 300 mg / mL) contained less than 0.01 EU / mg ELR. Thus, even at the highest ELR concentrations, endotoxin levels remained below the limit set by the FDA (EU 20 / biomedical device).

Polyacrylamide gel electrophoresis with SDS (in denaturing conditions, SDS-PAGE)

SDS-PAGE (sodium dodecyl sulfate–polyacrylamide gel electrophoresis) is a variant of polyacrylamide gel electrophoresis, an analytical method for the separation of charged

molecules in mixtures by their molecular masses in an electric field. It uses sodium dodecyl sulfate (SDS) molecules to help identify and isolate protein molecules. SDS acts as a surfactant, covering the proteins' intrinsic charge and conferring them very similar charge-to-mass ratios. The electrophoresis in polyacrylamide gels with SDS (5), entails the denaturation of the proteins (ELRs in our case) and the homogeneous distribution of negative charge for a migration dependent on their size. Considering that the migration is not dependent by the charge of the ELR or by the folding of the protein, this methodology allows to know the molecular weight (MW) of the ELRs, as well as the level of purity and degradation thereof. In this Thesis, it was used the vertical electrophoresis system "MiniVE" of Hoefer (Amersham Pharmacia Biotec). For the analysis by electrophoresis, around 1 mg/mL of ELR were loaded, according to the size of the well. After the electrophoresis, the polyacrylamide gels were stained with a 0.3 M solution of copper chloride. This staining works in a negative way; indeed, it does not stain the proteins, but copper interacts electrostatically with the SDS that contains the gel itself. Thus, the area containing the proteins are unstained, which appear as dark bands (6). The images of the gels were taken with the Gel Logic 100 Imaging System (Eastman Kodak) and analyzed with the Kodak 1D Image Analysis (Eastman Kodak) program.

Mass Spectrometry (MALDI-TOF)

In mass spectrometry, matrix-assisted laser desorption/ionization (MALDI) is an ionization technique that uses a laser energy absorbing matrix to create ions from large molecules with minimal fragmentation (7). MALDI methodology is a three-step process (Figure 2). First, the sample is mixed with a suitable matrix material and applied to a metal plate. Second, a pulsed laser irradiates the sample, triggering ablation and desorption of the sample and matrix material. Finally, the analyte molecules are ionized by being protonated or deprotonated in the hot plume of ablated gases, and then they are accelerated towards the detector (8). The type of a mass spectrometer most widely used with MALDI is the TOF (time-of-flight mass spectrometer), mainly due to its large mass range. The TOF measurement procedure is also ideally suited to the MALDI ionization process since the pulsed laser takes individual 'shots' rather than working in continuous operation. Mass spectrometry of the type "Matrix-assisted laser desorption / ionization -

Time-of-flight" (MALDI-TOF) allows to know exactly the MW. It is more accurate than the SDS-PAGE technique, hence it can be considered complementary to it. Mass Spectrometry has been carried out in the Laboratory of Instrumental Techniques (LTI) of the University of Valladolid (UVa) in the MALDI-TOF Voyager STR (Applied Biosystems).

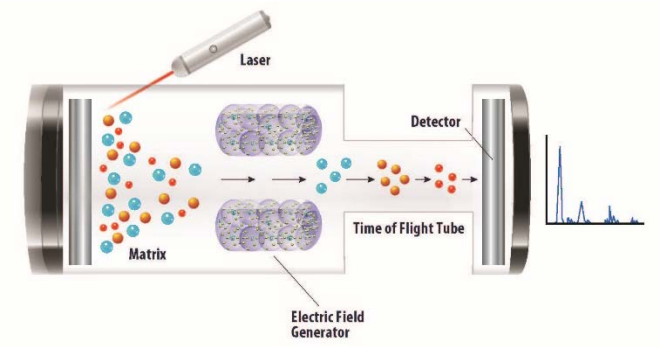

Figure 2. Schematic representation of the MALDI-TOF spectrometry.

Amino acid analysis (HPLC)

High-performance liquid chromatography (HPLC) is a technique used to separate, identify, and quantify each component in a mixture. It relies on pumps to pass a pressurized liquid solvent containing the sample mixture through a column filled with a solid adsorbent material. Each component in the sample interacts slightly differently with the adsorbent material, causing different flow rates for the different components and leading to the separation of the components as they flow out of the column. These interactions are physical in nature, such as hydrophobic (dispersive), dipole–dipole and ionic, most often a combination. HPLC is distinguished from traditional ("low pressure") liquid chromatography because operational pressures are significantly higher (50–350 bar), while ordinary liquid chromatography typically relies on the force of gravity to pass the mobile phase through the column. The analysis of ELR samples previously hydrolysed by "High-Performance Liquid Chromatography" (HPLC) allows to know the amino acid composition of the ELR molecules. First, ELR are hydrolyzed with 6M HCl, 1% phenol during 2.5 hours at 155˚C, and subsequently dried. Resulting powder is resuspended in 20mM HCl and diluted 1/10 for separation by HPLC. Quantification is done by comparing to standard patrons. A schematic representation of the process can be seen in Figure 3. This method has been carried out in the LTI of the UVa with the Waters 600 gradient HPLC equipment coupled to a Waters 2487 UV detector (Waters).

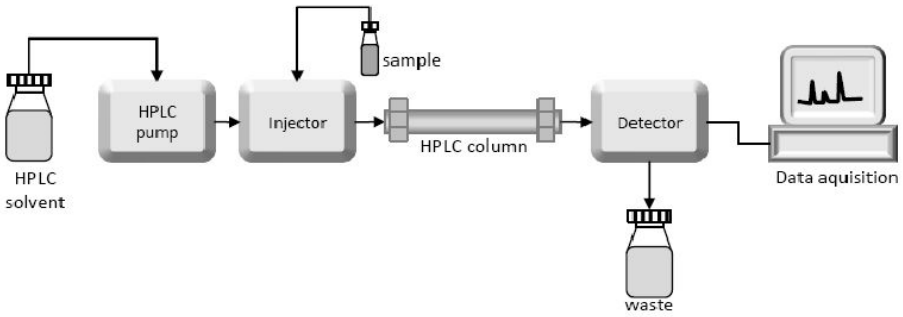

Figure 3. Schematic representation of the experimental set for amino acid analysis.

Differential Scanning Calorimetry (DSC)

Differential scanning calorimetry, or DSC is a thermoanalytical technique in which the difference in the amount of heat required to increase the temperature of a sample and reference is measured as a function of temperature. Both the sample and reference are maintained at the same temperature throughout the experiment. In our case, the sample is the ELR solution dissolved in milliQ water or in saline solution, whereas the reference is the corresponding solution without the ELR. In this Thesis, DSC analysis has been used to measure the T_t of the ELRs. The basic principle underlying this technique is that when the sample undergoes a physical transformation such as phase transitions, more or less heat will need to flow to it than the reference to maintain both at the same temperature. Whether less or more heat must flow to the sample depends on whether the process is exothermic or endothermic. When a phase change or transition occurs, if the amount of heat necessary to be supplied to the ELR solution to increase the temperature is greater than the reference, then it is an endothermic process. This means that the process consumes part of the energy supplied to the system during the transition. The ELRs were dissolved at 50 mg/mL in milliQ water or in PBS, the T_t was measured at different pH values. The experimental procedure consisted of a first isothermal stage at 0 °C for 10 minutes, followed by a heating step, from 0 to 60 °C, at a speed of 5 °C / min.

Fourier Transform Infrared Spectroscopy (FTIR)

Fourier-transform infrared spectroscopy (FTIR) is a technique that can be used to obtain information about the functional groups of the sample analyzed. The theory behind the technique resides in measuring how much light a sample absorbs at each wavelength. The molecules absorb specific frequencies that are characteristic of their structure. Fourier-transform spectroscopy shines a beam containing many frequencies of light at once and measures how much of that beam is absorbed by the sample. Next, the beam is modified to contain a different combination of frequencies, giving a second data point. This process is rapidly repeated many times over a short timespan. When the frequency of the IR is the same as the vibrational frequency of a bond, the absorption occurs. Afterwards, a computer takes all this data and the examination of the transmitted light reveals how much energy was absorbed at each frequency (or wavelength) revealing the presence of a certain chemical structure. In our case, the pure ELRs in the dry state were analyzed with a Bruker FTIR spectrophotometer (Bruker, USA). For each spectrum, a 512-scan interferogram was collected at single beam absorption mode with a 2 cm-1 resolution within the 4000 - 600 cm-1 region. For each sample, several FTIR absorption spectra were collected. Five measurements were averaged to obtain the final FTIR absorption spectrum of the sample. Residual water vapour absorption was interactively subtracted from the sample spectra. Finally, the spectral calculations were performed by the OPUS (version 4.2) software (MATTSON INSTRUMENT, INC.).

Proton nuclear magnetic resonance ^{1}H-NMR Spectroscopy

Proton nuclear magnetic resonance (^{1}H-NMR) is the application of nuclear magnetic resonance in NMR spectroscopy with respect to hydrogen-1 nuclei within the molecules of a substance, in order to determine the structure of its molecules (9). Nuclear magnetic resonance spectroscopy (NMR) studies the behaviour of certain atomic nuclei in the presence of an external magnetic field. When an atomic nucleus with non-zero total angular momentum is placed in an external electromagnetic field, they interact via the nuclear magnetic dipole moment. The applied magnetic field produces a split of the degenerated energy levels of the nuclear spin, so that transitions between them can be induced as a result of absorption of the adequate electromagnetic radiation. This specific

orientation of spins depends on the molecular structure and, therefore, is different for each molecule; and the whole NMR spectrum of a molecule can be considered as a fingerprint of it. Moreover, the proton NMR spectrum (^{1}H-NMR) of the bioproduced ELRs allows us to verify the absence of impurities for each one of them. The NMR analysis was performed with the NMR 500 (Agilent Technologies) equipment of the LTI. The measurements were carried out at 298 K with samples of 20–30 mg of the ELRs, purified and dissolved in DMSO-d6. The peak areas corresponding to three kind of hydrogen, namely -NH_2, -CH_3 and -CH- from the chain, were electronically integrated and compared to the calculated theoretical values.

Following ELRs characterization

Furthermore, according to the biomedical application for what the ELRs were designed, other analyses has been performed. For instance, in Chapter 3 it is reported the mechanical characterization of hydrogels by rheological measurements. In Chapter 4 the therapeutic capacity of the hydrogel-based on ELRs was evaluated with an *in vivo* study for osteochondral repair. Moreover, in Chapter 5 other types of characterization such as X-ray Photoelectron Spectroscopy and cell adhesion assay have been used to describe the new ELR-Peptide generated. Finally, in Chapter 6 an RNase A activity assay was assessed in order to monitor the allosteric control of the smart-ELRs generated. Many more methods of biomaterial characterization have been used along this Thesis, and they are all described in the following chapters.

Statistical analysis

All the values shown in this Thesis are expressed as mean ± standard deviation ($n \geq 3$ according to the specific experiment conditions). Depending on the group of data collected by each specific experiment, different statistical analyses has been used. Data were analyzed by performing the normality test Shapiro-Wilk. The parametric data were analyzed by one-way analysis of variance (ANOVA) followed by Tukey's Honestly Significant Difference (HSD) post hoc test; if only two groups were being compared, an unpaired t-test was used instead of ANOVA to assess the statistical difference. The nonparametric data were analyzed performing the Kruskal-Wallis test followed by Dunn's

multiple-comparison test. All statistical analyses were performed with GraphPad Prism. In all the cases, a P-value lower than 0.05 was considered statistically significant.

References

1. Girotti A, Reguera J, Arias FJ et al. Influence of the Molecular Weight on the Inverse Temperature Transition of a Model Genetically Engineered Elastin-like pH-Responsive Polymer. Macromolecules 2004; 37:3396-3400.

2. Rodríguez-Cabello JC, Girotti A, Ribeiro A et al. Synthesis of Genetically Engineered Protein Polymers (Recombinamers) as an Example of Advanced Self-Assembled Smart Materials. In: Navarro M, Planell JA (eds). Nanotechnology in Regenerative Medicine: Methods and Protocols. Totowa, NJ: Humana Press, 2012, 17-38.

3. Meyer DE, Chilkoti A. Protein purification by inverse transition cycling. In: Protein Interactions. New York (USA): Cold Spring Harbor Laboratory Press, 2002, 329-343.

4. Luis Jimenez, Narendra Rana, Kasey Travers, et al. Evaluation of the Endosafe® Portable Testing System™ for the Rapid Analysis of Biopharmaceutical Samples. PDA J Pharm Sci and Tech 2010; 64:211-221.

5. Laemmli UK. Cleavage of structural proteins during the assembly of the head of bacteriophage T4. Nature 1970; 227:680-5.

6. Lee C, Levin A, Branton D. Copper staining: a five-minute protein stain for sodium dodecyl sulfate-polyacrylamide gels. Anal Biochem 1987; 166:308-12.

7. Hillenkamp F, Karas M, Beavis R, Chait, Brian T. Matrix-assisted laser desorption/ionization mass spectrometry of biopolymers. Analytical Chemistry. 63 (24): 1193A–1203A. (1991) doi:10.1021/ac00024a002.

8. Karas M, Krüger R. Ion Formation in MALDI: The Cluster Ionization Mechanism. Chemical Reviews. 103 (2): 427–440. (2003) doi:10.1021/cr010376a.

9. R. M. Silverstein, G. C. Bassler and T. C. Morrill. Spectrometric Identification of Organic Compounds, 5th Ed., Wiley, (1991).

RESULTS

CHAPTER 3

CARTILAGE REGENERATION IN PREANNEALED SILK ELASTIN-LIKE CO-RECOMBINAMERS INJECTABLE HYDROGEL EMBEDDED WITH MATURE CHONDROCYTES IN AN EX VIVO CULTURE PLATFORM

Filippo Cipriani,[1] Melanie Krüger,[2] Israel González de Torre,[1,3] Luis Quintanilla Sierra,[3] Matilde Alonso Rodrigo,[1,3] Linda Kock,[2] José Carlos Rodríguez-Cabello,[1,3]

[1] Technical Proteins NanoBioTechnology (TPNBT) S.L., Valladolid, Spain

[2] LifeTec Group B.V., Eindhoven, The Netherlands

[3] Bioforge, University of Valladolid CIBER-BNN, Paseo de Belén 19, 47001 Valladolid, Spain

F. Cipriani, M. Krüger, I. González de Torre, L. Quintanilla Sierra, M. Alonso Rodrigo, L. Kock, J.C. Rodríguez-Cabello. Cartilage Regeneration in Preannealed Silk Elastin-Like Co-Recombinamers Injectable Hydrogel Embedded with Mature Chondrocytes in an Ex Vivo Culture Platform. *Biomacromolecules* (2018). doi: 10.1021/acs.biomac.8b01211.

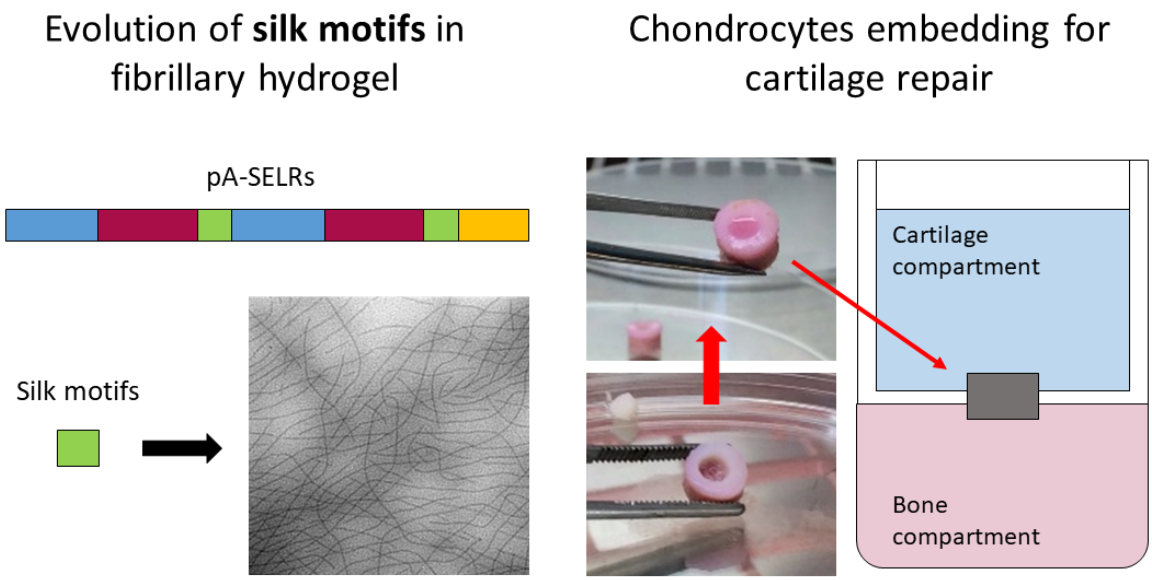

Keywords

Elastin-like Recombinamers; Polymers; Hydrogels; Cartilage repair; *Ex vivo* culture platform.

Abstract

Tissue engineering for cartilage repair requires biomaterials that show rapid gelation and adequate mechanical properties. Although the use of hydrogel is the most promising biomaterial, it often lacks in rigidity and anchorage of cells when they are surrounded by synovial fluid while they are subjected to heavy loads. We developed and produced the Silk Elastin co-Recombinamer (SELR), which contains both the physical interaction from elastin motifs and from silk motifs. In the first part of this work, we set up and optimized a pre-annealing treatment based on the evolution of silk motifs into β-sheet structures in order to fulfill the required mechanical properties of hydrogels for cartilage repair. The new pre-annealed SELRs ($pA(EIS)_2$-$(I_5R)_6$) were characterized with the combination of several experimental techniques (CD, TEM, SEM, and rheology) to provide a deep insight into the material features. Finally, the regeneration properties of the $pA(EIS)_2$-$(I_5R)_6$ hydrogel embedded with chondrocytes were evaluated. After 4 weeks of culturing in a standardized and representative *ex vivo* model, the biochemical and histological analysis revealed the production of glycosaminglycans and collagen. Moreover, the immunohistochemistry showed the absence of fibro-cartilage and the presence of hyaline cartilage. Hence, we conclude that the $pA(EIS)_2$-$(I_5R)_6$ hydrogel presents improved mechanical properties while conserving the injectability, which leads to successful regeneration of hyaline cartilage in an *ex vivo* model.

1. INTRODUCTION

Articular cartilage is central to the proper functioning of synovial joints. It covers the opposing articulating bones and, through its properties of high resiliency and deformability, it protects them from compressive joint loads (1). Moreover, it provides a smooth and gliding surface with a very low coefficient of friction (2). Many people suffer from cartilage degeneration due to genetic abnormalities, trauma, or osteoarthritis (3). One of the main issues in this regard is that articular cartilage possesses limited regeneration ability due to its avascular character, and the fact that only one cell type (chondrocytes) is present (4,5).

Because of the absence of self-repair abilities, various surgical interventions and biomaterials have been explored to facilitate regeneration of cells and cartilaginous matrix (5). The physical properties of the extra cellular matrix (ECM) often refer to its rigidity, porosity, insolubility, topography, and other characteristics that are essential for its scaffolding role in supporting tissue structure and integrity, and for its role in migration and anchorage of the cells (6). Moreover, another important parameter to take into account is the permeability of cartilage; it contributes to several tissue functions like the transport of nutrients to chondrocytes, the ability to carry heavy loads, and the maintenance of a lubricating fluid film between opposing articular surfaces (7). Permeability is a measure of the ability of fluid to flow through a porous-permeable material, such as an ECM, and is inversely proportional to the friction drag exerted by the fluid (8). The low permeability of articular cartilage prevents fluid from being quickly squeezed out of the matrix (9).

The purpose of surgery is the regeneration of the chondral defects to ultrastructural and biomechanical competent hyaline cartilage. From a scientific point of view, the clinical treatments are limited in their ability to functionally regenerate cartilage defects, as they often result in the formation of fibrotic tissue, which consists mainly of collagen type I and is therefore mechanically inferior to native cartilage.

Biomaterials with an elastic modulus in the range of 1-10 kPa are of widespread interest, as many native tissues also have moduli in this range (10,11). The hydrogels developed to

repair joint cartilage are more effective when their stress relaxation behavior matches with the native tissue, since such behavior affects load transfer and nutrient transport (12,13). Up to 80 % of articular cartilage wet weight consists of water (14). To replicate this environment, hydrogels have become a popular option for cartilage regeneration in situ and cartilage engineering *in vitro* (15-17). The purpose of these types of scaffold is not only to provide support for cell attachment and spreading, but also to have mechanical stability at the defect site; although it is important to take into account that, the aim of these scaffolds is not to substitute for the tissue, but to improve cartilage regeneration in order to obtain a mature tissue.

Natural polymers such as collagen and hyaluronic acid have some limitations; for instance, the insufficient mechanical integrity and the short lifetime in inflamed defects due to degradation by matrix metalloproteinases (18). From a biological point of view, the major drawback of synthetic polymer hydrogels such as polyglycolic acid (PGA) and polylactide acid (PLA) is that they do not provide specific biological functions (19). Moreover, synthetic polymer hydrogels do not fully recapitulate the chemical and biological features of ECM, considering that they generally regenerated fibro cartilage instead of hyaline cartilage (20).

Over the last few decades, recombinant DNA techniques have proven to be very powerful tools for the development of novel protein-based biomaterials that are able to self-assemble into different structures, such as hydrogels (21). These biomaterials include elastin-like recombinamers (ELRs), which are protein based polypeptides that comprise repetitive units of the Val−Pro−Gly−X−Gly $(VPGXG)_n$ pentapeptide, in which X (guest residue) could be any amino acid except L-proline. Moreover, they show thermo-responsiveness due to the change of the protein conformation above the so-called transition temperature (T_t), which itself depends on the amino acid composition of the polymer (22). Therefore, taking into account two ELRs with the same amino acid composition except for the guest amino acid, the T_t can be tuned depending on the polarity of the side chain for the guest residue in the X position of the pentapeptide (23, 24). Furthermore, ELRs can be designed so the phase transition occurring above the T_t is translated into a hydrophobically driven self-assembly of the molecules toward supramolecular hydrogels (25).

In this work we have used previously described amphiphilic Silk-Elastin-like Recombinamers (SELR) (26, 27) including two types of elastin-like domains, one hydrophilic and the other one hydrophobic. SELR also contains the amino acid sequences derived from other structural proteins like the GAGAGS hexapeptide (G: Glycine, A: Alanine, S: Serine) found in Bombyx mori silk fibroin, hence giving rise to SELR (28). Furthermore, the final sequence also contains the well-known RGD cell-adhesion sequence, which promotes specific cell attachment via integrins that provide a cell-friendly environment (29). This recombinamer contains a dual physical interaction that triggers gel formation, in order to obtain a rapid and stable gel that can be delivered into the area of interest via a simple injection. The elastin motifs have been reported to form elastomeric hydrogels, in which the hydrophilic blocks provide conformational elastic properties, and the hydrophobic blocks form cross-links by hydrophobic aggregation (30, 31). The silk motifs have been reported to be responsible for the supramolecular rearrangement into β-sheets, which increases the moduli of the hydrogels (26). However, the rearrangement of silk motifs into β-sheets with the consequent formation of a fibrillary structure takes time; the long time needed represents a drawback in terms of surgical application for the cartilage environment, which is surrounded by synovial fluid.

Furthermore, recent works have demonstrated that physical and structural features of the ECM, such as fibrils, are essential for its scaffolding role in supporting tissue structure and integrity (6, 32). The nanofiber environment plays an essential role in the migration and anchorage of the cells. Considering that one difficulty in nanofiber technology has been the placement of cells within a nanofibrillar structure (33), the purpose of this work is to design a system based on supramolecular self-assembly to form nanofibrillar matrices in situ, around the cells, without cellular damage.

This study focuses on the correlation between the elastin motifs and silk motifs, in order to understand how to improve the gelation properties of the hydrogel to obtain a system capable of forming an ECM fibrillary structure directly after injection. We set up and optimized a thermal treatment (pre-annealing treatment), which accelerates the β-sheet formation without losing the injectability of the material. The new $pA(EIS)_2$-$(I_5R)_6$ were characterized either with molecular analysis (Circular Dichroism and Transmission Electron Microscopy) or with rheological characterization, in order to investigate the

impact of the pre-annealing treatment on the arrangement of the silk motifs into β-sheet conformation. Moreover, the morphology of the hydrogel was checked using Scanning Electron Microscopy in order to verify the interconnected structure and an adequate porosity and permeability.

The incorporation of cells into biomaterial scaffolds include multiple aspects in cartilage repair; thus, considering that cells are the driving force of cartilage formation, they can significantly help orchestrate regeneration and overcome some of the limitations of using cells or biomaterials alone (34). The use of mature chondrocytes is based on the premise that native mature cells are best suited to guide regeneration (34). Moreover, the remarkable property of ELRs permits a homogeneous embedding of cells in the ELR solution at a temperature below T_t, while molecules can self-assemble into hydrogels above the T_t, thus allowing the use of the cell-scaffold system in injectable therapies perfectly suitable to the shape of the injured area (35). Therefore, although other ELR-based hydrogels have shown a minimal inflammatory response, confirming its high and extraordinary biocompatibility (36), we performed an *in vitro* study evaluating the metabolic activity of the chondrocytes embedded in the 3D hydrogel.

The potential properties of pA$(EIS)_2$-$(I_5R)_6$ hydrogel in cartilage repair were evaluated in an *ex vivo* osteochondral culture platform (37). The use of bioreactors has some advantages: first, bioreactors are devices in which biological or biochemical processes develop under a closely monitored and tightly controlled environment (38). Second, it must be taken into account that cartilage defect models in rodents and mature rabbits show spontaneous self-repair (39). In addition, there are some other disadvantages using an animal model: the limited control over physiological parameters, and the limited possibilities for monitoring and controlling the healing progress from a biological and biomechanical point of view, as well as the high costs of animal care and ethical issues (39, 40).

2. MATERIALS AND METHODS

2.1. $(EIS)_2$-$(I_5R)_6$ Design

Amino acid sequence: MESLLP-{[$(VPGVG)_2$-VPGEG-$(VPGVG)_2]_{10}$-$(VGIPG)_{60}$-[$V(GAGAGSG)_5]_2G$}-[$(VPGIG)_5$-AVTGRGDSPASS]$_6$V

The composition of this $(EIS)_2$-$(I_5R)_6$ is based on previously synthetized block co-recombinamers, which have silk-like motifs (SELR) (26, 41). The original block co-polymer was designed to comprise a hydrophobic block (containing isoleucine as the guest residue) with a low T_t, and a hydrophilic block (containing glutamic acid with a carboxylic group) with a high T_t (27). The final composition was further functionalized to include RGD cell-adhesion sequences (Figure 1). Initial SELRs were kindly provided by Technical Proteins Nanobiotechnology.

Figure 1. Graphical scheme of the composition of $(EIS)_2$-$(I_5R)_6$.

2.2. ELR biosynthesis and purification

The cloning and molecular biology for gene construction of $(EIS)_2$-$(I_5R)_6$ were performed using standard genetic-engineering methods. Production was carried out using recombinant techniques with *Escherichia coli* as the cell system, as described previously (42-45). Purification was performed using several cooling and heating purification cycles (Inverse Transition Cycling) following centrifugation.

2.3. Pre-Annealing treatment

The lyophilized recombinamer was dissolved in ultrapure water at a concentration of 50 mg/ml, and incubated at 37 °C for different time points: 12, 24, 36 and 48 h. The 50 mg/ml concentration for the pre-annealing treatment was selected considering the inability to form a gel even when using a long incubation time (up to 48 h). Afterwards, the solution was frozen and the polymer lyophilized again to finally obtain the pre-annealed SELRs: pA$(EIS)_2$-$(I_5R)_6$. The purity and molecular weight of the ELRs were verified by sodium

dodecyl sulfate polyacrylamide gel electrophoresis (SDS-PAGE), and matrix-assisted laser desorption/ionization time-of-flight (MALDI-TOF) mass spectroscopy using a Voyager STR apparatus from Applied Biosystems. Amino acid composition analysis was also performed. Additional characterization of ELRs was accomplished using infrared spectroscopy (FTIR), differential scanning calorimetry (DSC), and nuclear magnetic resonance (NMR) techniques (46) (Supporting Information Figures S1 - S5).

2.4. Circular Dichroism (CD)

Circular dichroism is an excellent method for rapidly evaluating the secondary structure and folding of proteins (47). It is known that the ELR conformational state is temperature-dependent as consequence of the ITT (Inverse Temperature Transition) behavior experienced by this class of molecules (41). For performing CD experiments, recombinamers $(EIS)_2$-$(I_5R)_6$ and $pA(EIS)_2$-$(I_5R)_6$ were dissolved at a final concentration of 1 mg/mL and were kept overnight at 4 °C. Just before performing each measurement, a 1:10 dilution was made. The CD spectrum was acquired using a Jasco J-815 150-S spectrometer (Servicios Centrales de Investigación, University of Almeria). A quartz cuvette with a path length of 0.1 cm was used. The scans were obtained over the wavelength range of 190−260 nm at the experimental temperatures of 4, 37 and 60 °C by acquiring points every 0.5 nm using a scan speed of 50 nm/min. Before each measurement, samples were equilibrated for 15 min. Spectra were corrected by subtraction of the corresponding blank solvent readings. The data was expressed as molar ellipticity [θ], which was calculated as follows:

$$[\theta] = \frac{\theta}{d \times M \times 10}$$

where θ is the ellipticity, d is the path length (cm) and M is the concentration (mol/L).

2.5. Transmission Electron Microscopy (TEM)

Nanostructure formation was checked by TEM. Solutions of $(EIS)_2$-$(I_5R)_6$ and $pA(EIS)_2$-$(I_5R)_6$ were prepared by dissolving pure, lyophilized products in Milli-Q water to a concentration of 25 µM. These solutions were kept at 4 °C overnight to allow complete dissolution of the proteins. The samples were incubated at 37 °C for 15 min and analyzed directly. TEM

measurements were performed using a JEOL JEM-1230 electron microscope operating at 120 kV. The specimens were prepared by placing a drop of the solution on a plasma-treated carbon-coated copper grid, followed by water evaporation at 37 °C.

2.6. Visualization and characterization of the Sol-Gel behavior

In order to check the capacity of pA$(EIS)_2$-$(I_5R)_6$ to rapidly form hydrogel and to remain stable in an excess of water, the pure recombinamers were dissolved in PBS (Phosphate-buffered saline) at 4 °C for 16 h at the concentrations of 100, 120, 150 and 180 mg/ml. Once the recombinamers were in a liquid state at 4 °C, they were placed inside an oven at 37 °C for 15 min and the Sol-Gel behavior was qualitatively observed tilting the Eppendorf containing the solution. Afterwards the hydrogels were removed and placed in an excess of water at 37 °C.

2.7. Rheological characterization

A strain-controlled AR-2000ex rheometer (TA Instruments) was employed to perform rheological experiments by using parallel plates of nonporous stainless steel (diameter = 12 mm).

Oscillatory measurements were carried out in shear deformation mode. The volume of the gel was 150 µl, a gap higher than 1000 µm was always reached after the sample relaxed until equilibrium. Measurements were performed at 37 °C, with the sample temperature being controlled and maintained using a Peltier device.

Firstly, the solution of pA$(EIS)_2$-$(I_5R)_6$ dissolved in PBS was placed over the plate at 37°C, and a time sweep experiment was performed up to 30 min with 1 % strain amplitudes and a frequency of 1 Hz; in this case, in situ gelation took place. Then, once the time sweep was over, two different measurements were carried out sequentially. First, the dynamic shear modulus was measured as a function of strain by a dynamic strain sweep with amplitudes ranging between 0.01% and 20% at a frequency of 1 Hz. This measurement was done to determine the range of strain amplitudes over which the gel exhibited a linear region of viscoelasticity. A second measurement consisted of the dynamic frequency

sweep between 0.1 and 50 Hz at a fixed strain (selected within the hydrogel linear region), with the aim of obtaining the dependence of the dynamic shear modulus and loss factor on the frequency. Rheological evaluation provided the storage modulus (G'), the loss modulus (G''), the complex modulus magnitude $|G^*|$, ($|G^*|^2 = (G')^2 + (G'')^2$), and the loss factor $\tan \delta \equiv (G'')/(G')$, where δ is the phase angle between the applied stimulus and the corresponding response as a function of strain amplitude or frequency.

In order to obtain the evolution of the viscosity of the $pA(EIS)_2$-$(I_5R)_6$ solutions with the shear rate, flow measurements were carried out at 4 °C. In this case, a parallel plate of 40 mm of diameter was used to improve the measurement sensitivity; the corresponding volume of the gel was 1300 µl. Initially, a conditioning step was accomplished at a constant shear rate of 0.1 s^{-1} for 1 min. Next, the shear rate was swept from 0.1 to 500 s^{-1} using a continuous ramp in a logarithmically ascending series of discrete steps. Specifically, 10 points were acquired for each order of magnitude and the complete measure took 5 min.

2.8. Scanning electron microscopy (SEM)

Scanning electron microscopy was employed to investigate the morphology of the hydrogel. Fully hydrated gels were dropped into liquid nitrogen, physically fractured, and immersed into liquid nitrogen again. Finally, they were freeze-dried. Images of lyophilized hydrogels were obtained by using a FEI Quanta 200 FEG with no prior coating procedures. Pictures were collected by SEM at Landing E of 7.00keV and Pressure of 0.7 Torr; afterwards they were analyzed with Image-J software.

2.9. Chondrocytes isolation

Pig chondrocytes were isolated from knee joints of Dutch Land Raise Hybrid pigs, male or female, 5-7 months of age, 100-110 kg live weight. Small cartilage pieces were removed from the cartilage of the knee joints and were digested in a solution of 0.5% (v/v) collagenase (PrepoTech) in high glucose DMEM (supplemented with 10% (v/v), fetal bovine serum (FBS; HyClone, (South America) Research Grade, GE Healthcare, Eindhoven, NL), 1% (v/v) penicillin/streptomycin (Lonza, Westburg, Leusden, NL), 1% (v/v) amphotericin B (Life Technologies, Bleiswijk, NL). Digestion in 8 ml collagenase solution

per gram of cartilage was executed for 16 h on a roller bank in the incubator. Subsequently, the cells were washed and filtered three times and stored in a cartilage medium until further use. The cartilage medium consisted of high glucose DMEM medium supplemented with 1% (v/v) penicillin/streptomycin, 1% (v/v) amphotericin B, 1 mM sodium pyruvate (LifeTechnologies, Bleiswijk, NL), 40 µg/ml L-proline (Sigma-Aldrich, Zwijndrecht, NL), 50 µg/ml L-ascorbic acid-2-phosphate (Sigma-Aldrich, Zwijndrecht, NL), 1% (v/v) ITS+ Premix (Corning, Fisher Scientific, Landsmeer, NL) and 100 nM dexamethasone (Sigma-Aldrich, Zwijndrecht, NL).

2.10. Hydrogel formation and embedding with chondrocytes

Freeze dried $pA(EIS)_2$-$(I_5R)_6$ was dissolved in plain DMEM (Dulbecco´s modified Eagle medium; Life Technologies, Bleiswijk, NL) for 16 h at 4 °C at 120 mg/ml. Afterwards, the solution was placed at 37 °C for 15 min and the gel was formed. For the hydrogel embedded with chondrocytes (20 million cells/ml), the cells were mixed with the solution of $pA(EIS)_2$-$(I_5R)_6$ dissolved in plain DMEM at 4 °C. The mixture was placed at 37 °C for 15 min, and the cell embedding gel was formed.

2.11. Cell viability assay

The viability of isolated chondrocytes embedded in $pA(EIS)_2$-$(I_5R)_6$ hydrogels at 120 mg/ml was assessed by measuring the metabolic activity with PrestoBlue® assay (A-13261, Invitrogen). Chondrocytes were isolated and mixed into the hydrogel according to the protocol described above. Of each hydrogel condition, 100 µl were pipetted into a 24 well Transwell® tissue culture plate (Costar, Kennebunk, USA) in quadruplicate and topped with 2 ml of cartilage medium. Culture time was 4 weeks at 37°C and 5% CO_2. After letting the cells adapt overnight, metabolic activity measurements were conducted on day 0, 14 and 28. For this purpose, 2 ml of a solution of cartilage medium containing 10 % PrestoBlue® Viability Reagent (Life Technologies, Eugene, USA) replaced the culture medium and was incubated in darkness for 2 h. Afterwards, 100 µl of medium from within the Transwell® insert, directly above the gel, was pipetted into a black 96 well plate in triplicate and fluorescence was read out at an excitation wavelength of 560 nm and an emission wavelength of 590 nm with a plate reader (CLARIOstar microplate reader, BMG

LABTECH GmbH, Ortenberg, D). The cell viability assay is not an end point measurement analysis, thereby, after each measurement the solution was removed and replaced with 2 ml of fresh cartilage medium.

2.12. *In vitro* Study

In order to evaluate the performance of the pA$(EIS)_2$-$(I_5R)_6$ hydrogel embedded with chondrocytes, a 4-week *in vitro* study was conducted. Firstly, silicone cylinders were produced with an inner diameter of 4 mm and a height of 2 mm, in correspondence to the simulated cartilage defect in the *ex vivo* study. After autoclaving, these silicone cylinders were attached to the bottom of a 24 well plate. 150 µl of the pre-annealed $(EIS)_2$-$(I_5R)_6$ hydrogel embedded with chondrocytes (20 million chondrocytes/ml), and the pA$(EIS)_2$-$(I_5R)_6$ hydrogel itself (as a control) were pipetted into the cylinders. After a gelation period of 15 min in the incubator at 37 °C, the cartilage compartment was topped with 3 ml of cartilage medium. The culture time was 28 days with medium changes every 3-4 days.

2.13. *Ex vivo* Study

2.13.1. Osteochondral explant isolation

Osteochondral explants (n=12) were isolated from knee joints of Dutch Land Raise Hybrid pigs, male or female, 5-7 months of age, 100-110 kg live weight. The knees were opened in a sterile manner and three explants were drilled from each medial femoral condyle with a dental drill bit of 8 cm diameter (MF Dental, Mantel, D). The site was cooled with cold, sterile phosphate-buffered saline (PBS; Sigma-Aldrich, Zwijndrecht, NL) with 2% (v/v) penicillin/streptomycin and 2% (v/v) amphotericin B and the explants were broken off from the bone with a custom-made tool. Successively, they were sewn to a bone length of 4 mm and incubated overnight in cartilage medium.

2.13.2 Cartilage defect creation, hydrogel incorporation and culture

To test the regenerative potential of the pA$(EIS)_2$-$(I_5R)_6$ hydrogel for cartilage repair, full depth cartilage defects of 4 mm diameter were created with a biopsy punch (PFM Medical

AG, Cologne, D) and the defect site was cleaned of remaining cartilage with a sharp spoon (MF Dental, Mantel, D) (Figure 2A). These osteochondral explants with defects were then mounted in an osteochondral culture platform developed by LifeTec Group BV as previously described (37). Briefly, the explants were mounted in an insert with an O-ring situated at the exact interface between the bone and the cartilage (Figure 2C). This insert was then suspended in a custom made six well plate, thereby resulting in two separate compartments for the bone and the cartilage. By using respective tissue-specific media, complete preservation of native extra cellular matrix composition was achieved over 56 days, thereby allowing regeneration studies in this *ex vivo* model. Once the explants were mounted in the described way into the insert, the $pA(EIS)_2$-$(I_5R)_6$ hydrogel itself (control), and the $pA(EIS)_2$-$(I_5R)_6$ hydrogel embedded with chondrocytes (20 million chondrocytes/ml) were pipetted into the defects (Figure 2B). In this manner, 30 µl of hydrogel itself, and 30 µl of hydrogel loading 600,000 chondrocytes filled each defect. After a gelation period of 15 min in the incubator at 37 °C, the cartilage compartment was topped with 3 ml of cartilage medium. The bone compartment was filled with 3 ml of bone medium consisting of high glucose DMEM medium supplemented with 10% (v/v) FBS, 1% (v/v) penicillin/streptomycin, 1% (v/v) amphotericin B, 50 µg/ml L-ascorbic acid-2-phosphate, 10 nM β-glycerophosphate (Sigma-Aldrich, Zwijndrecht, NL), and 100 nM dexamethasone. The medium was changed every 3-4 days and explants were cultured for 28 days at 37°C and 5% CO_2.

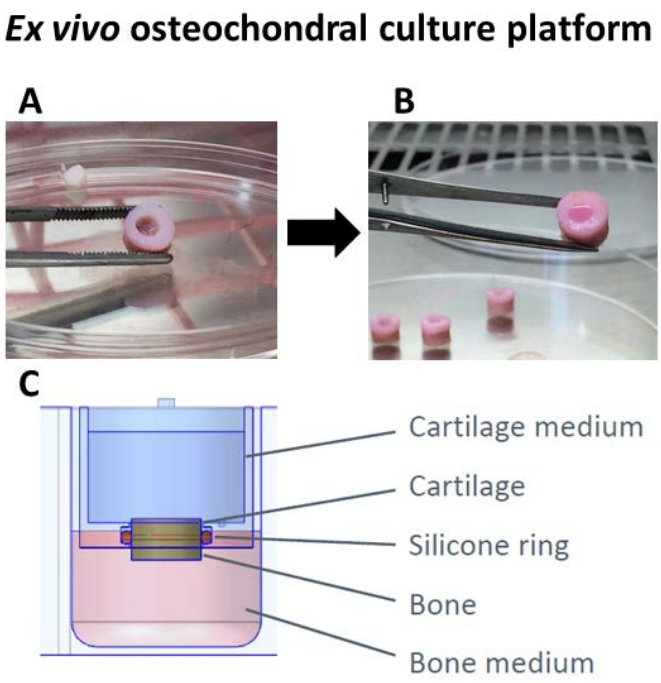

Figure 2. *Ex vivo* osteochondral culture platform mounting scheme. A: Creation of the full cartilage defects of 4 mm diameter with a biopsy punch. B: Filling of the defects with 30 µl of $pA(EIS)_2$-$(I_5R)_6$ hydrogel loaded with 600,00 chondrocytes and 30 µl of $pA(EIS)_2$-$(I_5R)_6$ hydrogel itself (control). C: Mounting of the explant in the insert with the O-ring situated at the exact interface between the bone and the cartilage.

2.14. Biochemical analysis

2.14.1. DNA quantification

The hydrogel samples were carefully and fully removed from the silicone cylinders (for the *in vitro* study), and from the osteochondral defect (for the *ex vivo* study) after the respective culturing period. They were then digested by a homogenizer (T 10 basic Ultra-Turrax® IKA) until the gel was completely disrupted. The DNA content was determined by Pico Green® assay. Briefly, Pico Green® analysis for DNA content was performed in 96-well plates with standard fluorescein wavelengths (excitation: 480 nm and emission: 520 nm) according to the manufacturer's instructions (Invitrogen) using an automated plate reader (*Bionova Cientifica, Molecular Devices*).

2.14.2. GAG quantification

GAG content was determined with a modified DMMB (Dimethylmethylene Blue) assay according to Farndale *et al. (*48). After the respective culturing period, the gels were removed, digested and centrifuged in the same manner as for the DNA analysis. In brief, 40 µl of centrifuged samples were pipetted into 96-well plates; the same volume was pipetted for standards, which are a shark cartilage chondroitin sulfate reference (Sigma, Zwijndrecht, NL). Afterwards, 150 µl of DMMB solution (containing 1-9-dimethylmethylene blue (Sigma-Aldrich, Zwijndrecht, NL)) was added in each well. Immediately afterwards, absorbance at 540 and 595 nm was measured with a plate reader (CLARIOstar microplate reader, BMG LABTECH GmbH, Ortenberg, D) and the GAG concentrations were calculated.

2.15. Histological analysis

For the histological analysis, all the samples were fixed in 4% formaldehyde in PBS 0.05M (pH 7.3) at 4°C for about 18 h. Afterwards the samples were dehydrated and infiltrated by paraffin following the automatic procedure performed by the MICROM Tissue Processor. The resulting blocks were cut using a rotary microtome (Leica RM 2125 RTS, Leica Biosystems, Germany) into slices with a thickness of 4 µm. For general histo-morphological evaluation, the sections were stained with Hematoxylin and Eosin (H/E) according to standard protocols. In order to evaluate the collagen and glycosaminoglycan content produced by chondrocytes, the sections were stained with Picro-Sirius Red Stain and Safranin-O/Fast Green, respectively, according to common methods. Immunohistochemistry for collagen type I and II was performed on 4 µm paraffin sections following the manufacturer's instructions and well-established protocols. The samples were immunostained with primary antibody Mouse monoclonal anti-collagen type I (dilution 1:100, Sigma), and with primary antibody Mouse monoclonal anti-collagen type II (dilution 1:00, Merck), then incubated with the secondary antibody Goat anti Mouse IgG conjugated with HRP (dilution 1:100, abcam). Immunostaining was developed using DAB (Thermo Scientific) followed by Hematoxylin counterstaining (Sigma, St. Louis, MO).

2.16. Statistical analysis

Values are expressed as mean ± standard deviation (SD). The data was examined with a one-way analysis of variance (ANOVA) followed by Tukey's Honestly Significant Difference (HSD) *post hoc* test. If only two groups were being compared, an unpaired *t*-test was used instead of ANOVA to assess the statistical difference. All statistical analyses were performed with GraphPad Prism. A *P*-value lower than 0.05 was considered statistically significant.

3. RESULTS

3.1. Circular dichroism

Circular dichroism (CD) was performed in order to investigate the impact of the pre-annealing treatment on the $(EIS)_2$-$(I_5R)_6$ on the consequent arrangement of the silk motifs into β-sheets. The silk motifs represented around 16% of the complete sequence of the $(EIS)_2$-$(I_5R)_6$. The conformational state of ELRs is temperature-dependent as a consequence of the T_t behavior experienced by this class of molecules (49); thus, the CD spectra were recorded at different temperatures (4, 37 and 60 °C) in order to verify if such temperature dependence remained operational for pA$(EIS)_2$-$(I_5R)_6$ with 12, 24, 36 and 48 h of pre-annealing time. A sample of $(EIS)_2$-$(I_5R)_6$ without pre-annealing was used as a control sample.

At 4 °C, (Figure 3A) an intensely negative band at 197 nm is displayed for all the curves, which indicates a predominant disordered structure; however, it is possible to see clearly the differences along the curves. The signal of the $(EIS)_2$-$(I_5R)_6$ (control) reaches lower values compare to the pA$(EIS)_2$-$(I_5R)_6$ values with different pre-annealing times. At this temperature, in the band at 197 nm, a trend is appreciable (corresponding to the pre-annealing samples) between the 4 curves regarding the different pre-annealing times. The 12 h curve values are lower than the 24, 36 and 48 h; moreover, the 24 h and 36 h curves show the same behavior, whereas the 48 h curve values are higher, showing a more ordered structure. Such a reduced negative band at 197 nm suggests the presence of a mixture of β-turns and β-sheet structures, and agrees with the contribution of elastin and silk moieties to the final conformation (50). A shoulder is also present at 4 °C at 210 nm

for all the curves where the signal of the control reaches lower values compare to the $pA(EIS)_2$-$(I_5R)_6$ values with a different pre-annealing time; all the curves maintain the same trend seen at 197 nm.

At 37 °C (Figure 3B), the CD spectra for all the curves clearly displays a less negative signal at 197 nm compared to 4 °C. Yet, at 37 °C, a clear difference is still present between the control curve and the $pA(EIS)_2$-$(I_5R)_6$ curves with different pre-annealing times. Furthermore, almost no difference is appreciable between the pre-annealed curves, apart from the 12 h curve which shows lower values compare to the 24, 36 and 48 h curves. Moreover, for all the curves, the magnitude of the signal at 210 nm increased, and such trend is also maintained when increasing the temperature to higher values (60 °C) (Figure 3C) which suggests the induction of a type II β-turn conformation with an increase in temperature, as it has previously been observed for EL macromolecules (47,49).

Finally, also at 60 °C, the 197 nm values recorded for the control curve are lower compared to the $pA(EIS)_2$-$(I_5R)_6$ curves with different pre-annealing times, which all show similar values.

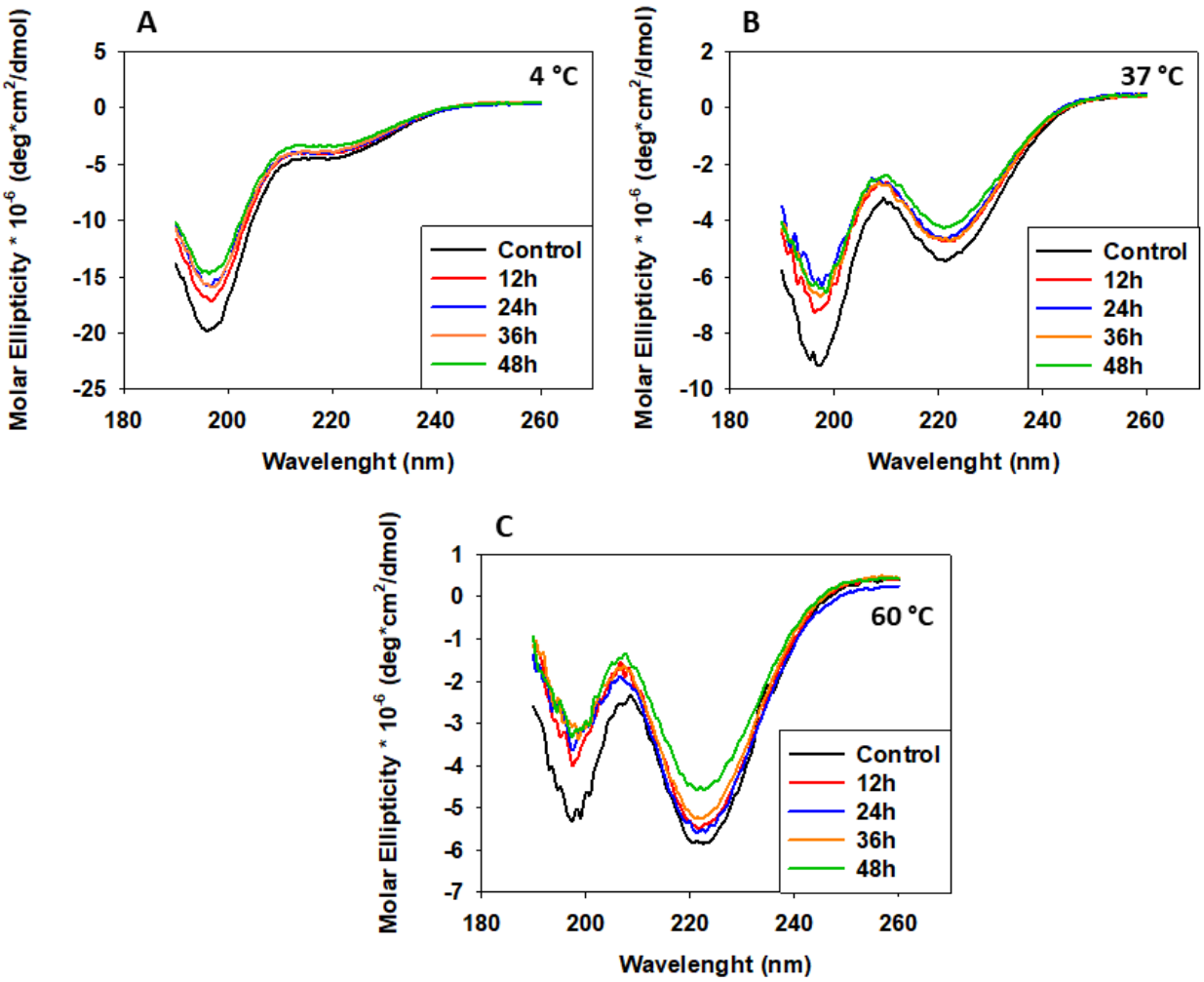

Figure 3. Circular dichroism spectra for $(EIS)_2$-$(I_5R)_6$ (control) and pA$(EIS)_2$-$(I_5R)_6$ with 12, 24, 36 and 48 h of pre-annealing time. CD spectra were recorded for the samples at 0.1 mg/mL in deionized water. For each sample, CD spectra was recorded at different temperatures. A: 4 °C; B: 37 °C: C: 60 °C.

3.2. Transmission Electron Microscopy (TEM)

Transmission electron microscopy (TEM) was used to visualize the supramolecular structures comparing $(EIS)_2$-$(I_5R)_6$ and pA$(EIS)_2$-$(I_5R)_6$ with 12, 24, 36 and 48 h of pre-annealing time. The TEM image for the $(EIS)_2$-$(I_5R)_6$ indicated the ability of this SELR to form spherical nanoparticles (Figure 4A). The TEM images for pA$(EIS)_2$-$(I_5R)_6$ with 12, 24, 36 and 48 h of pre-annealing time revealed the emergence of additional and different fibrillary structures (Figure 4B-4E). Moreover, a difference is appreciable in the density of the network of fibers between the 12 h treatment (Figure 4B) and the group of 24, 36 and

48 h (Figure 4C,4E), where a more dense network of fibers is evident for this group. Thus, the pre-annealing treatment enhanced the ability of the recombinamer to form a fibrillary structure.

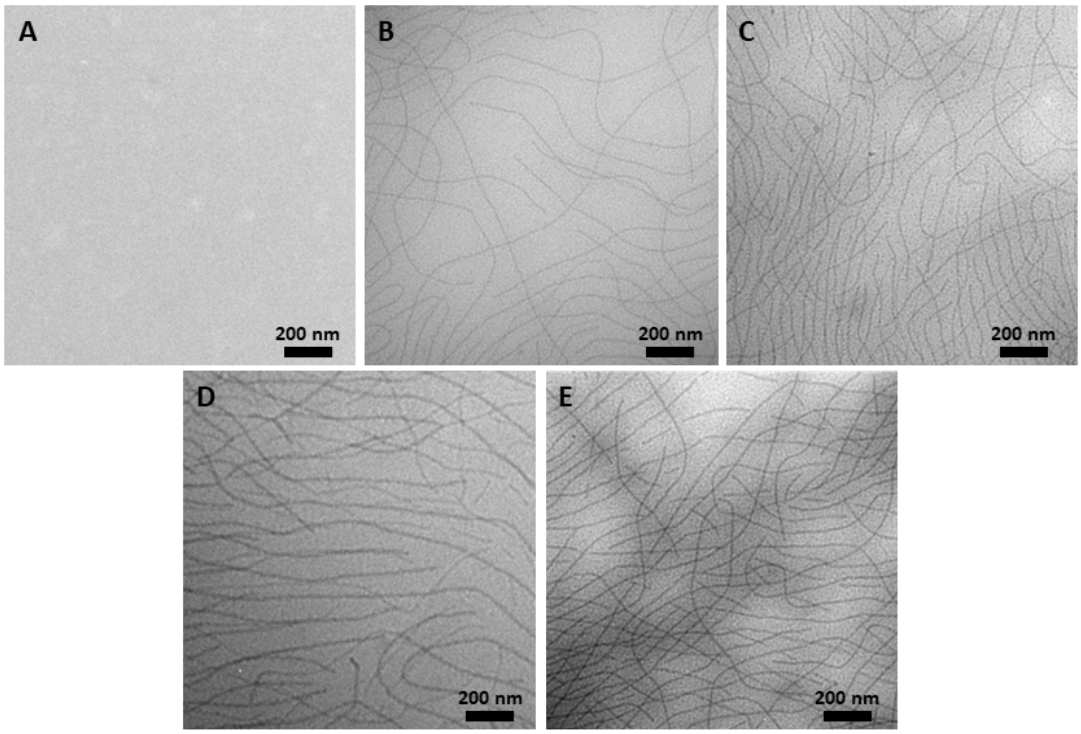

Figure 4. TEM images of the self-assembled nanoparticles formed by $(EIS)_2$-$(I_5R)_6$ at the concentration of 25 µM in Milli-Q water (A) and pA$(EIS)_2$-$(I_5R)_6$ with 12 h (B), 24 h (C), 36 h (D) and 48 h (E) of pre-annealing time.

3.3. Visualization of the Sol-Gel behavior

The pure recombinamers pA$(EIS)_2$-$(I_5R)_6$ at each pre-annealing time (12, 24, 36, 48 h) were dissolved in PBS at 4°C for 16 h at a concentration of 100, 120, 150 and 180 mg/ml. Afterwards the solutions were placed in an oven at 37 °C for 15 min. For all the pre-annealed $(EIS)_2$-$(I_5R)_6$ at different annealing times, the lowest concentration possible to form a hydrogel within 15 min was 120 mg/ml (Figure 5). Moreover, the solution of the $(EIS)_2$-$(I_5R)_6$ (without pre-annealing) subjected to the same procedure showed the incapacity to form a stable hydrogel. As it was already demonstrated by Fonseca *et al.*, where the minimum concentration to form a gel was 145mg/ml (27). In order to verify the stability of the hydrogel, identical parameters to our application were selected (see

hydrogel formation in Materials and Methods). The hydrogel at 120 mg/ml was placed in an excess of water and showed the ability to remain stable after 1 week at 37 °C (Figure 5E,F).

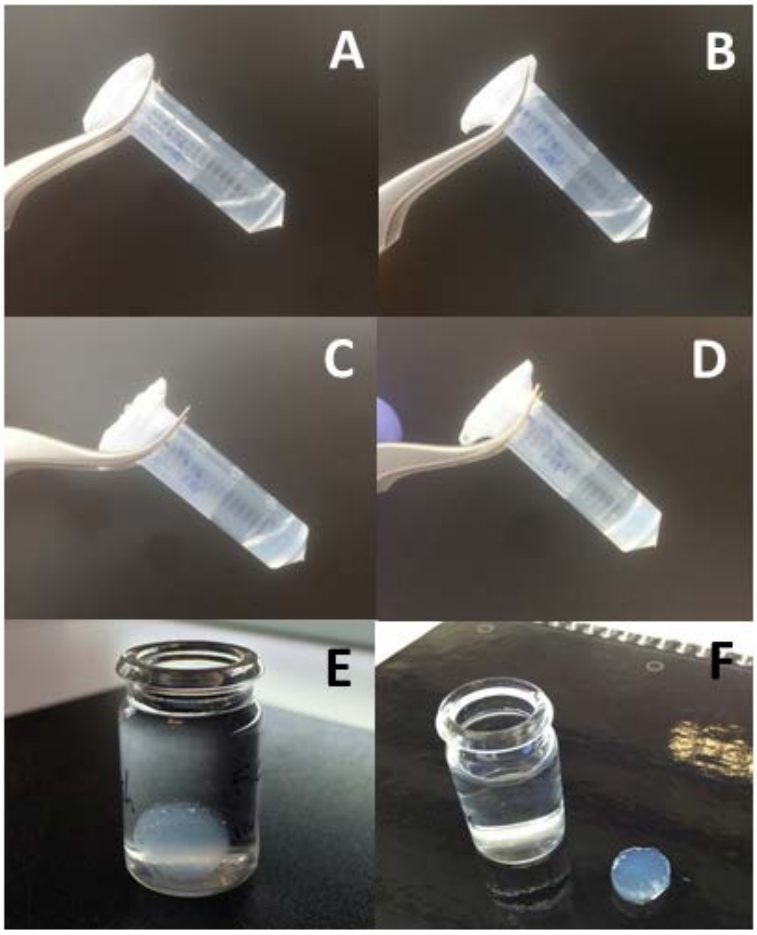

Figure 5. Pictures showing the visualization of the Sol-Gel behavior. 24 h pA$(EIS)_2$-$(I_5R)_6$ hydrogel at 100 mg/ml before (A) and after the incubation at 37 °C for 15 min (B). 24 h pre-annealed pA$(EIS)_2$-$(I_5R)_6$ hydrogel at 120 mg/ml before (C) and after the incubation at 37 °C for 15 min (D); finally, the hydrogel was placed in an excess of water (E) showing the ability to remain stable after 1 week at 37 °C (F).

3.4. Characterization of the Sol-Gel behavior

In order to understand the driving force of the gelation of the pA$(EIS)_2$-$(I_5R)_6$, a rheology study was performed. First of all, an in-situ gelation experiment was carried out for a solution of 120 mg/ml. The solutions dissolved in PBS at 4 °C for 16 h were placed in the

rheometer plate at 37 °C, where a time sweep experiment was carried out for 30 min (Figure 6A). The complex modulus increased with time in agreement with the study performed by Colino *et al*. (26). As can be seen, a clear difference is present between the $(EIS)_2$-$(I_5R)_6$ curve (control) and the $pA(EIS)_2$-$(I_5R)_6$ curves with different pre-annealing times. Along the pre-annealing conditions, no noticeable differences were observed in the complex modulus for the pre-annealing times of 24, 36 and 48 h at the end of the measuring time (around 1 kPa). Yet, a final complex modulus around 200 Pa was found for a pre-annealing time of 12 h.

Therefore, the pre-annealing time of 24 h was selected and several concentrations were considered (100, 120, 150 and 180 mg/ml) (Figure 6B). A clear difference was observed between the concentration of 100 mg/ml and the rest of the concentrations, in agreement with the Sol-Gel behavior qualitatively observed in Figure 5.

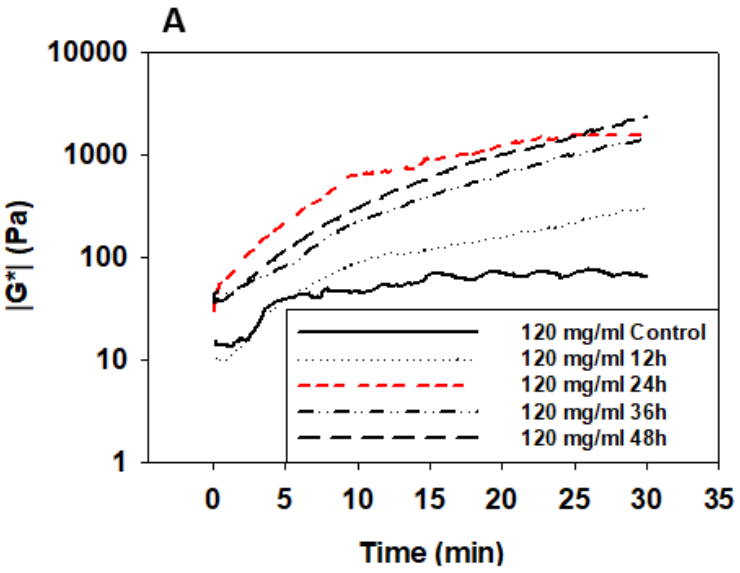

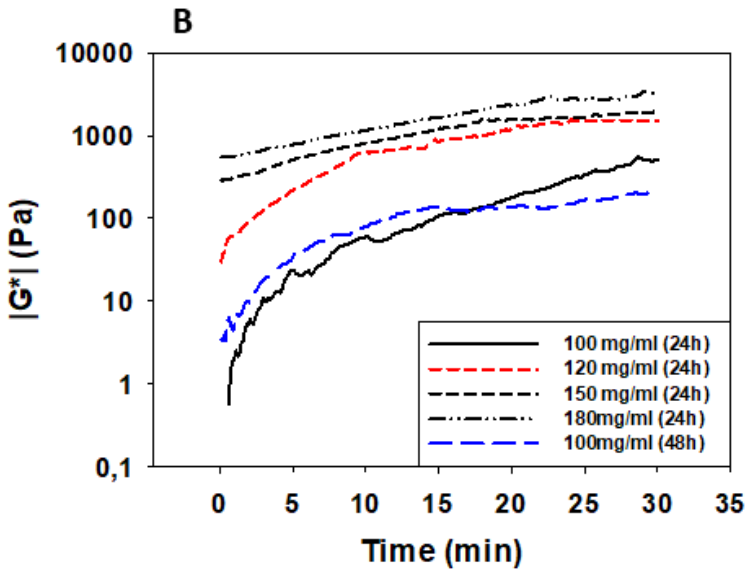

Figure 6. Time Sweep measurement at 37°C for A: $(EIS)_2$-$(I_5R)_6$ & pA$(EIS)_2$-$(I_5R)_6$ hydrogels at 120 mg/ml with 12, 24, 36 and 48 h of pre-annealing; B: pA$(EIS)_2$-$(I_5R)_6$ hydrogels with 24 h of pre-annealing at 100, 120, 150 and 180 mg/ml, and pA$(EIS)_2$-$(I_5R)_6$ hydrogel with 48 h of pre-annealing at 100 mg/ml.

Finally, the effect of the pre-annealing time for different concentrations can be found in Figure 6B, where the concentration of 100 mg/ml was pre-annealed for 48 h. It could be expected to find similar modulus for samples pre-annealed for 48 h at a concentration of 100 mg/ml and for samples pre-annealed for 24 h at a concentration of 120 mg/ml, considering that the lower concentration could be compensated by longer times of pre-annealing. Instead, as can be seen, the curves of 100 mg/ml for 24 and 48 h in Figure 6B are similar, and a lower complex modulus was obtained with respect to the concentration of 120 mg/ml pre-annealed for 24 h.

Therefore, the concentration of 120 mg/ml pre-annealed for 24 h presents a threshold for gelation, and these conditions were selected as the most suitable candidate for an injectable hydrogel for cartilage repair.

3.5. Viscosity measurements of the solutions

Rheological flow measurements were carried out in order to find the evolution of the viscosity of the pre-annealed $(EIS)_2$-$(I_5R)_6$ dissolutions with the shear rate. Since viscosity is the resistance of a fluid to flow upon the application of stress, the viscosity value and

its dependence on shear rate provide some insight about the interactions between the micro/nanostructures in our dissolution. These measurements provide some insight into the injectability of the solutions of 120 mg/ml for different pre-annealing times. To guarantee injectability, the solution should be of sufficiently low viscosity to allow the use of a small gauge needle (51).

In Figure 7, the dependence of the viscosity on the shear rate has been plotted in a lin-log scale for the control sample (without annealing), and for four pre-annealed samples at several annealing times (12, 24, 36 and 48 h). As can be seen, when the shear rate is higher than 200-300 s^{-1} all the curves overlap on a viscosity value around 70-80 mPa·s. Yet, a significantly different evolution of the viscosity is observed in the shear rate range of 0.1 - 50 s^{-1}. Whereas no evolution of the viscosity with the shear rate is observed for the control sample (Newtonian fluid), the annealed samples show a decrease of the viscosity (shear thinning) with an evident linear dependence of the viscosity in the lin-log scale. Specifically, two slopes are detected in the experimental data.

On the contrary, as can be seen in Figure S6 in Supporting Information (SI) obtained for an identical recombinamer lacking the silk motifs, no dependence of the viscosity with the shear rate for any annealing time was detected.

A noticeable difference was observed in the viscosity of samples for 24, 36 and 48 h with respect to the sample for 12 h (Figure 7). The viscosity for the sample at 48 h was slightly higher than that of the samples at 24 h and 36 h. This trend for $pA(EIS)_2$-$(I_5R)_6$ with different annealing time corroborates the behavior recorded with CD for at 4 °C (Figure 3A).

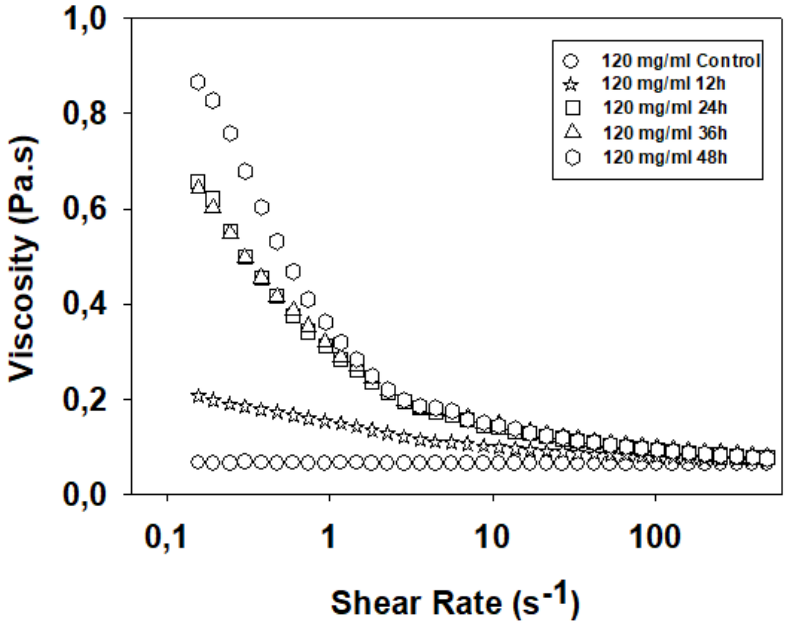

Figure 7. Dependence of the viscosity on the shear rate in a scale lin-log for $(EIS)_2$-$(I_5R)_6$ & $pA(EIS)_2$-$(I_5R)_6$ hydrogels with 12, 24, 36 and 48 h of pre-annealing. These parameters were calculated by numerical fitting of the experimental data to Equation (1). In each fitting $R^2 > 0.990$ was found.

Thus, from the viewpoint of injectability, the pre-annealing time of 24 h seems to be the most appropriate, considering enough maturation of the β-sheet structures and an adequate viscosity to make the injection process easier.

3.6. Rheological characterization of the hydrogels

Immediately after the 30 min of the *in situ* gelation of the hydrogels was finished, oscillatory rheological measurements were done, with special attention paid to the concentration of 120 mg/ml pre-annealed for 24 h. First, a sweep in the amplitude of the test signal was carried out in a strain sweep test, which provided the linear range where the rheological characterization should take place. According to Figure S7 (SI), a wide linear range was obtained. As a trade-off between linearity and noise, a strain of 1% was chosen for every subsequent rheological measurement. Moreover, this Figure also includes the results for the concentrations of 100, 150, and 180 mg/ml, showing a clear trend: the higher the concentration, the higher the complex modulus.

Dynamic frequency sweep measurements were performed in the frequency range of 0.1 and 50 Hz. The evolution of the storage modulus (G´), and the loss modulus (G´´) as a function of the frequency were represented in Figure 8A. Whereas a dependence of G' on frequency is observed, no significant dependence of G'' is found up to 10 Hz. It should be pointed out that the value of G´ is significantly higher than G´´, which is calculated by the loss factor tan δ ≡ G´´/G´ (Data not shown). Specifically, δ is around 12 - 13° for the frequency of 1 Hz, indicating a visco-elastic hydrogel behavior.

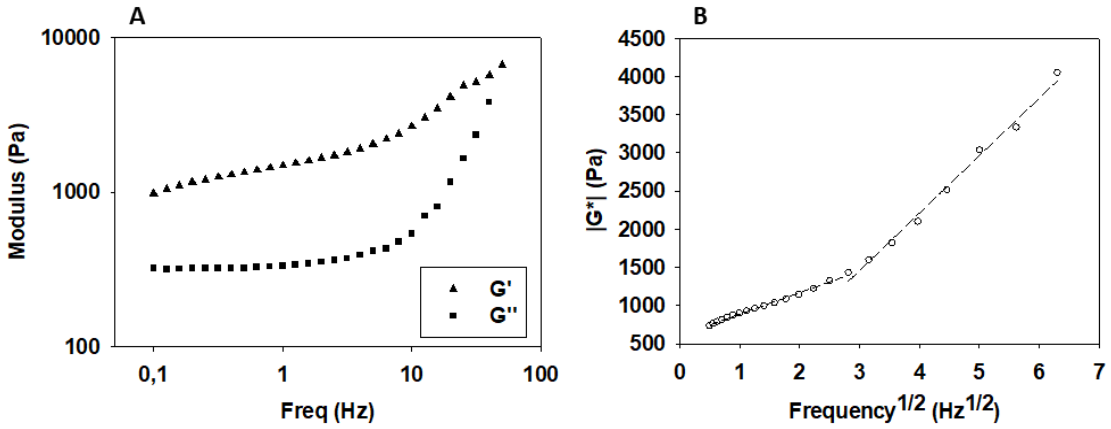

Figure 8. (A): Frequency dependence of the storage (G') and loss (G'') moduli for the pA$(EIS)_2$-$(I_5R)_6$ hydrogels at 120 mg/ml with 24 h of pre-annealing. (B): Dependence of the magnitude of the complex modulus on $f^{½}$ for the concentration of 120 mg/ml. The dashed lines correspond to the least-squares linear regressions of each linear region. In every case, R^2 is better than 0.990. Each curve corresponds to the average of three different samples measured.

In order to obtain some information about the physical mechanisms that determine the frequency dependence of |G*|, the dependence of |G*| on $f^{1/2}$ for the hydrogel of 120 mg/mL has been drawn in Figure 8B. A linear dependence based on two different slopes was found in the frequency range considered.

3.7. Scanning electron microscopy

pA$(EIS)_2$-$(I_5R)_6$ hydrogel at 120 mg/ml shows a pore size of 10.23 ± 2.87 µm and wall thickness of 0.71 ± 0.12 µm (Figure 9). pA$(EIS)_2$-$(I_5R)_6$ hydrogels at 150 & 175 mg/ml show, respectively, a pore size of 6.97 ± 2.30 µm & 5.22 ± 1.87 µm; and wall thickness of 1.85 ±

1.40 µm & 2.85 ± 1.11 µm (SI Figure S8). The pA$(EIS)_2$-$(I_5R)_6$ hydrogels at all of the concentrations showed a 3D porous environment with an interconnected structure.

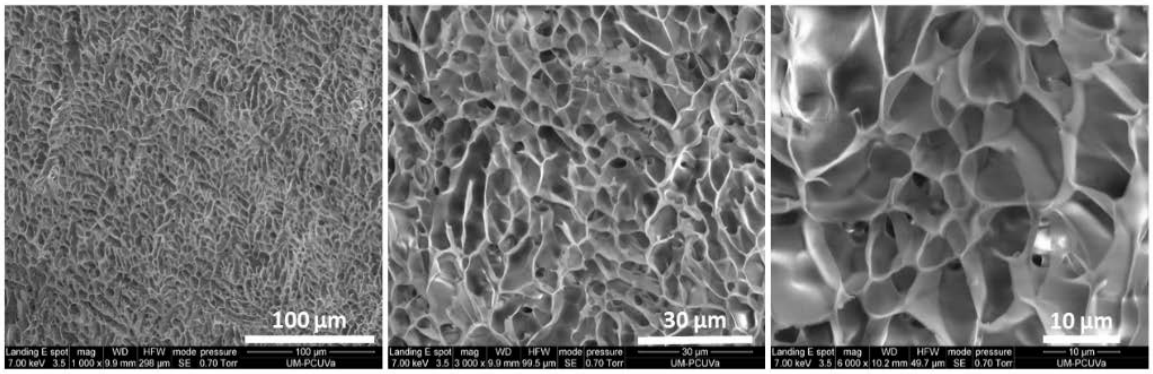

Figure 9. Representative SEM pictures for pA$(EIS)_2$-$(I_5R)_6$ hydrogel at 120 mg/ml at different magnifications.

3.8. Cell viability assay

The chondrocytes (20 million cells/ml) were mixed with the hydrogel as described in Material and Methods. The mixture was further stained with DAPI (nuclear counterstain) according to the standard protocol. As it can be seen in Figure S9 (SI) the cells were uniformly distributed. A metabolic activity assay was performed for the *in vitro* study at time 0, 2, and 4 weeks of culture. The cell viability analysis revealed an increase of metabolic activity, especially within the first 2 weeks, most likely due to the increase in number of cells; moreover, the viability of the cells remained high throughout the 4 weeks of culture, proving a suitable concentration of pA$(EIS)_2$-$(I_5R)_6$ hydrogel (Figure 10).

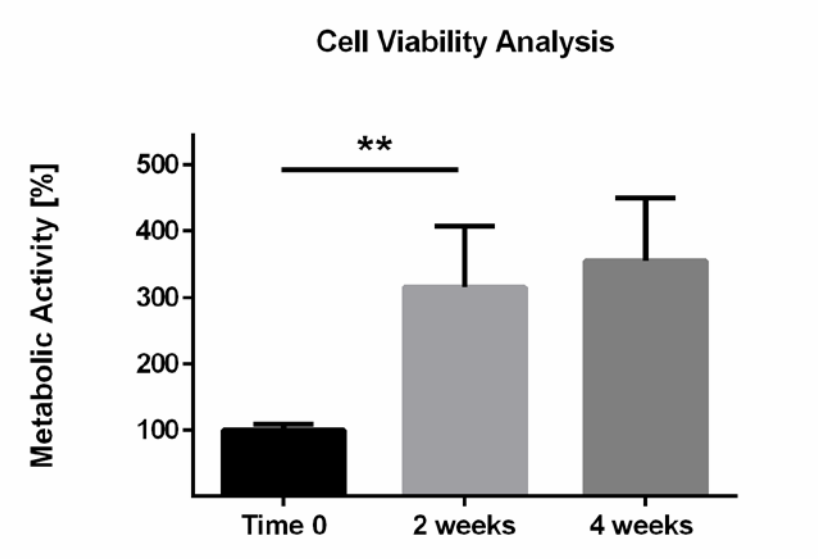

Figure 10. Cell viability test of pA$(EIS)_2$-$(I_5R)_6$ with 24h of pre-annealing at 120 mg/ml 3D gel embedded with pig chondrocytes (20 million/ml) at different time points (**P<0.01).

3.9. Biochemical analysis

In order to quantify the GAG and the DNA content of the hydrogel embedded with chondrocytes for the *in vitro* and *ex vivo* study at day 0 and 28, a biochemical analysis was performed. In both studies, an increase in DNA content was recorded with more significance in the *ex vivo* study (Figure 11). Moreover, at day 28 the DNA content of the *ex vivo* study was higher compare to the *in vitro* study with a significant difference (P<0.001).

The GAG content at day 0 has revealed the complete absence of polysaccharides, whereas at day 28 we recorded a large presence of glycosaminoglycan in both studies (Figure 11). Comparing the GAG content at day 28, the content was significantly higher in the *ex vivo* study than the content in the *in vitro* study (P<0.05) (Figure 11). Biochemical analysis of the hydrogel itself was performed for the *in vitro* and *ex vivo* study at day 0 and 28. As it can be seen in Figure S10 (SI), in both studies the values remained approximately zero, meaning the absence of contribution in GAG and DNA content from the surrounding tissue (in the case of *ex vivo* study).

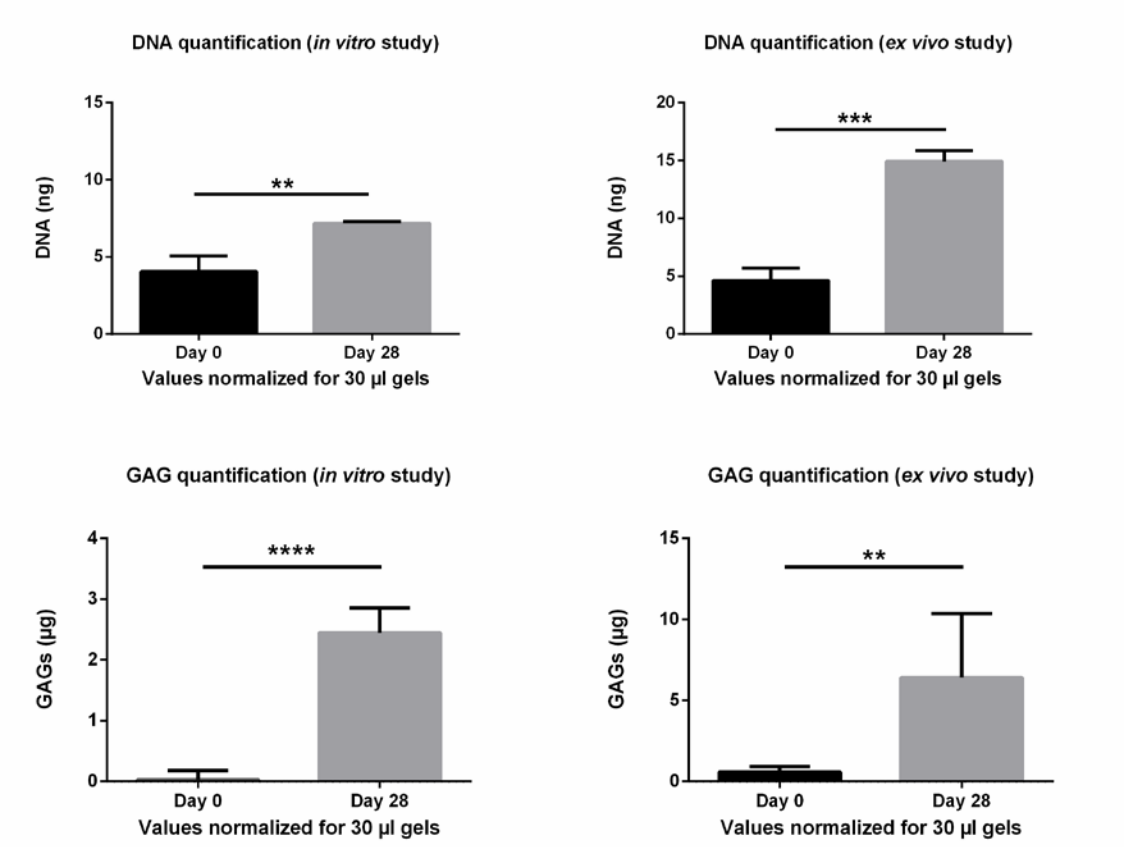

Figure 11. DNA and GAG content of the hydrogels embedded with chondrocytes for the *in vitro* and *ex vivo* study at day 0 and 28. All the values have been normalized for 30 µl volume of hydrogel (*P<0.05; **P<0.01; ***P<0.001; ****P<0.0001).

3.10. Histological analysis

Histological analyses were performed for the hydrogels embedded with chondrocytes at day 28 for the *in vitro* (Figure 12) and *ex vivo* study (Figure 13). For general histomorphological evaluation, the sections were stained with H/E; moreover, in order to evaluate the general collagen and GAG content produced by chondrocytes, the sections of hydrogels were stained with Picro-Sirius Red Stain and Safranin-O/Fast Green, respectively. For both studies, the H/E staining reveled a very homogenous distribution of chondrocytes embedded in the hydrogel. The Picro-Sirius Red Stain and Safranin-O/Fast Green demonstrated how the cells started to produce and secrete collagen and GAG, and thus began forming their own ECM, in Figure 12 (B & C) for the *in vitro* study and in Figure 13 (B & C) for the *ex vivo* study.

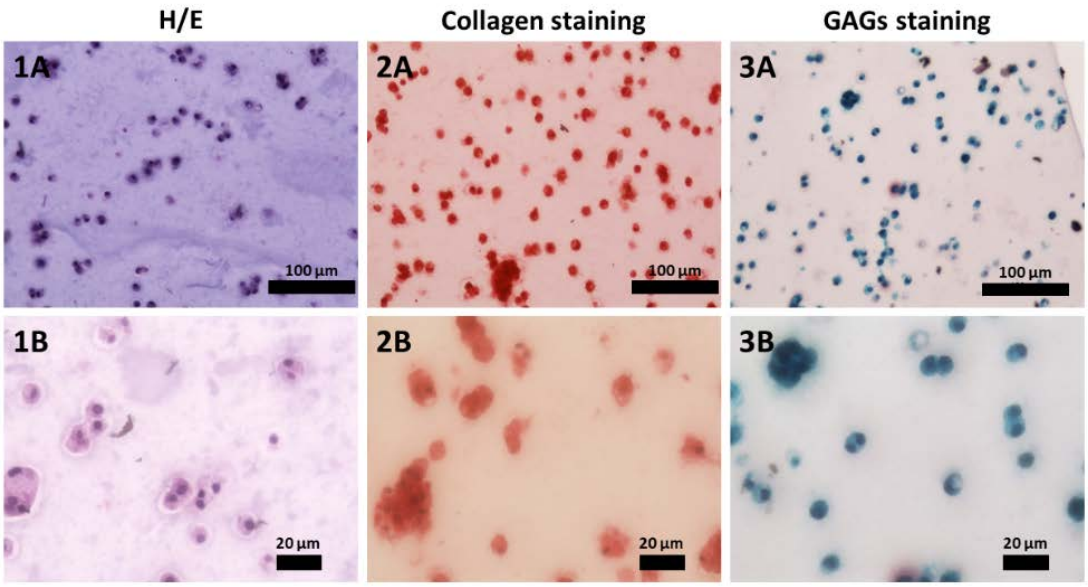

Figure 12. Histology of *in vitro* study with different staining, pictures collected at different magnifications (A&B): 1: H/E; 2: Collagen staining; 3: GAG staining.

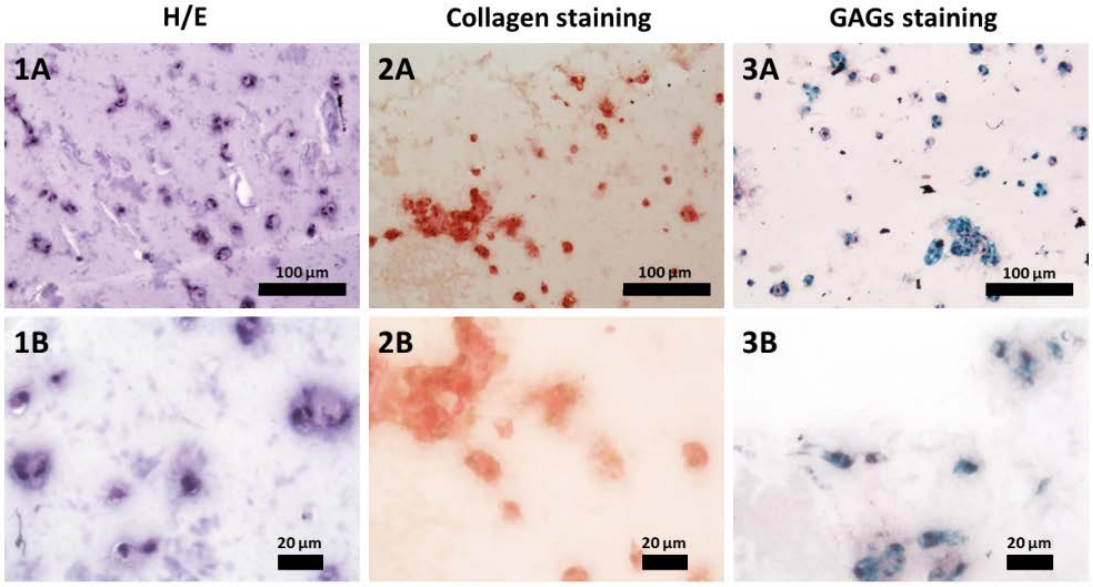

Figure 13. Histology of the *ex vivo* study with different staining, pictures collected at different magnifications (A&B): 1: H/E; 2: Collagen staining; 3: GAG staining.

3.11. Immunohistochemistry (IHC)

The sections of the samples from *in vitro* study and *ex vivo* study at day 28 were immunostained with primary antibody anti-collagen type I, and anti-collagen type II, in order identify the types of collagen stained by the general Picro-Sirius. The

immunohistochemistry revealed the absence of collagen type I produced by chondrocytes in both studies (Figure 14, B). The positive control for collagen type I was obtained embedding the hydrogel with HFF1 (Human foreskin fibroblasts 1). It's well known that HFF1 are responsible for the production of collagen type I, which is a sign of fibro-cartilage formation (52). Diversely, in both studies the IHC showed a clear signal for the antibody against collagen type II (hyaline cartilage), which is a sign of adequate cartilage regeneration (Figure 14, A).

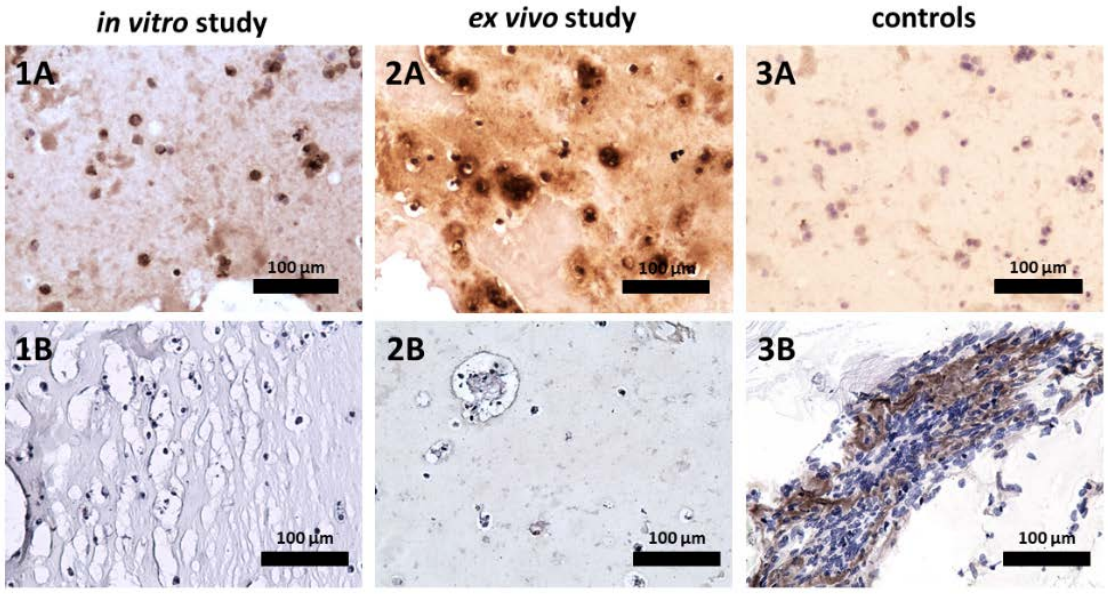

Figure 14. Immunohistochemistry of the *in vitro* and *ex vivo* study with Ab anti-collagen type II and Hematoxylin (respectively 1A & 2A). Immunohistochemistry of the *in vitro* study and of the *ex vivo* study with Ab anti-collagen type I and Hematoxylin (respectively 1B & 2B). 3A: Ctrl-: absence of Ab anti collagen type II; 3B: Ctrl+: IHC with Ab anti collagen type I and hematoxylin of hydrogel embedded with HFF1 cultured 21 days.

4. DISCUSSION

Tissue engineering for cartilage repair lacks biomaterials that have adequate mechanical properties capable of rapidly forming a gel that can be delivered into the area of interest via sample injection. Considering the unique properties of ELRs and silk, we have focused our attention on SELR obtained by recombinant techniques. The composition of this SELR is based on synthetized block co-recombinamers, which have silk motifs, elastin motifs and bioactive sequence (RGD). This SELR sequence contains the optimal content of silk

motifs for adequate thermosensitive properties and for the expression in bacteria (28). Moreover, a repetition of six RGD sequences was included in order to have a good cellular adhesion response (53). The elastin motifs were designed to comprise a hydrophobic and hydrophilic block. The copolymer structures have been reported to form elastomeric hydrogels, in which the hydrophilic blocks provide conformational elastic properties and the hydrophobic blocks form cross-links by hydrophobic aggregation (30, 31). Thus, SELR hydrogels are formed by the physical interactions from elastin motifs and silk motifs. In the first part of this study, we set up and optimized a pre-annealing treatment based on the evolution of silk motifs into β-sheet structures, in order to fulfill the required mechanical properties of hydrogels for cartilage repair. We finally obtained the proposed $pA(EIS)_2$-$(I_5R)_6$. Afterwards, we have carried out the characterization of our material with the combination of several experimental techniques (CD, TEM, SEM, and rheology), providing a deeper insight into the material features.

The CD spectra recorded at all the temperatures indicates a predominantly disordered structure, where a proportional trend towards a more ordered structure can be appreciated for increasing pre-annealing times. This trend is based on the increase of the magnitude of the signal at 210 nm and at 197 nm, associated with the presence of β-turns and β-sheet structures, respectively. Thus, CD has shown that the pre-annealing treatment speeds up the arrangement of silk motifs into β-sheet conformation.

It has already been investigated that a closely related ELR containing silk motifs is able to self-assemble into nanofibers through an evolution which is not immediate (26). The nanostructure formation of the $pA(EIS)_2$-$(I_5R)_6$ checked by TEM (Figure 4), shows how these gels are able to form a dense network of fibers immediately after injection. This is due to the phenomenon of thermal memory, by which the supramolecular rearrangement of the silk motifs into β-sheets has been enhanced by the pre-annealing treatment (and conserved by the freeze-drying step). The density of the network of fibers for the 12 h pre-annealing time appears lower than for the group of 24, 36 and 48 h.

The TEM results corroborate the CD analysis, where a similar trend has been observed. The visualization of sol-gel behavior (Figure 5) has shown that the rearrangement of silk motifs into β-sheet conformation has a direct influence on the gelation process, allowing

the gel formation at a lower concentration. Thereby, the gelation process for all the pA$(EIS)_2$-$(I_5R)_6$ processes was investigated by rheological characterization.

At the end of the measuring time (30 min) the corresponding complex modulus are: 100 mg/ml: 512 Pa; 120 mg/ml: 1537 Pa; 150 mg/ml: 2040 Pa; 180 mg/ml: 3190 Pa (Figure 6B). This modulus increase with the concentration is possibly attributed to the increase of the hydrophobic interactions between the elastin motifs.

When the concentration is fixed (120 mg/ml), the dependence of moduli with the pre-annealing time shows a lower stiffness for the pre-annealing time of 12 h, compared to longer annealing times. At the end of the measuring time (30 min), a similar modulus (around 1 kPa) is observed for the annealing time of 24, 36 and 48 h (Figure 6A). Since in this case the percentage of elastin is constant, these moduli are related to the presence of β-sheets. Thus, a similar maturation of β-sheets is suggested for annealing times from 24 to 48 h. This result agrees with the results obtained by using CD and TEM.

It has been reported that the concentration of 120 mg/ml represented a cut-off to obtain a significant effects of the pre-annealing treatment. Moreover, Figure 6B shows how for the pA$(EIS)_2$-$(I_5R)_6$ at 100 mg/ml there are no changes for 24 and 48 h annealing times.

The higher the concentration of pA$(EIS)_2$-$(I_5R)_6$ in the hydrogel, the more difficult it is to dissolve the material, but also to mix in cells, while still achieving a homogeneous cell distribution, due to the high viscosity. It can also be expected that more gel is lost during handling by attachment to syringes or pipet tips. Thus, solution viscosity is a significant parameter during the injection process.

The pre-annealing treatment affects the viscosity. It has been previously reported that the annealing time impacts the formation and maturation of the β-sheets existing in silk-based ELRs (26). Thus, this increased viscosity may be related to the different β-sheet structures induced by the annealing process. The dependence of viscosity on the shear rate (Figure 7) suggests modeling according to the equation

$$\eta\,(sh-rate) = \eta\infty + \sum_{i=1}^{2} Gi \cdot exp^{-\tau i \cdot (sh-rate)} \qquad (1)$$

based on a series of two decreasing exponential functions (Maxwell dependence), where τi are the relaxation time constants, and Gi are the weight of the τi-type relaxation to the overall relaxation process that is mainly dominated by each time constant within the corresponding shear rate range. Finally, η∞ corresponds to the viscosity at an enormous (infinite) shear rate.

The impact of the different annealing times on the viscosity corroborates the behavior recorded in the CD analysis at the same temperature (4 °C) (Figure 3A). Rheological flow measurements are in agreement with supramolecular analysis like CD and TEM. Moreover, considering that the temperature of the analysis for CD and rheological flow measurements is lower than the T_t of the SELRs, we can assume that the β-sheet structures formed by the pre-annealing treatment are conserved even after the freeze-drying step.

The experimental data of Figure 7 has been numerically fitted to Equation (1) and all the parameters have been obtained (Figure 15A and 15B). As can be seen, a threshold is again observed for the pre-annealing of 12 h both for the weights and the time constants of relaxation. For a fixed relaxation process, no noticeable changes are found for samples annealed for 24, 36 and 48 h, although for G1 the weight for the 48 h annealed sample is slightly higher. Relaxation process 1 shows a very short relaxation time (lower than 0.1 s), while the time constant of the second relaxation process is higher than 1 s.

Thus, the annealing time of 24 h has been selected in our work as a trade-off between enough maturation of the β-sheet structures and to make the injection process easier.

The rheological properties of the $pA(EIS)_2$-$(I_5R)_6$ hydrogels with 24 h of pre-annealing at 120 mg/ml are in agreement with the soft tissue engineering properties of hydrogel for biomedical application (54, 55). Dynamic frequency sweep measurements show at the frequency of 1 Hz a G': 1489 Pa and a G'': 334 Pa. As can be seen (where G' >> G''), the values of delta (specifically, δ is around 12 - 13° for the frequency of 1 Hz) for the $pA(EIS)_2$-$(I_5R)_6$ hydrogels at 120 mg/ml are in agreement with the viscoelastic behavior that has also been demonstrated in cartilage (56).

As for the physical mechanisms taking part in the rheological behavior of the hydrogel, the linear dependence of the complex modulus with $f^{1/2}$ (Figure 8B) indicates that a poroelastic mechanism dominates the viscoelastic behavior in this frequency range. In the poroelastic mechanism, viscous drag of interstitial fluid (water) through the porous recombinamer network and fluid–solid frictional interactions due to fluid pressurization are predominant (57, 58).

The slope is related to the hydrogel permeability that is a macroscopic measure of the ease with which a fluid can flow through the hydrogel matrix. In our case, two slopes are observed, whose values were numerically fitted: 282 ± 6 Pa/$Hz^{1/2}$ for $f^{1/2}$ < 2.5 $Hz^{1/2}$, and 753 ± 28 Pa/$Hz^{1/2}$ for $f^{1/2}$ > 2.5 $Hz^{1/2}$. Thus, the slope increases when the frequency exceeds 6.25 Hz. A slope increase was associated with a decrease in hydrogel permeability (54, 59). A similar behavior was reported for elastin-like catalyst free click gels (54) and hybrid elastin-like recombinamer-fibrin gels (60). However, in both cases, a single slope was obtained throughout the frequency range analyzed.

The pre-annealing treatment does have an effect on the gelation process. In fact, the observed increase in the storage modulus of $pA(EIS)_2$-$(I_5R)_6$ hydrogels (Figure 6A) indicates the contribution of the pre-annealing treatment on the gelation process by the increase of the crosslinking network. Moreover, the pre-annealing treatment has an impact on the concentration of the hydrogel, allowing the formation of the hydrogel at a lower concentration than observed by Fonseca *et al*. (27).

Fernandez-Colino *et al*. reported how the elastin contribution leads to the rapid and early formation of a hydrogel, whereas the silk domains can increase the modulus of the hydrogel over time (26). The same behavior has been recorded with the $pA(EIS)_2$-$(I_5R)_6$ hydrogels, with regards to the pre-annealing treatment that accelerate the β-sheet formation. CD and TEM confirms this phenomenon of thermal memory based on the growth-boosting of the β-sheet formation, which exerts an indirect influence on temperature trigger gelation.

Therefore, taking into account the two slopes observed both in the evolution of the complex modulus with f ½ and in the viscosity dependence on the shear rate, we

tentatively suggest that these two slopes are related to the two interactions existing in our silk-based ELR: the hydrophobic interaction associated with elastin, and the β-sheet interaction due to the silk-block. Both of them contribute to the crosslinking network of the physical hydrogel. In the oscillatory measurements, the higher slope, corresponding to a higher hindrance of the fluid flow through the hydrogel structure, might be associated with the β-sheet structures, which are stiffer and more rigid than the elastin interaction.

As for flow measurements, since more rigid blocks take more time to respond, the first process (characterized by G1 and τ1) might be related to the β-sheet structures. Following this idea, Figure 11 shows that both the β-sheets and the hydrophobic elastin interactions are affected by the pre-annealing time, although the former to a greater extent. Thus, it is suggested that both physical interactions are not independent, but that the maturation of the β-sheet structures the spatial location of the hydrophobic blocks modifies, altering this interaction, as it has been recently reported by Fonseca *et al*. (27).

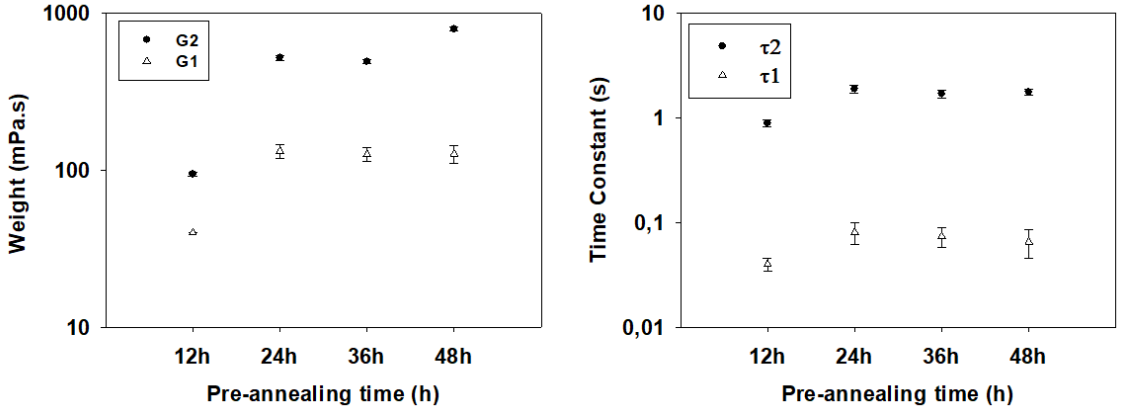

Figure 15. Fitted parameters according to Equation (1) obtained from the numerical fitting of the experimental curves of Figure 4. A: G1 and G2; B: τ1 and τ2.

The morphology of the pA(EIS)$_2$-(I$_5$R)$_6$ hydrogels at 120, 150 and 180 mg/ml was investigated by SEM (Figure 9 and Figure S8). The fibrillary structure, obtained by the pre-annealing treatment, does not negatively influence the porosity of the hydrogel; in fact, pA(EIS)$_2$-(I$_5$R)$_6$ hydrogels show a homogeneous porous environment with an interconnected structure. Porosity plays a critical role in the outcome of a tissue-engineered scaffold; the cells seeded in there rely heavily on the void spaces within the construct for cellular in-growth, exchange of nutrients, and removal of waste products

(61). In addition, the extent of ECM secretion also increases by increasing pore size (62). Moreover, the chondrocytes are the exclusive cells in articular cartilage, with a size of 10–13 µm diameters and are involved in the synthesis of the cellular matrix constituents (63). Considering the pore size of the pA$(EIS)_2$-$(I_5R)_6$ hydrogels at 120 mg/ml: 10.23 ± 2.87 µm, pA$(EIS)_2$-$(I_5R)_6$ hydrogel at 120 mg/ml presents a suitable pore size to create a 3D matrix embedded with chondrocytes.

In summary, the first part of the study intended to characterize the material proposed, and to understand the physical contribution of the silk motifs in relation to the elastin motifs for the cross-linkage of the hydrogel. We have paid particular attention to the characterization of the pA$(EIS)_2$-$(I_5R)_6$ hydrogels with different annealing times (12, 24, 36 and 48 h) and different concentrations (100, 120, 150, 180 mg/ml). From the combination of the experimental results obtained by various techniques, the concentration of 120 mg/ml pre-annealed for 24 h established a threshold for gelation, and these conditions were selected as the most suitable candidate as injectable hydrogel for cartilage repair. The second part of the study focused on the potential of the selected pA$(EIS)_2$-$(I_5R)_6$ hydrogels with 24 h of pre-annealing at 120 mg/ml, as a good candidate for cartilage repair.

A well-accepted tissue-engineering paradigm is that, the most successful scaffold for tissue repair is a biomaterial that mimics the functional properties of native tissue extra cellular matrix (ECM), facilitates encapsulation of reparative cells and is supportive of cell repair activities, including proliferation and *de novo* production of ECM (64). Although, the biocompatibility of ELR-based hydrogels formed through physical cross-linking has been extensively studied (53), in this study we have performed for the first time a 4 week culturing metabolic activity assay of the pA$(EIS)_2$-$(I_5R)_6$ hydrogel embedded with chondrocytes. The cell viability analysis has revealed that the selected concentration (120 mg/ml) supports cell viability and metabolic activity. In order to evaluate the regenerative abilities of our newly developed hydrogel-scaffold systems, a well established *ex vivo* model as a culture platform was used (37, 65). The biggest advantage of using this *ex vivo* model is to test biomaterials in a native environment for relevant culture period, with the possibility to oversee the healing process monitoring the physiological and biochemical contents of the regenerated tissue.

In Figure 11 DNA and GAG content is shown. In both cases, the content is obtained for a given volume of hydrogel analyzed (66, 67). The increase in DNA and GAG content recorded through biochemical analysis shows how the $pA(EIS)_2$-$(I_5R)_6$ hydrogel is an appropriate scaffold for chondrocytes embedding involved in cartilage repair. Furthermore, comparing the biochemical contents of the *in vitro* study with the *ex vivo* study, the DNA quantification shows how the osteochondral culture platform facilitates a better proliferation of chondrocytes. The same trend was observed with respect to GAG content, where the glycosaminoglycan content of the *ex vivo* study was higher compare to the *in vitro* study. According to the bibliography, the GAG density observed in our study was still not in the same range of mature cartilage (68). This was expected, considering that 28 days is a short time to obtain a mature regenerated cartilage. Anyway, comparing our scaffold with other hydrogel systems for cartilage repair, the media GAG content normalized to DNA obtained for our system (427 μg of GAG per μg of DNA), demonstrated a larger production of glycosaminoglycan (69).

The biochemical analysis for GAGs and DNA confirms that the *ex vivo* osteochondral culture platform is a good and representative model to evaluate the healing progress in created cartilage defects.

Histological analysis confirms the biochemical results, showing a higher amount of GAGs stained by Safranin-O/Fast Green in the *ex vivo* study. Moreover, the Picro-Sirius Red Stain staining revealed a larger production of collagen by the chondrocytes cultured in the *ex vivo* osteochondral culture platform. Finally, for both studies, the H/E staining demonstrated a very homogenous distribution of chondrocytes embedded in the hydrogel, showing efficient mixing of the matrix with the cells achieved by the adequate concentration of the hydrogel. Some cells look like they underwent a mitosis step (Figure 12: 1A, 2A and Figure 13: 1A, 2A), which results are in accordance with the values obtained by biochemical analysis for the DNA content.

Immunohistochemistry for collagen type I and collagen type II revealed the absence of collagen type I (a sign of undesired fibro-cartilage formation) in both studies. Diversely the IHC in both studies showed a clear signal for the antibody against collagen type II (hyaline cartilage); furthermore, the IHC revealed a better production and secretion of

collagen type II in the *ex vivo* study compared to the *in vitro* study. The absence of collagen type I and the production of collagen type II, which gives tensile strength to cartilage (70), proves that pA$(EIS)_2$-$(I_5R)_6$ hydrogel is an excellent candidate for osteochondral repair.

As it is widely reported in literature, agarose and PEG hydrogels are considered ones of the best alternative for cartilage tissue engineering, due to the good biological and mechanical properties (66,71,72). However, they do not provide specific biological functions, which could be obtained by the recombinant protein technique used in our study for a bioactive hydrogel. Moreover, after 28 days of culturing in the *ex vivo* platform, our hydrogel demonstrated a GAG production per µg of DNA around 10 times more than in the case of PEG or agarose based scaffolds (69).

Finally, the analysis recorded for the *ex vivo* study with the osteochondral culture platform confirms the importance of a native environment for the production of hyaline cartilage by mature chondrocytes.

5. CONCLUSIONS

We developed and produced the pre-annealed Silk Elastin co-Recombinamer (pA$(EIS)_2$-$(I_5R)_6$), which shows unique properties as a promising candidate for tissue engineering applications. We have focused on the need for biomaterials for cartilage repair, capable of being delivered into the area of interest, showing a rapid gelation and adequate mechanical properties when surrounded by synovial fluid. We have set up and optimized a pre-annealing treatment based on the evolution of silk motifs into β-sheet structures and on the phenomenon of thermal memory. In this study, we have carried out the physical characterization of our material in order to provide a deeper insight into the material features, analyzing the contribution of each component (Silk and Elastin) for the cross-linking formation. The pA$(EIS)_2$-$(I_5R)_6$ has shown a fast gelation, improved mechanical properties, and the presence of a fibrillary structure directly after injection of the hydrogel. Moreover, culturing the hydrogel embedded with chondrocytes in the *ex vivo* culture platform for weeks has exhibited good biocompatibility and remarkable advantages; such as the *de novo* ECM formation, the absence of fibro-cartilage and the production of hyaline cartilage. The addition of the silk allows to make hydrogels with

lower concentration, leading to larger pores, which is most likely responsible for better cell spreading, and proliferation. In conclusion, the pA$(EIS)_2$-$(I_5R)_6$ has shown to have new outstanding properties, which make the hydrogel a promising injectable scaffold in the field of cartilage regeneration.

ASSOCIATED CONTENT

Supporting Information

SDS-PAGE analysis, MALDI-TOF spectra, amino acid composition, FTIR spectra, DSC analysis and H-NMR spectra for the pA$(EIS)_2$-$(I_5R)_6$. Dependence of the viscosity for an identical recombinamer hydrogels lacking the Silk blocks with different pre-annealing times. Strain dependence of |G*| for the 24 h pre-annealed pA(EIS)2-(I5R)6 hydrogels at different concentrations. SEM analysis for the pA$(EIS)_2$-$(I_5R)_6$ hydrogels at different concentrations. Fluorescent microscope image of the hydrogel embedded with chondrocytes after DAPI staining. Biochemical analysis of the hydrogel alone for the *in vitro* and *ex vivo* study. This list of contents is supplied in Supporting Information.

AUTHOR INFORMATION

Corresponding Author

* E-mail: fcipriani@tpnbt.com

Author Contributions

The manuscript was written through contributions of all authors. All authors have given approval to the final version of the manuscript

Notes

The authors declare no competing financial interests.

Acknowledgment

This project has received funding from the European Union's Horizon 2020 research and innovation programme under the Marie Sklodowska-Curie grant agreement No 642687.

The authors are grateful for the funding from the European Commission (NMP-2014-646075), the Spanish Government (PCIN-2015-010, MAT2015-68901-R, MAT2016-78903-R, MAT2016-79435-R), Junta de Castilla y León (VA015U16) and Centro en Red de Medicina Regenerativa y Terapia Celular de Castilla y León.

References

1. Buckwalter, J.A. and H.J. Mankin, Articular cartilage: tissue design and chondrocyte-matrix interactions. Instructional course lectures, 1998. 47: p. 477-486.

2. Amadio, P.C., Friction of the Gliding Surface: Implications for Tendon Surgery and Rehabilitation. Journal of hand therapy: official journal of the American Society of Hand Therapists, 2005. 18(2): p. 112-119.

3. Tuli, R., W.-J. Li, and R.S. Tuan, Current state of cartilage tissue engineering. Arthritis Res Ther, 2003. 5(5): p. 235.

4. Huey, D.J., J.C. Hu, and K.A. Athanasiou, Unlike Bone, Cartilage Regeneration Remains Elusive. Science, 2012. 338(6109): p. 917-921.

5. Griffith, L.G. and G. Naughton, Tissue Engineering--Current Challenges and Expanding Opportunities. Science, 2002. 295(5557): p. 1009-1014.

6. Daley, W.P., S.B. Peters, and M. Larsen, Extracellular matrix dynamics in development and regenerative medicine. Journal of Cell Science, 2008. 121(3): p. 255-264.

7. Maroudas, A., et al., The permeability of articular cartilage. J Bone Joint Surg Br, 1968. 50(1): p. 166-77.

8. Kheir, E. and D. Shaw, Hyaline articular cartilage. Orthopaedics and Trauma, 2009. 23(6): p. 450-455.

9. Sophia Fox, A.J., A. Bedi, and S.A. Rodeo, The Basic Science of Articular Cartilage: Structure, Composition, and Function. Sports Health, 2009. 1(6): p. 461-468.

10. Erkamp, R.Q., et al., Measuring the Elastic Modulus of Small Tissue Samples. Ultrasonic Imaging, 1998. 20(1): p. 17-28.

11. Freeman, P.M., et al., Chondrocyte cells respond mechanically to compressive loads. Journal of Orthopaedic Research, 1994. 12(3): p. 311-320.

12. Mow, V.C., M.H. Holmes, and W. Michael Lai, Fluid transport and mechanical properties of articular cartilage: A review. Journal of Biomechanics, 1984. 17(5): p. 377-394.

13. Marijnissen, W.J.C.M., et al., Alginate as a chondrocyte-delivery substance in combination with a non-woven scaffold for cartilage tissue engineering. Biomaterials, 2002. 23(6): p. 1511-1517.

14. Muir, H., The chondrocyte, architect of cartilage—biomechanics, structure, function and molecular-biology of cartilage matrix macromolecules. Bioessays, 1995. 17(12): p. 1039-48.

15. Wall, A. and T. Board, Mesenchymal Cell-Based Repair of Large Full Thickness Defects of Articular Cartilage, in Classic Papers in Orthopaedics, P.A. Banaszkiewicz and D.F. Kader, Editors. 2014, Springer London: London. p. 441-443.

16. Dewan, A.K., et al., Evolution of Autologous Chondrocyte Repair and Comparison to Other Cartilage Repair Techniques. BioMed Research International, 2014. 2014: p. 11.

17. Caldwell, K.L. and J. Wang, Cell-based articular cartilage repair: the link between development and regeneration. Osteoarthritis Cartilage, 2015. 23: p. 351-62.

18. Nagaya, H., et al., Examination of synovial fluid and serum hyaluronidase activity as a joint marker in rheumatoid arthritis and osteoarthritis patients (by zymography). Ann Rheum Dis, 1999. 58: p. 186-188.

19. Shen, Y., et al., Biomaterial and mesenchymal stem cell for articular cartilage reconstruction. Curr Stem Cell Res Ther, 2014. 9: p. 254-67.

20. Armiento, A.R., et al., Biomaterials for articular cartilage tissue engineering: Learning from biology. Acta Biomaterialia, 2018. 65: p. 1-20.

21. Girotti, A., et al., Recombinant Technology in the Development of Materials and Systems for Soft-Tissue Repair. Advanced Healthcare Materials, 2015. 4(16): p. 2423-2455.

22. Urry, D.W., Molecular Machines: How Motion and Other Functions of Living Organisms Can Result from Reversible Chemical Changes. Angewandte Chemie International Edition in English, 1993. 32(6): p. 819-841.

23. Ribeiro, A., et al., Influence of the Amino-Acid Sequence on the Inverse Temperature Transition of Elastin-Like Polymers. Biophysical Journal, 2009. 97(1): p. 312-320.

24. McDaniel, J.R., D.C. Radford, and A. Chilkoti, A Unified Model for De Novo Design of Elastin-like Polypeptides with Tunable Inverse Transition Temperatures. Biomacromolecules, 2013. 14(8): p. 2866-72.

25. Martín, L., et al., Synthesis and Characterization of Macroporous Thermosensitive Hydrogels from Recombinant Elastin-Like Polymers. Biomacromolecules, 2009. 10(11): p. 3015-3022.

26. Fernández-Colino, A., et al., Self-Organized ECM-Mimetic Model Based on an Amphiphilic Multiblock Silk-Elastin-Like Corecombinamer with a Concomitant Dual Physical Gelation Process. Biomacromolecules, 2014. 15(10): p. 3781-3793.

27. Ibáñez-Fonseca, A., et al., Förster Resonance Energy Transfer-Paired Hydrogel Forming Silk-Elastin-Like Recombinamers by Recombinant Conjugation of Fluorescent Proteins. Bioconjugate Chemistry, 2017. 28(3): p. 828-835.

28. Cappello, J., et al., Genetic engineering of structural protein polymers. Biotechnology Progress, 1990. 6(3): p. 198-202.

29. Ruoslahti, E. and M.D. Pierschbacher, Arg-Gly-Asp: A versatile cell recognition signal. Cell, 1986. 44(4): p. 517-518.

30. Sallach, R.E., et al., Elastin-mimetic protein polymers capable of physical and chemical crosslinking. Biomaterials, 2009. 30(3): p. 409-22.

31. Martin, L., et al., Rapid micropatterning by temperature-triggered reversible gelation of a recombinant smart elastin-like tetrablock-copolymer. Soft Matter, 2010. 6(6): p. 1121-1124.

32. Friedl, P., Prespecification and plasticity: shifting mechanisms of cell migration. Current Opinion in Cell Biology, 2004. 16(1): p. 14-23.

33. Kuchler-Bopp, S., et al., Nanostructured hybrid materials for bone-tooth unit regeneration. Open Journal of Regenerative Medicine, 2013. Vol.02No.03: p. 6.

34. Bernhard, J.C. and G. Vunjak-Novakovic, Should we use cells, biomaterials, or tissue engineering for cartilage regeneration? Stem Cell Research & Therapy, 2016. 7(1): p. 56.

35. Rodríguez Cabello, J.C., et al., 12 - Elastin-like materials for tissue regeneration and repair A2 - Barbosa, Mário A, in Peptides and Proteins as Biomaterials for Tissue Regeneration and Repair, M.C.L. Martins, Editor. 2018, Woodhead Publishing. p. 309-327.

36. Sallach, R.E., et al., Long-term biostability of self-assembling protein polymers in the absence of covalent crosslinking. Biomaterials, 2010. 31(4): p. 779-791.

37. Schwab, A., et al., Ex vivo culture platform for assessment of cartilage repair treatment strategies. Vol. 34. 2016, Clinical Orthopaedics and Related Research. 17-26.

38. Plunkett, N. and F. O'Brien, IV.3. Bioreactors in tissue engineering. Vol. 19. 2011. 55-69.

39. Cook, J.L., et al., Animal models of cartilage repair. Bone and Joint Research, 2014. 3(4): p. 89-94.

40. Hurtig, M.B., et al., Preclinical Studies for Cartilage Repair. CARTILAGE, 2011. 2(2): p. 137-152.

41. Laura Martín, F.J.A., Matilde Alonso, Carmen García-Arévalo and José Carlos Rodríguez-Cabello Rapid micropatterning by temperature-triggered reversible gelation of a recombinant smart elastin-like tetrablock-copolymer. Soft Matter, 2010(6): p. 1121-1124.

42. Reguera, J., et al., Nanopore Formation by Self-Assembly of the Model Genetically Engineered Elastin-like Polymer [(VPGVG)2(VPGEG)(VPGVG)2]15. Journal of the American Chemical Society, 2004. 126(41): p. 13212-13213.

43. Girotti, A., et al., Influence of the Molecular Weight on the Inverse Temperature Transition of a Model Genetically Engineered Elastin-like pH-Responsive Polymer. Macromolecules, 2004. 37(9): p. 3396-3400.

44. García-Arévalo, C., et al., Immunomodulatory Nanoparticles from Elastin-Like Recombinamers: Single-Molecules for Tuberculosis Vaccine Development. Molecular Pharmaceutics, 2013. 10(2): p. 586-597.

45. Rodríguez-Cabello, J.C., et al., Synthesis of Genetically Engineered Protein Polymers (Recombinamers) as an Example of Advanced Self-Assembled Smart Materials, in Nanotechnology in Regenerative Medicine: Methods and Protocols, M. Navarro and J.A. Planell, Editors. 2012, Humana Press: Totowa, NJ. p. 17-38.

46. Costa, R.R., et al., Layer-by-Layer Assembly of Chitosan and Recombinant Biopolymers into Biomimetic Coatings with Multiple Stimuli-Responsive Properties. Small, 2011. 7(18): p. 2640-2649.

47. Urry, D.W., R.G. Shaw, and K.U. Prasad, Polypentapeptide of elastin: Temperature dependence of ellipticity and correlation with elastomeric force. Biochemical and Biophysical Research Communications, 1985. 130(1): p. 50-57.

48. Farndale, R.W., C.A. Sayers, and A.J. Barrett, A Direct Spectrophotometric Microassay for Sulfated Glycosaminoglycans in Cartilage Cultures. Connective Tissue Research, 1982. 9(4): p. 247-248.

49. Urry, D.W., et al., Circular dichroism and absorption of the polytetrapeptide of elastin: A polymer model for the β-turn. Biochemical and Biophysical Research Communications, 1974. 61(4): p. 1427-1433.

50. Eisaku Iizukat, J.T.Y., The Disordered and β Conformations of Silk Fibroin in Solution. Biochemistry 1968. 7(6): p. 2218–2228.

51. Portnov Tanya, T.R.S.a.M.Z., Injectable hydrogel-based scaffolds for tissue engineering applications. Reviews in Chemical Engineering, 2016. 33.1 p. 91-107.

52. Betz, P., et al., Immunohistochemical localization of collagen types I and VI in human skin wounds. Int J Legal Med, 1993. 106(1): p. 31-4.

53. Ibáñez-Fonseca, A., et al., Biocompatibility of two model elastin-like recombinamer-based hydrogels formed through physical or chemical cross-linking for various applications in tissue

engineering and regenerative medicine. Journal of Tissue Engineering and Regenerative Medicine, 2017. Volume12(Issue3): p. e1450-e1460.

54. González de Torre, I., et al., Elastin-like recombinamer catalyst-free click gels: Characterization of poroelastic and intrinsic viscoelastic properties. Acta Biomaterialia, 2014. 10(6): p. 2495-2505.

55. Staubli, S.M., et al., Control of angiogenesis and host response by modulating the cell adhesion properties of an Elastin-Like Recombinamer-based hydrogel. Biomaterials, 2017. 135(Supplement C): p. 30-41.

56. Hayes, W.C. and A.J. Bodine, Flow-independent viscoelastic properties of articular cartilage matrix. Journal of Biomechanics, 1978. 11(8): p. 407-419.

57. Han, L., et al., Time-Dependent Nanomechanics of Cartilage. Biophysical journal, 2011. 100(7): p. 1846-1854.

58. Lee, B., et al., Dynamic mechanical properties of the tissue-engineered matrix associated with individual chondrocytes. Journal of biomechanics, 2010. 43(3): p. 469.

59. Spiller, K.L., et al., Superporous hydrogels for cartilage repair: Evaluation of the morphological and mechanical properties. Acta Biomater, 2008. 4(1): p. 17-25.

60. Gonzalez de Torre, I., et al., Hybrid elastin-like recombinamer-fibrin gels: physical characterization and in vitro evaluation for cardiovascular tissue engineering applications. Biomaterials Science, 2016. 4(9): p. 1361-1370.

61. Kretlow, J.D., L. Klouda, and A.G. Mikos, Injectable matrices and scaffolds for drug delivery in tissue engineering. Adv Drug Deliv Rev, 2007. 59(4-5): p. 263-73.

62. Annabi, N., et al., Controlling the porosity and microarchitecture of hydrogels for tissue engineering. Tissue Eng Part B Rev, 2010. 16(4): p. 371-83.

63. Athanasiou, K.A., E.M. Darling, and J.C. Hu, Articular Cartilage Tissue Engineering. Synthesis Lectures on Tissue Engineering, 2009. 1(1): p. 1-182.

64. Guilak, F., et al., 2010 Nicolas Andry Award: Multipotent Adult Stem Cells from Adipose Tissue for Musculoskeletal Tissue Engineering. Clinical Orthopaedics and Related Research, 2010. 468(9): p. 2530-2540.

65. Mouser, V.H.M., et al., Ex vivo model unravelling cell distribution effect in hydrogels for cartilage repair. Altex, 2018. 35(1): p. 65-76.

66. Mouw, J.K., et al., Variations in matrix composition and GAG fine structure among scaffolds for cartilage tissue engineering. Osteoarthritis and Cartilage, 2005. 13(9): p. 828-836.

67. Pfeiffer, E., et al., The effects of glycosaminoglycan content on the compressive modulus of cartilage engineered in type II collagen scaffolds. Osteoarthritis and Cartilage, 2008. 16(10): p. 1237-1244.

68. Fermor, H.L., et al., Biological, biochemical and biomechanical characterisation of articular cartilage from the porcine, bovine and ovine hip and knee. Biomed Mater Eng, 2015. 25(4): p. 381-95.

69. DeKosky, B.J., et al., Hierarchically designed agarose and poly(ethylene glycol) interpenetrating network hydrogels for cartilage tissue engineering. Tissue Eng Part C Methods, 2010. 16(6): p. 1533-42.

70. Knudson, C.B. and W. Knudson, Cartilage proteoglycans. Seminars in Cell & Developmental Biology, 2001. 12(2): p. 69-78.

71. T Nguyen, Q., et al., Cartilage-like mechanical properties of poly (ethylene glycol)-diacrylate hydrogels. Vol. 33. 2012. 6682-90.

72. Ahearne, M. and D.J. Kelly, A comparison of fibrin, agarose and gellan gum hydrogels as carriers of stem cells and growth factor delivery microspheres for cartilage regeneration. Biomed Mater, 2013. 8(3): p. 035004.

SUPPORTING INFORMATION

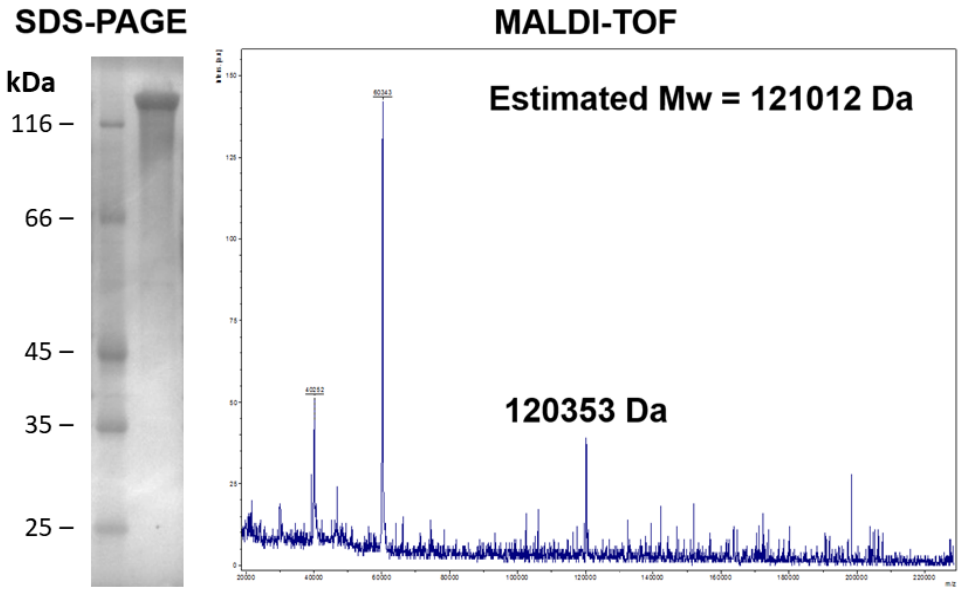

Figure S1. Molecular weight and purity assessment by SDS-PAGE and MALDI-TOF mass spectrometry for pA$(EIS)_2$-$(I_5R)_6$. MALDI-TOF spectra represent non-quantitative intensity (a.u.) against m/z (mass divided by net charge of the molecule) of the ELR.

Amino acid	Theoretical	Experimental
ASP+ASN	6+0	5.78
GLU+GLN	21	27.82
SER	39	31.91
HIS	-	-
GLY	576	577.62
THR	6	4.82
ARG	6	4.58
ALA	52	48.53
TYR	-	-
CYS	-	-

VAL	341	339.11
MET	1	1.45
TRP	-	-
PHE	-	-
ILE	150	154.44
LEU	2	2.36
LYS	-	-
PRO	257	257.24

Figure S2. Comparison between the theoretical number of each amino acid in $pA(EIS)_2$-$(I_5R)_6$ and the experimental values.

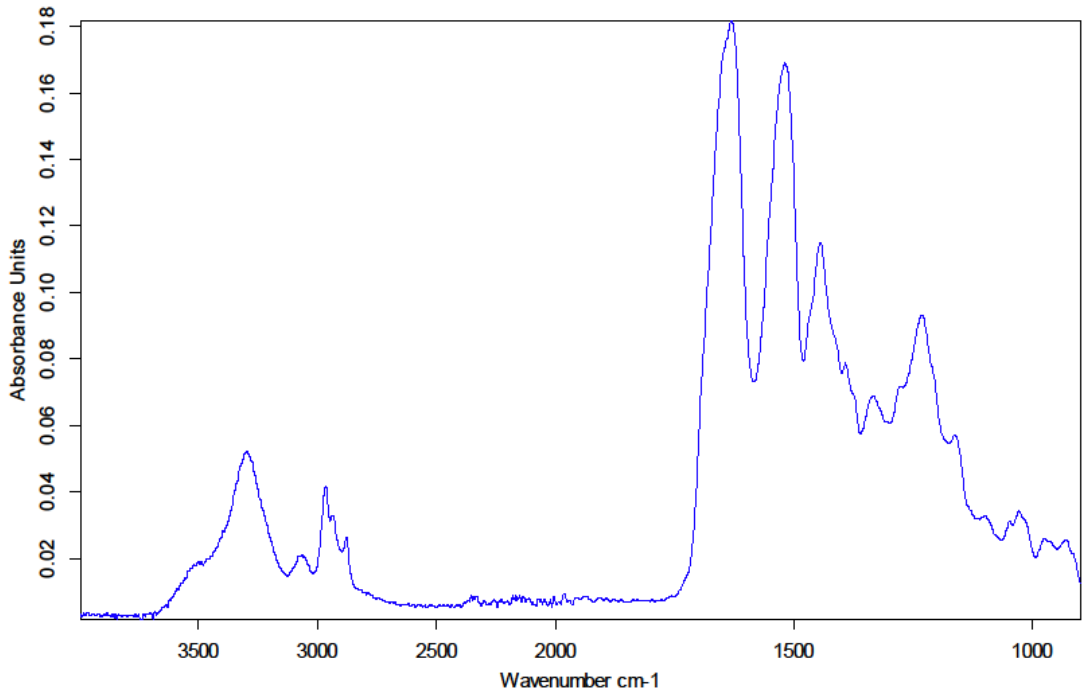

Figure S3. FTIR of $pA(EIS)_2$-$(I_5R)_6$.

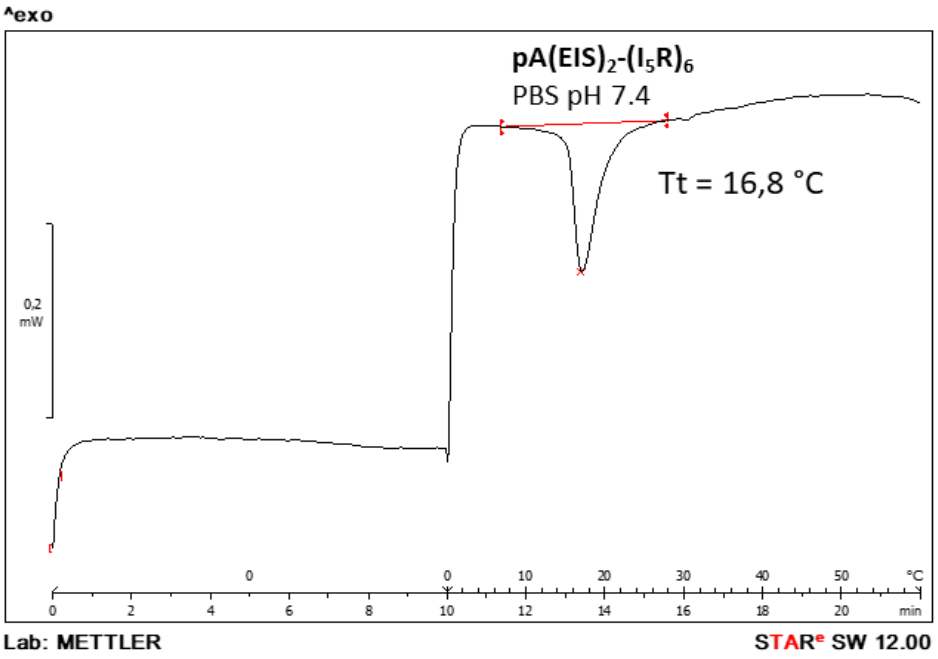

Figure S4. DSC graph of $pA(EIS)_2$-$(I_5R)_6$ showing the experimental Tt in PBS at physiological pH.

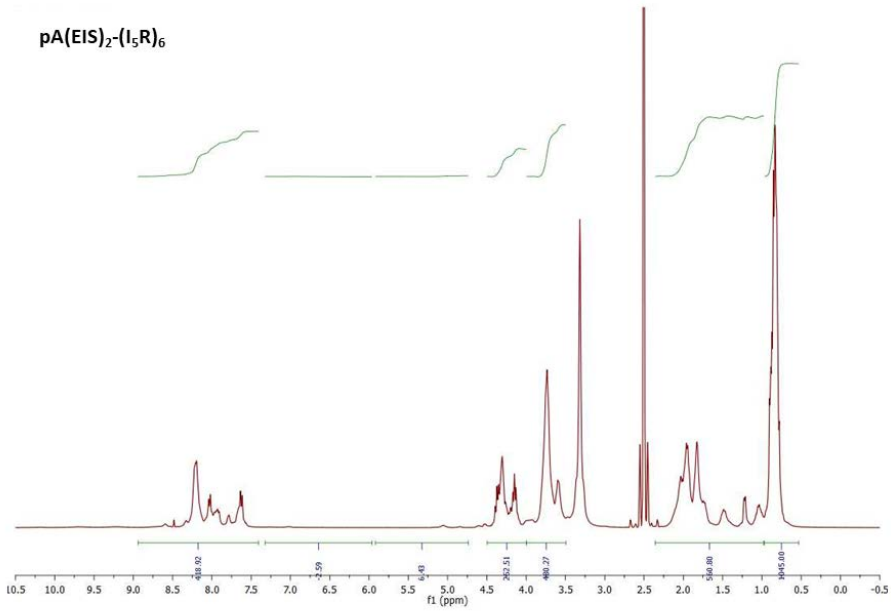

Figure S5. H-NMR spectrum of $pA(EIS)_2$-$(I_5R)_6$ showing the integration of the peaks corresponding to the different types of hydrogens.

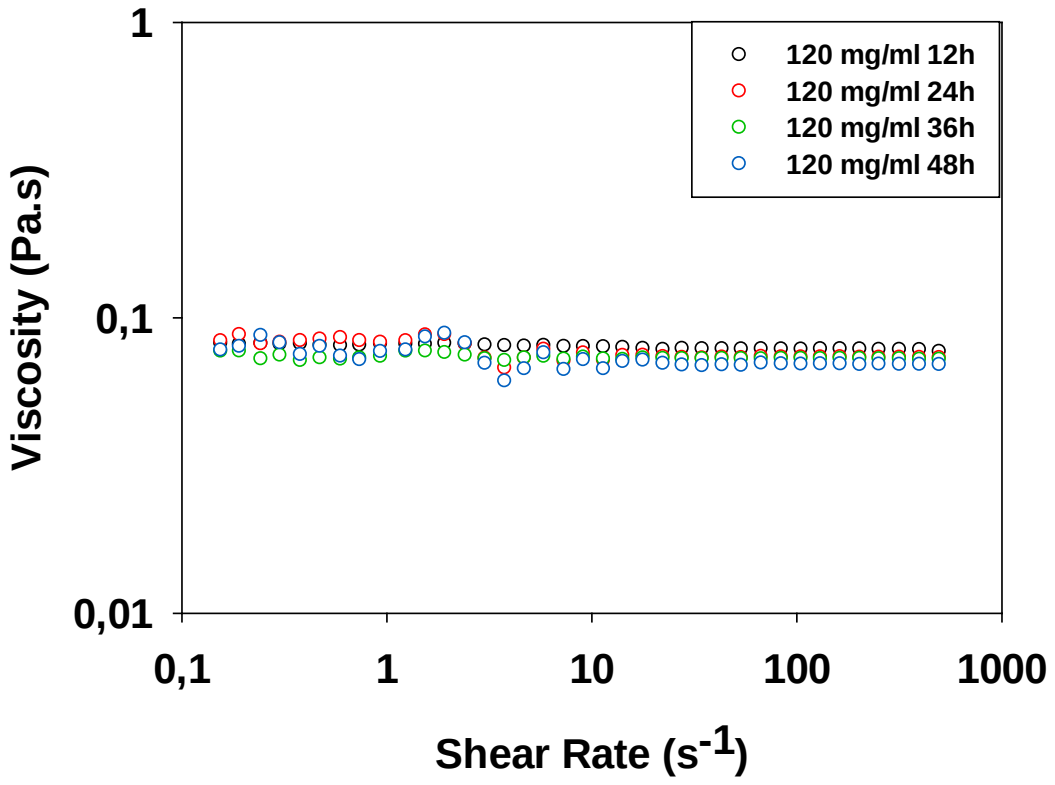

Figure S6: Dependence of the viscosity on the shear rate in a scale lin-log for an identical recombinamer hydrogels of $(EIS)_2$-$(I_5R)_6$ lacking the Silk blocks with 12 h, 24 h, 36 h and 48 h of pre-annealing.

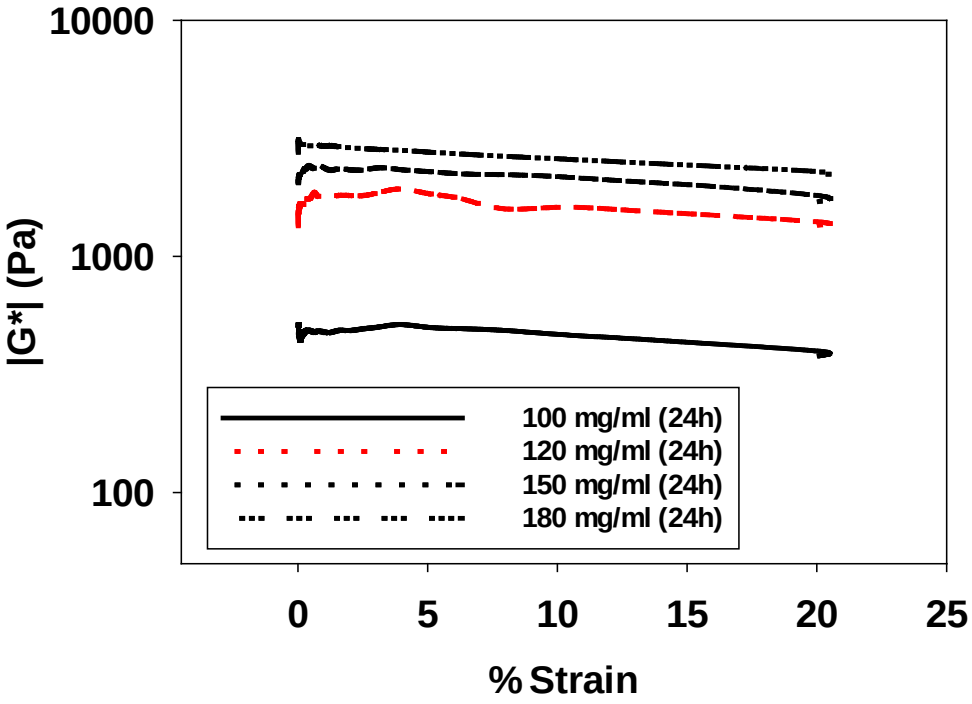

Figure S7. Strain dependence of |G*| for the 24 h pre-annealed pA(EIS)$_2$-(I$_5$R)$_6$ hydrogels at 100, 120, 150 and 180 mg/ml with a frequency of 1 Hz at 37°C.

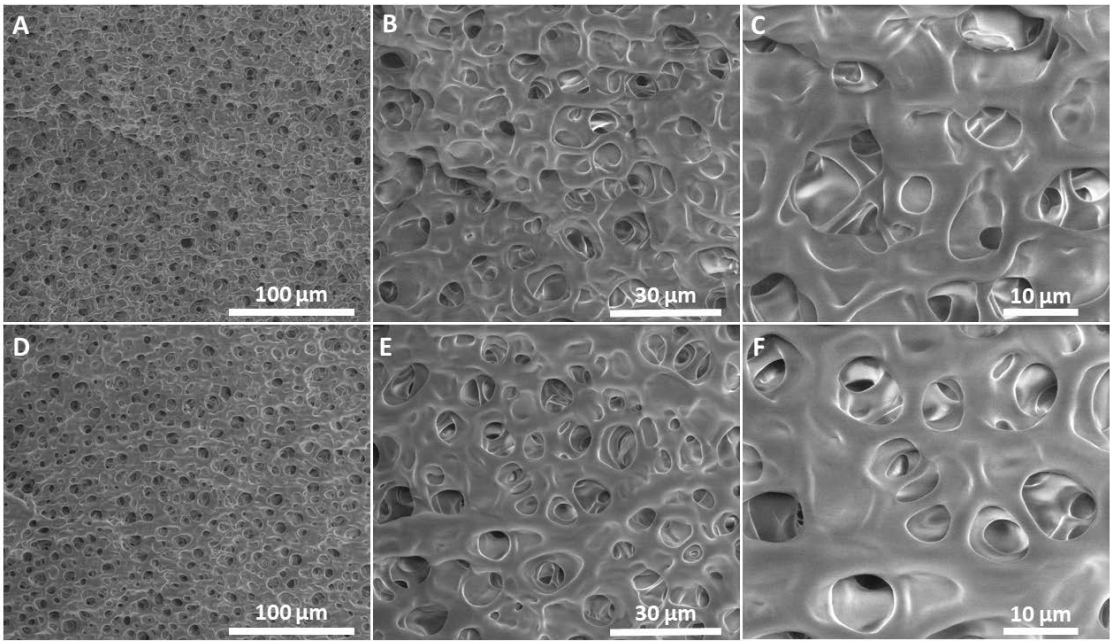

Figure S8. Representative SEM pictures for the pA(EIS)$_2$-(I$_5$R)$_6$ hydrogels at 150 mg/ml (A, B,C) and 180 mg/ml (D, E, F) at different magnification.

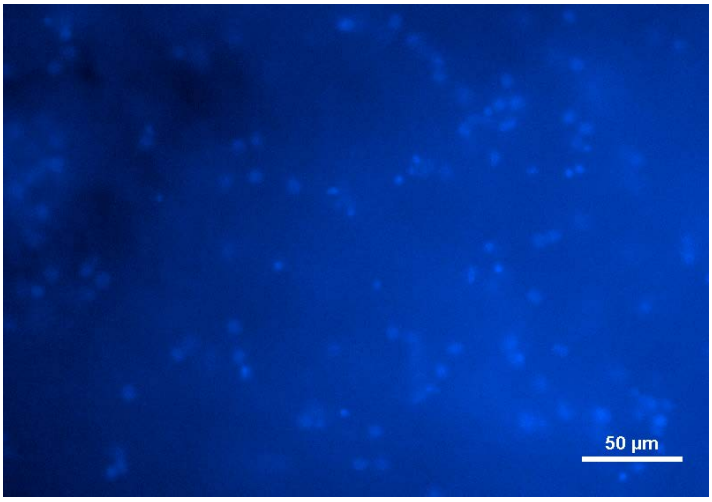

Figure S9. Fluorescent microscope image of the hydrogel embedded with chondrocytes after DAPI staining. The cell nuclei are in blue. The bluish background is due to the fluorescence of the hydrogel.

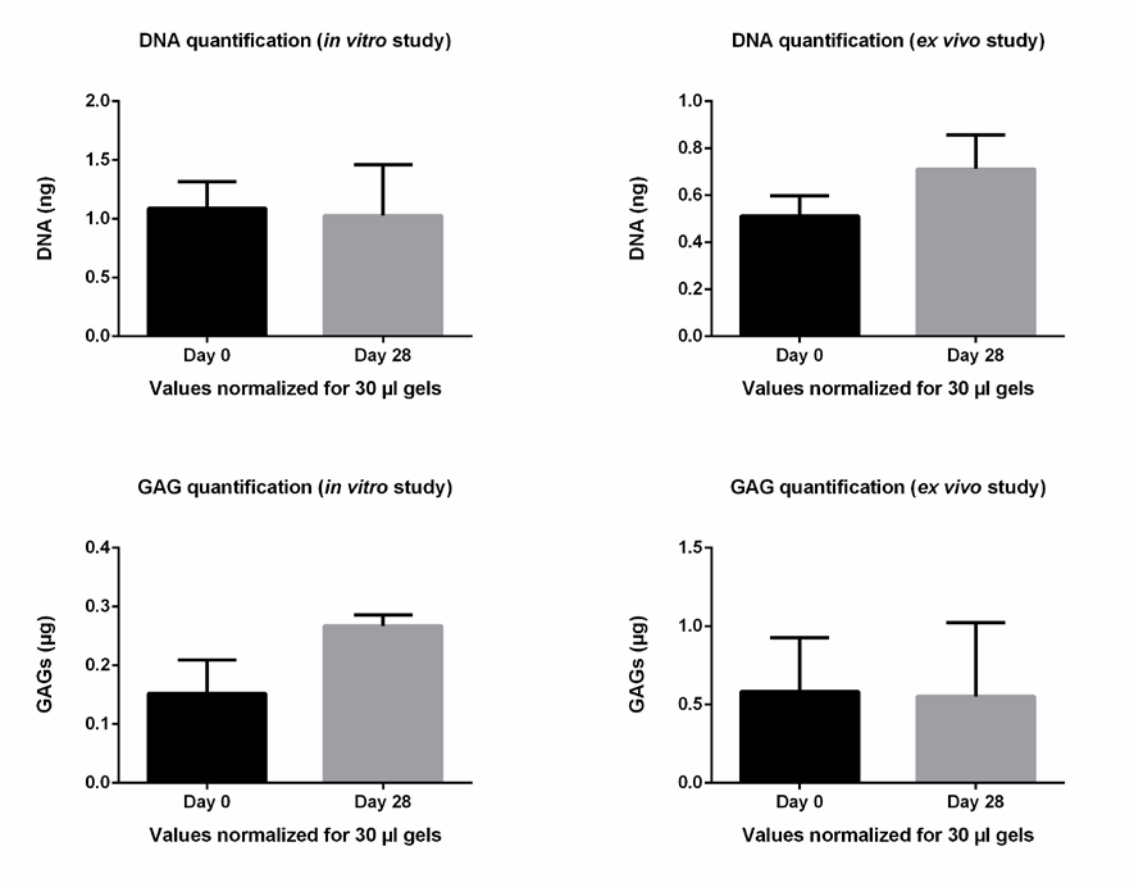

Figure S10. DNA and GAG content of the hydrogel itself for the *in vitro* and *ex vivo* study at day 0 and 28. All the values have been normalized for 30 µl volume of hydrogel.

CHAPTER 4

AN ELASTIN-LIKE RECOMBINAMER-BASED BIOACTIVE HYDROGEL EMBEDDED WITH MESENCHYMAL STROMAL CELLS AS AN INJECTABLE SCAFFOLD FOR OSTEOCHONDRAL REPAIR

Filippo Cipriani,[1] Blanca Ariño Palao,[2] Israel González de Torre,[1,3] Aurelio Vega Castrillo,[2] Héctor José Aguado Hernández,[2] Matilde Alonso Rodrigo,[1,3] Angel J Àlvarez Barcia,[4] Verónica García,[5] Monica Lopez Peña,[6] José Carlos Rodríguez-Cabello,[1,3]

[1] Technical Proteins Nanobiotechnology S.L., Paseo Belén 9A, 47001 Valladolid, Spain

[2] Hospital Clínico de Valladolid. Departamento de traumatología, Valladolid, Spain

[3] Bioforge, University of Valladolid CIBER-BNN, Paseo de Belén 19, 47001 Valladolid, Spain

[4] SIBA – UVa: servicio investigación y bienestar animal, University of Valladolid, Spain

[5] Instituto de Biología y Genética Molecular (IBGM), Universidad de Valladolid y CSIC, Valladolid, Spain

[5] Facultad de veterinaria, Campus Universitario, Lugo, Spain

F. Cipriani, B. Ariño Palao, I. González de Torre, A. Vega Castrillo, H. José Aguado Hernández, M. Alonso Rodrigo, A. J Àlvarez Barcia, V. García, Monica Lopez Peña, J.C. Rodríguez-Cabello. An elastin-like recombinamer-based bioactive hydrogel embedded with mesenchymal stromal cells as an injectable scaffold for osteochondral repair. *Regenerative Biomaterials* (2019). doi.org/10.1093/rb/rbz023.

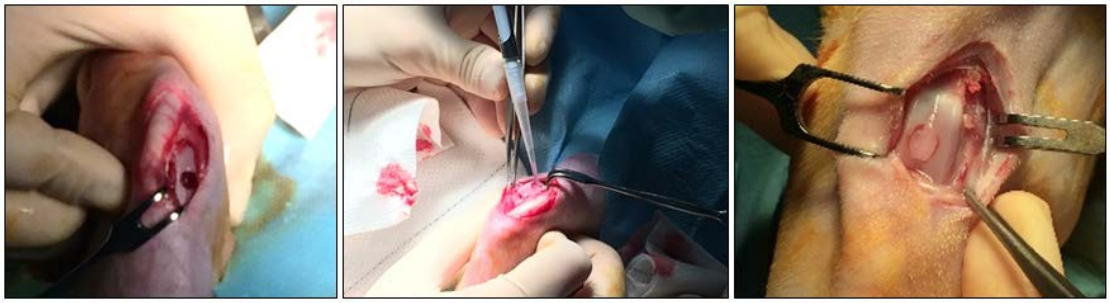

Abstract

The aim of this study was to evaluate injectable, *in situ* cross-linkable elastin-like recombinamers (ELRs) for osteochondral repair. Both the ELR-based hydrogel alone and the ELR-based hydrogel embedded with rMSCs were tested for the regeneration of critical subchondral defects in 10 New Zealand rabbits. Thus, cylindrical osteochondral defects were filled with an aqueous solution of ELRs and the animals sacrificed at 4 months for histological and gross evaluation of features of biomaterial performance, including integration, cellular infiltration, surrounding matrix quality and the new matrix in the defects. Although both approches helped cartilage regeneration, the results suggest that the specific composition of the rMSC-containing hydrogel permitted adequate bone regeneration, whereas the ELR-based hydrogel alone led to an excellent regeneration of hyaline cartilage. In conclusion, the ELR cross-linker solution can be easily delivered and forms a stable, well-integrated hydrogel that supports infiltration and *de novo* matrix synthesis.

1. INTRODUCTION

Chondral and osteochondral defects in the articular cartilage of the knee and in other joints caused by traumatic and non-traumatic injuries tend to progress to degenerative osteoarthritis over time. This scenario usually leads to total replacement of the joint with a prosthesis.(1) Several types of cartilage are known, including the articular hyaline cartilage, which is a smooth, pearly bluish layer with a width of 2 to 4 mm that covers the articular surfaces.(2) Articular hyaline cartilage is a highly specialized tissue characterized by its unique mechanical properties;(2) it has a structural role adsorbing the pressure overload the cartilage, and a functional role allowing the friction-less sliding of the articular surface.(3,4) When the cartilage layer is damaged, the structural components of hyaline cartilage (proteoglycans and glycosaminoglycans) tend to leak from it, reducing the ability to absorb the pressure overload.(5) Consequently, the functional capacity of friction-less sliding decreases, indeed, due to the remodeling of the layer, the water diffusion into the cartilage is reduced. Hyaline cartilage diseases bring synovitis, which progress to the inflammation of the articular layer.(6) In mammals, the ability of articular cartilage to durably repair decreases soon after birth and is almost completely lost by early adulthood.(7) Generally, the regenerated cartilage is rich in type I collagen (fibro cartilage) instead of containing type II collagen. Collagen type II provides tensile ability to the cartilaginous matrix and is essential for articular hyaline functional capacities,(8) whereas fibro cartilage is unable to maintain the biomechanical characteristics of articular cartilage.(2,4,5) All treatments currently used to restore the hyaline articular surface are unsatisfactory,(2) although several alternatives have been probed to promote the regeneration of damaged cartilage. In particular, the development of novel tissue-engineering methods has started to play an important role.(9,10) Mesenchymal stromal cell (MSC) therapy(11-13) is a method that utilizes pluripotent cells, which can differentiate into various cell types, such as chondrocytes and osteocytes. As a result, these cells are good candidates for the treatment of musculoskeletal lesions.(14,15) MSCs are available from different auto-, allo- and xenogeneic sources.(16) The first two options offer an immunologically safer approach, whereas the latter hugely increases the availability of MSCs.(17) Although there are several studies with successful results using xenogeneic MSCs in different animal hosts,(18) only autologous(19) or allogenic cells(13)

have been successfully used in humans, with negligible immunological response.(20) Moreover, in the case of osteochondral application, it must be taken into account that articular cartilage is considered an immunoprivileged tissue, indeed, due to its avascularity, the immune system has some limitations for the detection of the implanted tissue.(21) The suspension of MSCs in a scaffold as a cell-carrier enhances the persistence of the implanted cells at the treatment site.(2) Taking into account that the majority of wet articular cartilage is formed by water,(22) hydrogels represent one of the most promising solutions for cartilage repair applications. Moreover, it is important to consider that, during surgery, it is crucial to minimize the severity of the intervention.(23) One advantage of the arthroscopic technique is that it can reduce infection risk and recovery time compared to open joint surgery. In the light of this, the use of injectable hydrogels is of special interest because they are compatible with arthroscopic methods.(23)

The use of recombinant DNA techniques has brought new materials to the biomedical field, discovering new matrices for Tissue Engineering (TE) applications. An important role is played by elastin-like recombinamers (ELRs); they are based on the repetitive pentapeptide sequence Val−Pro−Gly−X−Gly (VPGXG)$_n$, where the guest residue (X) is any amino acid except L-proline.(24) The thermo-sensitivity shown by ELRs is defined by the transition temperature (T_t). It depends on the charge of protein conformations and on the polarity of the amino acids that composed the ELRs.(25,26) Moreover, a great advantage of the ELRs is the ability to form different structures, among which a hydrogel is one of the most common for regenerative medicine application.(9) As pointed out above, ELRs show thermo-sensitivity, thus meaning that hydrogels, which are stable at body temperature, can be formed whenever the transition temperature (T_t) of the ELR is lower than this temperature.(27) Several studies have shown how different types of ELRs can be used in some of the most challenging fields of tissue regeneration, such as cardiovascular,(28) ocular prosthesis(29) and osteochondral applications,(30,31) among others.(27)

The incorporation of cells into biomaterials can help to overcome some limitations of using cells or biomaterials alone. For instance, an ELR-based hydrogel can serve as a scaffold to allow MSCs to orchestrate tissue regeneration. Moreover, considering the

extraordinary compatibility of ELRs, the 3D hydrogel structure can mimic the properties of the ECM, thereby supporting the regeneration process.

In this study, in order to promote cell attachment and stimulate matrix production, we developed an appropriate ELR-based bioactive hydrogel composition that provides an adequate balance of properties, such as mechanical support,(32) to foster cell adhesion and proliferation. Given their recombinant nature, ELRs were designed to contain bioactive sequences, such as the extensively studied RGD sequence, which supports cell-adhesion via integrins,(33) CS5 human fibronectin REDV for efficient cell attachment(28,34) and VGVAPG as an elastase target domain (human leukocyte elastase I) to provide increased proteolytic sensitivity and increased functionality to the scaffold.(35,36) In this study, we obtained a homogeneous embedding of rMSCs (rabbit mesenchymal stromal cells) in the ELR solution at a temperature below body temperature, and injected this composition as a cell-scaffold system for osteochondral repair. This ELR-based bioactive hydrogel exhibited a cell-friendly environment, thus improving cartilage regeneration both with and without rMSCs embedded.

2. MATERIALS AND METHODS

2.1. Ethical approval

All procedures regarding the collection of rabbit MSCs (rMSCs) specified below were approved by the Ethics Committee of the University Hospital of Valladolid (Spain) in accordance with the Declaration of Helsinki (1975), as revised in 2013. All animal experiments were conducted in accordance with the institutional guidelines for the care and use of experimental animals of the University of Valladolid (Spain) in accordance with Directive 2010/63/EU (Resolution Number 2010/2/23).

2.2. Rabbit Mesenchymal Stem Cell collection

Bone marrow was extracted from the tibias and fibulas of white New Zealand male rabbits and collected in sterile tubes (Falcon® A Corning Brand, Ref. 352070) previously damped with a heparinized saline solution of Phosphate Buffered Saline (PBS, Gibco Ref. 20012-

068) and 5% Heparin Sodium (Chiesi Spain S.A.U) to avoid coagulation. Bone marrow samples were kept at 4 °C until they were processed within 24 hours. A fraction of mononuclear cells (MNCs) was selected using a density gradient method with Ficoll-Paque PREMIUM (GE Healthcare Ref. 17-5442-02). At the end of this process, counting and viability controls were performed using the Trypan Blue exclusion method with a Neubauer Chamber. After the selection process, MNCs were seeded at a density of $190 \cdot 10^3$ cells/cm^2 and kept in culture at 37 °C and 10% CO_2 with DMEM 4.5 g/L D-Glucose (Gibco, Ref: 31966-021) supplemented with 0.041 mg/mL of gentamicin (Gibco, Ref: 15710-049) and 20% Fetal Bovine Serum (FBS, Gibco). Every 3 or 4 days, the appearance of the cell monolayer was observed with an inverted microscope and the percentage growth recorded. If confluence was less than 60-80%, a change of medium was performed until cells covered 80% surface of culture. Then, dissociation and cellular expansion (passage) were carried out and the subcultures developed in order to increase and purify the MSC cell line. The cells obtained during this first step were cryopreserved in FBS and 10% DMSO (Dimethyl sulfoxide, Sigma Ref. D2650), and stored in liquid nitrogen at -196 °C. Then, when the cells were needed for the assays, they were thawed at 37 °C, seeded at a density of 1000 cells/cm^2 and kept in culture for approximately 7-10 days before use, changing the medium every 3 or 4 days.

2.3. ELR biosynthesis and purification

The gene construction was performed by molecular biology and recombinant DNA technique following standard methods previously described;(37,38) the purification process was carried out by several centrifugations preceded by inverse transition cycling. The ELRs obtained in this manner were dialyzed against MilliQ (MQ) water and lyophilized. Three ELRs extensively studied by Gonzalez et al., namely VKVx24, $HRGD_6$ and REDV, were employed in this study(28) (Figure 1). $HRGD_6$ was designed to contain the extensively studied RGD sequence, which supports cell-adhesion via integrins; REDV was designed to contain bioactive sequences such as the CS5 human fibronectin REDV for efficient cell attachment and VGVAPG as an elastase target domain (human leukocyte elastase I). The ELRs were further characterized by electrophoresis gel (SDS-PAGE), mass spectroscopy (MALDI-TOF), nuclear magnetic resonance (NMR), infrared spectroscopy (FTIR) and

differential scanning calorimetry (DSC).(39) The ELRs obtained were chemically modified and characterized by the transformation of the Ɛ-amine group in the lateral lysine chain to produce the cyclooctyne and azide groups necessary for subsequent “click chemistry” reactions, as reported previously.(28,40) The characterization results are provided in the Supporting Information (Figure S1- S9).

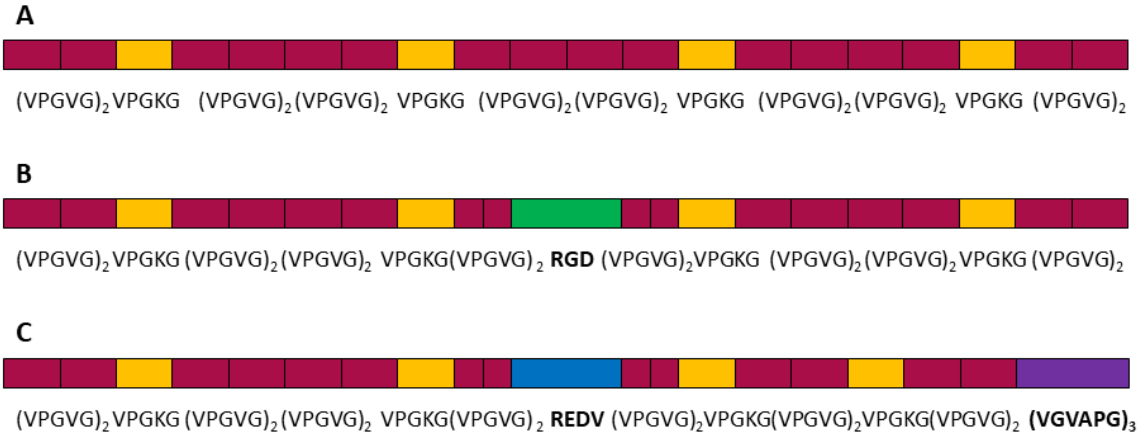

Figure 1. Graphical scheme of the ELR compositions: A: VKVx24; B: $HRGD_6$; C: REDV.

2.4. Gel formation

Freeze-dried ELRs were dissolved in plain DMEM (Dulbecco´s modified Eagle medium) for 16 h at 4 °C at a concentration of 75 mg/mL. The ELR-cyclooctyne solution comprised entirely VKVx24-cyclo, whereas the ELR-azide solution comprised REDV-N_3 and $HRGD_6$-N_3 (in equal amounts). To prepare the hydrogel embedded with rMSCs, the cells were mixed with the solution of VKVx24-cyclo and dissolved in neat DMEM at 4 °C. For gel formation, cold solutions of VKVx24-cyclo and REDV-N_3 and $HRGD_6$-N_3 were mixed together and the gel formed using catalyst-free click reactions between an azide group and an activated cyclooctyne group.

2.5. Rheological characterization

Rheological experiments were performed using a strain-controlled AR-2000ex rheometer (TA Instruments) with the hydrogel submerged in water. Cylindrical swollen gel samples were placed between parallel, nonporous stainless steel plates (diameter = 12 mm). The gap between the plates was adjusted by applying the minimum normal force to prevent

slippage. Before the measurements started, all the samples were relaxed until equilibrium; the temperature was controlled and maintained at 37 °C using a Peltier device. Shear deformation measurements were carried out. The dynamic shear modulus was measured by performing a dynamic strain sweep with amplitudes having a range between 0.1% and 20% at a fixed frequency of 1 Hz. Thus, the linear region of viscoelasticity was determined. Afterwards, a dynamic frequency sweep was carried out between 0.05 and 70 Hz at a fixed strain amplitude (1%), thus the dependence of the dynamic shear modulus and the loss factor on the frequency was obtained. Finally, the rheological characterization presented the storage modulus and the loss modulus, G' and G" respectively. As a results of those, the magnitude of the complex modulus |G*| ($|G^*|^2 = (G')^2 + (G'')^2$), and the loss factor ($\tan \delta \equiv (G'')/(G')$, where δ is a function of frequency or strain amplitude) were calculated.

2.6. Scanning electron microscopy (SEM)

The morphology of the hydrogel was investigated by SEM using a FEI Quanta 200 FEG instrument. No coating procedures were used during the sample preparation; briefly, hydrated hydrogels were submerged into liquid nitrogen, mechanically fractured and freeze-dried. Afterwards, the pictures were collected using the microscope at Landing E of 7.00keV and a pressure of 0.7 Torr and finally the images were analyzed using image-J software.

2.7. Cell viability assay

The viability of isolated rMSCs embedded in ELRs at 75 mg/mL was evaluated using the Alamar Blue assay (Invitrogen) according to the manufacturer's guidelines. Briefly, rMSCs were isolated according to the protocol described above and mixed with the hydrogels at a concentration of 8 million cells/mL. A 100 µL aliquot was then pipetted into a 24-well Transwell® tissue culture plate. After allowing the cells to adapt for four hours, the hydrogels were washed twice with PBS and metabolic activity measurements were conducted at 0, 3, 6, 9, 12 and 15 days of culture. For this purpose, 2 mL of a DMEM-containing 10% Alamar Blue solution was used to replace the culture medium and the cells were incubated in darkness for 2 h at 37 °C and under a 5% CO_2 atmosphere.

Subsequently, 70 µL of the reduced medium was transferred to a 96-well plate. The hydrogels were washed twice with PBS and the corresponding growth medium was added and incubated again in order to determine the metabolic activity at different times. Fluorescence (excitation: 560 nm; emission 590 nm) was measured using a SpectraMax M5e (Molecular Devices) microplate reader.(41) The fluorimetric reduction of 10% Alamar Blue reagent in the culture medium by the cells was measured at regular time intervals. Samples for the phase-contrast epifluorescence were fixed at 4% paraformaldehyde (Sigma-Aldrich) for 40 min. Staining was carried out after permeabilization of the sample with 0.2% Triton X-100 (Sigma-Aldrich) and stained with the fluorescent dyes Phalloidin–Alexa Fluor488R and DAPI (Invitrogen).

2.8. *In vivo* experimental model

Ten female New Zealand white rabbits with an age of 6 months and an average weight of 3 kg were used for the creation and treatment of the osteochondral defects. The number of animals was determined by power analysis and consideration of previous studies,(42-44) following the 3Rs principles formulated by Russell and Burch for animal experimentation.(45) The animals were anesthetized intramuscularly with medetomidine (0.5 mg/kg) (Braun) and ketamine (25 mg/kg) (Ritcherpharma). Afterwards, both knees were shaved and cleaned. The surgical procedure involved a parapatellar incision of the skin, which was performed under sterile conditions in order to expose the distal femur. A critical-size (4 × 4 mm full-thickness) osteochondral lesion was created with a drill (Figure 2A), following well-established surgical procedures.(46-49) The defect was deep enough to reach the osteochondral bone. The ELR-cyclooctyne and ELR-azide solutions were then mixed together and the cold solution (below T_t) was pipetted completely into the defect (Figure 2B). The gel was immediately formed by a catalyst-free click reaction between the azide group and activated cyclooctyne groups, filling the lesion created with the drill entirely (Figure 2C). Each animal was surgically operated at both knees and hydrogels with and without rMSCs embedded were pipetted into the right/left knee defects at random. Carprofen (50 mg/kg) (Norbrook) was administrated four hours after the surgical procedure. All animals were fed and watered ad libitum during the study period and maintained in individual cages. Animals were euthanized intravenously with pentobarbital

(200 mg/kg) at four months post-treatment and the distal femora extracted for further analysis.(17)

Figure 2. A: Creation of the osteochondral defect with critical size; B: Pipetting of the ELR solutions with and without cells embedded inside the defect; C: Formation of the gel via a catalyst-free click reaction, thereby entirely filling the lesion created.

2.9. Gross morphology

The entire knees of each rabbit were dissected and the distal part of each femur was extirpated. Samples for each group were photographed and examined for evaluation as per the International Cartilage Repair Society (ICRS) gross morphology assessment scale for cartilage repair.(50,51)

2.10. Histological analysis

A blind macro- and microscopic analysis was performed by trained histologists for all the samples previously fixed in 4% formaldehyde in PBS 0.05 M (pH 7.3) at 4 °C. The sections were stained with several stains: Hematoxylin and Eosin (H&E), Picro-Sirius Red Stain and Safranin-O/Fast Green, for collagen and glycosaminoglycan (GAGs) stains, respectively. The staining procedures were performed according to common methods. Moreover, immunohistochemistry was performed with primary antibody Mouse monoclonal anti-collagen type I and anti-collagen type II. Samples from each rabbit (n = 10 for each group) were graded by two observers using the ICRS visual histological assessment scale for cartilage repair.(52)

2.11. Statistical analysis

Values are expressed as mean ± standard deviation. Statistical analysis was evaluated by one-way analysis of variance using the Tukey's method. A *P*-value lower than 0.05 was considered statistically significant.

3. RESULTS

3.1. Rheological characterization

The linear viscoelastic region of the ELR hydrogels comprising 50% VKVx24-cyclo, 25% REDV-N_3 and 25% $HRGD_6$-N_3 at 75 mg/mL was determined by using strain sweep measurements from 0.01–20% strain at a frequency of 1 Hz (Figure 3A). The complex modulus (|G*|) at 75 mg/mL shows a constant value of 964 ± 156 Pa (at 1% strain) in this strain range. As such, a 1% strain was selected to carry out the dynamic frequency sweep measurements. Evolution of the storage (G') and loss moduli (G'') is represented in Figure 3B. At a frequency of 1 Hz, the value of G' is 960 ± 162 Pa, whereas the value of G'' is 28 ± 19 Pa. Moreover, the evolution of δ as a function of the frequency is represented in Figure 3C (the value of δ at 1 Hz is 1.6 ± 0.9°).

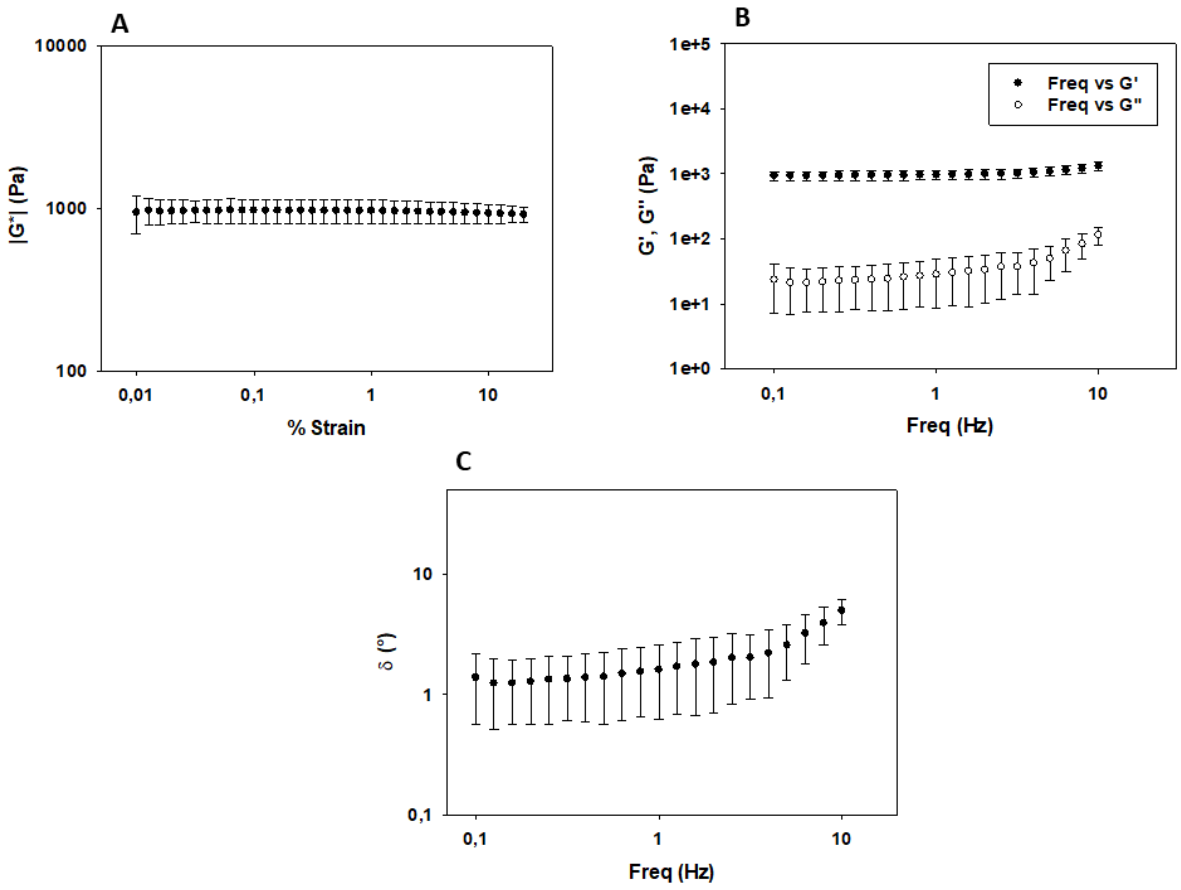

Figure 3. Rheological measurement for the ELR hydrogel at 37 °C and 75 mg/mL. A: Strain dependence of the complex modulus (|G*|); B: Frequency dependence of the storage (G') and loss (G'') modulus; C: Frequency dependence of δ. Each curve corresponds to the average of three different sample measurements.

3.2. Scanning electron microscopy (SEM)

ELR hydrogels at 75 mg/mL show a porous environment, with pore sizes ranging from around 3 µm to 20 µm and a wall thickness of 1.11 ± 0.34 µm (Figure 4). This large variety of pore size is due to the internal interconnected structure of the ELR, where small pores are able to merge to form larger pore structures.

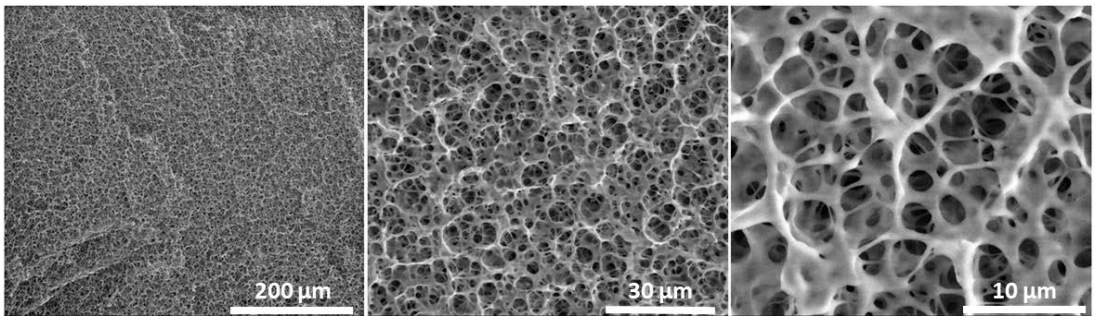

Figure 4. Representative SEM images for the ELR hydrogel at 75 mg/mL and different magnifications.

3.3. Cell viability assay

A cell viability assay was performed for two-week culturing of the ELR hydrogel at 75 mg/mL when embedded with rMSCs (8 million/mL). Assay data were recorded at different time points (0, 3, 6, 9, 12 and 15 days) in order to gain a better understanding of the metabolic activity of the rMSCs. The cell viability analysis revealed an increment in metabolic activity, with a significant difference between 0 and 3 days and a constant increase from day 3 to day 15 during the culture process (Figure 5). The biocompatibility demonstrated by our ELR-based hydrogel is in agreement with similarly cross-linked hydrogels previously studied.(53) Moreover, the curve trend of this viability assay was in accordance with typical cell-growth behavior, whereby the number of cells increases exponentially in the first part of the culture, subsequently reaching a stable value.

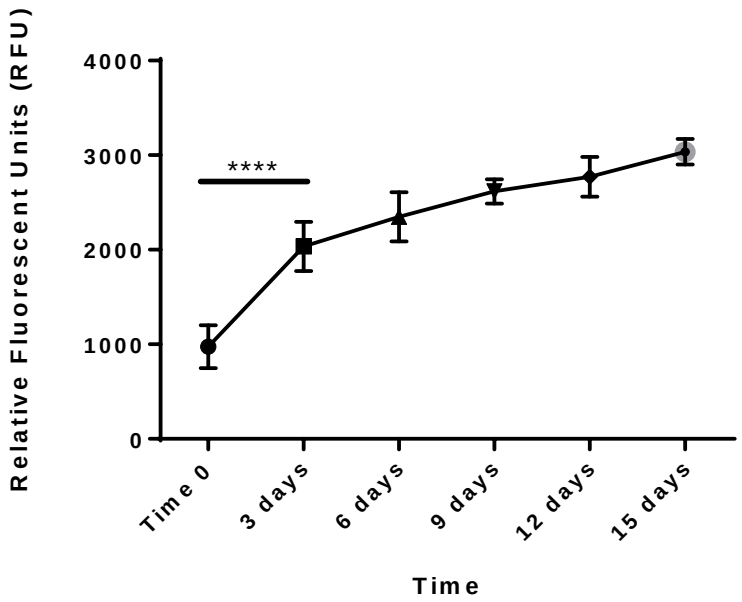

Figure 5. Cell viability test of a 3D ELR gel (75 mg/mL) embedded with rMSCs at different time points (****P<0.0001).

Furthermore, the Dapi/Phalloidin analysis (Figure 6) showed the morphology of the rMSCs embedded in the 3D structure after 15 days of culture. Mesenchymal stem cells are pluripotent cells that are able to differentiate into multiple cell-types widely used in both tissue engineering and regenerative medicine.(41) An extended and elongated cell shape, with long cytoplasmic processes, can be seen in all the different magnifications, thereby confirming colonization of the hydrogel over 15 days. The cells showed a well-spread morphology, with large extensions of their cytoskeleton actin filaments (green stained). The pictures collected at different magnifications (Figure 6A-C) help to visualize both the homogeneous distribution of the rMSCs and the colonization of the hydrogel at different focal points.

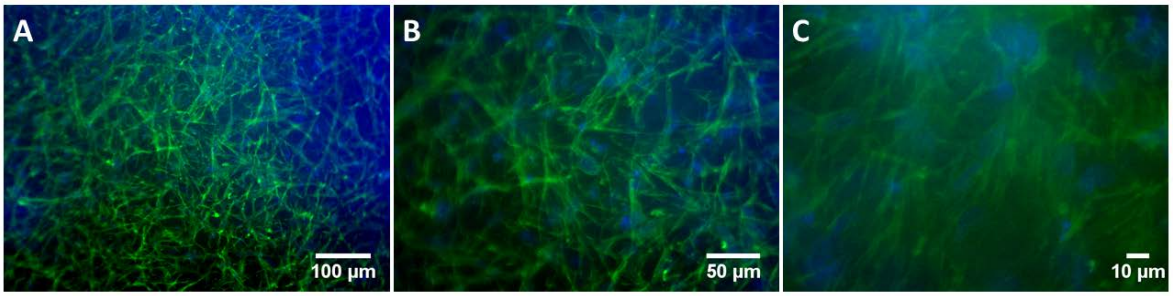

Figure 6. Optical microscope images of hydrogel colonization by rMSCs after culture for 15 days. Pictures collected at different magnifications (A,B,C).

3.4. *In vivo* study results

3.4.1. Macroscopic observation of repaired cartilage

Rabbits were euthanized 4 months after the surgical procedure and the performance of cartilage repair initially evaluated by macroscopic observation. The surface of the defects (Figure 7) showed that the defects in the central area of the trochlea were completely filled at 4 months post-surgery in all animals from both groups (ELR hydrogels & ELR hydrogels embedded with rMSCs). In addition, the defects were covered by a white layer of fibrous tissue in both groups. The regenerated tissue had a greyish color and could be easily recognized in both cases. As such, the regenerated tissue showed a good integration with the surrounding tissue; indeed, there was no clear boundary between the injured region and the surrounding chondral tissue. The regeneration rate was further evaluated based on macroscopic observation of the regenerated knee cartilage.

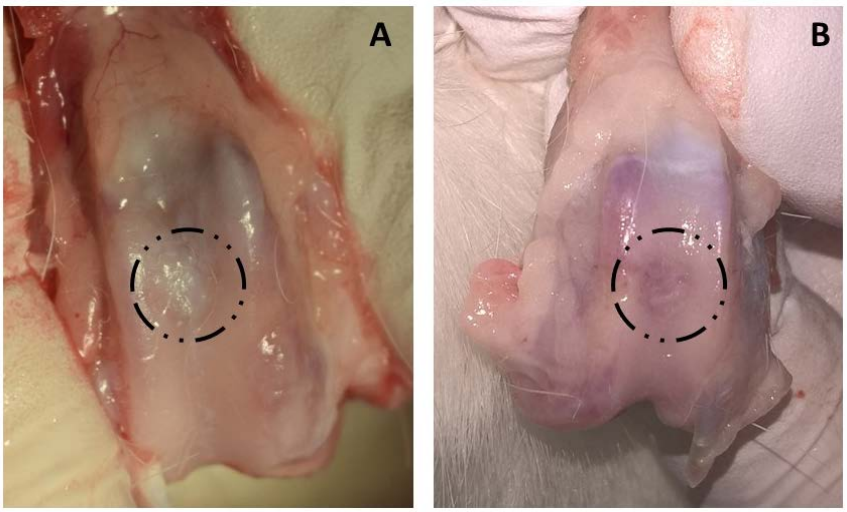

Figure 7. Macroscopic appearance of defects in the trochlear groove (4 mm in diameter) at 4 months post-surgery. A: ELR-based hydrogel embedded with rMSCs; B: ELR-based hydrogel alone. Defects are indicated with a black dashed line.

As noted above, the samples were evaluated using the ICRS gross morphology assessment scale. Briefly, this gross evaluation takes into consideration three parameters, namely the degree of defect repair, integration with the border zone and macroscopic appearance.(54) Each of these parameters is evaluated on a scale of 0 to 4, with a total score ranging from 0 to a maximum of 12. The average score for the ELR hydrogel group was 9.7 ± 1.3, whereas the ELR hydrogel embedded with rMSCs scored 9.5 ± 1.9 (Figure 8A).

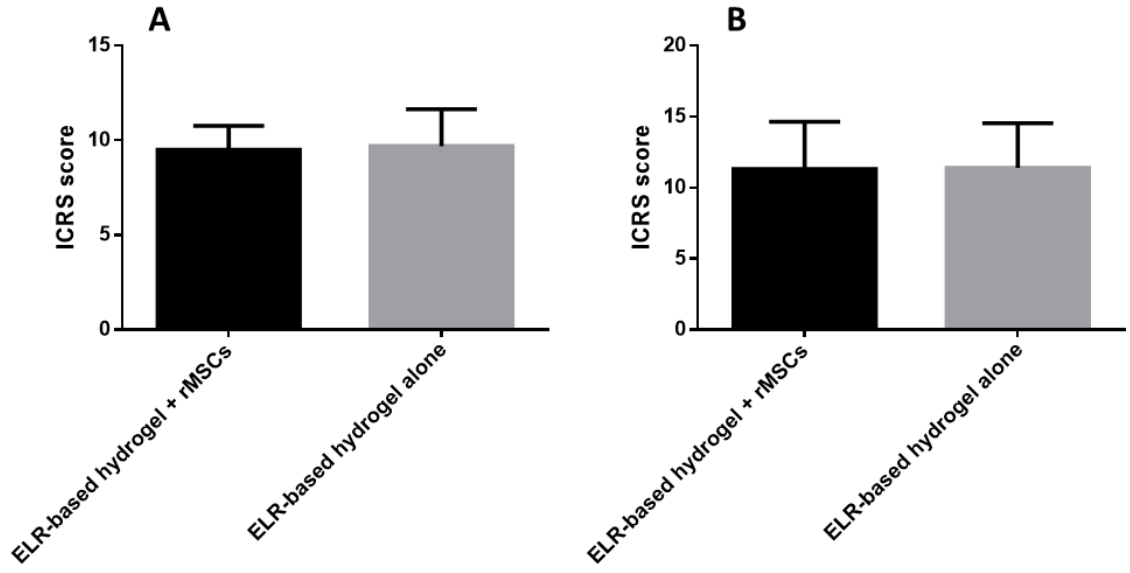

Figure 8. International Cartilage Repair Society (ICRS) macroscopic assessment scale. A: Gross morphology assessment; B: Histological and immunohistochemical assessment. Values are expressed as mean ± SD (n=10).

3.4.2. Histological analysis of repaired cartilage

Histological analyses were performed on the sections of the ELR-based hydrogel embedded with rMSCs (Figure 9) and on the ELR-based hydrogel alone (Figure 10). For histological analysis, all the sections were stained with H/E, Picro-Sirius Red Stain and Safranin-O/Fast Green, for morphological evaluation and detection of collagen and GAGs, respectively.

Histological analysis of the ELR-based hydrogel embedded with rMSCs (Figure 9) shows the absence of the hydrogel and that *de novo* bone tissue formation is present. It can also be seen that the new bone tissue exhibits the same porous and morphological structure as the native surrounding tissue. The upper bone region (underneath the cartilage layer) shows a less intense staining due to the degradation of the hydrogel combined to the uncompleted regeneration of the bone layer. Moreover, the collagen staining has the same intensity when comparing the regenerated cartilage with the native one. The regenerated cartilage layer also contained small egg-shaped cells, which is typical of the fibrocartilage-like tissue. Moreover, although GAG staining revealed glycosaminoglycan's production and secretion in the cartilage layer, metachromatic Safranin-O staining appeared to be less intense for the regenerated cartilage than for the surrounding cartilage. Furthermore, although the regenerated tissue at the articular surface of the samples exhibited an adequate thickness in comparison with the adjacent non-injured articular cartilage, the tissue had a fibrotic appearance. Finally, the subchondral bone was mostly regenerated.

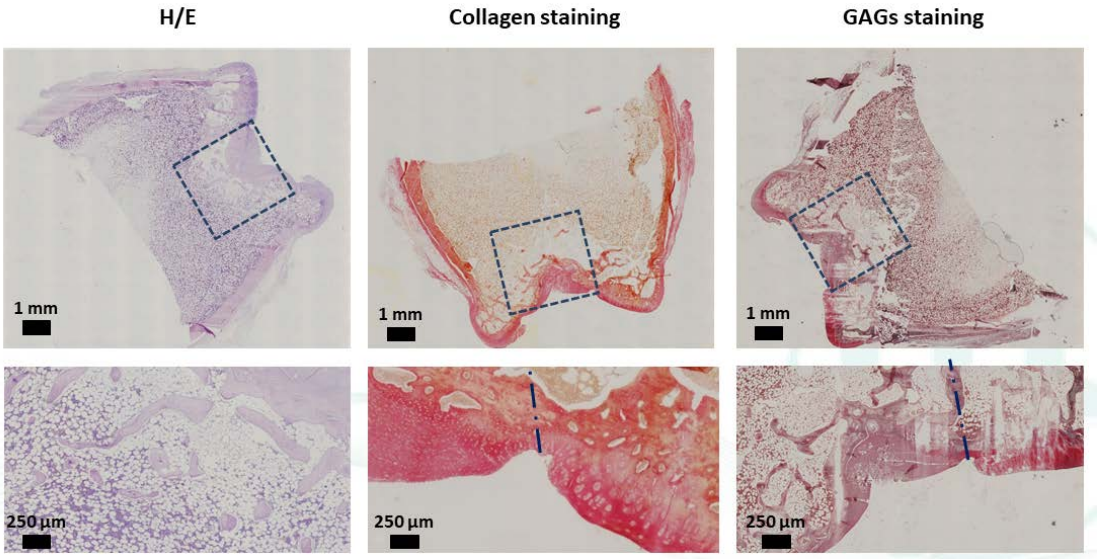

Figure 9. Representative histological staining of repaired cartilage for ELR-based hydrogel with rMSCs.

The first aspect that can be seen from the histological analysis of the ELR-based hydrogel alone (Figure 10) is the continued presence of the hydrogel within the created defect. Although the hydrogel remained intact in the inner part, it started to degrade from the periphery towards the center of the hydrogel. H/E staining clearly showed a difference

between native bone tissue and the hydrogel. In addition, in the boundary area of the hydrogel, a higher concentration of cells (revealed by the higher intensity of the staining) enrolled in the degradation of the hydrogel and in the *de novo* formation of bone tissue can be seen. Safranin-O staining revealed the presence of proteoglycan in the relatively thin repaired tissue. In addition, collagen staining indicated that the new tissue secretes an extracellular matrix. Histological staining revealed a columnar arrangement of the chondrocytes (typical of native cartilage) in the regenerated cartilage. The peripheral migration of these types of cells from the surrounding tissue towards the defect area displayed a smooth and regular surface of the regenerated cartilage, which, exhibited a complete integration with the adjacent non-injured cartilage. Moreover, the regenerated cartilage showed no structural differences with respect to healthy cartilage.

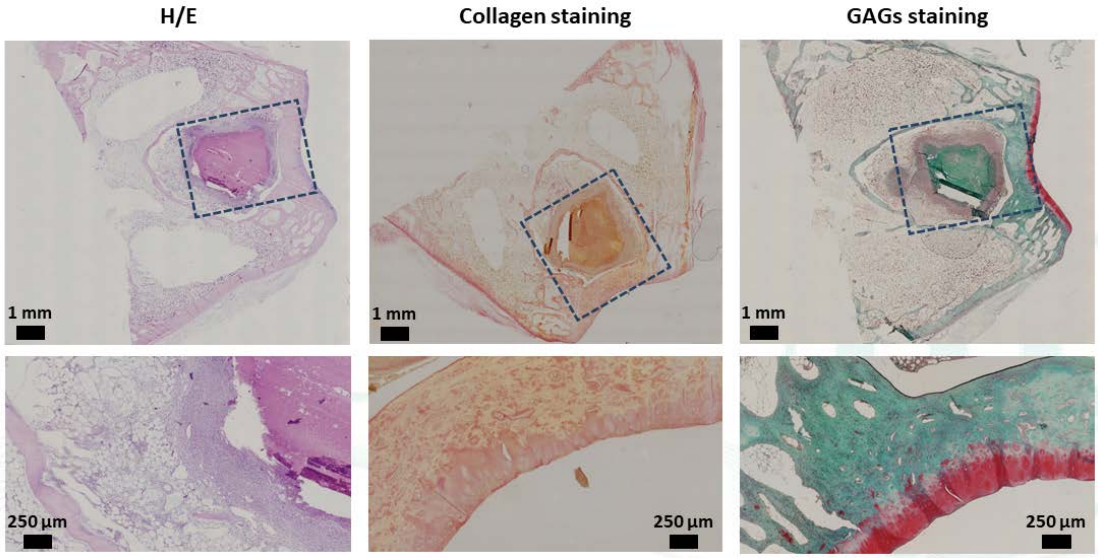

Figure 10. Representative histological staining of repaired cartilage for the ELR-based hydrogel alone.

The section of the ELR-based hydrogel embedded with rMSCs and the section of the ELR-based hydrogel alone were further analyzed by immunohistochemistry with primary antibody anti-collagen type I (fibro cartilage) and anti-collagen type II (hyaline cartilage), for detection of different types of collagen previously revealed by the general Picro-Sirius stain.

In the case of the ELR-based hydrogel embedded with rMSCs (Figure 11), no collagen type II was detected in the regenerated cartilage. This result is in accordance with the

histological analysis previously described, where a non-columnar arrangement of chondrocytes was revealed. The presence of collagen type II in the native cartilage ensures a correct staining performed for collagen type II. Moreover, the staining for collagen type I appears in a spot-like distribution throughout the section, possibly due to high exposure to this antibody, which is the signal for the non-appearance of collagen type I in the regenerated area. We can, therefore, conclude that the regenerative tissue in the ELR-based hydrogel embedded with rMSCs was mainly fibrous tissue with a small amount of hyaline-like tissue.

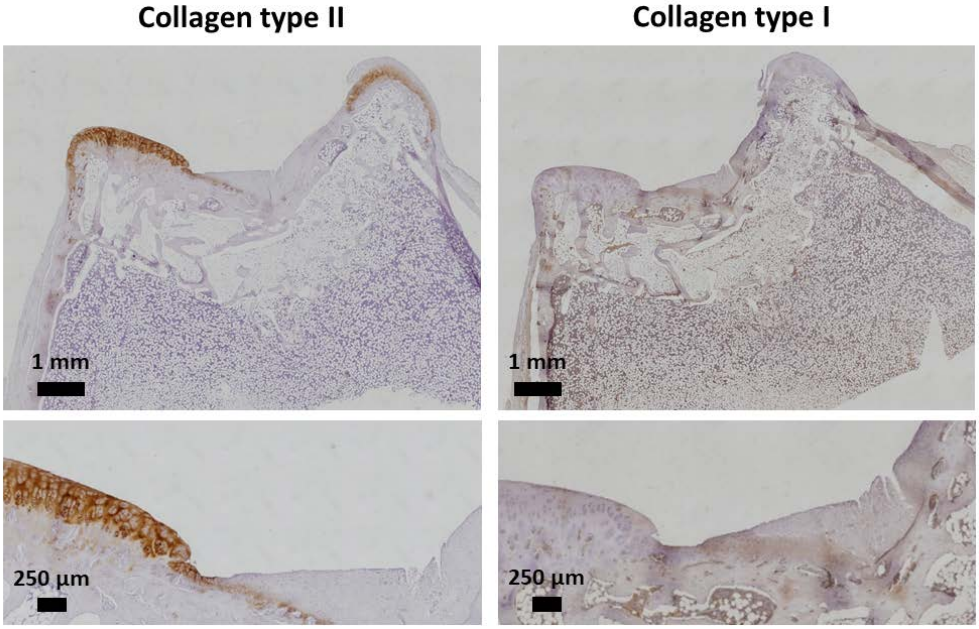

Figure 11. Representative immunohistochemistry study with anti-collagen type I & II for the cartilage regenerated using ELR-based hydrogels with rMSCs.

Notably, in the case of the ELR-based hydrogel alone (Figure 12), a marked production of collagen type II revealed the presence of hyaline cartilage in the regenerated layer. In addition, this result is in accordance with the histological analysis described previously, which exhibited a columnar disposition of the chondrocytes. Moreover, the immunohistochemistry study revealed how the chondrocytes involved in the regeneration process did not produce collagen type I, showing the absence of fibro cartilage.

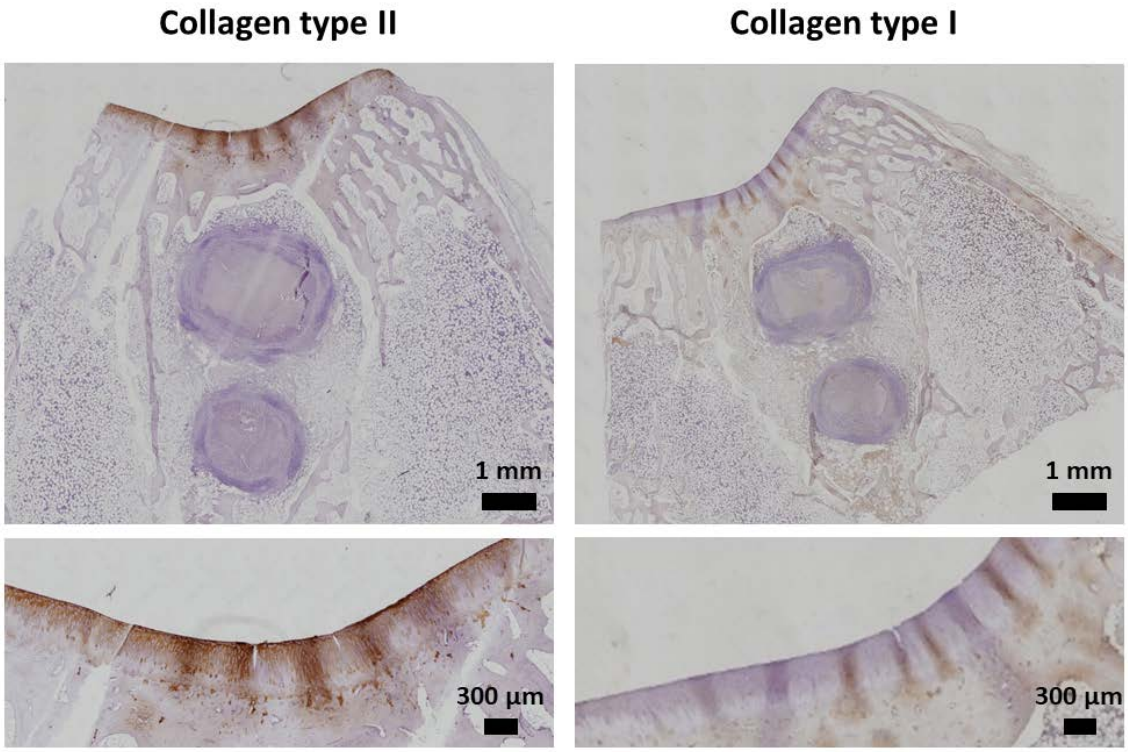

Figure 12. Representative immunohistochemistry study with anti-collagen type I &II for the cartilage regenerated using the ELR-based hydrogel alone.

As reported above, the samples were evaluated according to the ICRS visual histological assessment scale. The resulting score ranges from 0 to a maximum of 18, with the final score being the sum of six parameters, namely surface, matrix, cell distribution, cell population viability, subchondral bone and cartilage mineralization. Each of these parameters is given a value from 0 to 3. The average score in the ELR hydrogel group was 11.4 ± 3.1, whereas the ELR hydrogel embedded with rMSCs scored 11.3 ± 3.3 (Figure 8B).

4. DISCUSSION

It is well known that articular cartilage has a limited regeneration capacity after disease or trauma and that fibro cartilage is produced where the cartilage regeneration takes place.(55,56) This type of cartilage can easily degenerate and develop into osteoarthritis.(57) Considering that the clinical treatment of defective cartilage remains problematic,(58) the purpose of surgery is to regenerate the chondral defects in order to obtain a structurally and biomechanically competent hyaline cartilage. From a functional point of view, clinical treatments are not able to promote the proper regeneration of

cartilage defects; TE represents a new approach for articular cartilage repair,(51) it consists in reconstructing living tissue by associating cells with biomaterials. The 3D structure of the biomaterial plays a supporting role for the cells, thus helping them to proliferate under physiological conditions.(59) The application of new materials in tissue-engineered scaffolds has received particular interest,(60) and several studies have demonstrated how bioinspired materials can simulate the physiological characteristics, thereby enhancing the biological properties of the scaffold.(61-63) In this study, we have designed and developed an ELR-based hydrogel composed by VKVx24-cyclo, REDV-N_3 and $HRGD_6$-N_3, as reported in Figure 1. The specific composition of the ELR-based construct has been previously investigated by Staubli et al., demonstrating a good composition of the hydrogel tailored for a TE study; indeed, whereas the ELR VKV counterpart gives stability to the hydrogel, the combination of ELRs containing RGD sequence and elastase target domain is crucial for cell infiltration and material colonization.(64) In the light of this previous study, we designed our ELR-hydrogel to contain 25% of an ELR bearing the elastase target domain, thus allowing a slower degradation of the scaffold. Moreover, it has to be taken into account that natural polymers showed some limitations in terms of mechanical integrity. Indeed, both collagen and hyaluronic acid have a short lifetime due to degradation by matrix metalloproteinases.(65)

The composition of the hydrogel permits immediate gelation by click chemistry as it has been demonstrated by González et al.,(53) thus conferring the benefit of being an injectable scaffold on our system. The mechanical features of the scaffold are a crucial factor affecting cartilage repair. As it has been demonstrated, chemical cross-linkable ELR-hydrogels having similar Molecular Weight to our hydrogel,(53,66) showed no dependence between the swelling ratio and the concentration for the range 50 mg/mL - 150 mg/mL at 37 °C, maintaining a swelling ratio below 2. On the other hand, the hydrogel's concentration directly influences the mechanical properties of the hydrogel. Considering the remarkable results obtained in the application of this material at a concentration of 75 mg/mL in TE,(28) we decided to use our hydrogel at the same concentration. The rheological characterization of the ELR-hydrogel at 75 mg/mL showed a complex modulus of around 1 kPa, which is in accordance with the elastic modulus of many native tissues(67) and with the mechanical features of efficient scaffolds for TE

applications.(53,64) Moreover, the low values of δ obtained for the ELR hydrogel agree with the viscoelastic behavior demonstrated in the cartilage layer.(68) As it has been reported above, the δ is the phase angle between the applied stimulus and the corresponding response as a function of strain amplitude or frequency; the constant values of δ calculated demonstrated a highly elastic energy storing hydrogel at different frequency values. It is important to take into account that articular cartilage has unique biological properties (such as permeability and viscoelasticity) when compared with other cartilage.(69) Indeed, the structure and physiochemical properties of articular cartilage are similar to those of hydrogels. SEM analysis revealed the morphology of the hydrogel at 75 mg/mL, which shows an interconnected structure with adequate porosity and permeability, along with an appropriate pore size for the creation of a 3D scaffold embedded with rMSCs. The pore size determines the exchange of nutrients and waste products as a result of the void spaces where the cells are seeded and influences the *de novo* secretion of ECM.(70) Moreover, the fluid movement in the hydrogel determined by the pore size plays a fundamental role in the regeneration process, and in order to guarantee a good regeneration, it should be similar to that for native tissue.(71)

Cells play a critical role in the regeneration process; when incorporated into a biomaterial they can enhance tissue regeneration. Although it is well known that chondrocytes only form 1-5% volume of the mature articular cartilage,(72) it has been demonstrated that a higher MSCs seeding density results in better chondrogenesis.(73-76) We selected a seeding density of 8 x 10^6 cells/mL considering the outcomes of previous studies performed with a similar cell density.(77,78) The cell viability analysis revealed an increment in metabolic activity throughout the 15 days of culture, thus showing that the ELR-based hydrogel is a biocompatible scaffold for cell repopulation. Moreover, considering that the highest increase of metabolic activity was recorded within the first three days, the rMSCs appear to be more active when the hydrogel has a lower cell density, reaching a more quiescent state once the hydrogel starts to be repopulated.

The Dapi/Phalloidin analysis showed the morphology of the rMSCs embedded in the 3D structure after 15 days of culture. The specific composition of the ELR hydrogel, which contains RGD and REDV bioactive domains, permitted efficient cell attachment. Indeed, the colonization process indicates that this specific composition of the scaffold is able to

support the culture of embedded cells. Assuming that a suitable scaffold for TE should mimic the ECM functional properties, the *in vitro* study showed an adequate composition of the ELR hydrogel, thereby facilitating the encapsulation of reparative cells into a 3D matrix.(79) Moreover, the elastase target domain (VGVAPG sequence) fosters cell-mediated remodeling of the artificial scaffold. In addition, cell proliferation, and thus colonization of the scaffold, is guaranteed because of the action of proteases during the synthesis of new extracellular matrix.

In this study, we tested the ELR-based hydrogel embedded with rMSCs and the ELR-based hydrogel alone to repair cartilage defects *in vivo*. Macroscopic examination of the surface of the defects (Figure 7) showed that the defects were completely covered 4 months after the surgery in all animals. The scores on the ICRS gross morphology assessment scale for the two hydrogels are practically the same, thus suggesting that both groups aid cartilage regeneration, allowing for the defects to be filled. However, histological analysis of the dissected knees was necessary to determine which type of cartilage was regenerated, and whether the gel was fully replaced by newly formed tissue.

The H/E staining results for both groups showed no evident inflamed cells, such as neutrophilic granulocytes or lymphocytes, thus indicating that the ELR hydrogel has excellent biocompatibility. However, in contrast to the macroscopic evaluation, the histological analysis showed two different responses from the two groups as regards tissue, bone and cartilage. For the bone area, in the case of ELR-based hydrogel alone, a large quantity of intact hydrogel was present, whereas in the rMSCs group no intact hydrogel was present. In the boundary area of the ELR-based hydrogel alone, it was observed a higher concentration of cells enrolled in the degradation of the hydrogel and in the *de novo* formation of bone. This inflammatory cells infiltration in the hydrogel and the consequent degradation of the scaffold was mainly due to the presence of the elastase target domain. This behavior is in accordance with previous studies performed with ELR-based hydrogel containing protease target domains.(64) Moreover, in this case, the degradation came only from the surrounding tissue and the tissue-replacement process was not complete at 4 months post-surgery.

Finally, it is important to take into account that the rejection of engraftment depends essentially by the host immune response, whereby the proportion between inflammation

and pro-resolution is the key for successful implantation of the engineered tissue.(64,80) In contrast, the group treated with the ELR-based hydrogel containing rMSCs showed a much more marked degradation. Indeed, in that case, the degradation occurred both from the surrounding tissue and from the cells embedded in the hydrogel. For the cartilage layer, the histological and IHC staining showed how the group treated with the ELR-based hydrogel alone exhibited better cartilage regeneration compared to the group treated with the ELR-based hydrogel containing rMSCs. The group with no rMSCs exhibited all the typical features of hyaline cartilage, such as the columnar disposition of chondrocytes, excellent GAG staining, and the presence of collagen type II, that provides the tensile ability to the cartilage layer.(8) Moreover, the absence of fibro cartilage confirms that ELR-hydrogel is an attractive solution for cartilage regeneration. Although there is no significant difference in the scores for the ICRS visual histological assessment scale, we can conclude that the ELR-based hydrogel containing rMSCs leads to faster regeneration of the bone tissue and worse cartilage regeneration. In contrast, the ELR-based hydrogel alone enhanced the quality of the regenerated cartilage but the degradation of the hydrogel in the bone area was not complete. During the repair process, the hydrogel was gradually replaced by *de novo* tissue formation. Starting with the assumption that the purpose of this scaffold is to promote the bone and cartilage formation instead than merely substitute the tissue, it is important to evaluate either the capacity to support the cell adhesion and proliferation and the mechanical stability at the defect site. A crucial aspect was played by the 25% of the ELR containing the elastase domain, which allows for degradation of the hydrogel. As such, it could be of interest to test other hydrogel candidates that have different percentages of protease sequences in order to synchronize bone regeneration and cartilage repair. Moreover, another important aspect to take into consideration is the proportion between the RGD sequence and the REDV domain; as discussed recently by Flora et al., the ratio between these two bioactive domains can tailor the selectivity of the biomaterial towards specific cell lines.(81) Generally speaking, the degradation time of materials should match the production speed of the new tissue. Rapid degradation of the scaffold affects both repopulation of the hydrogel by rMSCs and their differentiation or the colonization of chondrocytes from the surrounding native tissue. A slow degradation could hinder cell proliferation and matrix secretion,(82,83) although we found that a high density of rMSCs

in our scaffold increased the regeneration of fibro cartilage instead of hyaline cartilage. Another important aspect that has to be taken in consideration is the cell-cell contact in the hydrogel, which regulates not only the cell behavior and the MSCs differentiation, but it is also crucial for the development of the tissue architecture. This parameter is strongly correlated to the cells density of the hydrogel. One of the major challenges for osteochondral repair is to obtain regenerated cartilage with adequate mechanical properties. This outcome is not completely fulfilled by synthetic hydrogels, which do not show the biological features of ECM and tend to regenerate fibro cartilage.(84)

Our ELR-hydrogel has been shown to have an adequate composition, with tunable degradation rate and adhesion behavior, exhibiting a good balance between the degradation rate and adhesion behavior, and allowing for the colonization of chondrocytes with an optimal secretion of extracellular matrix-collagen type II at the periphery of the hydrogel. Moreover, we observed excellent cartilage repair without the need for cellular implantation, which is a significant advantage in terms of eluding all the technical and ethical complications of cell implantation. Finally, these results are promising as regards the testing of other ELR-based hydrogels with higher degradation rates for bone regeneration, thus leading to an optimal system for osteochondral repair.

5. CONCLUSIONS

One of the biggest challenges in TE is to discover a new biomaterial that guarantees an adequate regeneration of either bone or cartilage tissue. In this study, we took advantage of the recombinant DNA technique to develop a bioactive ELR-based hydrogel with a specific composition as an injectable scaffold for osteochondral repair. The specific composition of this hydrogel allowed for faster bone regeneration when embedded with rMSCs compared to the injection of the hydrogel alone. Similarly, the specific composition of this bioactive hydrogel allowed for the infiltration and the recruiting of native cells (chondrocytes) to promote the repair and remodelling of articular cartilage. According to the outcomes revealed by this study, a promising therapy for osteochondral repair could be to develop a bilayer system based on ELR-hydrogels. This system would consist of a bottom layer composed by the hydrogel embedded with MSCs, which fill the sub-chondral bone cavity; whereas the upper layer would be composed by the hydrogel itself. In

conclusion, our bioactive ELR-based hydrogel alone was able to resemble native tissue in terms of hyaline cartilage content and the absence of fibro-cartilage, thus proving to be a promising scaffold for cartilage repair.

Acknowledgments

This project has received funding from the European Union's Horizon 2020 research and innovation programme under the Marie Sklodowska-Curie grant agreement No 642687. The authors are grateful for the funding from the European Commission (NMP-2014-646075), the Spanish Government (PCIN-2015-010, MAT2015-68901-R, MAT2016-78903-R, MAT2016-79435-R), Junta de Castilla y León (VA015U16) and Centro en Red de Medicina Regenerativa y Terapia Celular de Castilla y León. The authors also wish to thank Maria Victoria Saez Velasco for her important contribution to cell culture experiments.

Conflict of Interest

The authors declare no competing financial interest.

References

1. Mankin HJ. The response of articular cartilage to mechanical injury. J Bone Joint Surg Am 1982;64:460-6.

2. Rodríguez Cabello JC, De Torre IG, Cipriani F et al. 12 - Elastin-like materials for tissue regeneration and repair A2 - Barbosa, Mário A. In: Martins MCL (ed). Peptides and Proteins as Biomaterials for Tissue Regeneration and Repair: Woodhead Publishing, 2018, 309-327.

3. Altman RD, Lozada CJ. Practice guidelines in the management of osteoarthritis. Osteoarthritis and Cartilage 1998;6:22-24.

4. Sharma A, Wood LD, Richardson JB et al. Glycosaminoglycan profiles of repair tissue formed following autologous chondrocyte implantation differ from control cartilage. Arthritis Research & Therapy 2007;9:R79.

5. Gagliardi JA, Chung EM, Chandnani VP et al. Detection and staging of chondromalacia patellae: relative efficacies of conventional MR imaging, MR arthrography, and CT arthrography. AJR Am J Roentgenol 1994;163:629-36.

6. Smolen JS, Aletaha D, Steiner G. Does damage cause inflammation? Revisiting the link between joint damage and inflammation. Ann Rheum Dis 2009;68:159-62.

7. Correa D, Lietman SA. Articular cartilage repair: Current needs, methods and research directions. Seminars in Cell & Developmental Biology 2017;62:67-77.

8. Knudson CB, Knudson W. Cartilage proteoglycans. Seminars in Cell & Developmental Biology 2001;12:69-78.

9. Girotti A, Orbanic D, Ibáñez-Fonseca A et al. Recombinant Technology in the Development of Materials and Systems for Soft-Tissue Repair. Advanced Healthcare Materials 2015;4:2423-2455.

10. Kerker JT, Leo AJ, Sgaglione NA. Cartilage Repair: Synthetics and Scaffolds: Basic Science, Surgical Techniques, and Clinical Outcomes. Sports Medicine and Arthroscopy Review 2008;16:208-216.

11. Vaquero J, Forriol F. Knee chondral injuries: Clinical treatment strategies and experimental models. Injury 2012;43:694-705.

12. Vijayan S, Bartlett W, Bentley G et al. Autologous chondrocyte implantation for osteochondral lesions in the knee using a bilayer collagen membrane and bone graft. a two- to eight-year follow-up study 2012;94-B:488-492.

13. Vega A, Martin-Ferrero MA, Del Canto F et al. Treatment of Knee Osteoarthritis With Allogeneic Bone Marrow Mesenchymal Stem Cells: A Randomized Controlled Trial. Transplantation 2015;99:1681-90.

14. Kessler MW, Ackerman G, Dines JS et al. Emerging Technologies and Fourth Generation Issues in Cartilage Repair. Sports Medicine and Arthroscopy Review 2008;16:246-254.

15. Trattnig S, Ba-Ssalamah A, Pinker K et al. Matrix-based autologous chondrocyte implantation for cartilage repair: noninvasive monitoring by high-resolution magnetic resonance imaging. Magnetic Resonance Imaging 2005;23:779-787.

16. Zhang J, Huang X, Wang H et al. The challenges and promises of allogeneic mesenchymal stem cells for use as a cell-based therapy. Stem Cell Research & Therapy 2015;6:234.

17. Pescador D, Ibanez-Fonseca A, Sanchez-Guijo F et al. Regeneration of hyaline cartilage promoted by xenogeneic mesenchymal stromal cells embedded within elastin-like recombinamer-based bioactive hydrogels. J Mater Sci Mater Med 2017;28:115.

18. Li J, Ezzelarab MB, Cooper DKC. Do mesenchymal stem cells function across species barriers? Relevance for xenotransplantation. Xenotransplantation 2012;19:273-285.

19. Orozco L, Munar A, Soler R et al. Treatment of knee osteoarthritis with autologous mesenchymal stem cells: a pilot study. Transplantation 2013;95:1535-41.

20. Garcia-Sancho J, Sanchez A, Vega A et al. Influence of HLA Matching on the Efficacy of Allogeneic Mesenchymal Stromal Cell Therapies for Osteoarthritis and Degenerative Disc Disease. Transplant Direct 2017;3:e205.

21. Revell CM, Athanasiou KA. Success rates and immunologic responses of autogenic, allogenic, and xenogenic treatments to repair articular cartilage defects. Tissue Eng Part B Rev 2009;15:1-15.

22. Muir H. The chondrocyte, architect of cartilage—biomechanics, structure, function and molecular-biology of cartilage matrix macromolecules. Bioessays 1995;17:1039-48.

23. Hou Q, Bank. PAD, Shakesheff KM. Injectable scaffolds for tissue regeneration. J Mater Chem 2004;14:1915-1923

24. Meyer DE, Chilkoti A. Genetically Encoded Synthesis of Protein-Based Polymers with Precisely Specified Molecular Weight and Sequence by Recursive Directional Ligation: Examples from the Elastin-like Polypeptide System. Biomacromolecules 2002;3:357-367.

25. Ribeiro A, Arias FJ, Reguera J et al. Influence of the Amino-Acid Sequence on the Inverse Temperature Transition of Elastin-Like Polymers. Biophysical Journal 2009;97:312-320.

26. McDaniel JR, Radford DC, Chilkoti A. A unified model for de novo design of elastin-like polypeptides with tunable inverse transition temperatures. Biomacromolecules 2013;14:2866-2872.

27. J. Carlos Rodriguez-Cabello AIF, Matilde Alonso, Leander Poocza, Filippo Cipriani, Israel González de Torre. Elastin-Like Polymers: Properties, Synthesis, and Applications. In: Wiley (ed). Encyclopedia of Polymer Science and Technology, 2017, 1-36.

28. de Torre IG, Wolf F, Santos M et al. Elastin-like recombinamer-covered stents: Towards a fully biocompatible and non-thrombogenic device for cardiovascular diseases. Acta Biomaterialia 2015;12:146-155.

29. Srivastava GK, Martín L, Singh AK et al. Elastin-like recombinamers as substrates for retinal pigment epithelial cell growth. Journal of Biomedical Materials Research Part A 2011;97A:243-250.

30. Vila M, García A, Girotti A et al. 3D silicon doped hydroxyapatite scaffolds decorated with Elastin-like Recombinamers for bone regenerative medicine. Acta Biomaterialia 2016;45:349-356.

31. Cipriani F, Kruger M, de Torre IG et al. Cartilage Regeneration in Preannealed Silk Elastin-Like Co-Recombinamers Injectable Hydrogel Embedded with Mature Chondrocytes in an Ex Vivo Culture Platform. Biomacromolecules 2018;19:4333–4347.

32. Meller D, Li DQ, Tseng SCG. Regulation of Collagenase, Stromelysin, and Gelatinase B in Human Conjunctival and Conjunctivochalasis Fibroblasts by Interleukin-1β and Tumor Necrosis Factor-α. Investigative Ophthalmology & Visual Science 2000;41:2922-2929.

33. Ruoslahti E, Pierschbacher MD. Arg-Gly-Asp: A versatile cell recognition signal. Cell 1986;44:517-518.

34. Di Zio K, Tirrell DA. Mechanical Properties of Artificial Protein Matrices Engineered for Control of Cell and Tissue Behavior. Macromolecules 2003;36:1553-1558.

35. Rodríguez-Cabello JC, Martín L, Alonso M et al. "Recombinamers" as advanced materials for the post-oil age. Polymer 2009;50:5159-5169.

36. Rodríguez-Cabello JC, Pierna M, Fernández-Colino A et al. Recombinamers: Combining Molecular Complexity with Diverse Bioactivities for Advanced Biomedical and Biotechnological Applications. In: Nyanhongo GS, Steiner W, Gübitz G (eds). Biofunctionalization of Polymers and their Applications. Berlin, Heidelberg: Springer Berlin Heidelberg, 2011, 145-179.

37. Girotti A, Reguera J, Arias FJ et al. Influence of the Molecular Weight on the Inverse Temperature Transition of a Model Genetically Engineered Elastin-like pH-Responsive Polymer. Macromolecules 2004;37:3396-3400.

38. Rodríguez-Cabello JC, Girotti A, Ribeiro A et al. Synthesis of Genetically Engineered Protein Polymers (Recombinamers) as an Example of Advanced Self-Assembled Smart Materials. In: Navarro M, Planell JA (eds). Nanotechnology in Regenerative Medicine: Methods and Protocols. Totowa, NJ: Humana Press, 2012, 17-38.

39. Costa RR, Custódio CA, Arias FJ et al. Layer-by-Layer Assembly of Chitosan and Recombinant Biopolymers into Biomimetic Coatings with Multiple Stimuli-Responsive Properties. Small 2011;7:2640-2649.

40. Baskin JM, Bertozzi CR. Bioorthogonal Click Chemistry: Covalent Labeling in Living Systems. QSAR & Combinatorial Science 2007;26:1211-1219.

41. Testera AM, Girotti A, de Torre IG et al. Biocompatible elastin-like click gels: design, synthesis and characterization. J Mater Sci Mater Med 2015;26:105.

42. Dormer NH, Singh M, Zhao L et al. Osteochondral interface regeneration of the rabbit knee with macroscopic gradients of bioactive signals. Journal of biomedical materials research. Part A 2012;100:162-170.

43. Løken S, Jakobsen RB, Årøen A et al. Bone marrow mesenchymal stem cells in a hyaluronan scaffold for treatment of an osteochondral defect in a rabbit model. Knee Surgery, Sports Traumatology, Arthroscopy 2008;16:896-903.

44. Dashtdar H, Rothan HA, Tay T et al. A preliminary study comparing the use of allogenic chondrogenic pre-differentiated and undifferentiated mesenchymal stem cells for the repair of full thickness articular cartilage defects in rabbits. J Orthop Res 2011;29:1336-42.

45. Franco NH, Olsson IAS. Scientists and the 3Rs: attitudes to animal use in biomedical research and the effect of mandatory training in laboratory animal science. Laboratory Animals 2013;48:50-60.

46. Lam J, Lu S, Lee EJ et al. Osteochondral defect repair using bilayered hydrogels encapsulating both chondrogenically and osteogenically pre-differentiated mesenchymal stem cells in a rabbit model. Osteoarthritis and cartilage 2014;22:1291-1300.

47. Kim K, Lam J, Lu S et al. Osteochondral tissue regeneration using a bilayered composite hydrogel with modulating dual growth factor release kinetics in a rabbit model. Journal of Controlled Release 2013;168:166-178.

48. Holland TA, Bodde EWH, Cuijpers VMJI et al. Degradable hydrogel scaffolds for in vivo delivery of single and dual growth factors in cartilage repair. Osteoarthritis and Cartilage 2007;15:187-197.

49. Guo X, Park H, Young S et al. Repair of osteochondral defects with biodegradable hydrogel composites encapsulating marrow mesenchymal stem cells in a rabbit model. Acta Biomaterialia 2010;6:39-47.

50. van den Borne MPJ, Raijmakers NJH, Vanlauwe J et al. International Cartilage Repair Society (ICRS) and Oswestry macroscopic cartilage evaluation scores validated for use in Autologous Chondrocyte Implantation (ACI) and microfracture. Osteoarthritis and Cartilage 2007;15:1397-1402.

51. Cao L, Yang F, Liu G et al. The promotion of cartilage defect repair using adenovirus mediated Sox9 gene transfer of rabbit bone marrow mesenchymal stem cells. Biomaterials 2011;32:3910-3920.

52. Mainil-Varlet P, Aigner T, Brittberg M et al. Histological assessment of cartilage repair: a report by the Histology Endpoint Committee of the International Cartilage Repair Society (ICRS). J Bone Joint Surg Am 2003;85-A Suppl 2:45-57.

53. González de Torre I, Santos M, Quintanilla L et al. Elastin-like recombinamer catalyst-free click gels: Characterization of poroelastic and intrinsic viscoelastic properties. Acta Biomaterialia 2014;10:2495-2505.

54. Jia S, Wang J, Zhang T et al. Multilayered Scaffold with a Compact Interfacial Layer Enhances Osteochondral Defect Repair. ACS Applied Materials & Interfaces 2018;10:20296-20305.

55. Roach HI, Aigner T, Soder S et al. Pathobiology of Osteoarthritis: Pathomechanisms and Potential Therapeutic Targets. Current Drug Targets 2007;8:271-282.

56. Richter W. Mesenchymal stem cells and cartilage in situ regeneration. J Intern Med 2009;266:390-405.

57. Peterson L, Vasiliadis HS, Brittberg M et al. Autologous Chondrocyte Implantation: A Long-term Follow-up. The American Journal of Sports Medicine 2010;38:1117-1124.

58. Wakitani S, Goto T, Young RG et al. Repair of large full-thickness articular cartilage defects with allograft articular chondrocytes embedded in a collagen gel. Tissue Eng 1998;4:429-44.

59. Iwasa J, Engebretsen L, Shima Y et al. Clinical application of scaffolds for cartilage tissue engineering. Knee Surgery, Sports Traumatology, Arthroscopy 2009;17:561-577.

60. Fong EL, Watson BM, Kasper FK et al. Building bridges: leveraging interdisciplinary collaborations in the development of biomaterials to meet clinical needs. Adv Mater 2012;24:4995-5013.

61. Perka C, Spitzer RS, Lindenhayn K et al. Matrix-mixed culture: new methodology for chondrocyte culture and preparation of cartilage transplants. J Biomed Mater Res 2000;49:305-11.

62. Lee KY, Mooney DJ. Hydrogels for Tissue Engineering. Chemical Reviews 2001;101:1869-1880.

63. Jin R, Moreira Teixeira LS, Dijkstra PJ et al. Injectable chitosan-based hydrogels for cartilage tissue engineering. Biomaterials 2009;30:2544-51.

64. Staubli SM, Cerino G, Gonzalez De Torre I et al. Control of angiogenesis and host response by modulating the cell adhesion properties of an Elastin-Like Recombinamer-based hydrogel. Biomaterials 2017;135:30-41.

65. Nagaya H, Ymagata T, Ymagata S et al. Examination of synovial fluid and serum hyaluronidase activity as a joint marker in rheumatoid arthritis and osteoarthritis patients (by zymography). Ann Rheum Dis 1999;58:186-188.

66. Trabbic-Carlson K, Setton LA, Chilkoti A. Swelling and Mechanical Behaviors of Chemically Cross-Linked Hydrogels of Elastin-like Polypeptides. Biomacromolecules 2003;4:572-580.

67. Erkamp RQ, Wiggins P, Skovoroda AR et al. Measuring the Elastic Modulus of Small Tissue Samples. Ultrasonic Imaging 1998;20:17-28.

68. Hayes WC, Bodine AJ. Flow-independent viscoelastic properties of articular cartilage matrix. Journal of Biomechanics 1978;11:407-419.

69. Broom ND, Oloyede A. The importance of physicochemical swelling in cartilage illustrated with a model hydrogel system. Biomaterials 1998;19:1179-88.

70. Annabi N, Nichol JW, Zhong X et al. Controlling the porosity and microarchitecture of hydrogels for tissue engineering. Tissue Eng Part B Rev 2010;16:371-83.

71. Mow VC, Holmes MH, Michael Lai W. Fluid transport and mechanical properties of articular cartilage: A review. Journal of Biomechanics 1984;17:377-394.

72. Bhosale AM, Richardson JB. Articular cartilage: structure, injuries and review of management. British Medical Bulletin 2008;87:77-95.

73. Erickson IE, Kestle SR, Zellars KH et al. Improved cartilage repair via in vitro pre-maturation of MSC-seeded hyaluronic acid hydrogels. Biomed Mater 2012;7:024110.

74. Hui TY, Cheung KM, Cheung WL et al. In vitro chondrogenic differentiation of human mesenchymal stem cells in collagen microspheres: influence of cell seeding density and collagen concentration. Biomaterials 2008;29:3201-12.

75. Huang CY, Reuben PM, D'Ippolito G et al. Chondrogenesis of human bone marrow-derived mesenchymal stem cells in agarose culture. Anat Rec A Discov Mol Cell Evol Biol 2004;278:428-36.

76. Goldberg A, Mitchell K, Soans J et al. The use of mesenchymal stem cells for cartilage repair and regeneration: a systematic review. Journal of orthopaedic surgery and research 2017;12:39-39.

77. Li Z, Kupcsik L, Yao SJ et al. Chondrogenesis of human bone marrow mesenchymal stem cells in fibrin-polyurethane composites. Tissue Eng Part A 2009;15:1729-37.

78. Jia Z, Liu Q, Liang Y et al. Repair of articular cartilage defects with intra-articular injection of autologous rabbit synovial fluid-derived mesenchymal stem cells. Journal of translational medicine 2018;16:123-123.

79. Guilak F, Estes BT, Diekman BO et al. 2010 Nicolas Andry Award: Multipotent Adult Stem Cells from Adipose Tissue for Musculoskeletal Tissue Engineering. Clinical Orthopaedics and Related Research 2010;468:2530-2540.

80. Crupi A, Costa A, Tarnok A et al. Inflammation in tissue engineering: The Janus between engraftment and rejection. Eur J Immunol 2015;45:3222-36.

81. Flora T, de Torre IG, Quintanilla L et al. Spatial control and cell adhesion selectivity on model gold surfaces grafted with elastin-like recombinamers. European Polymer Journal 2018;106:19-29.

82. Bettinger CJ. Biodegradable elastomers for tissue engineering and cell-biomaterial interactions. Macromol Biosci 2011;11:467-82.

83. Kosuge D, Khan WS, Haddad B et al. Biomaterials and scaffolds in bone and musculoskeletal engineering. Curr Stem Cell Res Ther 2013;8:185-91.

84. Armiento AR, Stoddart MJ, Alini M et al. Biomaterials for articular cartilage tissue engineering: Learning from biology. Acta Biomaterialia 2018;65:1-20.

SUPPORTING INFORMATION

Differential Scanning Calorimetry (DSC) measurements

DSC experiments were performed using the Mettler Toledo 822^e DSC with a liquid nitrogen cooler accessory and under a nitrogen atmosphere. All samples were equilibrated for 5 min at 0 °C inside the sample chamber before the experiment started, and then, heated from 0 to 60 °C with a speed of 5 °C/min.

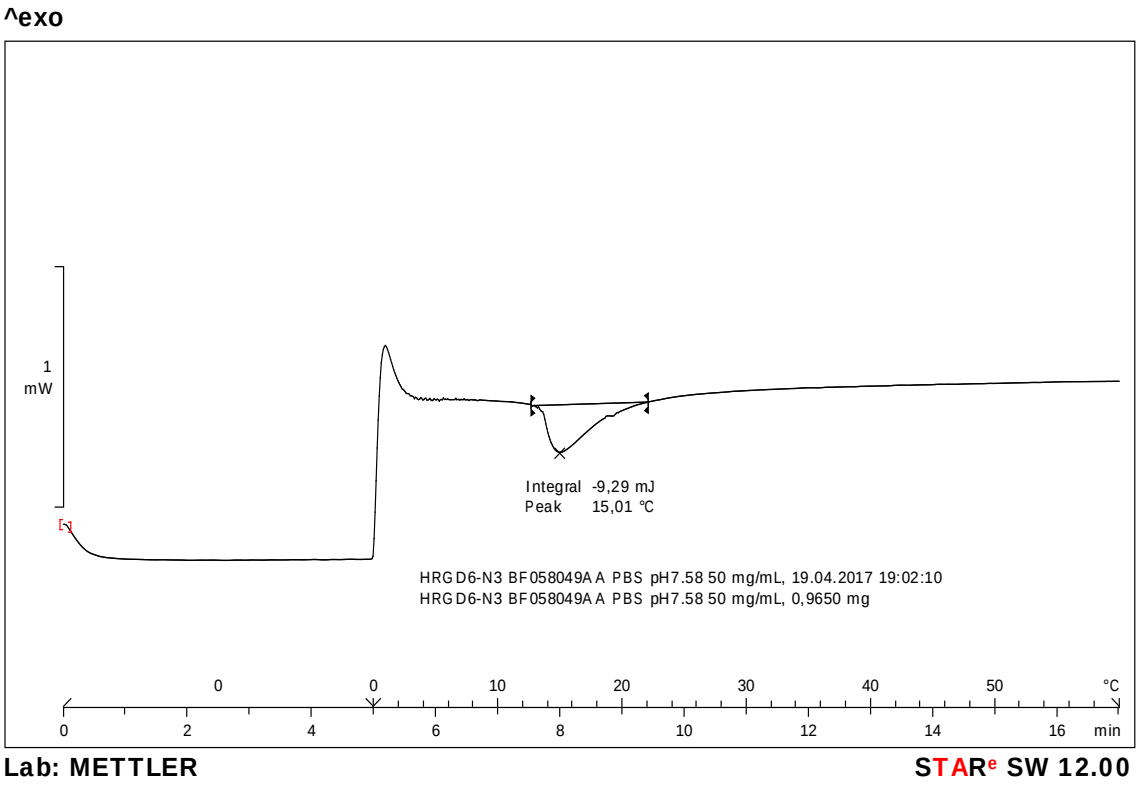

Figure S1. DSC graph of $HRGD_6$-N_3 showing the experimental T_t in PBS at physiological pH.

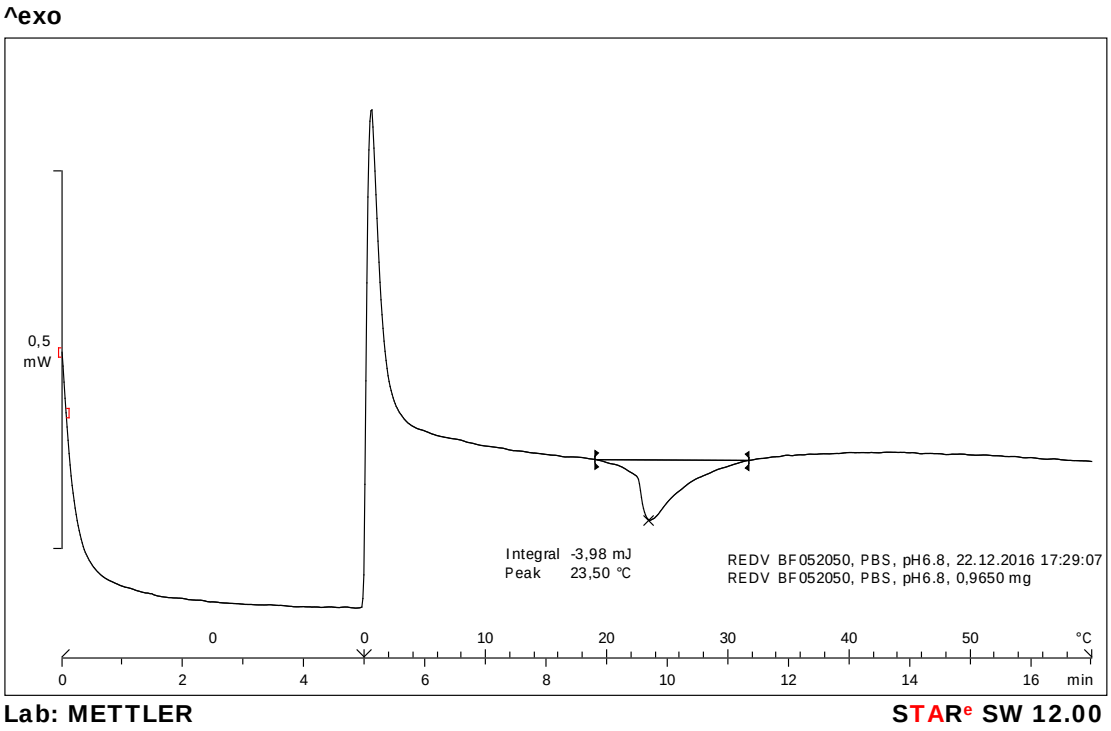

Figure S2. DSC graph of REDV-N_3 showing the experimental T_t in PBS at physiological pH.

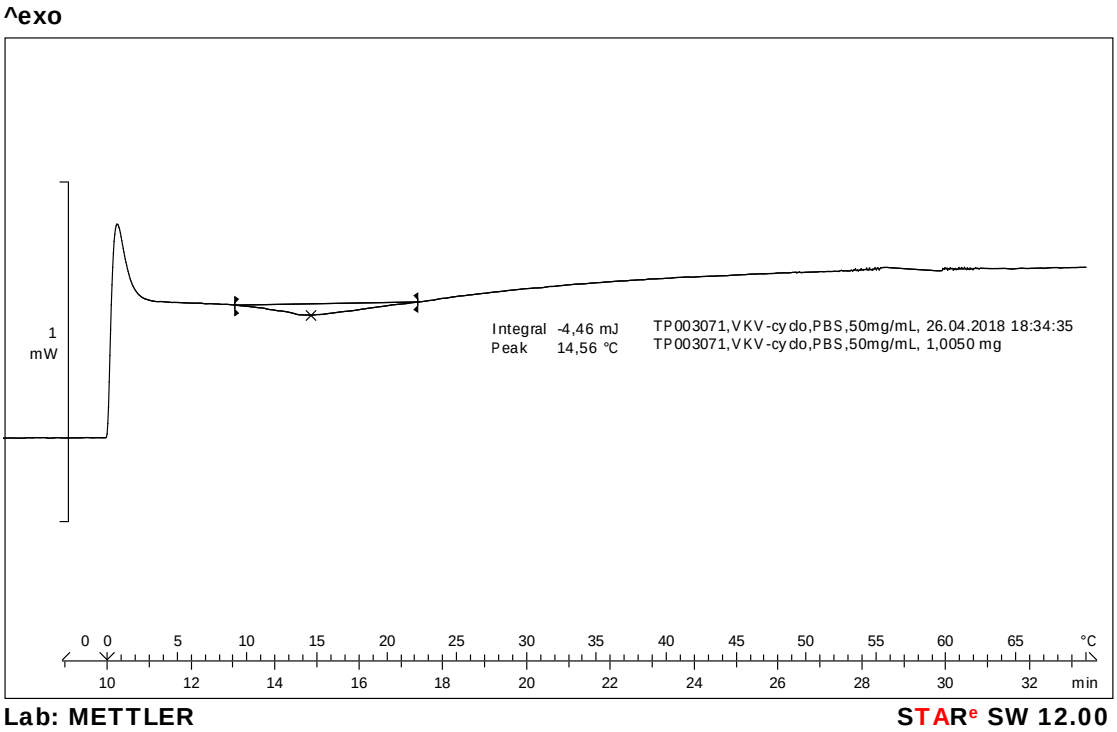

Figure S3. DSC graph of VKV-Cyclo showing the experimental T_t in PBS at physiological pH.

Fourier Transform Infrared Spectroscopy (FTIR).

FTIR analysis was carried out using a Bruker FTIR spectrophotometer (Bruker, USA), whereas the spectral calculations were performed by the OPUS (version 4.2) software

(Mattson Instrument INC.). For each spectrum, a 512-scan interferogram was collected at single beam absorption mode with a 2 cm^{-1} resolution within the 4000- 600 cm^{-1} region. Measurements were performed in triplicates and averaged to obtain the final FTIR absorption spectrum of the sample. Residual water vapour absorption was interactively subtracted from the sample spectra.

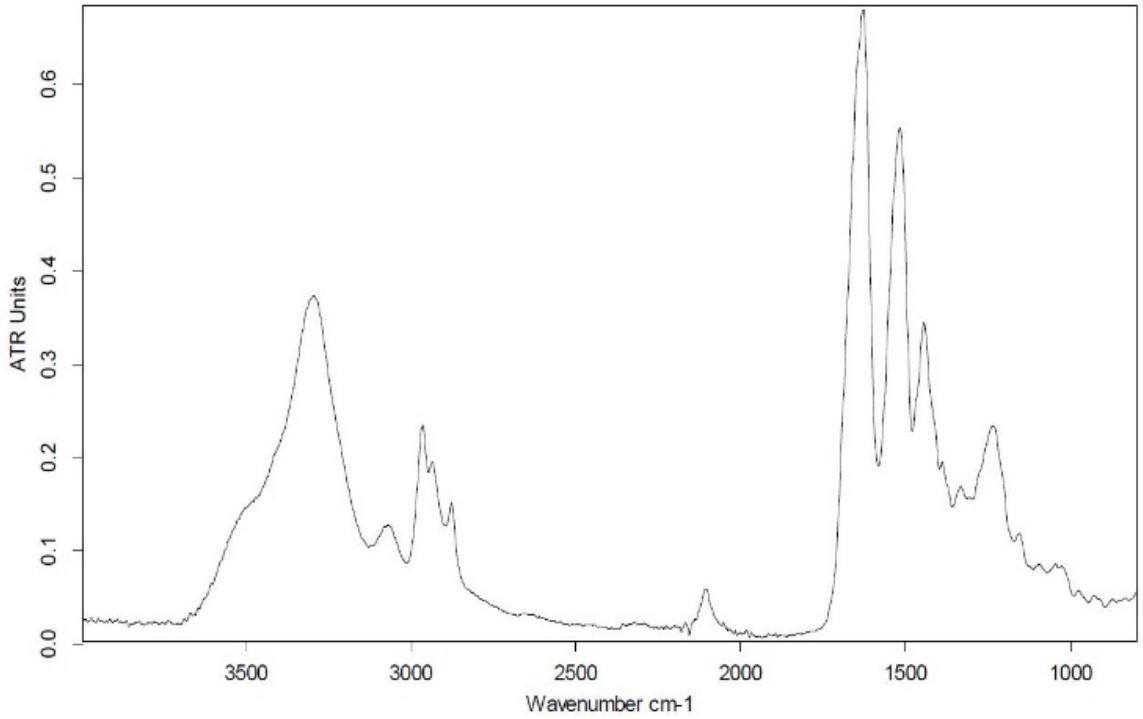

Figure S4. FTIR of $HRGD_6$-N_3.

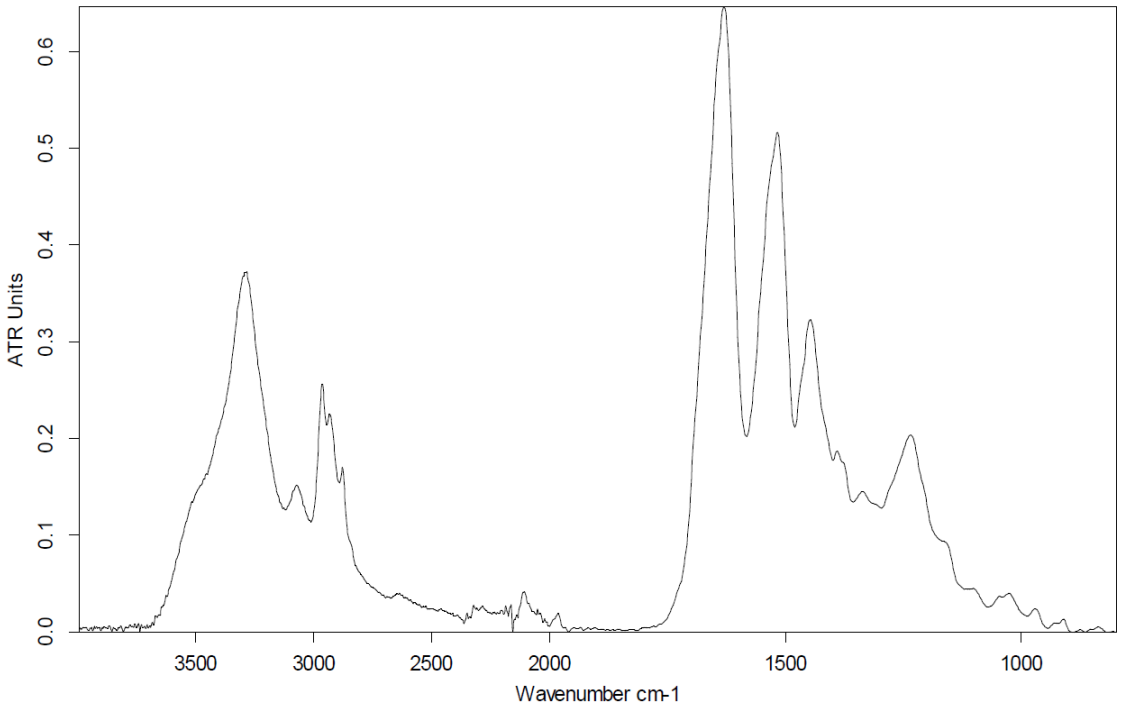

Figure S5. FTIR of REDV-N_3.

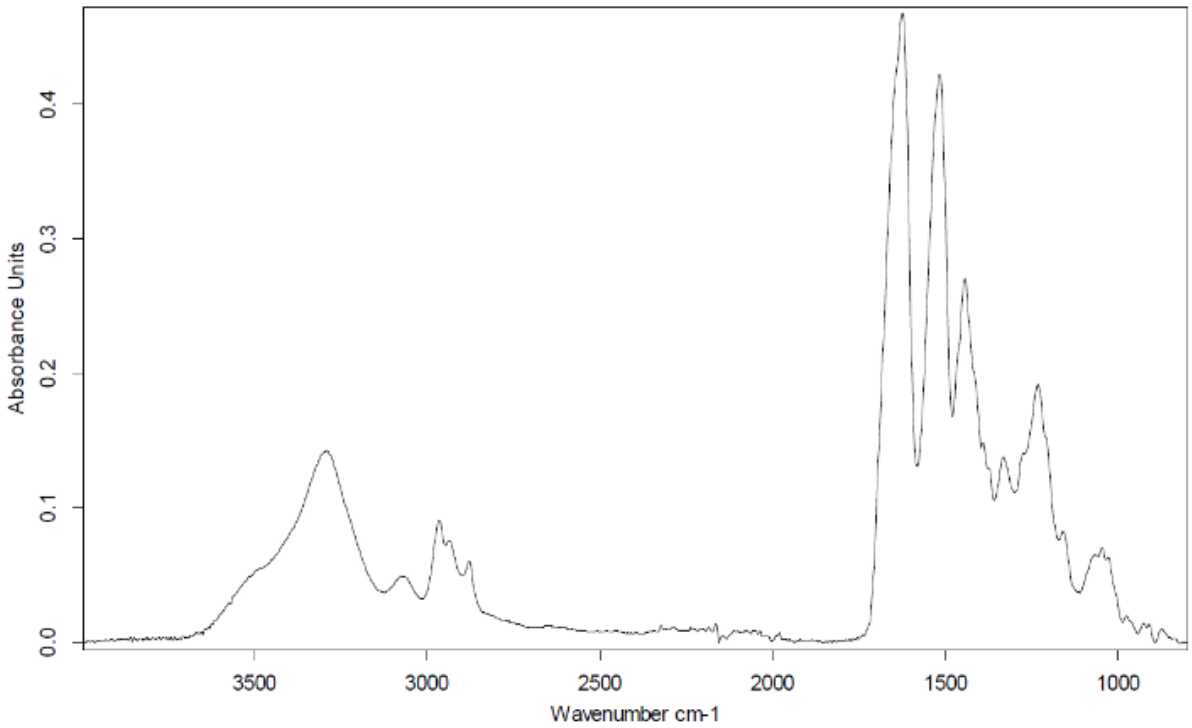

Figure S6. FTIR of VKV-Cyclo.

Proton nuclear magnetic resonance ^{1}H-NMR Spectroscopy

NMR analysis was carried out using a 400 MHz Agilent Technologies equip with an Agilent MR console 400 and a One NMR probe. The measurements were carried out at 298 K with samples of 20–30 mg of the modified elastin like recombinamers, purified, and dissolved in DMSO-d6. Chemical shifts (δ) are given in ppm.

The no deuterated dimethyl sulfoxide peaks at d ¼ 2.5 ppm and d ¼ 39.51 ppm were used as internal reference for 1H and 13C NMR spectra, respectively.

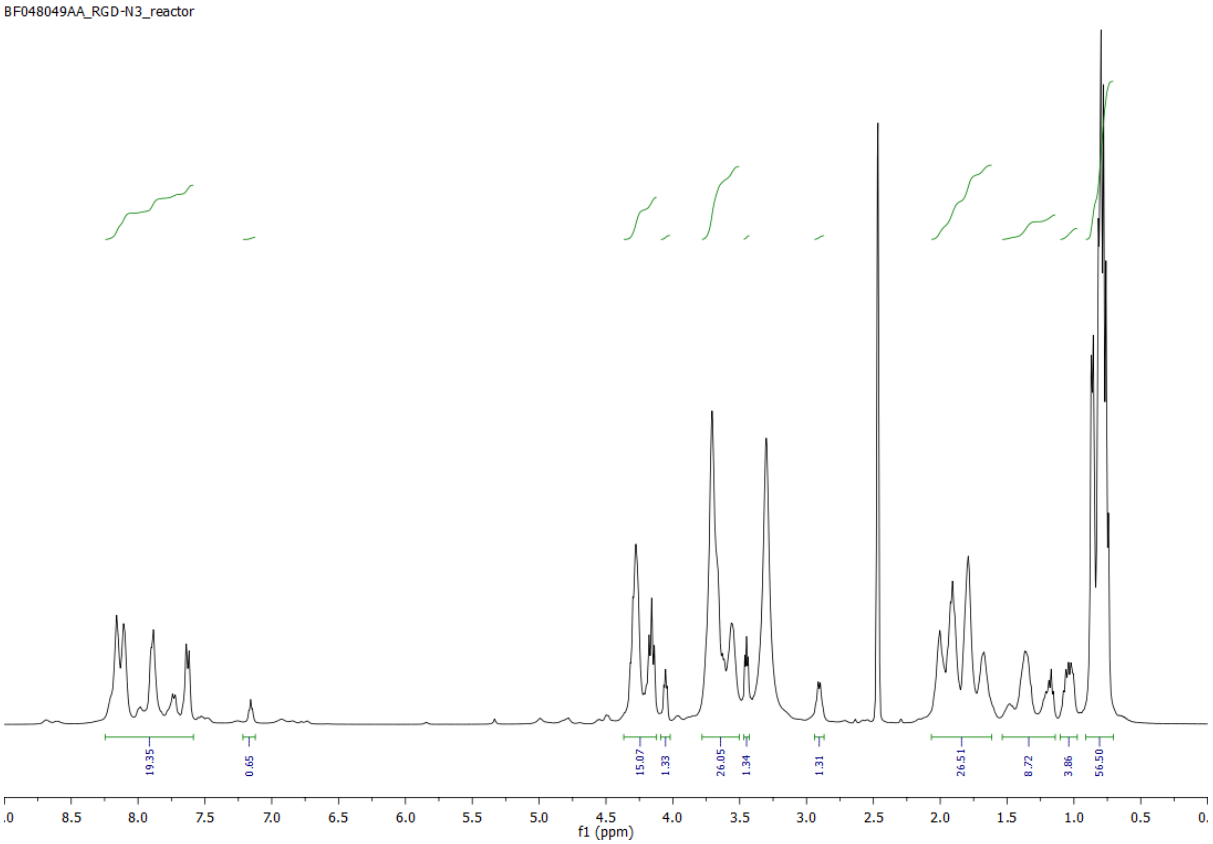

Figure S7. H-NMR spectrum of $HRGD_6$-N_3 showing the integration of the peaks corresponding to the different types of hydrogens.

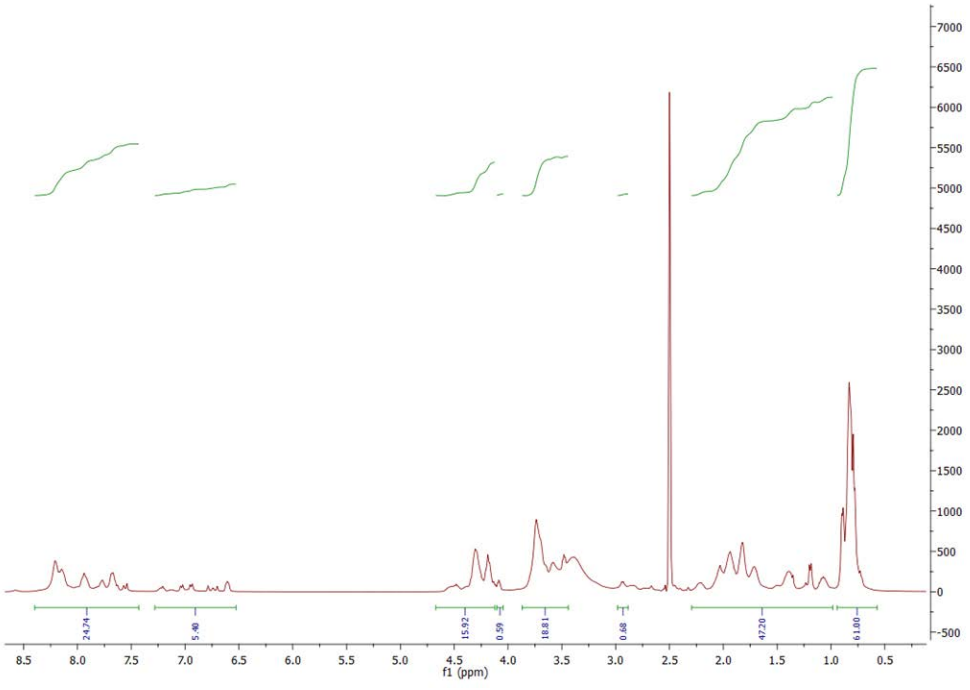

Figure S8. H-NMR spectrum of REDV-N_3 showing the integration of the peaks corresponding to the different types of hydrogens.

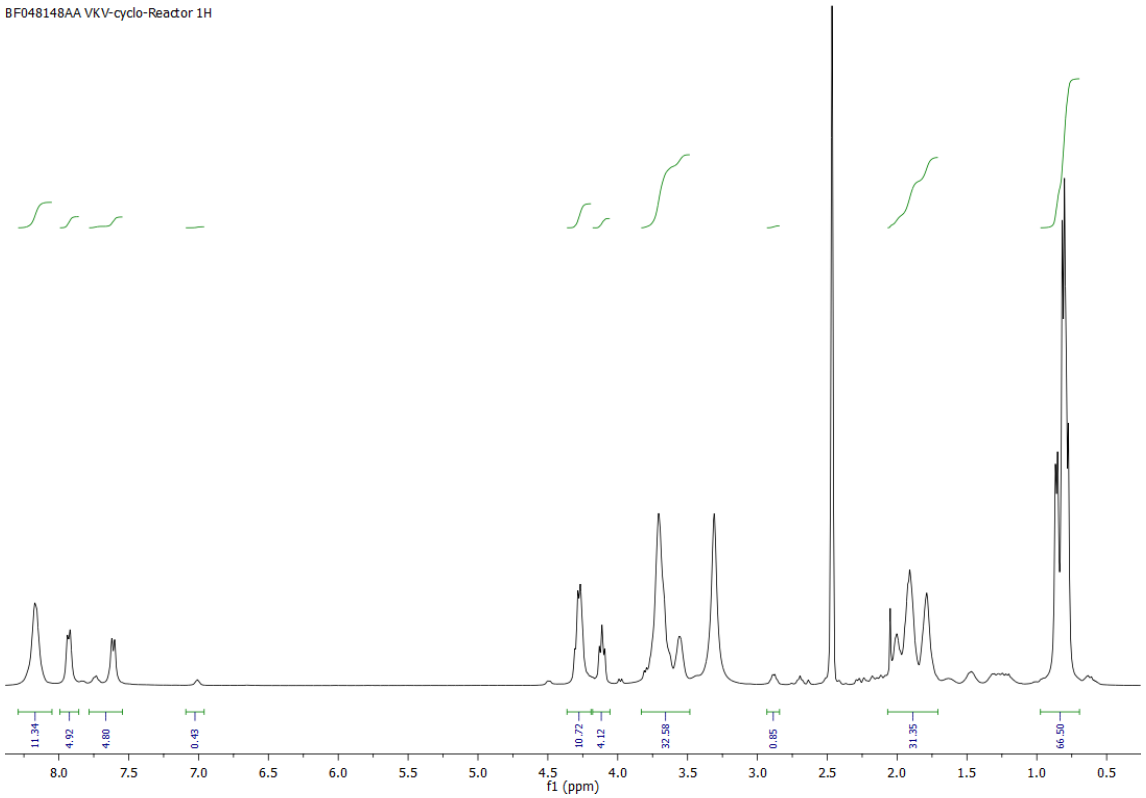

Figure S9. H-NMR spectrum of VKV-Cyclo showing the integration of the peaks corresponding to the different types of hydrogens.

CHAPTER 5

BICYCLIC RGD PEPTIDES WITH INTEGRIN $\alpha_v\beta_3$ AND $\alpha_5\beta_1$ AFFINITY PROMOTE CELL ADHESION ON ELASTIN-LIKE RECOMBINAMERS

Filippo Cipriani,[1] Dominik Bernhagen,[2] Carmen García-Arévalo,[3] Israel González de Torre,[1,3] Peter Timmerman,[2,4] José Carlos Rodríguez-Cabello,[1,3]

[1] Technical Proteins Nanobiotechnology S.L., Paseo Belén 9A, 47001 Valladolid, Spain

[2] Pepscan Therapeutics, Zuidersluisweg 2, 8243 RC Lelystad, the Netherlands

[3] Bioforge, University of Valladolid CIBER-BNN, Paseo de Belén 19, 47001 Valladolid, Spain

[4] Van't Hoff Institute for Molecular Sciences, University of Amsterdam, Science Park 904, 1098 XH Amsterdam, the Netherlands

F. Cipriani, D. Bernhagen, C. García-Arévalo, I. González de Torre, P. Timmerman, J.C. Rodríguez-Cabello. Bicyclic RGD peptides with high integrin $\alpha_v\beta_3$ and $\alpha_5\beta_1$ affinity promote cell adhesion on elastin-like recombinamers. *Biomedical Materials* (2018). doi: 10.1088/1748-605X/aafd83

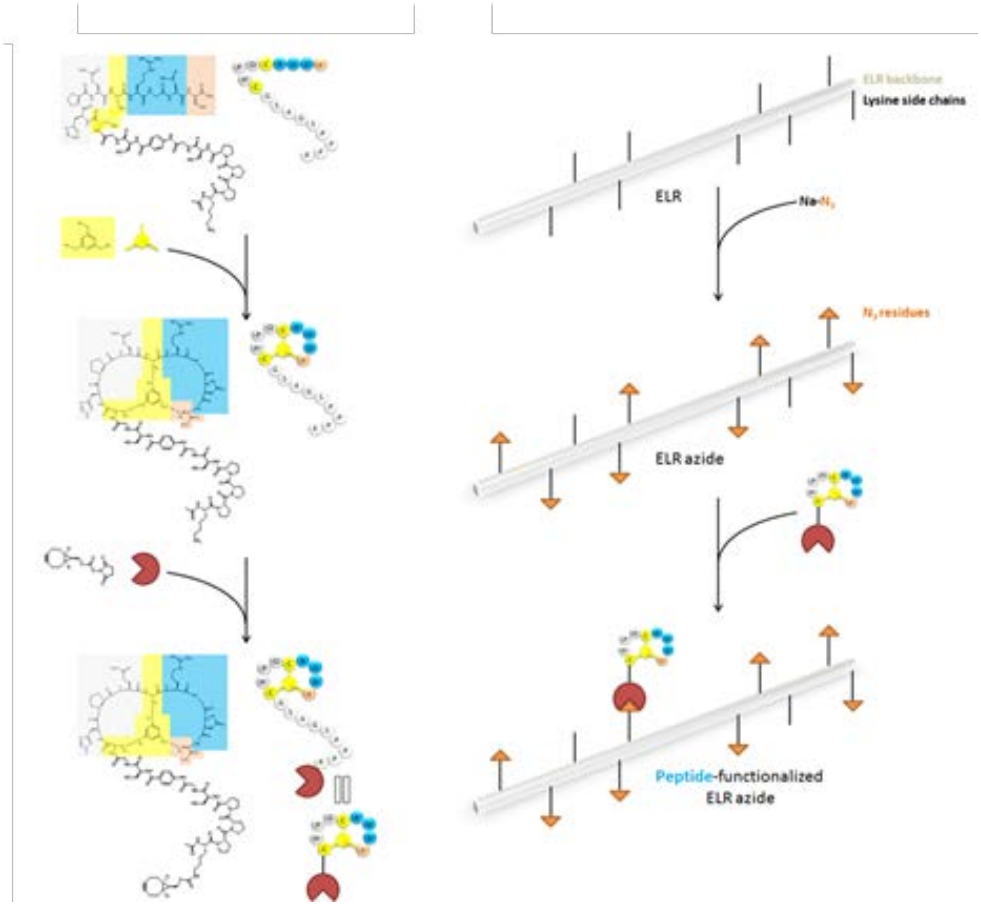

Abstract

Biomaterial design in tissue engineering aims to identify appropriate cellular microenvironments in which cells can grow and guide new tissue formation. Despite the large diversity of synthetic polymers available for regenerative medicine, most of them fail to fully match the functional properties of their native counterparts. In contrast, the few biological alternatives employed as biomaterials lack the versatility that chemical synthesis can offer. Herein, we studied the HUVEC adhesion and proliferation properties of elastin-like recombinamers (ELRs) that were covalently functionalized with each three high-affinity and selectivity $\alpha_v\beta_3$- and $\alpha_5\beta_1$-binding bicyclic RGD peptides. Next to the bicycles, ELRs were also functionalized with various integrin-binding benchmark peptides, i.e. knottin-RGD, cyclo-[KRGDf] and GRGDS, allowing for better classification of the obtained results. Covalent functionalization with the RGD peptides, as validated by MALDI-TOF analysis, guarantees flexibility and minimal steric hindrance for interactions with cellular integrins. In addition to the covalently modified RGD-ELRs, we also synthesized another benchmark ELR comprising RGD as part of the backbone. HUVEC adhesion and proliferation analysis using the PicoGreen® assay revealed a higher short-term adhesion and proliferative capacity of cells on ELR surfaces functionalized with high affinity, integrin-binding bicyclic RGD-peptides compared with the ELRs containing RGD in the backbone.

1. INTRODUCTION

A central goal of research in tissue engineering and regenerative medicine is the design of biomaterials that can be used to control critical aspects of cellular behaviour. Such materials should guide cells toward the phenotypes and architectures that are needed to restore tissue function or induce cells from surrounding tissue to infiltrate implanted matrices (1), including vascular grafts (2), bone grafts (3), wound dressings (4), and injectable drug depots (5). One major problem that still remains is the inadequate interaction between polymer and cells, which leads to foreign body reactions such as inflammation, infections, and implant encapsulation, as well as thrombosis and embolization, *in vivo*. Research into the surface modification of polymeric materials to guide cellular activity in biomaterials (6-8) designed for tissue-engineering applications has mostly focused on the use of natural extracellular matrix (ECM) proteins and short peptides such as the integrin-binding tripeptide RGD (9,10). The use of small peptides offers several advantages, such as straightforward synthesis and a low immunogenic potential (11, 12). Moreover, they tend to exhibit high stability towards sterilization conditions, heat treatment, pH-variation and storage (13, 14). However, it is important to take into account that the peptide stability is strongly dependent on the sequence. In particular, peptides containing methionine, cysteine or tryptophan are prone to oxidation with resultant loss of bioactivity (15).

While a large variety of modified synthetic polymers have been extensively explored in regenerative medicine, only a few biological materials, mostly purified proteins from animal tissues, have been studied in detail to date (16). In this regard, recombinant proteins have recently received interest as an attractive alternative for tissue-engineering applications and surface functionalization (17, 18). Elastin-like recombinamers (ELRs) are some of the most intensively studied groups of recombinant proteins over the past decade (19). ELRs comprise repetitive sequences comprising the pentapeptide “Val-Pro-Gly-X-Gly”, where the guest residue “X” can be any amino acid except proline. These polypeptides are highly flexible due to weak hydrophobic interactions and hydrogen bonds that enable the chains to extend and retract similarly to a spring (20-22). ELRs can be codified in synthetic genes and expressed in *Escherichia coli* in large quantities, thus

allowing greater control of the amino acid sequence and molecular weight when compared with the chemical synthesis of large polypeptides (18). Furthermore, due to their inverse temperature transition property, they can easily be separated from the raw protein mixture (23), thereby resulting in a purified, biocompatible, biodegradable, and non-immunogenic engineered protein (24). ELRs have several advantages as regards tissue engineering applications, such as their defined macromolecular structure, controlled swelling behaviour and porosity, degradability, and controllable mechanical properties (25, 26).

First described in 1992 by Nicol *et al*. (27), ELRs comprising integrin-binding motifs such as RGD (1, 28-30) or REDV (30, 31) have been investigated as possible materials for biomaterial applications. However, thus far, recombinant synthesis has limitations in the incorporation of non-canonical amino acids and does not allow the formation of cyclized peptides (32). Despite this, ELR hydrogels covalently functionalized with a peptide mimic of the receptor-binding region of VEGF (vascular endothelial growth factor) showed enhanced HUVEC proliferation over non-functionalized hydrogels (33).

One drawback of the non-integrin-selective RGD sequence is the inability to elicit responses based on closely defined intracellular pathways (34). An elegant approach to circumvent this limitation, and an additional lever for the control of cell adhesion and proliferation, is orthogonal post-functionalization with peptides via modified lysine side-chains, for example, via maleimide-thiol coupling (34). Functionalization via biorthogonal chemistry is a well-known strategy for the manufacturing of hydrogels and multifaceted cell culture scaffolds (35, 36). Another possibility to functionalize biomaterials with peptides is via copper-free click chemistry (37). For instance, Krause *et al*. applied a metal free click reaction to functionalize alginate with a cyclic RGD peptide (38).

The integrin-binding RGD motif is generally applied in either linear or cyclic format, with the cell adhesion-promoting properties of these peptides depending on the material applied. Linear RGD derivatives, such as GRGDS, are still the most widely applied cell-adhesion sequences despite the fact that cyclic RGD peptides or RGD peptidomimetics provide much higher integrin affinities and selectivities (39, 40). For example, ELRs functionalized with *cyclo*-[KRGDf] showed a 100% improved mouse osteoblast adhesion in comparison with ELRs functionalized with linear FGRGDS (16). However, this study

focused on the chemical functionalization of ELRs and did not include recombinant synthesized RGD-ELRs as a benchmark. In contrast, spider silk proteins genetically fused to GRGDSPG showed similar fibroblast adhesion and proliferation properties compared to spider silk proteins covalently modified with *cyclo*-[KRGDf] (41).

Recently, Bernhagen and coworkers reported short bicyclic RGD-peptides that bind to either integrin $\alpha_v\beta_3$, or to both integrins $\alpha_5\beta_1$ and $\alpha_v\beta_3$, with high affinity (42). For example, for integrin $\alpha_5\beta_1$, the bicyclic peptide **C_{T3}**RGD**C_{T3}**AYJ**C_{T3}** (J: D-Leucine, **C_{T3}** represents cysteines that were constrained using the trivalent scaffold 1,3,5-tris(bromomethyl)benzene) exhibited much higher inhibition (IC_{50}: 90 nM) compared with monocyclic RGD-peptide *cyclo*-KRGDf or linear GRGDS (each IC_{50}: >10 µM) (43). Hence, bicyclic RGD-peptides potentially represent a new group of ligands that boost cellular adhesion and proliferation in biomaterials more than commonly applied linear RGD peptides.

In this study, we have created RGD-functionalized ELRs by conjugating various high-affinity integrin-binding bicyclic RGD-peptides to ELRs using copper-free click chemistry (44). We then evaluated the cell adhesion and proliferation properties of peptide-ELR conjugates for HUVECs. ELRs functionalized with high-affinity bicyclic peptides were compared with ELRs functionalized with benchmark RGD peptides and ELRs that comprised RGD as part of their backbone at the short, medium and long term.

2. MATERIALS AND METHODS

2.1. ELR biosynthesis, modification and characterization

The ELRs used in this work were obtained using standard genetic engineering techniques (31). They were purified using several cycles of temperature-dependent reversible precipitations by centrifugation below and above their transition temperature (T_t), thus making use of the intrinsic thermal behavior of these compounds (31). The ELRs were subsequently dialyzed against purified water and freeze-dried. Two different ELRs, namely VKVx24, a structural recombinamer lacking a bioactive sequence, and $HRGD_6$, a recombinamer containing the universal cell adhesion epitope (RGD) repeated six times per ELR molecule, were obtained. The purity and chemical characterization of these ELRs

were verified by sodium dodecyl sulfate polyacrylamide gel electrophoresis (SDS–PAGE) and matrix-assisted laser desorption/ionization time-of-flight mass spectrometry (MALDI-TOF MS) amino acid composition analysis, differential scanning calorimetry (DSC) and nuclear magnetic resonance (NMR) spectroscopy (31, 45). ELRs were chemically modified by the transformation of the Ɛ-amine group in the lateral lysine chain to bear azide groups (46, 47). VKVx24-N_3 and $HRGD_6$-N_3 were prepared and characterized by NMR, Fourier transform infrared spectroscopy (FTIR), and DSC (Supporting information).

2.2. Reagents and chemicals

Incubation and washing buffers were prepared using standard protocols. Amino acids were purchased from Iris Biotech (Marktredwitz, Germany) and Matrix Innovation (Quebec, Canada). Resins were purchased from Rapp Polymere (Tübingen, Germany) and Merck (Darmstadt, Germany). 1,3,5-Tris(bromomethyl) benzene (T3) and (1*R*,8*S*,9*S*)-Bicyclo[6.1.0]non-4-yn-9-ylmethyl *N*-succinimidyl carbonate (BCN-NHS) were purchased from Sigma-Aldrich (Steinheim, Germany). 2-Azidoethyl (2,5-dioxopyrrolidin-1-yl) carbonate was purchased from GalChimia (A Coruña, Spain).

2.3. Peptide synthesis

Linear peptide **3c** and linear precursor peptides of **1a-1c**, **2a-2c**, **3a** and **3b** (Figure 1) were synthesized using a fully automated peptide synthesizer from Gyros Protein Technologies (Symphony) by Fmoc-based solid-phase peptide synthesis on Rink-amide resin using standard coupling protocols. Folding of knottin-RGD peptide **3a** and backbone cyclization of cyclic RGD peptide **3b** were performed according to previously published protocols (48). For the formation of bicyclic peptides (**1a-c**, **2a-c**), purified linear peptides were dissolved at 0.5 mM in 1:3 MeCN/H_2O, and 1.1 equiv. 1,3,5-tris(bromomethyl) benzene (**T3**) dissolved in MeCN (10 mM) and 1.4 equiv. ammonium carbonate (0.2 M in H_2O) were added. After completion (30-60 min, monitored by UPLC/MS), the reaction was quenched with 10% TFA/H_2O to pH < 4, followed by lyophilization. All peptides were purified by preparative HPLC on an RP-C18 column (Reprosil-Pur 120 C18-AQ 150x20 mm, Dr. Maisch GmbH, Ammerbuch, Germany) using a MeCN/milliQ gradient (5-65%) including 0.05% TFA followed by lyophilization (Christ Alpha 2-4 LDplus). An overview of all peptides can be found in Table 1.

2.4. Synthesis of peptide-cyclooctyne conjugates

BCN-NHS ester (1.1 equiv.) and 10 equiv. *N*,*N*-diisopropylethylamine were added to the peptides dissolved in DMSO (5 mM, TEC218 10 mM). After completion of the reaction (15-30 min, monitored by UPLC/MS), the reaction was quenched with 10% TFA/DMSO to pH < 4. The product was directly purified by preparative HPLC using a MeCN/milliQ gradient (5-65%) including 0.05% TFA, followed by lyophilization. Conjugation was verified by matrix-assisted laser desorption/ionization time-of-flight (MALDI-TOF) mass spectroscopy using a Voyager STR apparatus from Applied Biosystems.

2.5. Formation of peptide-functionalized ELRs

The ELRs comprising 5% or 10% peptide functionalization were modified based on the following calculations: azide-functionalized ELRs (62809 Da) comprised 24 lysine molecules, 80% of which were functionalized with azides (NMR), corresponding to 19.2 azide groups per ELR molecule. The application of 1 equiv. BCN-functionalized peptide would result in the functionalization of 5.21% of the azide groups. Hence, application of 0.96/1.92 equiv. BCN-functionalized peptide would result in 5%/10% functionalization. As such, the application of 3 equiv. and 4 equiv. BCN-functionalized peptide would result in 15% and 20% functionalization. The conjugation of ELRs with BCN-functionalized peptides was performed as follows: azide-functionalized ELRs were dissolved in milliQ water (4 °C, 20 mg/mL). BCN-functionalized peptides were dissolved at 5 mM in milliQ water (**2a** in 50% MeCN/milliQ) and added to the ELR solutions. After shaking the copper-free click reactions for at least 24 h at 4 °C, the products were freeze-dried. Conjugation was subsequently verified by MALDI-TOF MS.

2.6. Analysis of turbidity by UV/Vis-spectroscopy

The ELRs comprising 5% or 10% peptide functionalization were dissolved in milliQ water (4°C, 1 mg/mL), and turbidity measurements were performed at a wavelength of 350 nm (Agilent Technologies Cary Series UV/Vis Spectrophotometer). The transition temperature (T_t) of each RGD peptide-functionalized ELR (ELR-Peptide) was detected by performing a temperature ramp analysis.

2.7. Adsorption of peptide-functionalized ELRs on TCPS

The ELRs comprising 5% or 10% peptide functionalization were dissolved at 1 mg/mL in DPBS (Dulbecco's Phosphate Buffered Saline) –Ca –Mg (O/N at 4 °C) then added to a 96-well tissue culture polystyrene (TCPS) plate for incubation with ELR-Peptide solution O/N at 4 °C with gentle shaking. A positive control was obtained by incubating fibronectin at 10 µg/mL in DPBS –Ca –Mg, whereas a negative control was obtained by incubating BSA at 5 mg/mL in DPBS –Ca –Mg. The plates were subsequently sterilized using an ultraviolet (UV) lamp for 20 min, the solutions removed and the wells washed twice with DPBS –Ca –Mg. Plates were then incubated with a 5 mg/mL BSA blocking solution at 37 °C for 2 h. Finally, the solution was removed and the plates washed twice with DPBS –Ca –Mg prior to cell seeding.

2.8. Contact Angle measurements

Contact angle (CA) measurements were performed using the sessile drop method on a Data Physics OCA20 System instrument. The drop profile images during micro-syringe dispensation were recorded using an adapted CCD video camera. Measurements were taken at ambient temperature 5 s after application of the drops to the surfaces. The contact angle values are the average of ten measurements, including standard deviation, for different locations on each surface in order to ensure a representative value of the contact angle.

2.9. X-ray Photoelectron Spectroscopy (XPS)

XPS experiments were carried out using a Physical Electronics (PHI) 5500 spectrometer equipped with a monochromatic X-ray source (Al Ka line, energy: 1486.6 eV and 350 W). The pressure inside the analysis chamber was 10^{-7} Pa. All measurements were performed at an angle of 45° with respect to both the X-ray source and analyzer. Survey scans were taken in the range 0–1100 eV, with a beam diameter of 200 µm, and high-resolution scans were obtained for C_{1s}, N_{1s}, O_{1s}. The elemental surface composition was estimated from the area of the different photoemission peaks taken from the survey scans modified by their corresponding sensitivity factors.

2.10. Cell culture and cell adhesion assay

Human umbilical vein endothelial cells (HUVECs) (Cat.# C-015-10C; Gibco) at passage 2 were used in all experiments. HUVECs were cultured in Medium 200 (Gibco) supplemented with Low Serum Growth Supplement (LSGS) kit (Gibco), thus resulting in the following final concentrations: fetal bovine serum (FBS) 2% (v/v); hydrocortisone 1 µg/mL; human epidermal growth factor 10 ng/mL; basic fibroblast growth factor 10 ng/mL and heparin 10 µg/mL. A separate vial of Gentamicin/Amphotericin solution (Gibco) was also incorporated at a final concentration of 10 and 0.25 µg/mL, respectively. HUVECs were incubated at 37 °C and 5% CO_2 and harvested at 90% confluence by trypsin–EDTA treatment.

HUVECs were seeded at a density of 5300 cells/cm^2 in serum-free Medium 200 (Gibco) for 30 min on different surfaces (n = 3), and allowed to adhere for 30 min, after which time Medium 200 was removed and the cells cultured in LSGS-supplemented Medium 200 for 14 days. HUVEC adhesion and spreading were evaluated after incubation for 30 min, 4 h and 1, 3, 5, 7 and 14 days. Cultures were provided with fresh media daily, up to the time of the staining period or DNA quantification.

2.11. DNA Analysis

DNA content was determined using the PicoGreen® assay after incubation for 4 h and 1, 3, 5, 7 and 14 days. Briefly, the cells were lysed with a solution of 0.1% Triton X-100 (Sigma Aldrich) in phosphate buffered saline (PBS) (v/v) (49), and the PicoGreen® analysis for DNA content was performed in 96-well plates at standard fluorescein wavelengths (excitation at 480 nm and emission at 520 nm) according to the manufacturer's instructions (Invitrogen) using an automated plate reader (*Bionova Cientifica, Molecular Devices*). Fluorescence intensities were transformed into cell numbers using a calibration curve obtained by measuring the fluorescence of defined cell amounts (n = 0, 100, 1000, 10,000 and 100,000):

n = (y+4.4615)/0.0157 (n: number of cells, y: fluorescence emission)

2.12. 2D Immunofluorescent Staining

Immunofluorescent staining of actin (red), vinculin (green), and nuclei (blue) were performed to visualize the HUVECs on different surfaces. After cell culture, cells were fixed with 4% (w/v) paraformaldehyde, permeabilized with 0.1% Triton-X 100 and blocked with 1% bovine serum albumin (BSA) in PBS solution. Focal contact formation was evaluated by incubating overnight at 4 °C antivinculin rabbit monoclonal antibody (AlexaFluor® 488) (1:200) (Abcam). Cell actin cytoskeletons and nuclei were stained with Rhodamin phalloidin (1:80) (Invitrogen) and DAPI (1:10000) (Lonza), respectively. Cell adhesion and morphological changes were examined using an inverted fluorescence microscope (Nikon Eclipse Ti E) and its associated software. A scan of each surface at low magnification (10x) was analyzed for this study. The images are representative of the morphology found in the samples studied, with at least two to three captures per well being taken. Quantitative image analysis of cell spreading area has been performed at short time incubation (4h); the cell area was calculated by the software associated with the microscope Nikon Eclipse Ti E.

2.13. Statistical analysis

Values are expressed as mean ± standard deviation (SD). Data were analyzed by performing the normality test Shapiro-Wilk. The parametric data were analyzed by one-way analysis of variance (ANOVA) followed by Tukey's Honestly Significant Difference (HSD) *post hoc* test; if only two groups were being compared, an unpaired *t*-test was used instead of ANOVA to assess statistical difference. The nonparametric data were analyzed performing the Kruskal-Wallis test followed by Dunn's multiple-comparison test. All statistical analyses were performed with GraphPad Prism. A *P*-value lower than 0.05 was considered to be statistically significant.

3. RESULTS

3.1. Selection and synthesis of RGD peptides

For this work, we selected three high-affinity integrin $\alpha_v\beta_3$- and $\alpha_5\beta_1/\alpha_v\beta_3$-binding bicyclic peptides for the synthesis of peptide-cyclooctyne conjugates (Figure 1). The $\alpha_v\beta_3$-binding

peptides are K(BCN)-linker-**C$_{T3}$**HPQ**c$_{T3}$**RGD**c$_{T3}$** (**1a**), K(BCN)-linker-**C$_{T3}$**HPQ**C$_{T3}$**RGD**c$_{T3}$** (**1b**), and K(BCN)-linker-**C$_{T3}$**HSQ**C$_{T3}$**RGD**c$_{T3}$** (**1c**), whereas the $\alpha_5\beta_1/\alpha_v\beta_3$-binding peptides are K(BCN)-linker-**C$_{T3}$**RGD**c$_{T3}$**AYJ**C$_{T3}$** (**2a**), K(BCN)-linker-**C$_{T3}$**RGD**c$_{T3}$**AWG**C$_{T3}$** (**2b**), and K(BCN)-linker-**C$_{T3}$**RGD**c$_{T3}$**AYa**C$_{T3}$** (**2c**). The linker sequence PPPSG-(Abz)-SG was designed based on the HexPPP spacer reported by Pallarola *et al.* (50) "**T3**" stands for the scaffold derived from 1,3,5-tris(bromomethyl) benzene, "Abz" represents 4-aminobenzoic acid, and "J" stands for D-Leucine. The selection of the linker will be explained below. In addition to these bicycles, we selected K(BCN)-linker-knottin-RGD (**3a**), *cyclo*-[K(K(BCN)-linker-)RGDf] (**3b**) and K(BCN)-linker-GRGDS (**3c**) as benchmark peptides.

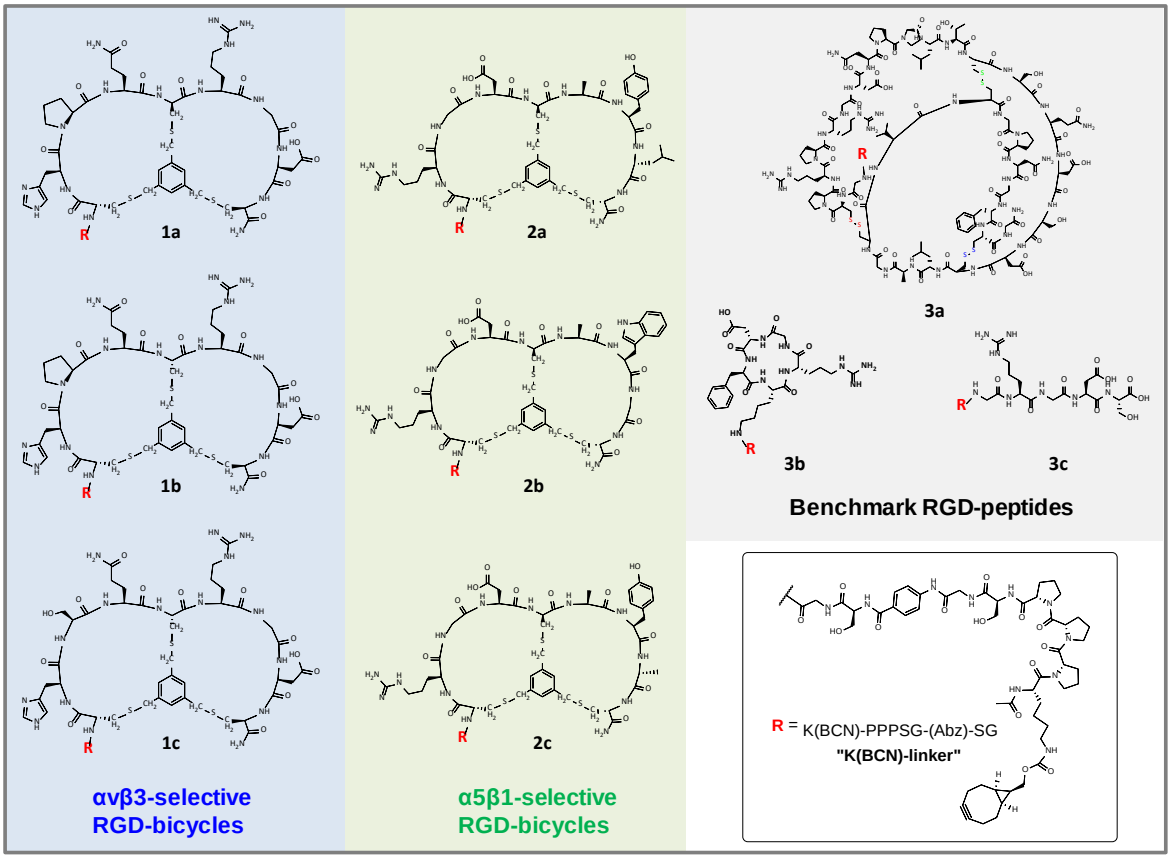

Figure 1. Overview of RGD-peptide–cyclooctyne conjugates for the functionalization of ELRs. **1a:** K(BCN)-linker-**C$_{T3}$**HPQ**c$_{T3}$**RGD**c$_{T3}$**; **1b:** K(BCN)-linker-**C$_{T3}$**HPQ**C$_{T3}$**RGD**c$_{T3}$**; **1c:** K(BCN)-linker-**C$_{T3}$**HSQ**C$_{T3}$**RGD**c$_{T3}$**; **2a:** K(BCN)-linker-**C$_{T3}$**RGD**c$_{T3}$**AYJ**C$_{T3}$** (J: D-Leu); **2b:** K(BCN)-linker-**C$_{T3}$**RGD**c$_{T3}$**AWG**C$_{T3}$**; **2c:** K(BCN)-linker-**C$_{T3}$**RGD**c$_{T3}$**AYa**C$_{T3}$**; **3a:** K(BCN)-linker-G**C$_{S\text{-}S}$**RPRPRGDNPPLT**C$_{S\text{-}S}$**SQDSD**C$_{S\text{-}S}$**LAG**C$_{S\text{-}S}$**V**C$_{S\text{-}S}$**GPNGF**C$_{S\text{-}S}$**G (K(BCN)-linker-knottin-RGD); **3b:** *cyclo*-[K[K(BCN)-linker]RGDf]; **3c:** K(BCN)-linker-GRGDS. Abz: 4-aminobenzoic acid.

For the synthesis of peptide-cyclooctyne conjugates, we chose an approach in which the integrin-binding sequence was coupled to a peptide linker in solid phase peptide synthesis. Pallarola et al. explored the role of the linker system attached to cyclic RGD peptides in the inhibition of binding of immobilized vitronectin to the soluble integrin $\alpha_v\beta_3$ (50); in their study, linkers comprising a triple- (HexPPP), hexa- (HexPPPPPP) or nonaproline (HexPPPPPPPPP) motif did not significantly decrease the inhibition ability. Hence, we added a linker that is similar to the HexPPP linker, but with some variations, to all the RGD peptides. In order to improve solubility in water-based solvents, we included two additional serine residues, and for practical reasons, we used 4-aminobenzoic acid instead of a triazole group. Furthermore, we incorporated an N-terminal acetylated lysine comprising a free amine in the side chain that allows for conjugation with BCN. Linear peptides comprising RGD in one loop and a tripeptide motif providing integrin-selectivity and additional affinity in the other, both enclosed by cysteine residues, were transformed into bicyclic peptides via trivalent scaffold 1,3,5-tris(bromomethyl)benzene followed by reaction with BCN-NHS to form bicyclic RGD peptide-cyclooctyne conjugates. A table of calculated and theoretical molecular weights obtained via UPLC/MS analysis can be found in the Supporting Information (Table S1).

ELR reference	Azide functionalization degree [%]	ELR modification or coating	Integrin selectivity
P1a **P1a-10**	5 10	K(BCN)-linker-**C**$_{T3}$HPQ**c**$_{T3}$RGD**c**$_{T3}$	αvβ3*
P1b **P1b-10**	5 10	K(BCN)-linker-**C**$_{T3}$HPQ**C**$_{T3}$RGD**c**$_{T3}$	αvβ3*
P1c **P1c-10**	5 10	K(BCN)-linker-**C**$_{T3}$HSQ**C**$_{T3}$RGD**c**$_{T3}$	αvβ3*
P2a **P2a-10**	5 10	K(BCN)-linker-**C**$_{T3}$RGD**c**$_{T3}$AYJ**C**$_{T3}$	α5β1, (αvβ3)*
P2b **P2b-10**	5 10	K(BCN)-linker-**C**$_{T3}$RGD**c**$_{T3}$AWG**C**$_{T3}$	α5β1, (αvβ3)*
P2c **P2c-10**	5 10	K(BCN)-linker-**C**$_{T3}$RGD**c**$_{T3}$AYa**C**$_{T3}$	α5β1, (αvβ3)*
P3a **P3a-10**	5 10	K(BCN)-linker-G**C**$_{ox}$PRPRGDNPPLT**C**$_{ox}$ QDSD**C**$_{ox}$LAG**C**$_{ox}$V**C**$_{ox}$GPNGF**C**$_{ox}$G	αvβ3, α5β1, αvβ5*
P3b **P3b-10**	5 10	*cyclo*-[DfK(K(BCN)-linker)RG]	αvβ3, αvβ5*
P3c **P3c-10**	5 10	K(BCN)-linker-GRGDS	multiple*
P0-RGD	–	RGD as part of the ELR-backbone	multiple
P0	–	–	–
P0-FN	–	Fibronectin	αvβ3, α5β1
P0-BSA	–	Bovine serum albumin (BSA)	–

J: D-Leu

Table 1. Overview of ELRs investigated in this study, including degree of functionalization, RGD peptide, and integrin selectivity. ELR labels containing "**P0**" serve as controls that were not covalently modified via copper-free click reaction. * Data from competition ELISA (43).

3.2. ELR functionalization and MALDI-TOF MS analysis

We subsequently functionalized the ELR azides with the peptide-cyclooctyne conjugates via copper-free click chemistry. This orthogonal reaction does not require catalysts and can be performed at room temperature at short reaction time (below one hour). Due to the need to maintain the ELRs in solution (below the T_t), the functionalization of ELRs and ELR azides was performed at 5 °C overnight. Six bicyclic RGD-peptides (**1a-c**, **2a-c**) and three non-selective RGD-peptides (**3a-c**) were used to functionalize either 5% or 10% of the ELR azide groups to receive a total of 18 ELR-peptide conjugates (Table 1). MALDI-

TOF-MS analysis was performed to verify functionalization of the ELRs with the RGD peptides. Selected spectra (**P0**, **P1a**, **P2a**, and **P3a–c**) are shown in Figure 2. The peaks at around m/z 62,200 represent non-functionalized ELR, whereas additional peaks reveal ELRs that were mono-, di-, tri- or even tetra-functionalized with RGD peptides (Table 2).

5%	Mono-functionalization
10%	Di-functionalization
15%	Tri-functionalization
20%	Tetra-functionalization

Table 2. Comparison between the different rates of functionalization and the peaks detected during MALDI-TOF MS analysis.

All the spectra in Figure 2 reveal differences between 5% functionalization and 10% functionalization. In the spectra representing ELRs with 5% peptide functionalization, the peaks for monovalent functionalization have a higher intensity than those for bivalent functionalization. In contrast, the spectra representing ELRs with 10% peptide functionalization show different peak ratios, with the mono- and di-functionalization peaks showing higher intensity than the respective peaks for 5% functionalization. Moreover, additional peaks for tri- and tetravalent-functionalization of ELRs appear in the spectra for ELRs with 10% peptide functionalization.

P0

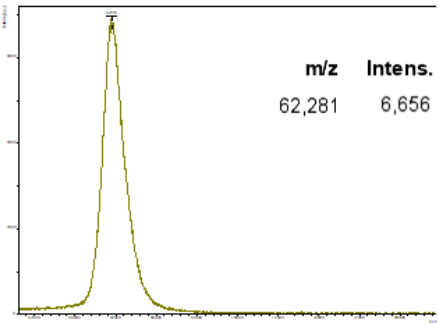
m/z Intens.
62,281 6,656

P2a

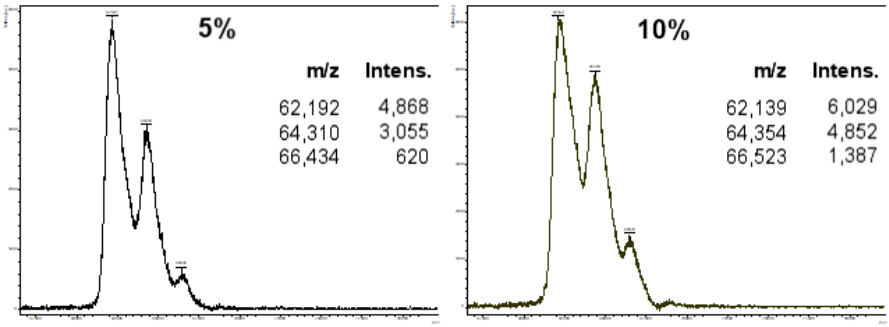
5%
m/z Intens.
62,192 4,868
64,310 3,055
66,434 620
10%
m/z Intens.
62,139 6,029
64,354 4,852
66,523 1,387

P3b

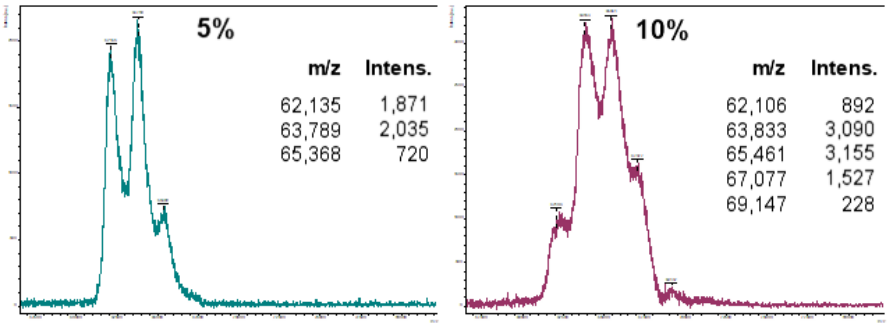
5%
m/z Intens.
62,135 1,871
63,789 2,035
65,368 720
10%
m/z Intens.
62,106 892
63,833 3,090
65,461 3,155
67,077 1,527
69,147 228

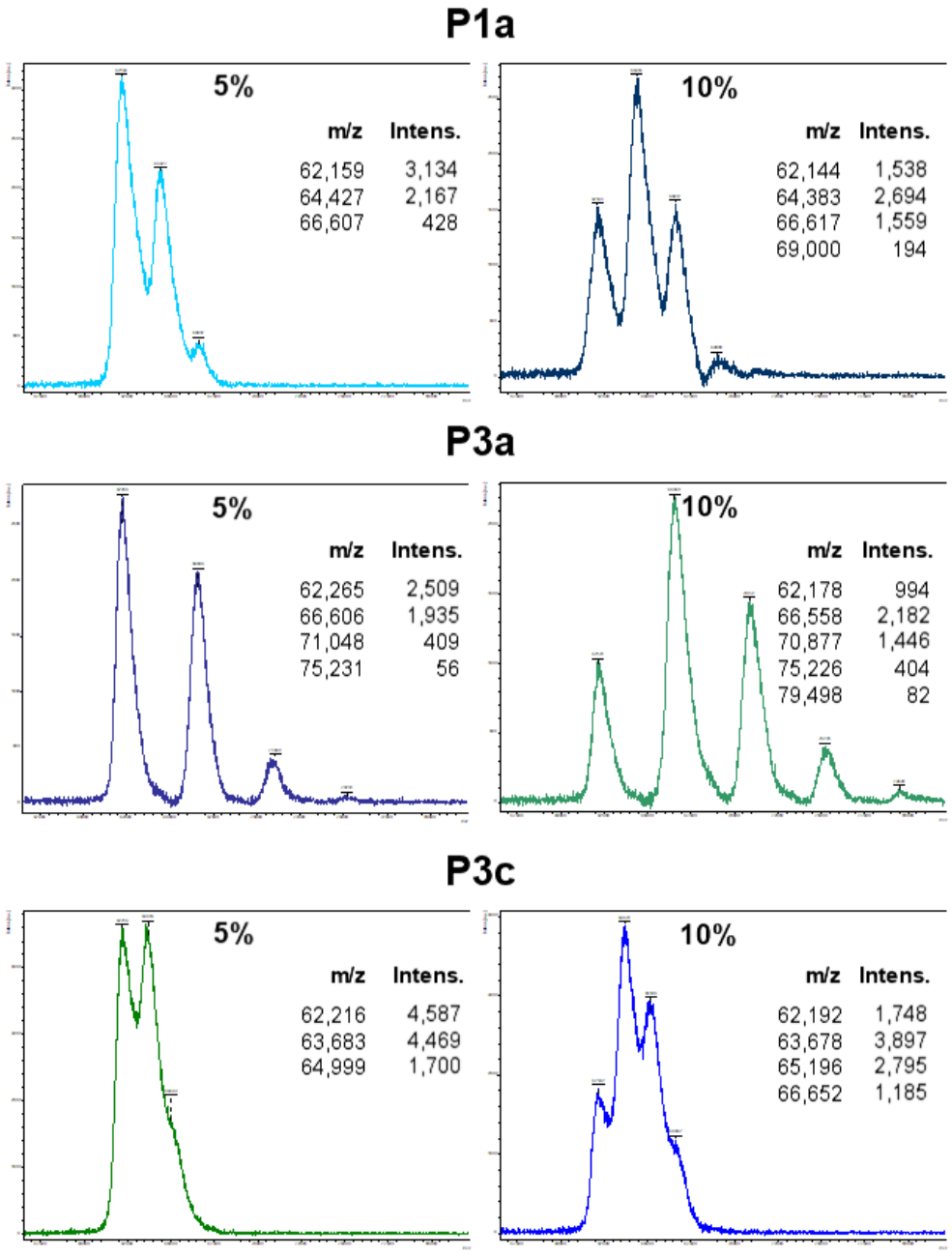

Figure 2. MALDI-TOF MS spectra for non-functionalized ELR and ELRs functionalized with 5%/10% of bicyclic RGD peptides **1a**, **2a** and control RGD peptides **3a–c**.

3.3. Analysis of turbidity by UV/Vis-spectroscopy

A turbidity study was performed for all the functionalized ELRs. In all the cases, a slight shift in T_t to lower values was observed as compared to the non-functionalized ELR (VKV-N_3). The turbidity measurements are reported in the Supporting Information (Figures S9-S11).

3.4. Contact Angle

Static aqueous contact angle analysis was performed in order to verify the correct adsorption of ELRs and ELR-Peptides onto tissue culture polystyrene surfaces (TCPS). Measurements were taken using ultrapure water drops on four different surfaces: TCPS, VKV adsorbed on TCPS (VKV), VKV-N_3 adsorbed on TCPS (VKV-N_3), ELR bearing peptides adsorbed on TCPS (ELR-Peptide). The results (Figure 3) show that TCPS is moderately hydrophobic (Θ= 71.6° ± 0.5°), whereas VKV and VKV-N_3 are markedly hydrophilic (Θ= 24.2° ± 1.5° and Θ= 23.3° ± 3.3°, respectively). ELR-Peptides was the most hydrophilic (Θ= 15.6° ± 1.6°), with the difference with respect to VKV-N_3 being significant ($p < 0.0001$), thereby suggesting a hydrophilic contribution from the peptides. Measurements were repeated in different regions in order to confirm the homogeneous adsorption of ELRs and ELR-peptide onto TCPS.

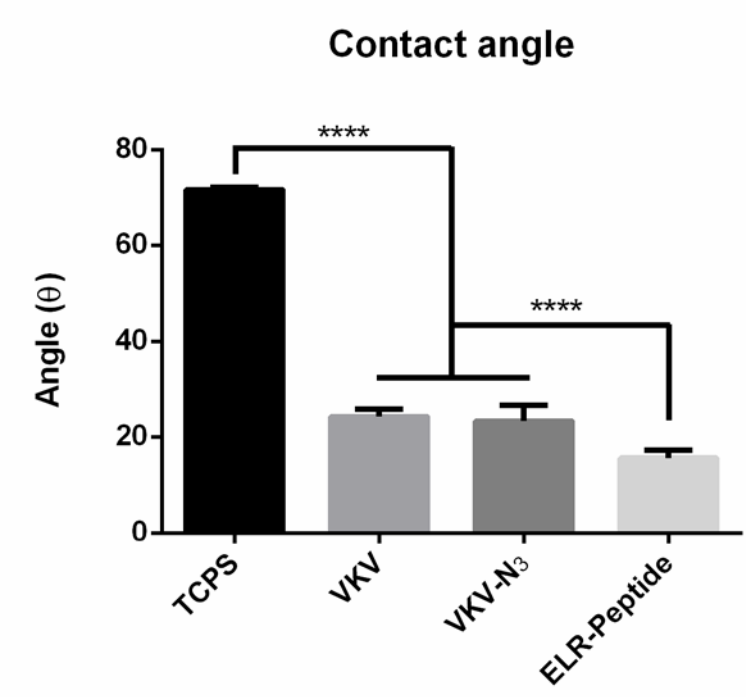

Figure 3. Contact angle analysis performed 5 s after application of the drops to the surfaces: TCPS; VKV adsorbed on TCPS (VKV); VKV-N_3 adsorbed on TCPS (VKV-N_3); ELR-bearing peptides adsorbed on TCPS (ELR-Peptide). (*P<0.05; **P<0.01; ***P<0.001; ****P<0.0001).

3.5. XPS

XPS was used to characterize the TCPS surface adsorbed with ELRs and ELR-Peptides. The surface compositional results from XPS analysis, shown in Table 3, indicate a reduction in C1s upon comparing untreated TCPS with VKV-N_3 adsorbed on TCPS (VKV-N_3) and ELR-bearing peptides adsorbed on TCPS (ELR-Peptide). XPS analysis also revealed a clear enrichment of nitrogen, passing from 0.8% for TCPS to 16.49% and 13.97%, respectively, for VKV-N_3 and ELR-Peptide. Finally, oxygen also exhibited a slight increase compared with the TCPS surface.

	C1s	N1s	O1s
TCPS	85.64 ± 1.82	0.74 ± 0.09	13.63 ± 1.73
VKV	68.69 ± 0.57	15.13 ± 0.28	16.18 ± 0.28
VKV-N_3	68.28 ± 1.29	15.71 ± 1.10	16.01 ± 0.20
ELR-Peptide	69.79 ± 0.20	14.33 ± 0.51	15.89 ± 0.32

Table 3. XPS analysis performed on different surfaces: TCPS; VKV adsorbed on TCPS (VKV); VKV-N_3 adsorbed on TCPS (VKV-N_3); ELR-bearing peptides adsorbed on TCPS (ELR-Peptide). All the measurements were performed in triplicate. Values are expressed in % (average ± st. dev).

3.6. Cell-adhesion assay

3.6.1. Time-dependent cell quantification studies

The capacity to promote cell adhesion and proliferation of HUVECs on the modified ELRs was evaluated at short, medium and long term. Figure 4 shows the time-dependent cell quantification for VKV-N_3 (**P0**) and ELRs functionalized with 5% (**P1a**) and 10% modification (**P1a-10**). The cell count for all time points (except after 14 d) show a significant difference upon comparing **P0** with **P1a** and **P1a-10**. However, no significant difference was observed between **P1a** and **P1a-10** at any time point. Similar behavior was found for the remaining ELR-peptides (Supporting Information, Figure S7), and the various high-affinity integrin-binding peptides used in this study did not show any difference for the two concentrations used. As such, we decided to analyze the results for ELR-peptides functionalized at 5% (Figures 5–7).

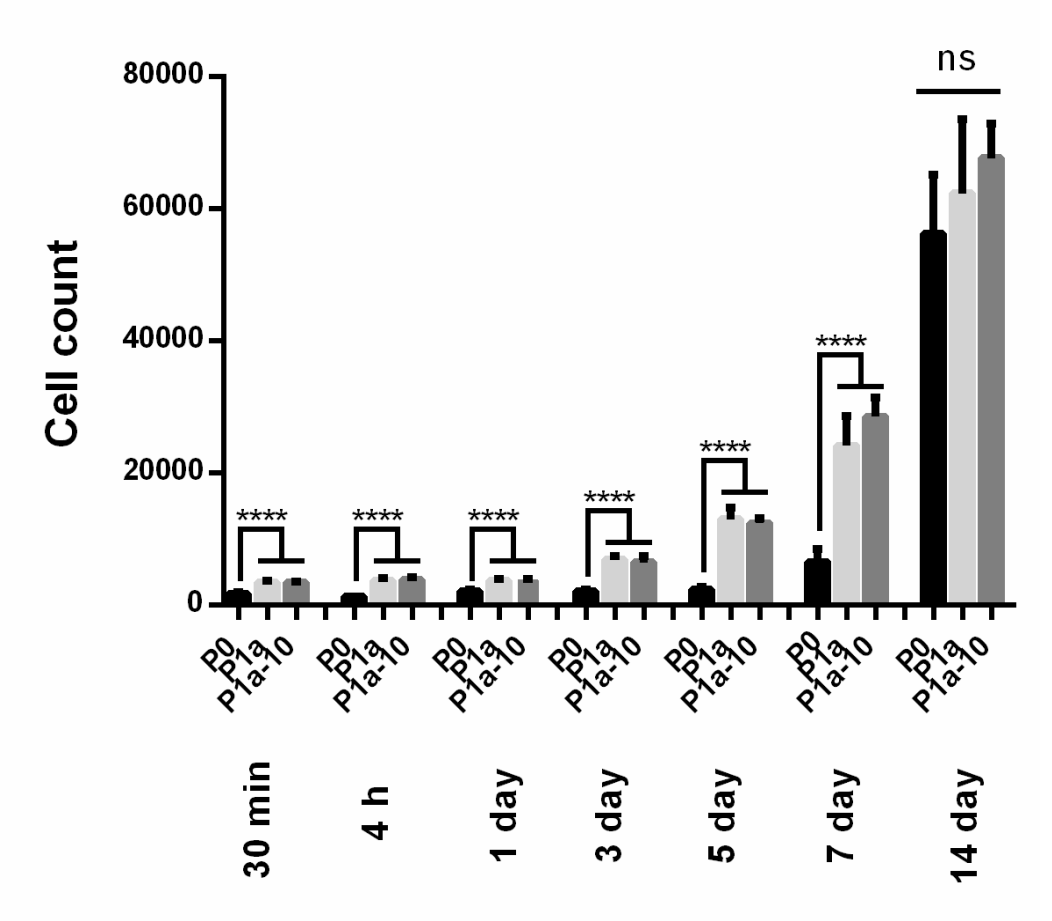

Figure 4. Time-dependent cell quantification for VKV-N_3 (**P0**), P1a 5% (**P1a**) and P1a 10% (**P1a-10**) at different time points (30 min, 4 h, 1 d, 3 d, 5 d, 7 d, 14 d). All experiments were carried out in triplicate and error bars show standard deviations (*P<0.05; **P<0.01; ***P<0.001; ****P<0.0001). There was no statistically significant difference between **P1a** and **P1a-10** at any time point.

All the PicoGreen® data collected were subdivided into different groups based on the different time points: short-term (30 min, 4 h, 1 d; Figure 5), medium-term (3 d, 5 d; Figure 6) and long-term (7 d, 14 d; Figure 7). In order to make the bar charts clearer, the ELR-Peptides have been arranged and clustered into different groups: ELRs functionalized with $\alpha_v\beta_3$-binding bicycle peptides **1a–c** (red bars); ELRs functionalized with $\alpha_v\beta_3$ and $\alpha_5\beta_1$-binding bicyclic peptides **2a–c** (green bars); and benchmark RGD peptides **3a–c** (blue bars). The grey scale bars represent other controls, namely the RGD in the ELR-backbone (**P0-RGD**), ELR with no RGD peptide (**P0**), fibronectin coating (**P0-FN**) and coating with BSA (**P0-BSA**). The positive (**P0-FN**) and negative controls (**P0-BSA**) remained between the highest and lowest, respectively, thus confirming the reliability of the study.

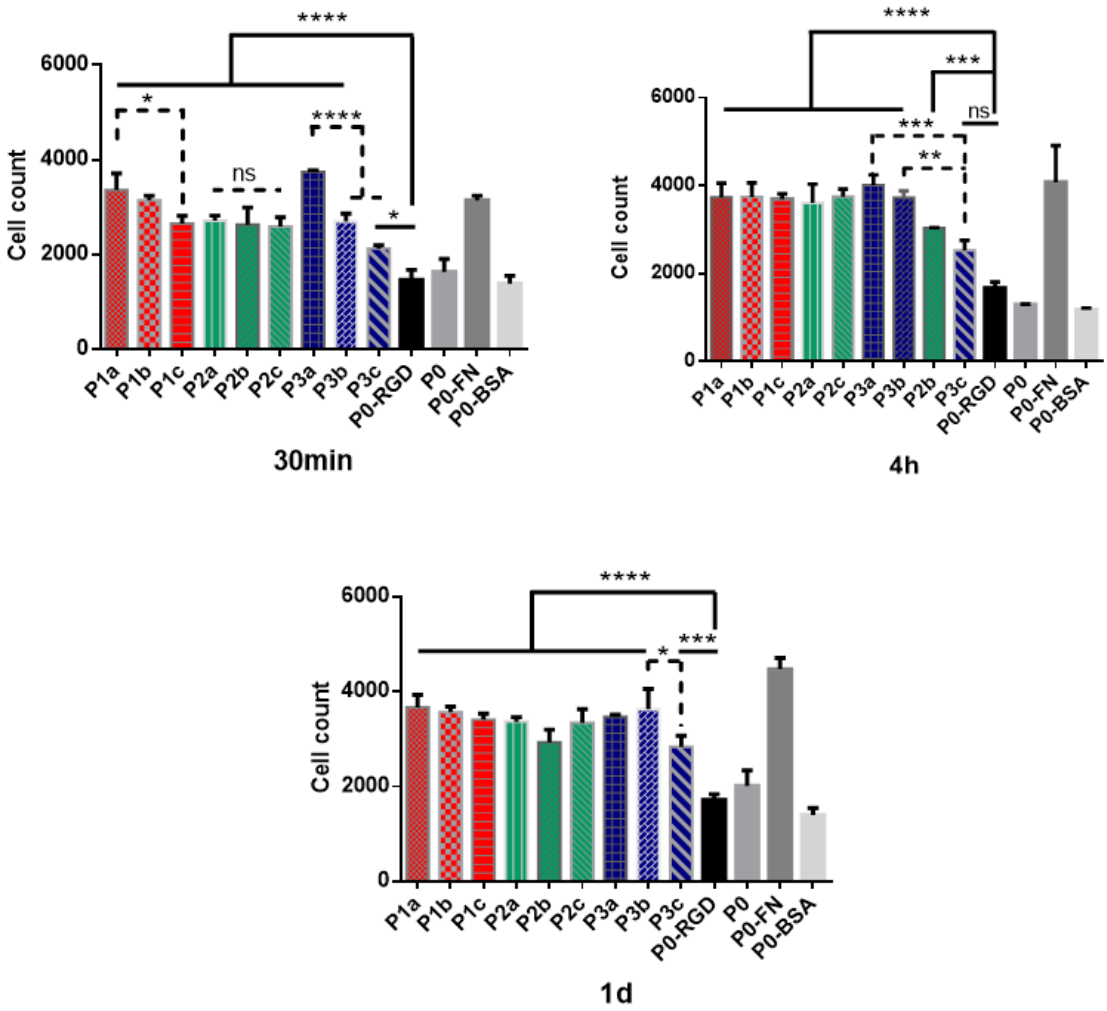

Figure 5. Short-term time-dependent cell quantification (30 min, 4 h, 1 d). Number of cells determined for ELRs containing bicyclic peptides **1a–c** (red bars) and **2a–c** (green bars), and control RGD peptides **3a–c** (blue bars), RGD in the ELR-backbone (**P0-RGD**), ELR with no RGD peptide (**P0**), fibronectin coating (**P0-FN**) and coating with BSA (**P0-BSA**). The amount of cells was calculated from fluorescence intensities using a calibration curve. All experiments were carried out in triplicate and error bars show standard deviations. (*P<0.05; **P<0.01; ***P<0.001; ****P<0.0001).

For the short-term study (30min, 4h, 1 d; Figure 5), the peptides included after click modification supported higher levels of cells than the recombinant ELR-RGD (**P0-RGD**). At 30 min all the ELR-Peptides, except for **P3c**, showed the maximum statistical difference with **P0-RGD**. The differences in cell numbers remained high for almost all ELR-Peptides when compared with the **P0-RGD** for the whole short-term study. In contrast, no significant difference was observed between the recombinant ELR-RGD (**P0-RGD**) and the

ELRs lacking RGD (**P0**). The second comparison (indicated by a dashed line) shows the differences between the ELR-Peptide groups, in other words bicyclic peptides **1a–c** (red bars), **2a–c** (green bars), and control RGD peptides **3a–c** (blue bars). Essentially no significant differences were found between the bicyclic peptide groups, with the only exception being for the group of non-selective RGD-peptides (**3a-c**), for which a greater variability and significance were evident. The ELR functionalized with **3a** supported cell adhesion most efficiently within this group, with cell counts similar to those for ELRs functionalized with integrin-selective bicycles (**1a-c** and **2a-c**), whereas **3c** showed the lowest number of cells among the covalently functionalized ELRs at this time point, albeit still higher than for **P0-RGD**.

The data collected at 4 h are similar to those obtained at 30 min, with all ELR-Peptides except **P3c** showing the same statistical difference with respect to **P0-RGD**. The inter-group comparisons were in accordance with the trend observed at 30 min, with the bicyclic peptide groups **1a–c** (red bars), **2a–c** (green bars) showing no significant differences except for the group of non-selective RGD-Peptides (**3a-c**).

After 1 day, the differences between groups tended to decrease further, although the previous trends were maintained. A slight increase in cell counts at this time point suggests an incipient proliferation, although this is not particularly pronounced at this cell stage.

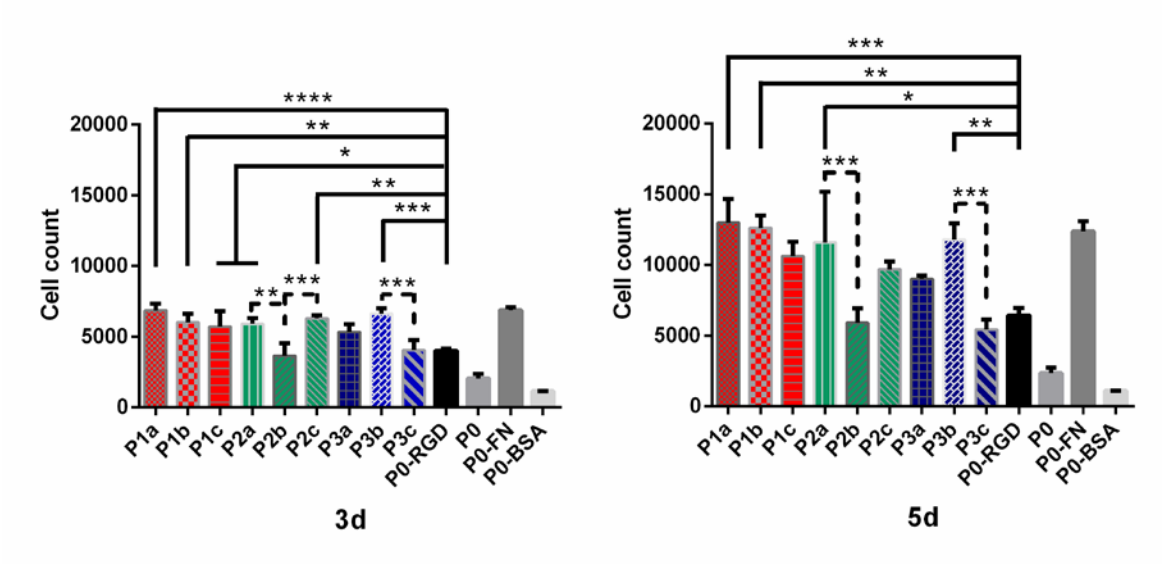

Figure 6. Medium-term time-dependent cell quantification (3 d, 5 d). Number of cells determined for ELRs containing bicyclic peptides **1a–c** (red bars) and **2a–c** (green bars), and control RGD peptides **3a–c** (blue bars), RGD in the ELR-backbone (**P0-RGD**), ELR with no RGD peptide (P0), fibronectin coating (**P0-FN**) and coating with BSA (**P0-BSA**). The number of cells was calculated from fluorescence intensities using a calibration curve. All experiments were carried out in triplicate and error bars show standard deviations. (*P<0.05; **P<0.01; ***P<0.001; ****P<0.0001).

In the medium-term study (3 d, 5 d; Figure 6), the number of cells practically doubled for almost all conditions, with a similar trend as for the initial adhesion, although with some exceptions. However, the comparison between the ELR-Peptides and **P0-RGD** appears less clear than for the short-term culture. Thus, despite showing good initial adhesion, **P2b** proliferation on slowed down over longer time periods. In contrast, the difference between **P0-RGD** and **P0** became more evident. A comparison within the same group revealed statistically significant differences only for **P2a-c** and **P3b - P3c** at day 3, and **P2a - P2b** and **P3b - P3c** at day 5.

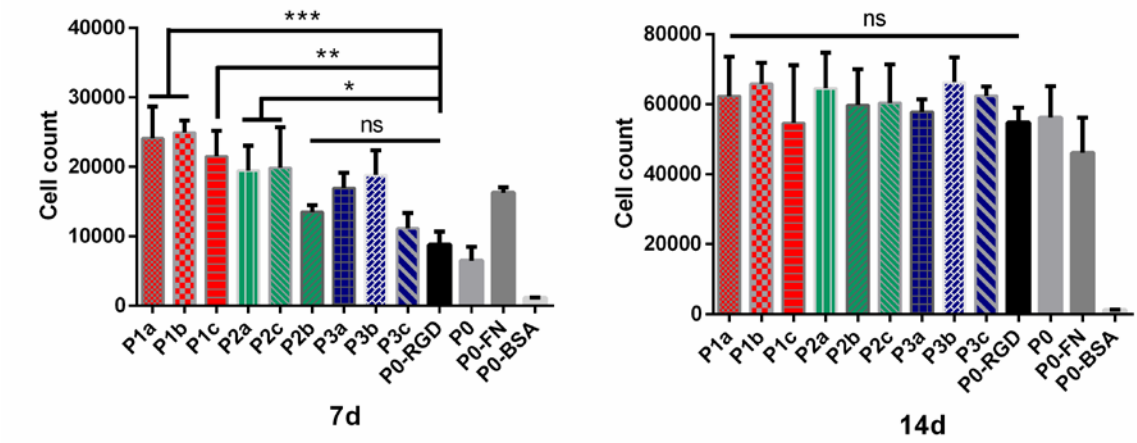

Figure 7. Long-term time-dependent cell quantification (7 d, 14 d). Number of cells determined for ELRs containing bicyclic peptides **1a–c** (red bars) and **2a–c** (green bars), and control RGD peptides **3a–c** (blue bars), RGD in the ELR-backbone (**P0-RGD**), ELR with no RGD peptide (**P0**), fibronectin coating (**P0-FN**) and coating with BSA (**P0-BSA**). The number of cells was calculated from fluorescence intensities using a calibration curve. All experiments were carried out in triplicate and error bars show standard deviations. (*P<0.05; **P<0.01; ***P<0.001; ****P<0.0001).

Long-term proliferation studies (7 d, 14 d) revealed that HUVEC growth tends to reduce the difference in the ability to promote cell adhesion by the various high-affinity integrin-binding peptides (Figure 7). Thus, after 7 days almost all the bicyclic peptides, i.e. **P1a-c**, **P2a** and **P2c**, showed a significant difference compared with **P0-RGD**, whereas **P3a-c** and **P2b** exhibited no clear difference. No significant difference was found within ELR-Peptide groups. Finally, after 14 days all conditions except the negative control **P0-BSA** exhibited similar amounts of cells. Indeed, cell counts after 14 days were approximately threefold higher that after culture for 7 days under all conditions.

3.6.2. Morphology studies

The ELR-Peptides were also characterized by morphological *in vitro* studies to investigate cell attachment, cell spreading, cytoskeletal reorganization and formation of focal adhesions. In order to investigate the time-dependent morphology of the cells, they were stained with rhodamin/phalloidin (actin skeleton), DAPI (nuclei) and a fluorescent mAb (vinculin) and examined by fluorescence microscopy (Figures 8 and 9).

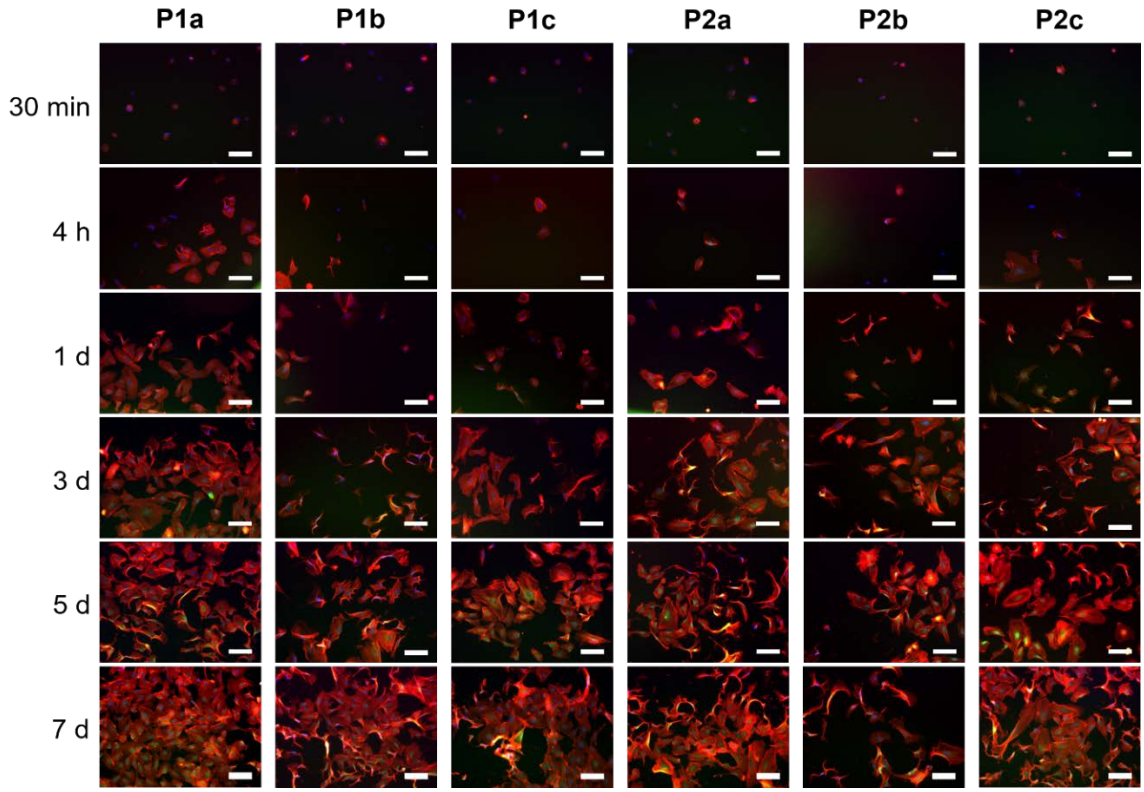

Figure 8. Immunostaining of actin (red), vinculin (green), and nuclei with DAPI (blue) of HUVEC cells cultured for different time points (30 min, 4 h, 1 d, 3 d, 5 d, 7 d) on ELRs functionalized with bicycles 1a–c **(P1a-c)** and 2a–c **(P2a-c)**. Scale bars: 100 µm.

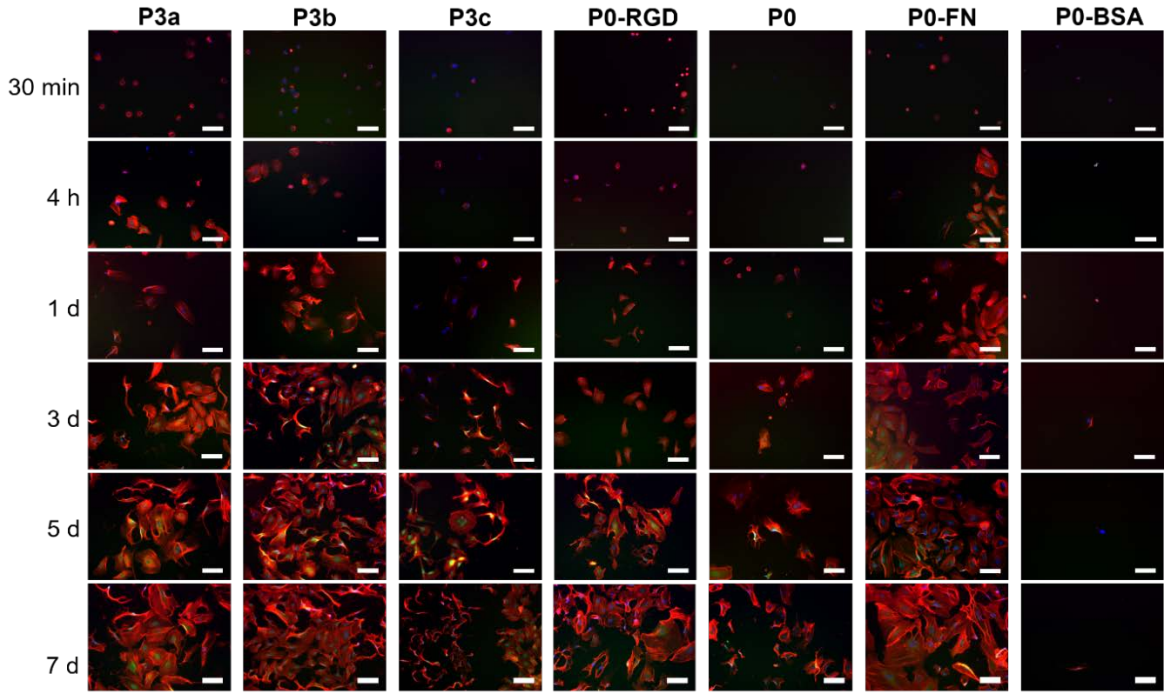

Figure 9. Immunostaining of actin (red), vinculin (green), and nuclei with DAPI (blue) of HUVEC cells cultured for different time points (30 min, 4 h, 1 d, 3 d, 5 d, 7 d) on ELRs functionalized with controls 3a–c **(P3a-c)**, and comprising RGD in the ELR-backbone **(P0-RGD)**, no RGD peptide **(P0)**, fibronectin coating **(P0-FN)** and coating with BSA **(P0-BSA)**. Scale bars: 100 µm.

Since non-adhered cells were discarded after seeding for 30 minutes, those that remained adhered, although small and spherically shaped, nevertheless showed small protrusions at the periphery or ring-shaped adhesions at the onset of cell culture (30 min) under practically all conditions tested (Supporting Information, Figure S8). At early time points, the focal contacts are circumscribed to the perinuclear zone, whereas at longer times a yellow coloration was found when overlapping actin and vinculin captures.

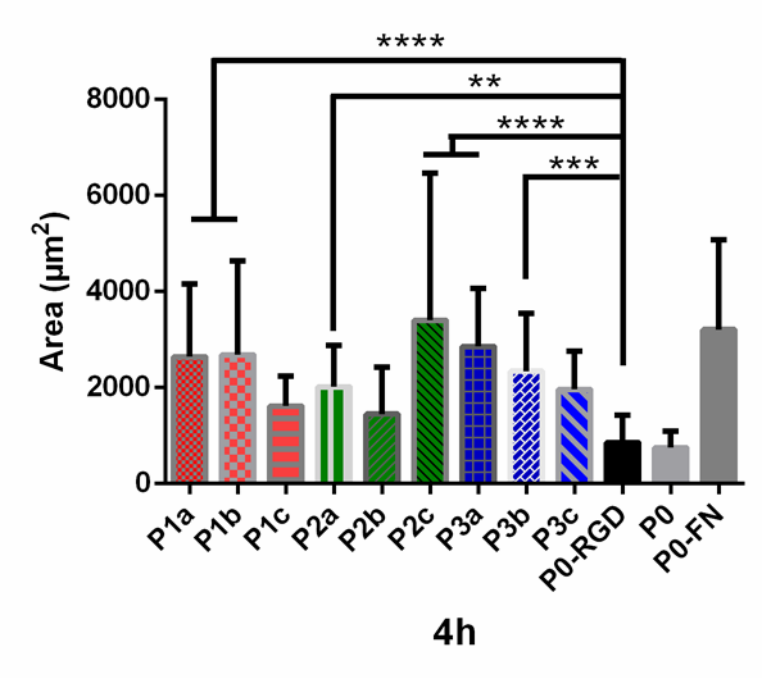

Figure 10. Quantitative image analysis of cell spreading area after 4 h. Cell area has been determined for ELRs containing bicyclic peptides **1a–c** (red bars) and **2a–c** (green bars), and control RGD peptides **3a–c** (blue bars), RGD in the ELR-backbone (**P0-RGD**), ELR with no RGD peptide (**P0**) and fibronectin coating (**P0-FN**). A minimum of 25 images have been analyzed per sample, except for **P1c**, **P2b**, **P3b-c** and **P0** where the number of images were less than 25 but in any case more than 10. The results correspond to a single independent experiment. The values are is expressed μm^2; the error bars show standard deviations. (*P<0.05; **P<0.01; ***P<0.001; ****P<0.0001).

The quantitative image analysis of cell spreading area has been performed after short time incubation (4 h) (Figure 10). **P1a-b**, **P2c** and **P3a** showed the highest statistical difference as compared with **P0-RGD**, whereas the difference between **P3b** and **P2a** was less significant. All the remaining ELR-Peptides (**P1c**, **P2b** and **P3c)** did not exhibit significantly different cell spreading as compared with **P0-RGD**. In any cases, no significant differences were found within the same peptide group. **P2b** showed the largest error bars, reflecting the vast population of cells having a different spreading area (Figure 10). In contrast, the negative control **P0-BSA** does not appear since no cells were present, (Figure 9). The data collected by quantitative image analysis after 4 h are similar to those obtained by cell quantification analysis reported in Figure 5. In both analyses, **P2b** and **P3c** showed less difference as compared with **P0-RGD**. With respect to the cell spreading area analysis,

also **P3b** and **P2a** showed a less significant difference compared to **P0-RGD,** whereas for **P1c** no significant differences were found. When comparing cell spreading areas on ELRs within the same group, the trends observed were in accordance with cell quantification analysis, where no significant differences were shown, except for the group of non-selective RGD-Peptides (**3a-c**).

4. DISCUSSION

The focus of biomaterials research often lies with the biomaterial itself rather than the cell-adhesion sequence (51), especially given that the surface-protein interaction determines the nature of subsequent cell-surface behavior. Herein we have created peptide-functionalized ELRs by conjugating various high-affinity integrin-binding, bicyclic RGD-Peptides to ELRs via copper-free click chemistry in order to overcome the known limitations of recombinant synthesis; for instance, the inability to incorporate non-canonical amino acids and to form cyclized peptides. Furthermore, this strategy allows the bioactive ligand to maintain the flexibility and minimal steric hindrance required for cellular interactions. The purpose of this study was to improve the cell-adhesion and proliferation abilities of the recombinant and biocompatible substrate ELRs by conjugating a very small number (one or two molecules per ELR) of high integrin affinity peptides. The choice of the different conditions and peptides was based on very recent studies by Bernhagen *et al*., who reported an exhaustive investigation of high-affinity integrin $\alpha_v\beta_3$- and $\alpha_5\beta_1$-binding bicyclic RGD-Peptides (42, 43). Remarkably, in the same studies the researchers also found that linear GRGDS (non-functionalized version of **3c**), which is probably the most common cell-adhesive ligand in hydrogels, showed relatively low integrin $\alpha_v\beta_3$ and $\alpha_5\beta_1$ affinity, whereas the monocyclic peptide *cyclo*-KRGDf (non-functionalized equivalent to **3b**) showed a high affinity for integrins $\alpha_v\beta_3$ and $\alpha_5\beta_1$. Similarly, the 32-mer knottin-RGD peptide (origin of **3a**) published by Kimura *et al.* (52) non-selectively bound all integrins $\alpha_v\beta_3$, $\alpha_v\beta_5$ and $\alpha_5\beta_1$ with high affinity. Finally, a battery of nine RGD-Peptides was successfully synthesized and conjugated with cyclooctyne using an approach in which the integrin-binding sequence was coupled to a peptide linker. Moreover, and discussed above, the solubility in water-based solvents was improved by the inclusion of additional serine residues. All the cyclooctyne-functionalized peptides

were conjugated to ELR azides via copper-free click chemistry. Functionalization was carried out as a mono-functionalization (5%) and di-functionalization (10%), and the ELR-Peptides were further analyzed by MALDI-TOF MS. Although MALDI-TOF MS analysis does not allow the degree of functionalization to be determined quantitatively, a comparison of the spectra in Figure 2 reveals different degrees of functionalization depending on the type and amount of peptide applied, thus confirming the successful conjugation of two different quantities of peptides on the ELRs. Furthermore, a turbidity study was performed for all the functionalized ELRs, with a slight shift in T_t to lower values beings observed for all ELR-Peptides in comparison with the non-functionalized ELR. This essentially negligible T_t shift is likely due to the very small quantity of peptide molecules conjugated to the ELRs (one molecule for 5% functionalization and two molecules for 10% functionalization) and to the low molecular weight of the peptides. These data show how this functionalization strategy does not affect the physical properties of the ELR, represented by the T_t value (Supporting Information, Figures S9-S11).

The ELRs comprising 5% or 10% peptide functionalization were adsorbed onto TCPS in order to further investigate the cell adhesion behavior and proliferation over these surfaces. XPS and CA analysis were used to confirm the correct adsorption. Thus, XPS analysis revealed a change in the surface composition, as can be seen from Table 3 for ELRs and ELR-Peptides, with a clear enrichment in nitrogen and a reduction in carbon, and oxygen increasing slightly compared with the TCPS surface. These changes in chemical composition confirm an adequate adsorption of ELRs and ELR-Peptides onto TCPS (53-55). CA measurements help to characterize the affinity of a solution or suspension towards a certain surface, with the CA value decreasing as the number and strength of these interactions increases. The adsorption of ELRs onto the surface increases the hydrophilicity with respect to TCPS and, given the XPS results, this is likely due to the enrichment in electronegative atoms like nitrogen and oxygen and to the reduction in carbon. This enrichment in electronegative atoms increases the number and strength of interactions, such as hydrogen bonds, with the aqueous solution. Surprisingly, the ELR containing peptides adsorbed on TCPS was the most hydrophilic surface, with the difference with respect to the other ELRs being significant. This suggests a hydrophilic contribution from the peptides, which likely expose their electronegative atoms

outwards, thereby increasing the number and strength of interactions with the aqueous solution. As reported previously, the hydrophilicity of a solid surface is an essential requirement for cell-surface interactions (56) and, in this case, combines with a correct exposure of RGD peptide sequences.

HUVECs were chosen to investigate the cell adhesion behavior, proliferation and morphology by culture thereof on ELR and ELR-Peptide adsorbed surfaces. Endothelial cells form part of a highly specialized tissue for vessel formation that provides stable structural support for new vessels. Endothelial cells cover the blood vessels and are metabolically very active, being responsible for maintaining vascular homeostasis. In this study we have synthesized a battery of nine peptides, which can be sub-divided into groups of three with high affinity for $\alpha_v\beta_3$, $\alpha_5\beta_1/\alpha_v\beta_3$, and multiple integrins (Table 1). According to the literature, the remodeling of blood vessels and concomitant reorganization of the cytoskeleton requires the involvement of integrins (57). In mammals, this family of integrins comprises at least 20 different αβ heterodimers, which are expressed on the surface of endothelial cells (57). Different combinations of integrin subunits on the cell surface allow cells to recognize and respond to a variety of extracellular matrix proteins under different physiological conditions; for example, the $\alpha_v\beta_1$ and $\alpha_5\beta_1$ fibronectin receptors are highly expressed in quiescent endothelial cells, whereas the $\alpha_v\beta_3$ fibronectin and vitronectin receptor is expressed only during angiogenesis (57, 58). Herein we have evaluated either the functional avidity or proliferation of HUVECs on ELR and ELR-peptide adsorbed surfaces. Loosely adhered or unbound cells were removed from the surfaces after incubation for 30 min in order to determine the cell fate as a function of the extent of initial attachment to the different surfaces and, therefore, the avidity of the cells for the adhesion sequences exposed.

The adhesion behavior was investigated in a short-term study (up to 1 day, Figure 5), which revealed that ELR-bearing peptides supported higher levels of cells than the recombinant ELR-RGD. This difference involves either the bicyclic peptides **1a–c** or **2a–c**, each of which exhibits high-affinity for $\alpha_v\beta_3$ and $\alpha_5\beta_1/\alpha_v\beta_3$ integrins, or the control RGD peptides, which exhibit high affinity for multiple integrins **3a–c**. It should be noted that the backbone-RGD functionalized ELR (**P0-RGD**) comprises six RGD motifs per molecule, while the covalently functionalized ELR-Peptides only comprise one RGD moiety per

molecule. This suggests either a higher adhesion capacity for the high-affinity integrin-binding peptides to HUVECs or a better exposure of these peptides after protein adsorption. It is well known from the literature that cell attachment is influenced by several factors, one of the most important of which is the RGD concentration (59-61). By creating RGD-Peptides functionalized via copper-free click chemistry, we have improved the cell attachment capacity while reducing the RGD concentration on the surface, although the RGD-concentration function varies for each different bioactive surface and cell line (62, 63).

Surprisingly, the adhesion and proliferation results for the different high-affinity integrin-binding peptides used in this study showed no difference when compared with the same ELR-Peptide for the two concentrations selected. This identical behavior for ELRs having 5% and 10% peptide functionalization is likely due to the similar and very low number of peptide molecules (one and two molecules for 5% and 10%, respectively) on the ELR substrate. In contrast, the presence of RGD in the backbone (**P0-RGD**) did not affect the adhesion behavior of cells in the short-term culture when compared with the ELR lacking RGD (**P0**). This could be related to the adsorption process of ELR-RGD molecules, which may have not allowed an optimal outwards exposure of the RGD sequence. Overall, the short-term results demonstrate a greater avidity of the cells for the bicycle-functionalized ELRs. According to the cell adhesion and proliferation results obtained for ELR-Peptides functionalized at 5%, the differences observed in the short-term cultures could be explained by considering that signal transduction after interaction with a specific integrin can trigger different or preferential cellular responses (proliferation, migration and/or organization into networks characteristic of early angiogenesis, for example). A comparison within the same groups of ELR-Peptides also revealed clear differences for various peptides at certain time points. However, these differences do not follow a trend as they arise due to the design and synthesis of the different peptides which, although they have the same composition, exhibit different affinities for the integrins expressed on the HUVEC membrane. The PicoGreen® study is in accordance with the morphological study, whereby the focal contacts, which are initially circumscribed to the perinuclear zone, give way to vinculin clustering of activated integrins, as can be inferred from the yellow coloration found when overlapping actin and vinculin captures. In addition, these

were numerous and not restricted to the nuclear periphery. The morphological study reveals that short-term capability to support cell adhesion is higher for the surface adsorbed with bicycle-functionalized ELRs than for all the other benchmarks. Moreover, the cell spreading area at a short time incubation (4 h) followed the same trend of cell adhesion, suggesting that bicyclic RGD peptides support cell adhesion and cell cytoskeleton.

The differences in cell numbers were highest in the short-time study for almost all the peptide-bearing ELRs when compared with the recombinant ELR-RGD**.** However, a comparison between the ELR-Peptides and ELR-RGD showed much smaller differences in the long term, with HUVEC growth tending to minimize the initial difference in the ability to promote cell adhesion by the various high-affinity integrin-binding peptides. Differences within the same groups of ELR-Peptides were also relatively small. Intercellular contacts between HUVECs inhibit their proliferation and growth stops. A possible explanation for the similar cell numbers in long-term cultures (7 d, 14 d, Figure 7) is that the rapid proliferation corresponds to the earlier confluence with respect to the cells that do not exhibit intercellular contacts. However, in contrast to the group of non-selective RGD-Peptides, which exhibit high affinity for multiple integrins, almost all the bicyclic peptides exhibited the highest proliferation data at longer times, showing a significant difference with respect to ELR-RGD. The cell quantification data show that essentially similar proliferation rates were observed for the bicyclic peptides optimized for both $\alpha_v\beta_3$ and $\alpha_5\beta_1$ affinity/selectivity, thus enabling either active or quiescent HUVECs to be targeted. The morphological study shows how the surfaces that have performed a better adhesion at short times, are those where the cells exhibit more expanded and less sharped morphology at longer times. Given that a similar situation is found for cells cultured on fibronectin (positive control), the peptide-bearing ELRs appear to be a better substrate for cell stretching compared with the recombinant-synthesized ELR-RGD (**P0-RGD**) and ELR itself (**P0**). However, these differences became less apparent as cell cultures were maintained for longer periods, probably as a result of the analysis chosen for this cell type.

In the light of these results, the various high-affinity integrin-binding peptides used in this study appear to play an important role, especially during short-term culture. RGD Peptide-

functionalized ELRs enhance the ability to promote cell adhesion compared with recombinant-synthesized ELR-RGD, irrespective of the lower net RGD concentration of covalently functionalized ELRs. Moreover, taking into account the limitations of *in vitro* culture, an *in vivo* study would be required to determine whether active HUVECs involved in angiogenesis could be selectively targeted with bicycle-functionalized ELRs optimized for high $\alpha_v\beta_3$ integrin affinity (**P1a**-**P1c**). Similarly, bicycle-functionalized ELRs optimized for $\alpha_5\beta_1$ affinity (**P2a**-**P2c**) could exhibit a specific interaction with endothelial cells in a quiescent state. Finally, we have opened up a new application for ELRs as a biocompatible substrate in studies to determine which integrins need to be targeted for optimal cell adhesion and proliferation.

5. CONCLUSIONS

The *in vitro* studies of ELRs functionalized with high-affinity integrin $\alpha_v\beta_3$- and $\alpha_5\beta_1$-binding RGD bicycles suggest that these bicycles provide an interesting alternative to promote fast cell adhesion on 2D biomaterial surfaces compared with well-known linear or monocyclic RGD peptides. Our initial hypothesis that high-affinity integrin-binding RGD bicycles, as determined in solid-phase immunoassays (43), should improve integrin-mediated cell adhesion and proliferation to a significantly greater extent than monocyclic and linear RGD was partially verified. Furthermore, we have shown that covalent RGD-functionalization of ELRs via copper-free click reaction is more efficient for inducing integrin-mediated cell adhesion and proliferation than the recombinant synthesis of ELRs comprising RGD as part of their backbone. This strategy could be used to ensure correct exposure of the bioactive sequence, thereby guaranteeing an optimal cell-material interaction. Finally, we believe that ELRs functionalized with integrin-selective RGD-bicycles represent an attractive and efficient way to design integrin-selective polymer surfaces with the potential to evaluate cell-adhesion behavior and tailor high integrin peptides for specific biomedical applications.

Notes

Pepscan is the inventor of the CLIPS technology and holds a patent on the synthesis of bicyclic peptides using this technique.

Acknowledgments

The authors are grateful for the funding from the European Commission (NMP-2014-646075, MSCA-ITN-2014-ETN-642687), MINECO of the Spanish Government (PCIN-2015-010, MAT2015-68901-R, MAT2016-78903-R), Junta de Castilla y León (VA015U16) and Centro en Red de Medicina Regenerativa y Terapia Celular de Castilla y León.

References

1. Liu, J.C. and D.A. Tirrell, Cell Response to RGD Density in Cross-Linked Artificial Extracellular Matrix Protein Films. Biomacromolecules, 2008. 9(11): p. 2984-2988.

2. Sagnella, S.M., et al., Human microvascular endothelial cell growth and migration on biomimetic surfactant polymers. Biomaterials, 2004. 25(7-8): p. 1249-1259.

3. Eid, K., et al., Effect of RGD coating on osteocompatibility of PLGA-polymer disks in a rat tibial wound. J Biomed Mater Res, 2001. 57(2): p. 224-31.

4. Fong, E., S. Tzlil, and D.A. Tirrell, Boundary crossing in epithelial wound healing. Proceedings of the National Academy of Sciences, 2010. 107(45): p. 19302-19307.

5. Waite, C.L. and C.M. Roth, Binding and transport of PAMAM-RGD in a tumor spheroid model: the effect of RGD targeting ligand density. Biotechnol Bioeng, 2011. 108(12): p. 2999-3008.

6. Rasal, R.M., A.V. Janorkar, and D.E. Hirt, Poly(lactic acid) modifications. Progress in Polymer Science, 2010. 35(3): p. 338-356.

7. Wong, L.S., F. Khan, and J. Micklefield, Selective Covalent Protein Immobilization: Strategies and Applications. Chemical Reviews, 2009. 109(9): p. 4025-4053.

8. Desmet, T., et al., Nonthermal Plasma Technology as a Versatile Strategy for Polymeric Biomaterials Surface Modification: A Review. Biomacromolecules, 2009. 10(9): p. 2351-2378.

9. Punet, X., et al., Enhanced cell-material interactions through the biofunctionalization of polymeric surfaces with engineered peptides. Biomacromolecules, 2013. 14(8): p. 2690-702.

10. R., T., Surface functionalization of materials to initiate auto-biocompatibilization in vivo. Materialwissenschaft und Werkstofftechnik, 2001. 32(12): p. 949-952.

11. Leslie-Barbick, J.E., et al., The promotion of microvasculature formation in poly(ethylene glycol) diacrylate hydrogels by an immobilized VEGF-mimetic peptide. Biomaterials, 2011. 32(25): p. 5782-9.

12. Santulli, G., et al., In vivo properties of the proangiogenic peptide QK. Journal of Translational Medicine, 2009. 7: p. 41-41.

13. Yoshihiro, I., K. Masako, and I. Yukio, Materials for enhancing cell adhesion by immobilization of cell-adhesive peptide. Journal of Biomedical Materials Research, 1991. 25(11): p. 1325-1337.

14. Boxus, T., et al., Synthesis and evaluation of RGD peptidomimetics aimed at surface bioderivatization of polymer substrates. Bioorganic & Medicinal Chemistry, 1998. 6(9): p. 1577-1595.

15. Grob, N.M., et al., Methoxinine - an alternative stable amino acid substitute for oxidation-sensitive methionine in radiolabelled peptide conjugates. J Pept Sci, 2017. 23(1): p. 38-44.

16. Kaufmann, D., et al., Chemical conjugation of linear and cyclic RGD moieties to a recombinant elastin-mimetic polypeptide--a versatile approach towards bioactive protein hydrogels. Macromol Biosci, 2008. 8(6): p. 577-88.

17. Rodríguez Cabello, J.C., et al., 12 - Elastin-like materials for tissue regeneration and repair A2 - Barbosa, Mário A, in Peptides and Proteins as Biomaterials for Tissue Regeneration and Repair, M.C.L. Martins, Editor. 2018, Woodhead Publishing. p. 309-327.

18. Nettles, D.L., A. Chilkoti, and L.A. Setton, Applications of elastin-like polypeptides in tissue engineering. Adv Drug Deliv Rev, 2010. 62(15): p. 1479-85.

19. Carlos Rodríguez-Cabello, J., et al., Developing functionality in elastin-like polymers by increasing their molecular complexity: the power of the genetic engineering approach. Progress in Polymer Science, 2005. 30(11): p. 1119-1145.

20. Desai, M.S. and S.W. Lee, Protein-based functional nanomaterial design for bioengineering applications. Wiley Interdiscip Rev Nanomed Nanobiotechnol, 2015. 7(1): p. 69-97.

21. Trabbic-Carlson, K., L.A. Setton, and A. Chilkoti, Swelling and Mechanical Behaviors of Chemically Cross-Linked Hydrogels of Elastin-like Polypeptides. Biomacromolecules, 2003. 4(3): p. 572-580.

22. Desai, M.S., et al., Elastin-Based Rubber-Like Hydrogels. Biomacromolecules, 2016. 17(7): p. 2409-2416.

23. McDaniel, J.R., D.C. Radford, and A. Chilkoti, A unified model for de novo design of elastin-like polypeptides with tunable inverse transition temperatures. Biomacromolecules, 2013. 14(8): p. 2866-2872.

24. Meyer, D.E. and A. Chilkoti, Purification of recombinant proteins by fusion with thermally-responsive polypeptides. Nat Biotechnol, 1999. 17(11): p. 1112-5.

25. Almine, J.F., et al., Elastin-based materials. Chemical Society Reviews, 2010. 39(9): p. 3371-3379.

26. Rodríguez-Cabello, J.C., et al., Elastin-like polypeptides in drug delivery. Advanced Drug Delivery Reviews, 2016. 97: p. 85-100.

27. Nicol, A., D.C. Gowda, and D.W. Urry, Cell adhesion and growth on synthetic elastomeric matrices containing ARG-GLY–ASP–SER–3. Journal of Biomedical Materials Research, 1992. 26(3): p. 393-413.

28. Costa, R.R., et al., Stimuli-Responsive Thin Coatings Using Elastin-Like Polymers for Biomedical Applications. Advanced Functional Materials, 2009. 19(20): p. 3210-3218.

29. Straley, K.S. and S.C. Heilshorn, Independent tuning of multiple biomaterial properties using protein engineering. Soft Matter, 2009. 5(1): p. 114-124.

30. Putzu, M., et al., Elastin-like-recombinamers multilayered nanofibrous scaffolds for cardiovascular applications. Biofabrication, 2016. 8(4): p. 045009.

31. Girotti, A., et al., Design and bioproduction of a recombinant multi(bio)functional elastin-like protein polymer containing cell adhesion sequences for tissue engineering purposes. Journal of Materials Science: Materials in Medicine, 2004. 15(4): p. 479-484.

32. Link, A.J., M.L. Mock, and D.A. Tirrell, Non-canonical amino acids in protein engineering. Current Opinion in Biotechnology, 2003. 14(6): p. 603-609.

33. Cai, L., C.B. Dinh, and S.C. Heilshorn, One-pot Synthesis of Elastin-like Polypeptide Hydrogels with Grafted VEGF-Mimetic Peptides. Biomaterials science, 2014. 2(5): p. 757-765.

34. Ravi, S., et al., Maleimide-thiol coupling of a bioactive peptide to an elastin-like protein polymer. Acta Biomater, 2012. 8(2): p. 627-35.

35. Azagarsamy, M.A. and K.S. Anseth, Bioorthogonal Click Chemistry: An Indispensable Tool to Create Multifaceted Cell Culture Scaffolds. ACS Macro Lett, 2013. 2(1): p. 5-9.

36. Sletten, E.M. and C.R. Bertozzi, Bioorthogonal chemistry: fishing for selectivity in a sea of functionality. Angew Chem Int Ed Engl, 2009. 48(38): p. 6974-98.

37. Deforest, C.A., E.A. Sims, and K.S. Anseth, Peptide-Functionalized Click Hydrogels with Independently Tunable Mechanics and Chemical Functionality for 3D Cell Culture. Chemistry of materials: a publication of the American Chemical Society, 2010. 22(16): p. 4783-4790.

38. Krause, A., A. Kirschning, and G. Drager, Bioorthogonal metal-free click-ligation of cRGD-pentapeptide to alginate. Org Biomol Chem, 2012. 10(29): p. 5547-53.

39. Mas-Moruno, C. and R. Fraioli, alphavbeta3- or alpha5beta1-Integrin-Selective Peptidomimetics for Surface Coating. 2016. 55(25): p. 7048-67.

40. Kapp, T.G., et al., A Comprehensive Evaluation of the Activity and Selectivity Profile of Ligands for RGD-binding Integrins. Sci Rep, 2017. 7: p. 39805.

41. Wohlrab, S., et al., Cell adhesion and proliferation on RGD-modified recombinant spider silk proteins. Biomaterials, 2012. 33(28): p. 6650-9.

42. Dominik Bernhagen, N.G.Q., Vanessa Jungbluth, Jakub Dostalek, Paul B. White, Peter Timmerman., Bicyclic RGD-peptides with Exquisite Selectivity for the Integrin αvβ3 Receptor using a 'Random Design' Approach. 2018. (Manuscript in press).

43. Dominik Bernhagen, N.G.Q., Vanessa Jungbluth, Jakub Dostalek, Paul B. White, Peter Timmerman., High Affinity α5β1 Integrin-Binding Bicyclic RGD-Peptides Identified via Screening of Partially Randomized Libraries. 2018. (Manuscript in press).

44. González de Torre, I., et al., Elastin-like recombinamer catalyst-free click gels: Characterization of poroelastic and intrinsic viscoelastic properties. Acta Biomaterialia, 2014. 10(6): p. 2495-2505.

45. Costa, R.R., et al., Layer-by-Layer Assembly of Chitosan and Recombinant Biopolymers into Biomimetic Coatings with Multiple Stimuli-Responsive Properties. Small, 2011. 7(18): p. 2640-2649.

46. Baskin, J.M. and C.R. Bertozzi, Bioorthogonal Click Chemistry: Covalent Labeling in Living Systems. QSAR & Combinatorial Science, 2007. 26(11-12): p. 1211-1219.

47. de Torre, I.G., et al., Elastin-like recombinamer-covered stents: Towards a fully biocompatible and non-thrombogenic device for cardiovascular diseases. Acta Biomaterialia, 2015. 12(Supplement C): p. 146-155.

48. Bernhagen, D., L. De Laporte, and P. Timmerman, High-Affinity RGD-Knottin Peptide as a New Tool for Rapid Evaluation of the Binding Strength of Unlabeled RGD-Peptides to alphavbeta3, alphavbeta5, and alpha5beta1 Integrin Receptors. 2017. 89(11): p. 5991-5997.

49. Chen, Y., et al., Validation of a PicoGreen-Based DNA Quantification Integrated in an RNA Extraction Method for Two-Dimensional and Three-Dimensional Cell Cultures. Tissue Engineering Part C: Methods, 2011. 18(6): p. 444-452.

50. Pallarola, D., et al., Interface Immobilization Chemistry of cRGD-based Peptides Regulates Integrin Mediated Cell Adhesion. Adv Funct Mater, 2014. 24(7): p. 943-956.

51. Hersel, U., C. Dahmen, and H. Kessler, RGD modified polymers: biomaterials for stimulated cell adhesion and beyond. Biomaterials, 2003. 24(24): p. 4385-415.

52. Kimura, R.H., et al., Engineered cystine knot peptides that bind alphavbeta3, alphavbeta5, and alpha5beta1 integrins with low-nanomolar affinity. Proteins, 2009. 77(2): p. 359-69.

53. Hirano, Y., et al., Cell-attachment activities of surface immobilized oligopeptides RGD, RGDS, RGDV, RGDT, and YIGSR toward five cell lines. Journal of Biomaterials Science, Polymer Edition, 1993. 4(3): p. 235-243.

54. Bearinger, J.P., D.G. Castner, and K.E. Healy, Biomolecular modification of p(AAm-co-EG/AA) IPNs supports osteoblast adhesion and phenotypic expression. J Biomater Sci Polym Ed, 1998. 9(7): p. 629-52.

55. Lin, Y.S., et al., Growth of endothelial cells on different concentrations of Gly-Arg-Gly-Asp photochemically grafted in polyethylene glycol modified polyurethane. Artif Organs, 2001. 25(8): p. 617-21.

56. Ma, Z., Z. Mao, and C. Gao, Surface modification and property analysis of biomedical polymers used for tissue engineering. Colloids Surf B Biointerfaces, 2007. 60(2): p. 137-57.

57. Short, S.M., G.A. Talbott, and R.L. Juliano, Integrin-mediated signaling events in human endothelial cells. Mol Biol Cell, 1998. 9(8): p. 1969-80.

58. Baranska, P., et al., Expression of Integrins and Adhesive Properties of Human Endothelial Cell Line EA.hy 926. Cancer Genomics - Proteomics, 2005. 2(5): p. 265-269.

59. Kantlehner, M., et al., Surface coating with cyclic RGD peptides stimulates osteoblast adhesion and proliferation as well as bone formation. Chembiochem, 2000. 1(2): p. 107-14.

60. Jeschke, B., et al., RGD-peptides for tissue engineering of articular cartilage. Biomaterials, 2002. 23(16): p. 3455-63.

61. Danilov, Y.N. and R.L. Juliano, (Arg-Gly-Asp)n-albumin conjugates as a model substratum for integrin-mediated cell adhesion. Exp Cell Res, 1989. 182(1): p. 186-96.

62. Maheshwari, G., et al., Cell adhesion and motility depend on nanoscale RGD clustering. J Cell Sci, 2000. 113 (Pt 10): p. 1677-86.

63. Service, R.F., Tissue engineers build new bone. Science, 2000. 289(5484): p. 1498-500.

SUPPORTING INFORMATION

Differential Scanning Calorimetry (DSC) measurements

DSC experiments were performed on a Mettler Toledo 822^e DSC with a liquid nitrogen cooler accessory.

Both temperature and enthalpy were calibrated with an indium standard at the same experimental conditions used for the studied materials. Water solutions of ELRs at 50 mg mL^{-1} were prepared at different values of pH. In a typical DSC run, 20 µL of the solution was placed inside a standard 40 µL aluminium pan hermetically sealed. The same volume of water was placed in the reference pan. As for ELR-hydrogel analysis, 20 mg of the hydrated hydrogel was placed in the sample pan. To account for the exact amount of polymer in the assayed hydrogel, the sample was lyophilized and weighted after DSC run.

All samples were equilibrated for 10 min at 0ºC inside the sample chamber just before the beginning of each experiment, and then, heated from 0 to 60 ºC at a heating rate of 5ºC/min. The scans were run under a nitrogen atmosphere.

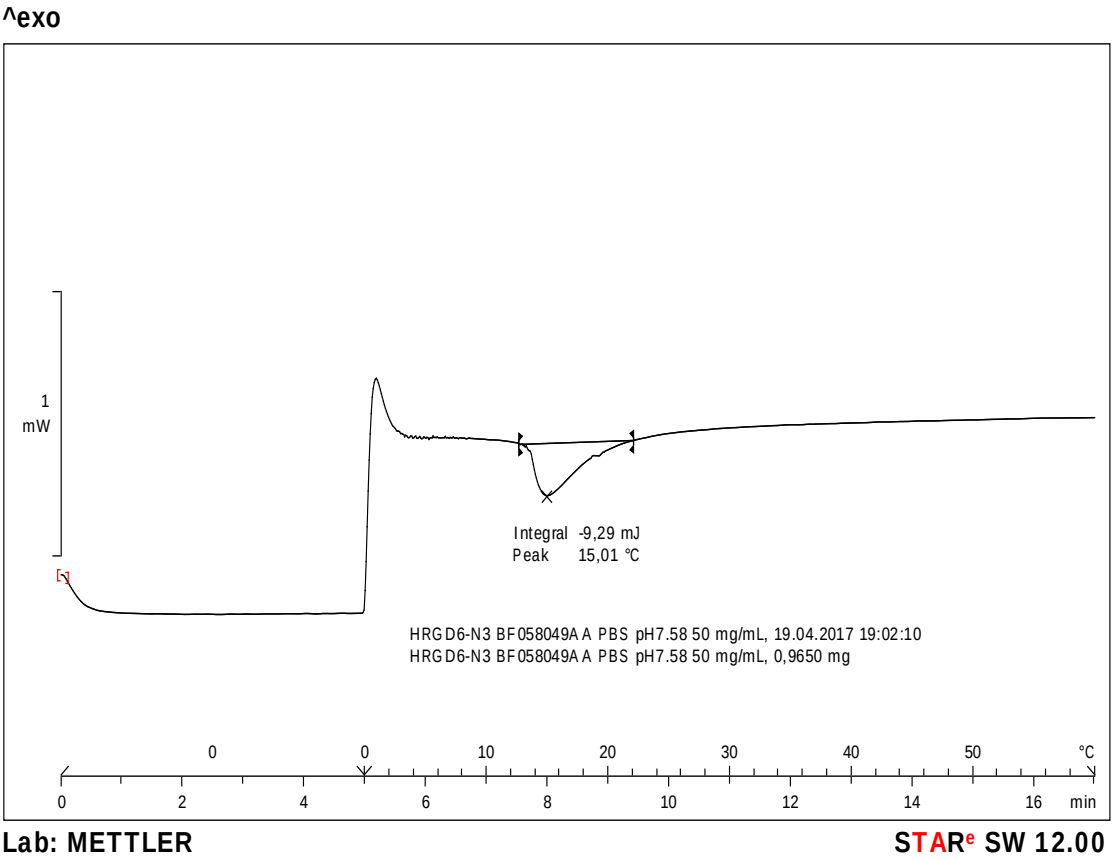

Figure S1. DSC graph of $HRGD_6$-N_3 showing the experimental T_t in PBS at physiological pH.

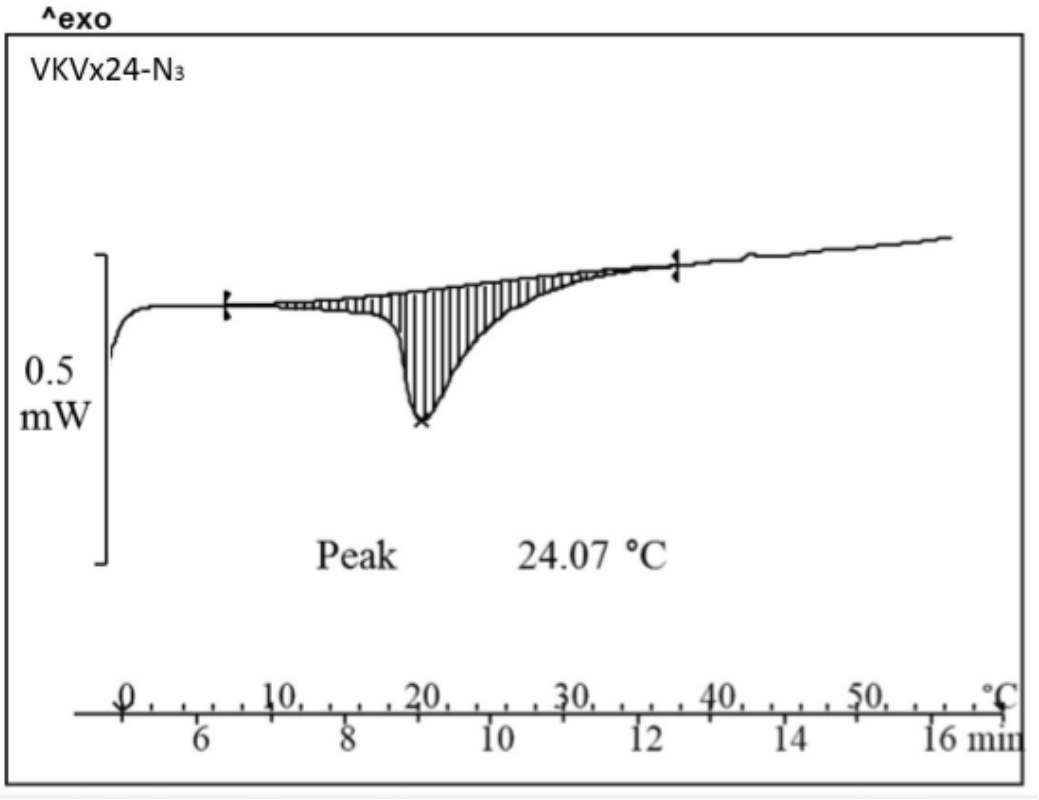

Figure S2. DSC graph of VKV-N_3 showing the experimental T_t in PBS at physiological pH.

Fourier Transform Infrared Spectroscopy (FTIR)

FTIR analysis was conducted with a Bruker FTIR spectrophotometer (Bruker, USA). For each spectrum, a 512-scan interferogram was collected at single beam absorption mode with a 2 cm^{-1} resolution within the 4000- 600 cm^{-1} region. For each sample several FTIR absorption spectra were collected. Five measurements were averaged to obtain the final FTIR absorption spectrum of the sample. Residual water vapour absorption was interactively subtracted from the sample spectra.

Spectral calculations were performed by the OPUS (version 4.2) software (MATTSON INSTRUMENT, INC.).

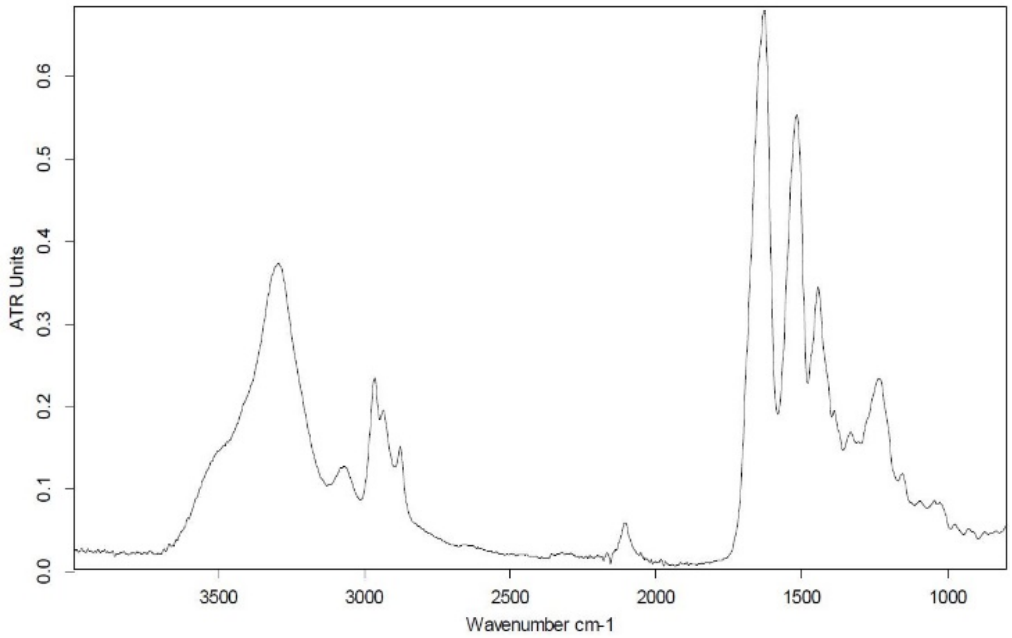

Figure S3. FTIR of $HRGD_6$-N_3.

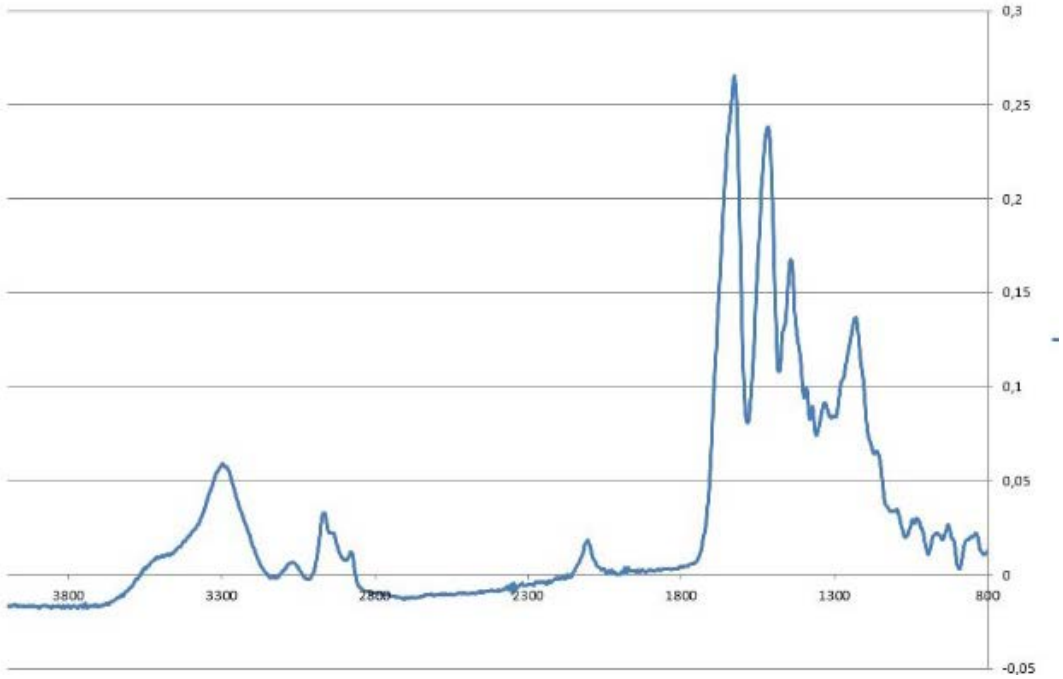

Figure S4. FTIR of VKV-N_3.

Proton nuclear magnetic resonance ^{1}H-NMR Spectroscopy

NMR analysis was carried out using a 400 MHz Agilent Technologies equip with an Agilent MR console 400 and a One NMR probe. The measurements were carried out at 298 K with samples of 20–30 mg of the modified elastin like recombinamers, purified and dissolved in DMSO-d6. Chemical shifts (δ) are given in ppm.

The no deuterated dimethyl sulfoxide peaks at d ¼ 2.5 ppm and d ¼ 39.51 ppm were used as internal reference for 1H and 13C NMR spectra, respectively.

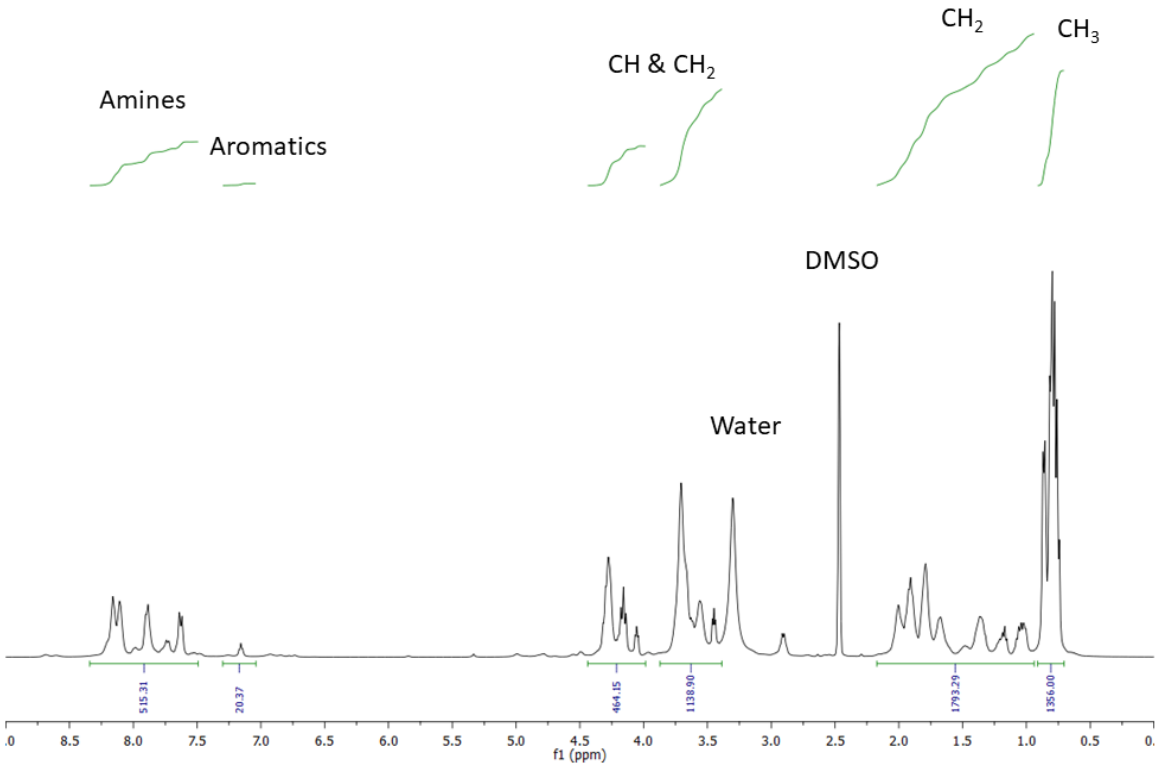

Figure S5. H-NMR spectrum of $HRGD_6$-N_3 showing the integration of the peaks corresponding to the different types of hydrogens.

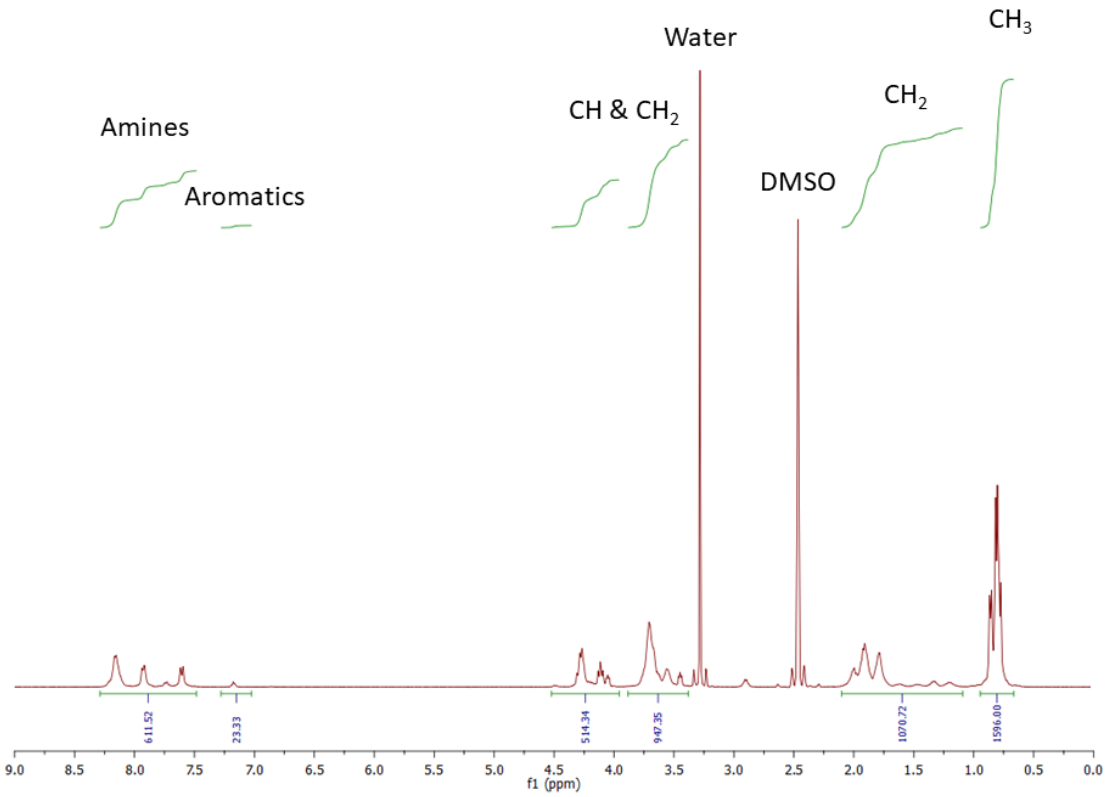

Figure S6. H-NMR spectrum of VKV-N_3 showing the integration of the peaks corresponding to the different types of hydrogens.

Peptide	Sequence	M_{found} [Da]	M_{calc} [Da]
1a	K(BCN)PPPSG[Abz]SG-**C**$_{T3}$HPQ**c**$_{T3}$RGD**c**$_{T3}$	2176,78	2176,47
1b	K(BCN)PPPSG[Abz]SG-**C**$_{T3}$HPQ**C**$_{T3}$RGD**c**$_{T3}$	2176,59	2176,47
1c	K(BCN)PPPSG[Abz]SG-**C**$_{T3}$HSQ**C**$_{T3}$RGD**c**$_{T3}$	2166,43	2166,43
2a	K(BCN)-PPPSG[Abz]SG-**C**$_{T3}$RGD**c**$_{T3}$AYJ**C**$_{T3}$	2162,34	2161,50
2b	K(BCN)-PPPSG[Abz]SG-**C**$_{T3}$RGD**c**$_{T3}$AWG**C**$_{T3}$	2129,34	2128,43
2c	K(BCN)-PPPSG[Abz]SG-**C**$_{T3}$RGD**c**$_{T3}$AYa**C**$_{T3}$	2119,40	2119,41
3a	K(BCN)-PPPSG[Abz]SG-knottin-RGD	4337,85	4336,81
3b	*cyclo*-[K(K(BCN)-PPPSG[Abz]SG)RGDf]	1648,57	1648,84
3c	K(BCN)-PPPSG[Abz]SG-GRGDS	1534,37	1534,65

J: D-Leu

Table S1. Molecular weights of all cyclooctyne (BCN)-functionlized RGD peptides as obtained from UPLC/MS analysis. Calculated masses were determined using ChemDraw software.

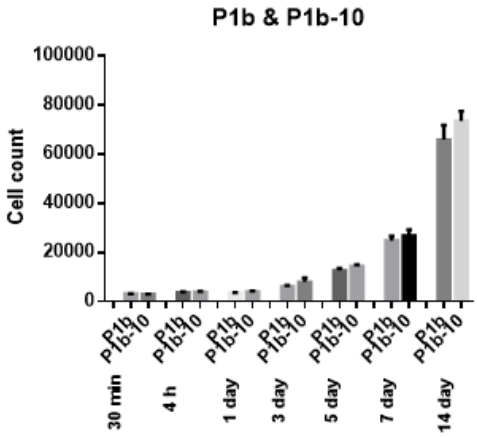
P1b & P1b-10
Cell count
100000
80000
60000
40000
20000
0
P1b
P1b-10
30 min
4 h
1 day
3 day
5 day
7 day
14 day

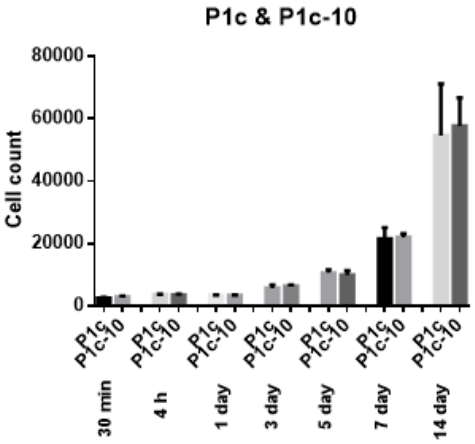
P1c & P1c-10
Cell count
80000
60000
40000
20000
0
P1c
P1c-10
30 min
4 h
1 day
3 day
5 day
7 day
14 day

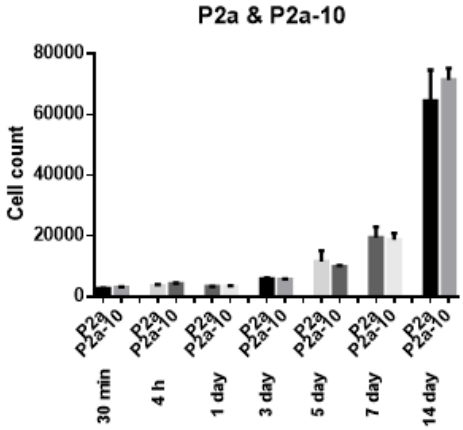
P2a & P2a-10
Cell count
80000
60000
40000
20000
0
P2a
P2a-10
30 min
4 h
1 day
3 day
5 day
7 day
14 day

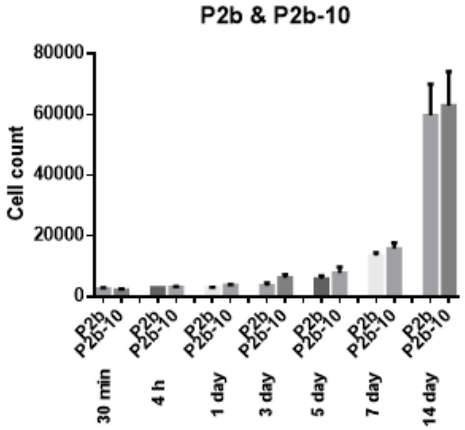
P2b & P2b-10
Cell count
80000
60000
40000
20000
0
P2b
P2b-10
30 min
4 h
1 day
3 day
5 day
7 day
14 day

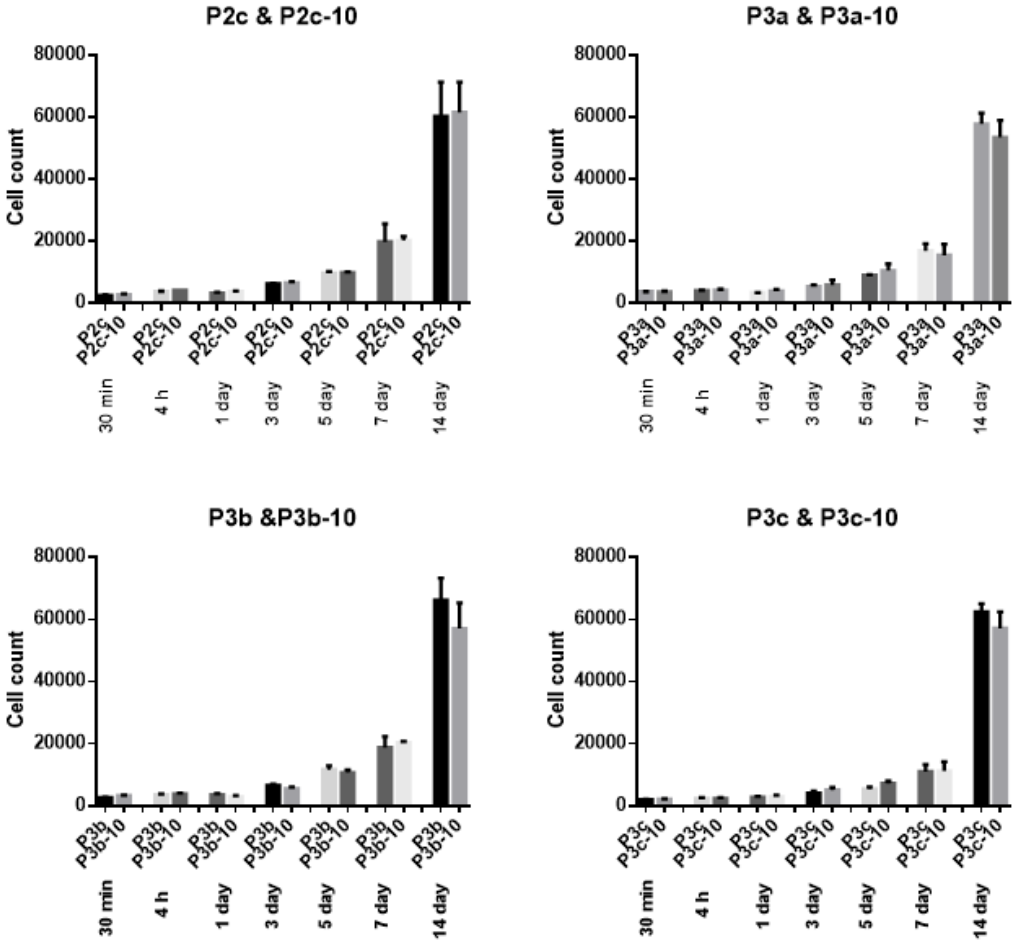

Figure S7. Time-dependent cell quantification for ELRs containing peptides at 5% and 10%; 1a–c (red bars) and 2a–c (green bars), and control RGD peptides 3a–c (blue bars), at different time points (30 min, 4 h, 1 d, 3 d, 5 d, 7 d, 14 d). All experiments were carried out in triplicate and error bars show standard deviations. There was no statistically significant difference between 5% and 10% at any time point.

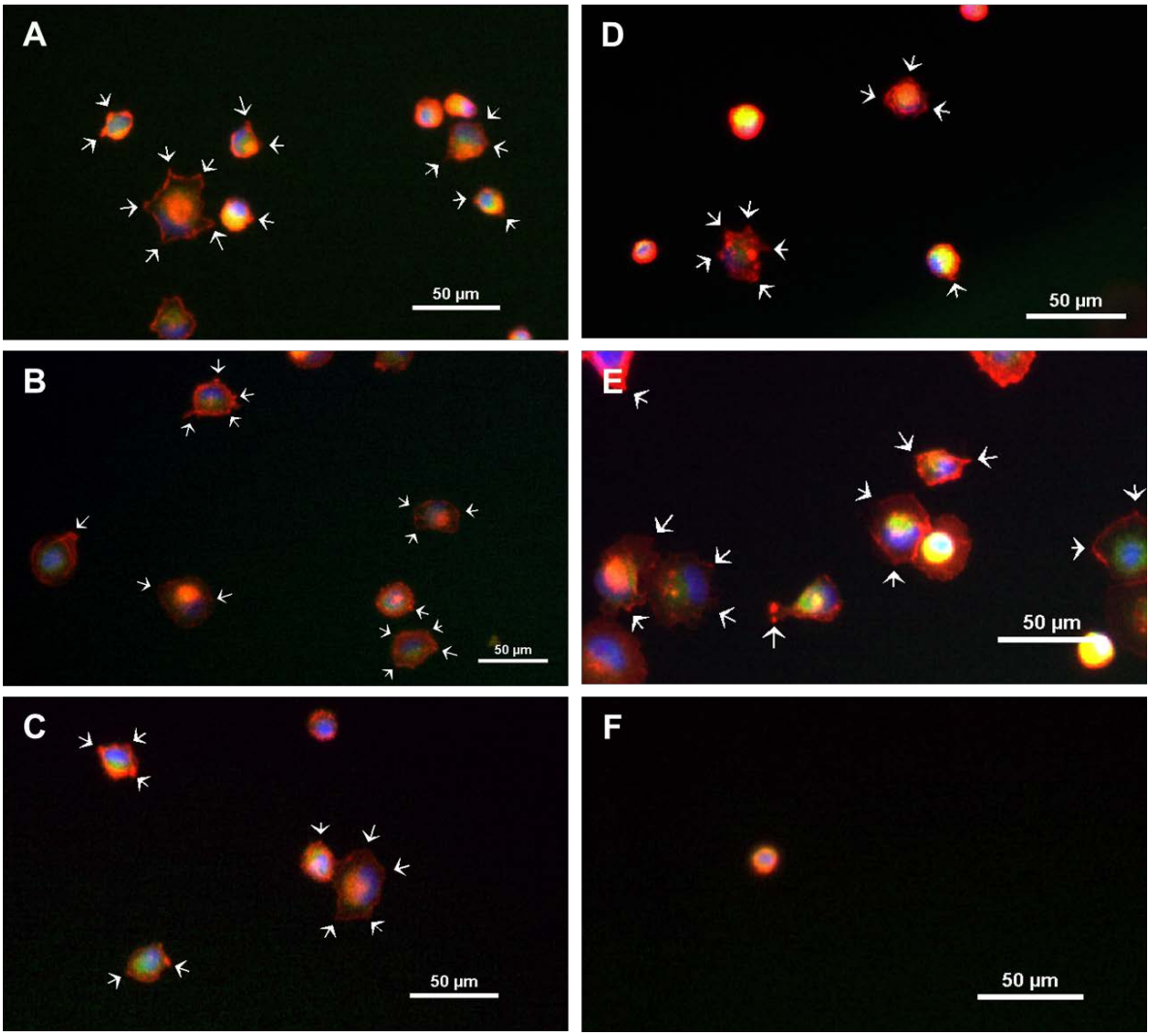

Figure S8. Some examples of magnified captures of immunostained HUVEC cells seeded on P1a (A), P3a (B), P2c (C); P0-RGD (D), P0-FN (E) and P0-BSA (F) that remained adhered after 30 min of incubation and washing. Actin is stained in red, vinculin in green, and nuclei with DAPI in blue. Small protrusions are marked with white arrows. Scale bars are 50 µm.

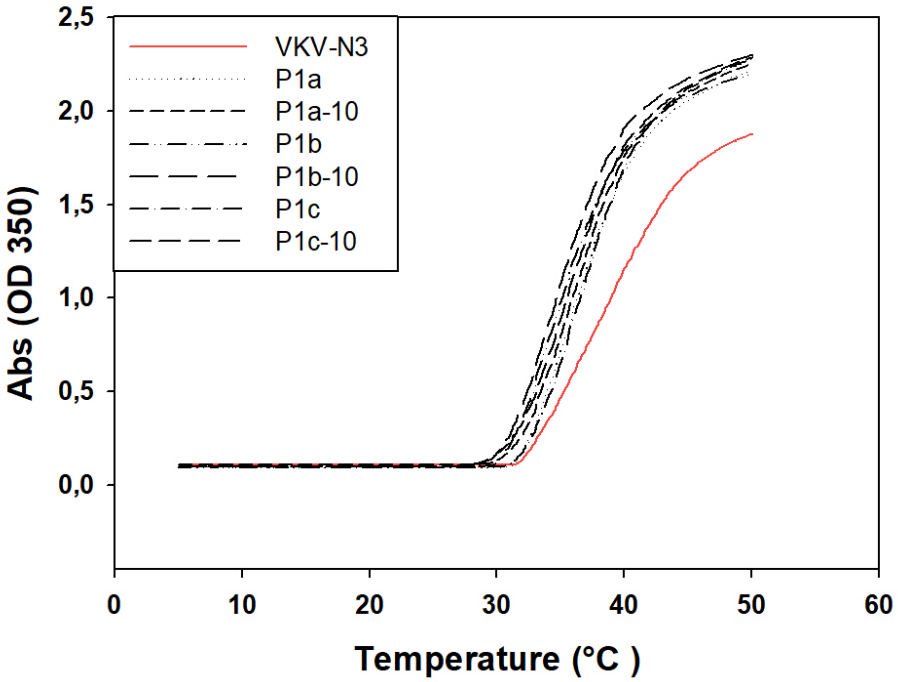

Figure S9. Turbidity analysis of VKV-N_3 and ELRs functionalized with bicycles 1a–c at 5% **(P1a-c)** and 10% **(P1a-c-10)**.

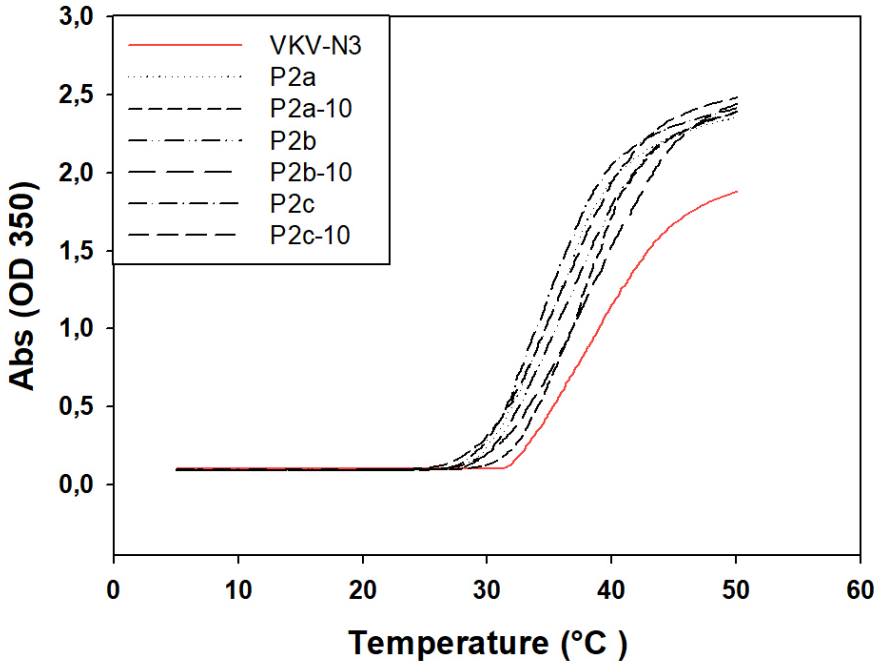

Figure S10. Turbidity analysis of VKV-N_3 and ELRs functionalized with bicycles 2a–c at 5% **(P2a-c)** and 10% **(P2a-c-10)**.

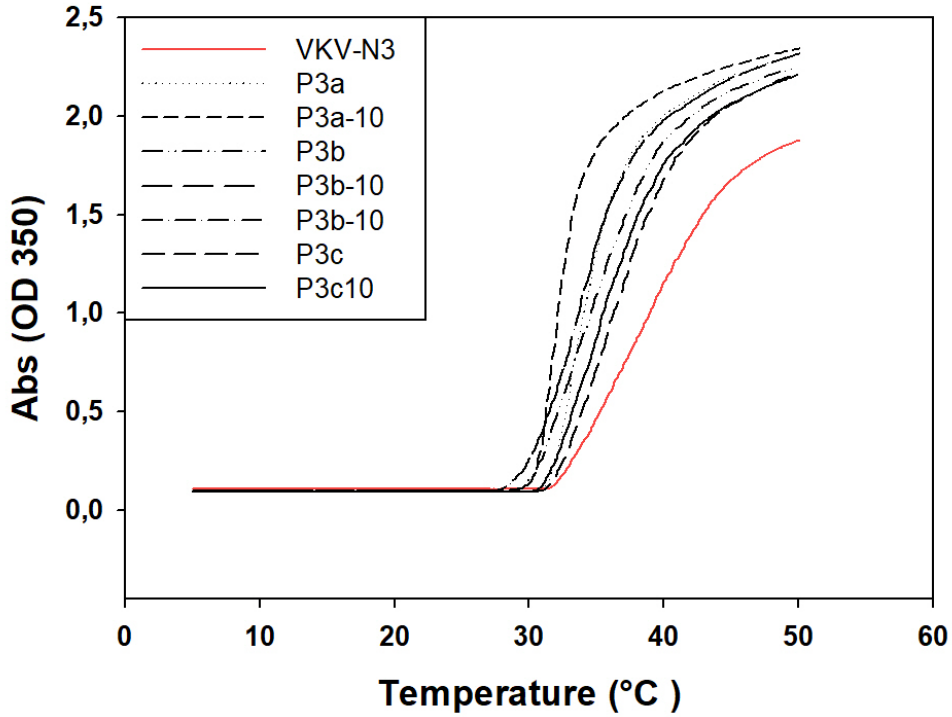

Figure S11. Turbidity analysis of VKV-N_3 and ELRs functionalized with controls 3a–c at 5% **(P3a-c)** and 10% **(P3a-c-10)**.

CHAPTER 6

SELECTIVE ENZYMATIC RESPONSIVE SMART-ELRs WITH ALLOSTERIC CONTROL OF RNase A ACTIVITY

Filippo Cipriani,[1] Leander Poocza,[2] Israel González de Torre,[1,2] Matilde Alonso Rodrigo,[1,2] José Carlos Rodríguez-Cabello.[1,2]

[1] Technical Proteins Nanobiotechnology S.L., Paseo Belén 9A, 47001 Valladolid, Spain

[2] Bioforge, University of Valladolid CIBER-BNN, Paseo de Belén 19, 47001 Valladolid, Spain

(In Progress)

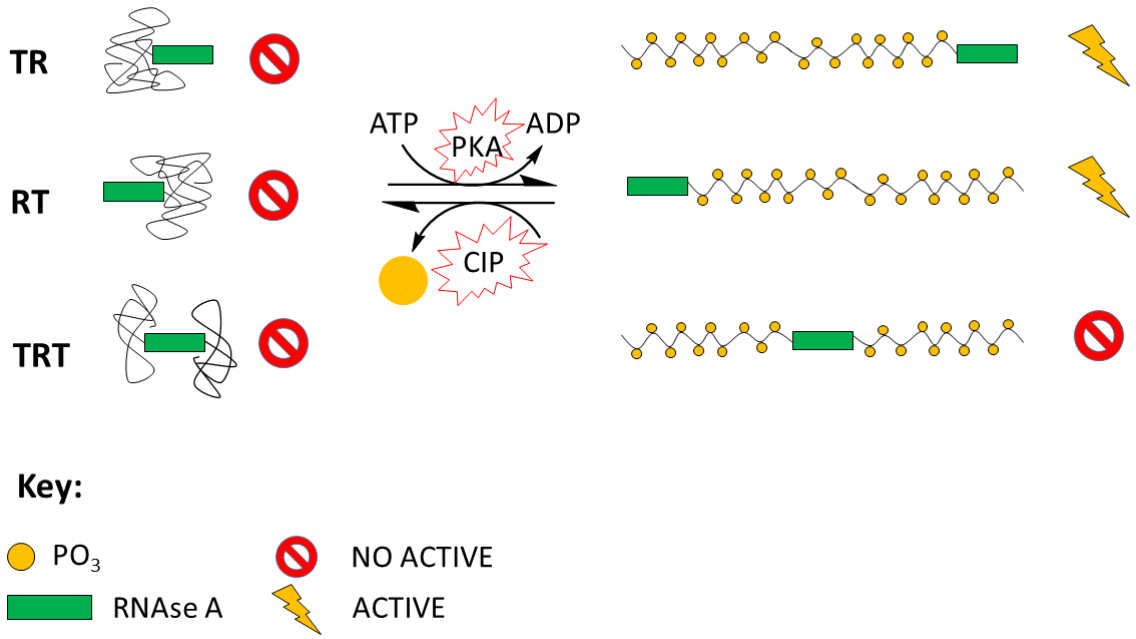

Abstract

A new generation of smart biomaterials that show multiple modular behaviour is a real challenge for targeting complex biomedical system. Herein we developed a smart biomaterial based on Elastin-like Recombinamers with allosteric control of RNase A activity. Taking advantages by the recombinant DNA techniques, we obtained a smart-ELRs containing bioactive sequences sensible to external stimuli. It was designed containing 10 consensus sequence phosphorylation sites regularly distributed along the ELR, and by the Ribonuclease A active sequence (RNase A). According to the position of RNase A relative to the ELR backbone, several variants of the smart-ELR have been produced. The smart-ELRs were further characterized by several experimental techniques (SDS-PAGE, FTIR and HPLC-HR-MS), showing the capacity to be fully phosphorylated and further de-phosphorylated. This reversible system was then investigated by turbidity analysis, demonstrating an evident shift in Temperature transition (T_t) value due to the (de-)phosphorylation. Finally, the allosteric control of the RNase A catalytic activity was evaluated for all the different variants of the smart-ELR. The allosteric control of RNase A activity by the selective phosphorylation was demonstrated. Moreover, the different designs of the smart-ELRs exhibited different catalytic activity, showing the importance of the RNase A position according to the ELR backbone.

1. INTRODUCTION

Research is moving towards the development of new materials capable to combine modular features in order to tailor custom applications. Smart materials have gained widespread interest in material science, they have been used in a large variety of applications (1-4). In particular, this new class of material opened new frontiers in the biomedical fields, such as for tissue engineering, regenerative medicine application and for medical diagnostics (5, 6). The concept of smart, intelligent or stimuli-responsive materials derived from the development of materials that show large conformational changes in response to small environmental stimuli such as temperature, ionic strength, solvent polarity, electric/magnetic field, or light (7). Above the variety of all the stimuli that can be employed, an increasingly important concept is about biomaterials with enzyme responsiveness due to the enzyme's ability to perform in mild conditions, and to their high selectivity in reaction they catalyze (8). The escalation in the development of enzyme-responsive materials is driven by the motivation to mimic bio-molecular recognition processes (9). One of the most common application is therapeutic delivery; for instance, Fouladi *et al.* developed enzyme-responsive liposomes for delivery of anticancer drugs (10). Moreover, it is important to take into account the versatility of this new class of biomaterial, considering which type of biomaterial has been chosen to be engineered and for which purpose. For example, Overstreet at al. developed a novel thermoreversible copolymer of poly-NIPAAm with collagenase-sensitive solubility behaviour (11). Considering that for the most biomedical applications based on enzymes it is often essential to switch on or off the enzymatic reaction, Kim *et al*., performed a study where the use of conducting polymers was employed for building a "bio-switch chip" based on nanostructured polymers and entrapped enzyme; the authors demonstrated the switching of enzyme (glucose oxidation) in real time (12). Therefore, enzyme-responsive smart biomaterials can be applied not only in biomedical applications; Yang e al. created a controllable switching of enzyme activity by Poly(N-isopropylacrylamide)-based microgels through mineralization of calcium carbonate in high-pressure CO_2 (13). Allosteric regulated enzymes are very functional; in many cases, protein functionality is related to changes in the conformational state of certain parts of the molecule; whereby these changes render molecules active or inactive. The features

that have to be taken into account for the development of smart biomaterial with allosteric domains are the ability to be post-translationally and reversibly modified by enzymatic reaction, and the capacity to exhibit a movable solubility frontier close to the body temperature. The common strategy for the development of enzyme-responsive material is to covalently link enzymatic substrates to amphiphilic copolymers (14, 15). In addition to that strategy, there is also a supramolecular strategy for the preparation of enzyme-responsive biomaterials, which features the non-covalent integration of enzymatic substrates into assemblies (16, 17). A promising and powerful strategy extensively study for the design of bioactive biomaterials is the genetic engineering strategy based on recombinant DNA techniques (18). One of the most important biomaterials taking part in this category is Elastin-like Recombinamers (ELRs). ELRs are protein based polypeptides that comprise repetitive units of the Val−Pro−Gly−X−Gly (VPGXG)n pentapeptide, in which X (guest residue) could be any amino acid except L-proline. ELRs shows several advantages of designing smart biomaterials. First, they exhibit thermo-responsiveness due to the change of the protein conformation above the so-called transition temperature (T_t), which itself depends on the amino acid composition of the polymer (19). ELRs are soluble below their T_t and become insoluble and aggregate at a temperature above their T_t, thereby, ELRs are close to a frontier between solubility and insolubility (20-22). This feature is important considering that gives the possibility to begin the design of temperature triggered self-assembling polymers using a repeated motif that is intrinsically responsive to its environment (23). Second, the genetic engineering method enables biosynthesis of fusion constructs with precise control over chain length and protein position which, makes their sensitivity to the environment highly tuneable (24, 25). Third, the design of the ELR can be engineered in order to be responsive to other triggers in the context of self-assembly (26, 27). Finally, taking advantage from the ability of ELRs to modify the activity of functional proteins, they can be used for the development of natural systems with added allosteric control of their function (28, 29).

There are many examples of smart biomaterials based on ELR (smart-ELR); for biomedical and biomimetic applications (30-34), some of them are smart-ELR with enzyme-responsiveness (23, 35-37). Du *et al.* fused an ELR to the D-amino acid oxidase, thereby increasing the solubility and stability of that enzyme (38). Later, in a paper from the same

group, Gao *et al.* (39) fused ELRs to two enzymes to form ELR-fusion R-ω-transaminase and ELR-fusion D-amino acid oxidase, which, at temperatures above the T_t of the ELR part, assembled to form two-enzyme complexes with significantly improved catalytic efficiency. Herein, we propose a new type of enzymatic responsive smart-ELR with allosteric control of enzymatic activity. The smart-ELR enzyme was designed containing the consensus sequence for the Kinase/Phosphorylase enzyme. Furthermore, it was engineered with the sequence of RNase A which is a type of digestive enzyme used to specifically cleave single-stranded RNA (40). RNase A was chosen as the modular enzyme, considering its relatively small protein structure consisting of only 124 amino acid (41), and its well-known optimal refolding properties (42, 43). Finally, taking into account that the folding of the smart-ELR into the 3D structure can alter the enzymatic activity it was carefully designed three different variants of the smart-ELR according to the position of the RNase A domain relative to the ELR backbone. Finally, the RNase A activity modulated by the enzymatic phosphorylation/de-phosphorylation was evaluated, and a comparison between the different variants has been made.

2. MATERIALS AND METHODS

2.1. ELR biosynthesis and purification

The cloning and molecular biology for gene construction were performed using standard genetic-engineering methods (44). In this study, four different smart-ELRs were designed (Figure 1). The four smart-ELR designed differ among each other for the composition of bioactive sequences and for the disposition of those sequences. All of the smart-ELRs were designed containing ten consensus sequence for the Kinase/Phosphorylase enzyme (45); in order to provide a better exposition of the consensus sequence, the consensus sequence was flanked by hydrophilic sites. Moreover, all the smart-ELRs were composed by hydrophobic blocks having Isoleucine as the guest amino acid. Finally, the smart-ELRs was further engineered with the RNase A sequence. According to the position of the RNase A domain relative to the ELR backbone, four different types of smart-ELRs were generated: TI, TR, RT and TRT.

TI is composed of the hydrophilic sequence and the hydrophobic block. *MESLLP-[(VDLDVPIPGRFDRRVSVAAE(VGIPG)$_{10}$]$_{10}$V*

TR has the same composition of TI, plus the RNase A sequence at the N-terminal. *MESLLP[(VDLDVPIPGRFDRRVSVAAE(VGIPG)$_{10}$]$_{10}$VETAAAKFERQHMDSSTSAASSSNYCNQM MKSRNLTKDRCKPVNTFVHESLADVQAVCSQKNVACKNGQTNCYQSYSTMSITDCRETGSSKYPNC AYKTTQANKHIIVACEGNPYVPVHFDASV*

RT has the same composition of TR, plus the RNase A sequence located at the C-terminal. *MESLLPVETAAAKFERQHMDSSTSAASSSNYCNQMMKSRNLTKDRCKPVNTFVHESLADVQAVCS QKNVACKNGQTNCYQSYSTMSITDCRETGSSKYPNCAYKTTQANKHIIVACEGNPYVPVHFDAS-[(VDLDVPIPGRFDRRVSVAAE(VGIPG)$_{10}$]$_{10}$V*

TRT has the identical composition of TR and RT, but in this case, the RNase A domain was located exactly in the middle of the ELR backbone sequence.

MESLLP[(VDLDVPIPGRFDRRVSVAAE(VGIPG)$_{10}$]$_5$VETAAAKFERQHMDSSTSAASSSNYCNQMM KSRNLTKDRCKPVNTFVHESLADVQAVCSQKNVACKNGQTNCYQSYSTMSITDCRETGSSKYPNCA YKTTQANKHIIVACEGNPYVPVHFDAS-[(VDLDVPIPGRFDRRVSVAAE(VGIPG)$_{10}$]$_5$ V

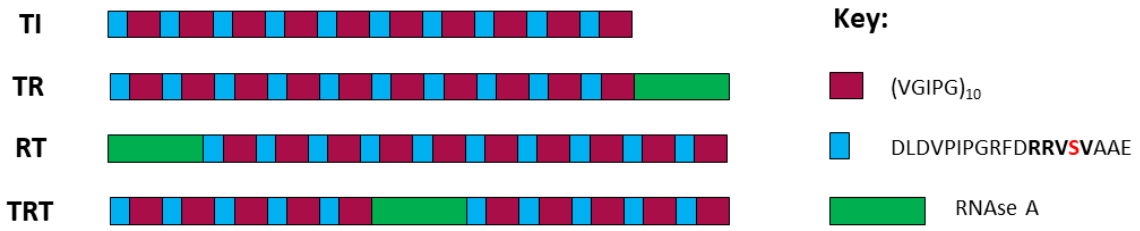

Figure 1. Graphical scheme of the smart-ELRs. The hydrophilic sequence containing the consensus sequence is represented by the blue block; according to the key, the consensus sequence is marked in bold, and the Serine residue where occurs the phosphorylation/de-phosphorylation is marked in red. The hydrophobic block is represented by the red block. RNase A sequence is represented by the green block.

Production was carried out by recombinant techniques using Escherichia coli as the cell system, as described previously (44, 46-48). Purification was performed by several cooling and heating purification cycles (Inverse Transition Cycling) following centrifugation; the ELRs obtained in this manner were dialyzed against MilliQ (MQ) water and lyophilized.

The purity and molecular weight (MW) of the ELRs were verified by sodium dodecyl sulfate polyacrylamide gel electrophoresis (SDS-PAGE). Amino acid composition analysis and infrared spectroscopy (FTIR) was also performed (49). The characterization results are provided in the Supporting Information (Figure S1 – S7).

2.2. Smart-ELRs phosphorylation and de-phosphorylation

Phosphorylation and de-phosphorylation reactions were performed to modulate the smart-ELR state. The smart-ELRs were dissolved at a concentration of 5 mg/mL either for phosphorylation or de-phosphorylation reaction. Specific buffers were prepared for the two reactions. For the phosphorylation: the phosphorylation buffer was composed by NEBuffer for protein Kinases (PK) 1X (New England BioLabs), Adenosine 5'-Triphosphate (ATP) 200 µM (New England Biolabs), and milliQ water. The concentration of ATP was in excess according to the stoichiometry of the reaction (2,6 times more), in order to guarantee the presence of phosphates groups for complete phosphorylation of the ELRs. The cAMP-dependent Protein Kinase (PKA) catalytic Subunit (New England BioLabs) was added to the solution buffer with a ratio of 5000 Units of enzyme per mL of reaction buffer. The solution was further incubated 3 h at 20 °C (temperature on which the ELRs were at dissolved state) under shaking. For the de-phosphorylation: the de-phosphorylation buffer was composed by CutSmart Buffer 1X (New England BioLabs), and milliQ water. The Alkaline Phosphatase, Calf Intestinal (CIP) (New England BioLabs) was added to the solution buffer with a ratio of 100 Units of enzyme per mL of reaction buffer. The solution was further incubated 3 h at 20 °C under shaking. According to the design of the biomaterial, ten phosphate groups can theoretically be transferred/removed to each smart-ELR. After both the reactions, the enzymes (PKA and CIP) were removed in the same way: the solution was heated up to 80 °C for 15 min in order to inactivate and unfold the enzyme. Afterwards, quick centrifugation was performed and the pellet was re-dissolved in MilliQ water at 1 mg/mL O/N at 4 °C under shaking. Then, quick centrifugation at 4 °C was performed to remove the unfolded enzyme from the solution. Finally, the solution went through dialysis and freeze-drying steps.

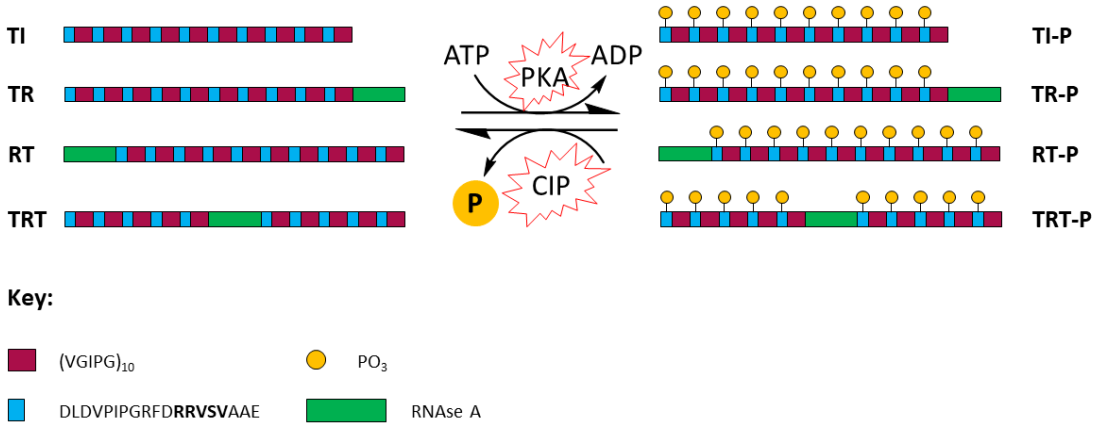

Figure 2. Graphical scheme of the phosphorylation and de-phosphorylation reaction of the smart-ELRs. Ten phosphate groups can theoretically be transferred/removed to each smart-ELR.

2.3. Mass analysis (HPLC-HR-MS)

The phosphorylation/de-phosphorylation rate of the four different smart-ELRs was analyzed by High-Performance Liquid Chromatography-High Resolution-Mass spectrometry (HPLC-HR-MS). Mass spectra were performed using an ultra-high-resolution QTOF instrument (MAXIS II, BRUKER, Bremen-Germany). Electrospray ionization source in positive mode was used for all the analyses and the parameters were adjusted as follows: Capillary voltage 3400 V, End plate offset 500 V, in-source Collision Induced Dissociation energy (isCID) 130 eV. Nitrogen was used as nebulizer gas (pressure of 3 Bar) and drying gas (heated to 250°C, flow 4 L/min). The scans of MS spectra were conducted in the m/z range of 1000 to 12000. For accurate high-resolution mass spectrometry (HRMS) external calibration was performed after each chromatographic run by means of a mixture of phosphazenes. Prior to mass detection samples were separated in a HPLC instrument (HP1100 Series, Agilent Technologies) using a Vydac-C4 Protein column (300 Å, 250 mm, 4.6 mm id, 5 mm particle size), the flow rate was set to 0.5 mL/min, solutions of 0.2% trifluoroacetic acid in water (v/v) and 0.1% trifluoroacetic acid in acetonitrile (v/v) were used as mobile phases A and B respectively. For each sample, a 4 mg/mL solution was prepared in DMSO and 100 µL of it was loaded on the column. The separation was achieved by a 25 min linear gradient from 30% to 80% B, afterwards, isocratic conditions were kept for a 60 min total run time. Finally, the MaxEnt algorithm was applied to the

protein spectrum to de-convolute the multi-charged signals in order to obtain the neutral intact mass protein.

2.4. Turbidity analysis

The T_t of all the ELRs was verified by Turbidity using the Cary Series UV-Vis Spectrophotometer (Agilent Technologies). The analysis for the determination of the T_t shift before and after the phosphorylation and the de-phosphorylation was recorded for ELRs at 5 mg/mL. For all the turbidity analysis (including buffer and concentration dependence experiments), a thermal ramp was carried out at 1 °C/min and the turbidity was recorded at a wavelength of 350 nm.

2.5. Dynamic Light Scattering (DLS)

Light scattering measurements were performed using a BI-200SM multi-angle goniometer (Brookhaven Instrument, Holtsville, NY) with a 33mWHe−Ne vertically polarized laser at a wavelength of 632.8 nm and a digital correlator (BI-9000AT). All the ELRs solutions were prepared by dissolving the ELRs in RNase buffer, thus stored at 4 °C overnight to allow the complete dissolution of the smart-ELRs and filtered using 0,45 µm PVDF syringe filter. Afterwards, the samples were introduced into the polystyrene cuvette and stabilized for 5 min at 37 °C to allow supramolecular assembly. DLS measurements were performed to calculate the size distribution (Volume mean (nm)) and polydispersity index (PDI). All the measurements were performed in triplicates.

2.6. RNase A activity analysis

The RNase A activity of each smart-ELRs was evaluated either for the phosphorylated or dephosphorylated state. The assay was performed following the general ribonuclease assay using methylene blue (50). The buffer of the assay was adjusted for the RNase A activity. Briefly, the RNase buffer was prepared (50 mM Tris HCl, 250 mM KCl, 3 mM $MgCl_2$, 10 mM DTT); Methylene Blue buffer was obtained dissolving Methylene Blue (Sigma-Aldrich) in RNase buffer at 0,1 mg/mL, whereas RNA solution was obtained dissolving RNA from yeast (Roche) in RNase buffer at 10 mg/mL. RNA solution (100 µL) was mixed with the methylene blue buffer (400 µL) and pre-incubated at 37 °C for 10 min in the dark. Afterwards 500 µL of the ELRs solution (1 mg/mL) was added to reach a final

volume of 1 mL and an ELRs concentration of 0,5 mg/mL. Afterwards the solution was incubated at 37 °C for 15 min in the dark, and then the spectrophotometer analysis was performed at 688 nm.

2.7. Statistical analysis

Values are expressed as mean ± standard deviation (SD). The data were examined with a one-way analysis of variance (ANOVA) followed by Tukey's Honestly Significant Difference (HSD) post hoc test. All statistical analyses were performed with GraphPad Prism. A P-value lower than 0.05 was considered statistically significant.

3. RESULTS

3.1. Smart-ELRs phosphorylation and de-phosphorylation

The design of our smart-ELR was composed by the inclusion of ten (de-)phosphorylation consensus sequence regularly distributed along the ELR, moreover, the consensus domain was flanked by a hydrophilic sequence for better accessibility to the Kinase (PKA) and Phosphatase (CIP). Finally, the Isoleucine was selected as a guest amino acid in order to have a counter hydrophobic-part tailoring our smart-ELR for mild conditions. Furthermore, according to the position of RNase A sequence in relation to the ELR backbone, three different versions of the smart-ELRs were obtained by DNA recombinant techniques (TR, RT, TRT) (Figure 1).

The phosphorylation/de-phosphorylation rate of all the smart-ELRs was analyzed by HPLC-HR-MS. Mass Spectrometry spectra are shown in Supporting Information (Figure S8-S11). In table 1 there are reported the values of all the smart-ELRs in different states, where Native means before phosphorylation, Phosphorylated means after phosphorylation, and De-Phosphorylated means after De-phosphorylation.

HPLC-HR-MS (Da)	Native	Phosphorylated	Dephosphorylated	Δ Native - Phosphorylated
TI	65077	65873	65075	796
TR	78611	79410	78612	799
RT	78612	79412	78610	800
TRT	78609	79411	78613	802

Table 1. HPLC-HR-MS of all the smart-ELRs in different states. Native: before Phosphorylation; Phosphorylated: after Phosphorylation; De-Phosphorylated: after De-phosphorylation. Mass values are expressed in Dalton (Da).

In the case of TI, the mass measured in the native state is 65077 Da; whereas the phosphorylated state showed a mass of 65873 Da; finally, the de-phosphorylated TI mass was 65075 Da. The difference between the Native and the Phosphorylated Mass of TI was 796 Da, which coincides with the difference in MW recorded between the Phosphorylated and the De-phosphorylated state of TI (798 Da). On the other hand, the mass values recorded for TR, RT and TRT in their native state are higher than the mass of TI in the native state, due to the presence of RNase A sequence. These values were 78611 Da for TR, 78612 Da for RT and 78609 Da for TRT; whereas after the phosphorylation it was recorded 79410 Da, 79412 Da and 79411 Da, for TR, RT and TRT respectively. As it was recorded for TI, also for TR, RT and TRT the difference between the Native and the Phosphorylated Mass was in around 800 Da, which coincides, also for the last ones, with the difference recorded between the Phosphorylated and the de-Phosphorylated state.

The thermally driven aggregation of the ELRs was investigated using the turbidity approach. The increment in temperature beyond the critical point results in a sharp increase in turbidity (51, 52). The T_t is defined as the temperature at 50% maximal turbidity (51). Turbidity was measured as a function of the temperature of ELR solutions to investigate the aggregation temperature. The turbidity analysis was performed for all smart-ELRs in order to verify the smart-ELR state modulation by the enzymatic phosphorylation and de-phosphorylation. As it has reported above, a thermal ramp was recorded before and after the phosphorylation (Figure 4, red lines), and before and after the de-phosphorylation (Figure 4, black lines). All the smart-ELRs showed a sharp peak in

turbidity when they turned to aggregate states; this subsequently stabilized over the entire temperature range analyzed, with a maximum optical density (OD) of around 2.5.

In all the cases, a clear shift in temperature was recorded. The difference in T_t for TI between before and after phosphorylation was of 15 °C, passing from 26 °C to 41 °C. Whereas for TR, RT and TRT the T_t shift was around 12 °C in all the cases. The smart-ELRs dissolved in the phosphorylase buffer showed lower T_t compared to the kinase buffer due to the different saline composition (Figure 4, red dashed line compared to the black continuous line). The difference in T_t between the smart-ELRs before and after de-phosphorylation was in all the cases less evident than after the phosphorylation. After the de-phosphorylation, TI showed a T_t shift of 13 °C; whereas for TR, RT and TRT the T_t shift was around 8 °C. Although the delta (Δ) in T_t shift recorded after the de-phosphorylation was lower than after the phosphorylation, the T_t of the de-phosphorylated smart-ELRs was similar to the T_t of the native smart-ELRs in all the cases. Indeed, for TR, RT and TRT the T_t before phosphorylation (Figure 4 B, C, D red continuous lines) coincides with the T_t after the de-phosphorylation (Figure 4 B, C, D black dashed lines). The turbidity analysis for TI before phosphorylation (Figure 4 A red continuous lines) showed a T_t slightly higher (26 °C) than the T_t after the de-phosphorylation (24 °C) (Figure 4 A black dashed lines).

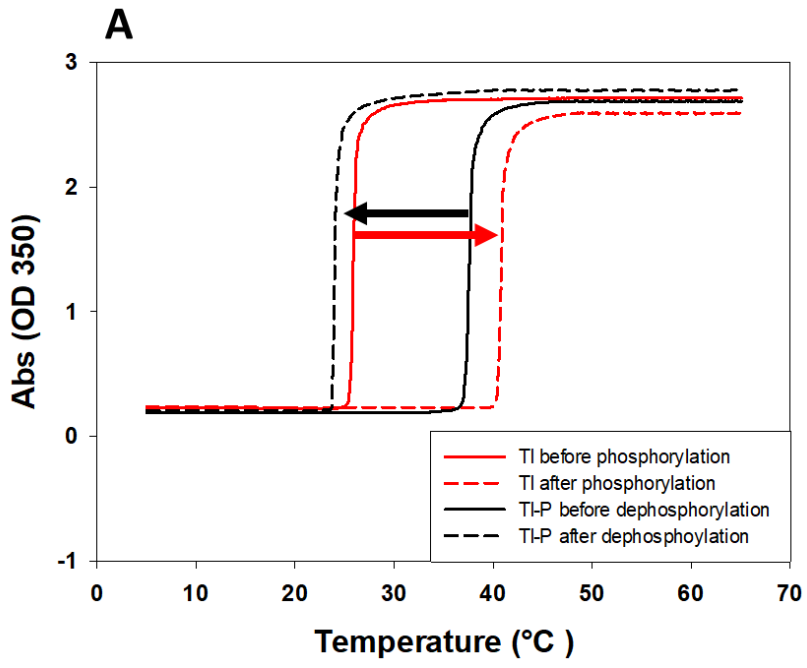

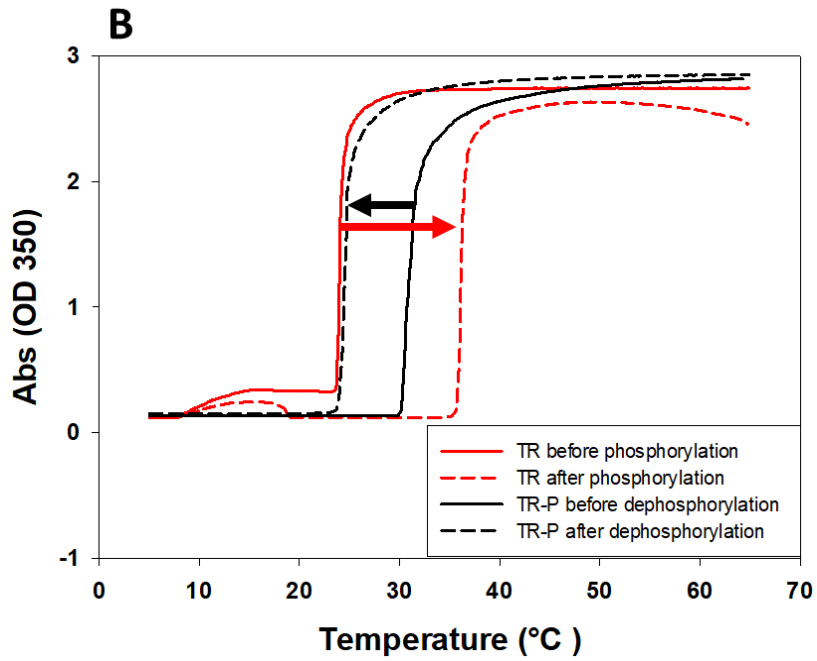
B
Abs (OD 350)
Temperature (°C)
TR before phosphorylation
TR after phosphorylation
TR-P before dephosphorylation
TR-P after dephosphorylation

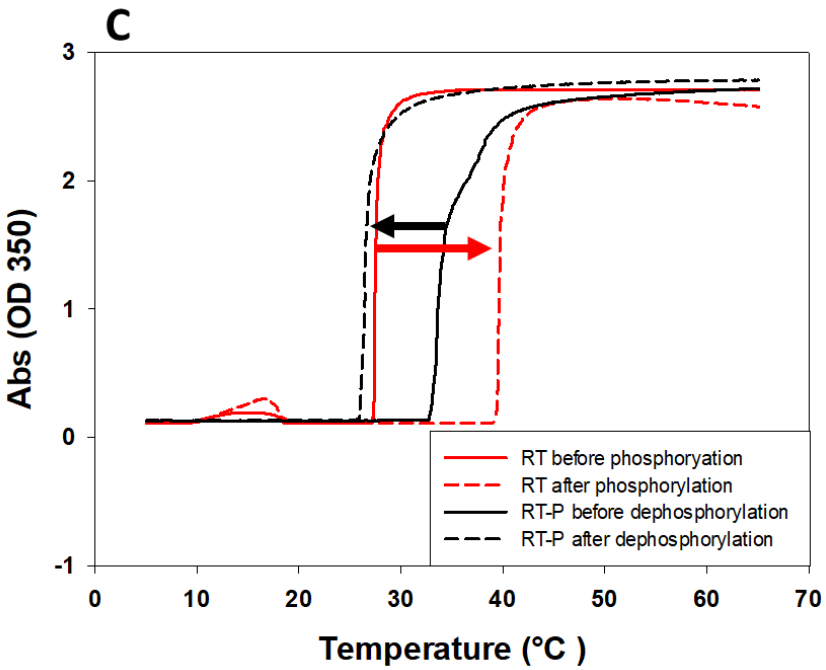
C
Abs (OD 350)
Temperature (°C)
RT before phosphoryation
RT after phosphorylation
RT-P before dephosphorylation
RT-P after dephosphorylation

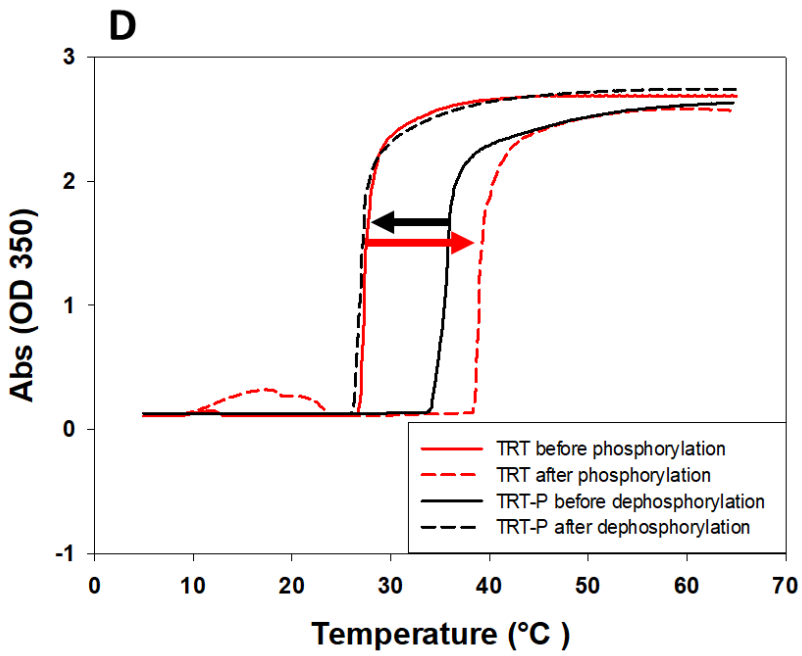

Figure 4. Turbidity analysis of TI (A), TR (B), RT (C), TRT (D). All the samples were measured at 5 mg/mL carrying out thermal ramp at 1 °C/min for the range between 5 and 65 °C. Red lines show the turbidity behavior of the smart-ELR before phosphorylation (continuous line) and after phosphorylation (dashed line). Black lines show the turbidity behavior of the smart-ELR before de-phosphorylation (continuous line) and after de-phosphorylation (dashed line).

In order to see the effect of saline buffer on the T_t, a turbidity analysis was performed dissolving TI in milliQ (Figure 5A). The T_t shift recorded in MQ was much higher than the T_t shift in saline buffer. Indeed, the T_t shift caused by phosphorylation was of 41 °C, passing from 35 °C for the TI before phosphorylation to 76 °C for the TI after phosphorylation. Moreover, the T_t before phosphorylation (Figure 5A, black line) coincides with the T_t after the de-phosphorylation (Figure 5A, orange line).

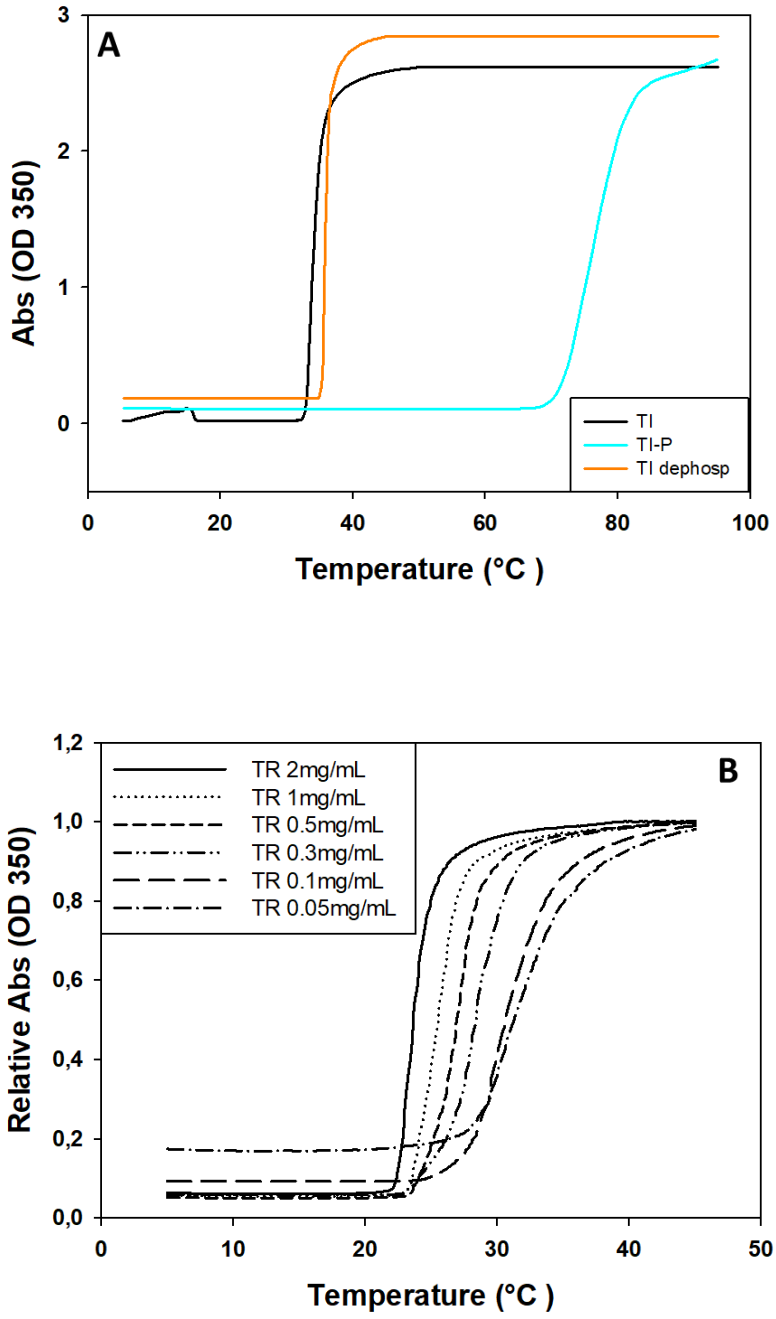

Figure 5. (A): Turbidity analysis performed in milliQ at 5 mg/mL carrying out thermal ramp at 1 °C/min for the range between 5 and 65 °C of TI before phosphorylation (black line), after phosphorylation (light blue line) and after de-phosphorylation (orange line). (B) Turbidity analysis of TR performed in RNase buffer at different concentration carrying out thermal ramp at 1 °C/min for the range between 5 and 45 °C. For all the measurements a thermal ramp was carried out at 1 °C/min and the turbidity was recorded at a wavelength of 350 nm.

In order to see the dependence of concentration on the T_t, a comparison between concentrations was also performed as it is reported in Figure 5B. A turbidity analysis was

performed dissolving TR in RNase buffer at several concentrations. The highest concentration analyzed was 2 mg/mL, showing a T_t of 24 °C; whereas the lowest concentration analyzed was 0,05 mg/mL, showing a T_t of 32 °C. The concentration of 0,5 mg/mL showed a T_t of 27 °C, and it was selected for RNase A activity analysis.

Once that the concentration was fixed at 0,5 mg/mL, a turbidity analysis of the smart-ELRs in RNase buffer was performed. As it is reported in Figure 6, the turbidity behavior of each smart-ELRs was evaluated in its three different forms: native-ELR (before the phosphorylation) represented with the black, phosphorylated smart-ELR (after the phosphorylated) represented with the blue line, and de-phosphorylated smart-ELR (after the de-phosphorylated) represented with the light green line. TI showed a T_t shift of 25 °C after the phosphorylation, passing from around 29 °C to 54 °C. Whereas for TR and RT the T_t shift was around 28 °C. On the other hand, TRT showed a T_t shift around 19 °C; in this case, the native and de-phosphorylated TRT showed a T_t of 36 °C, which was higher compared to the T_t of the other smart-ELRs in the same state. Moreover, all the smart-ELRs containing RNase A sequence showed a less sharply curved, especially at the phosphorylated state compared to TI. Finally, the T_t shifts recorded for every smart-ELRs dissolved in RNase buffer at 0,5 mg/mL (Figure 6) are much higher than the ones recorded in Kinase or Phosphatase buffer at 5 mg/mL (Figure 4).

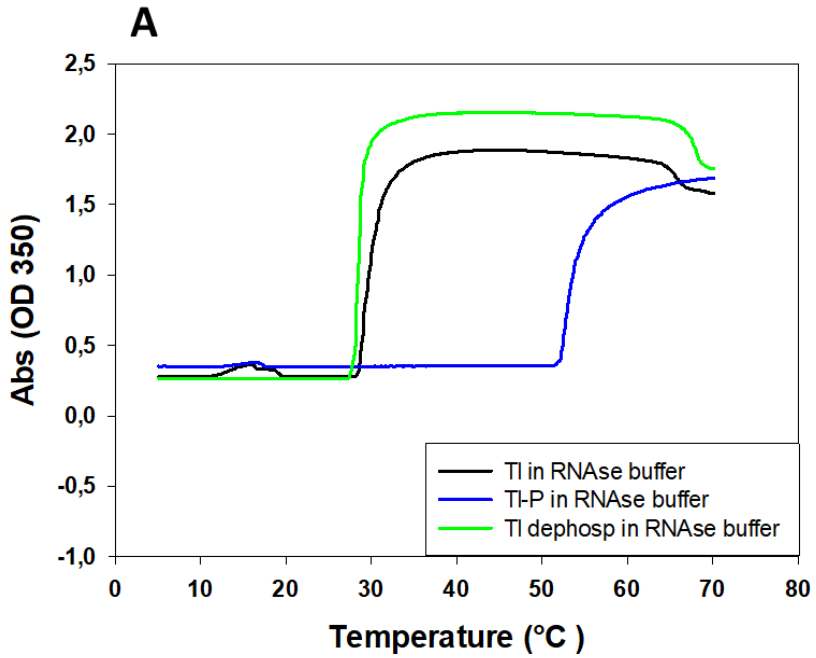

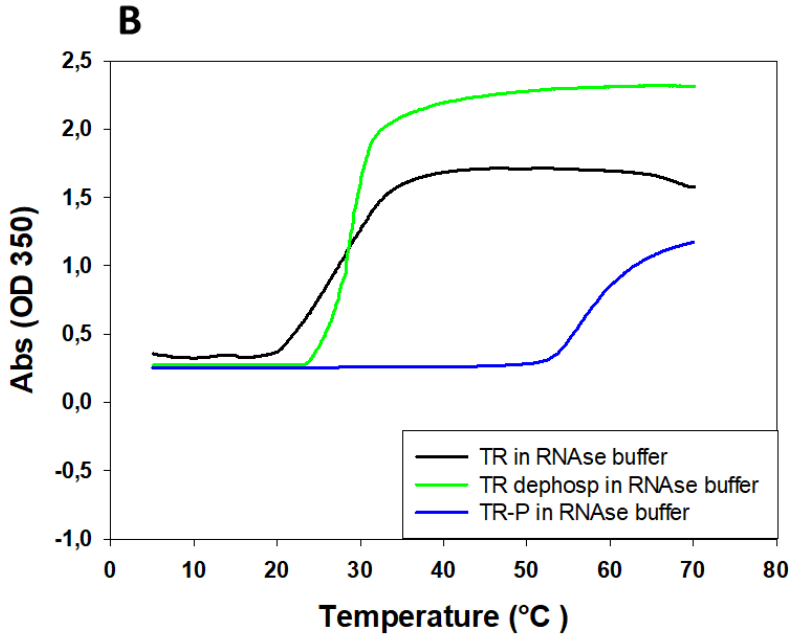
B
Abs (OD 350)
2,5
2,0
1,5
1,0
0,5
0,0
-0,5
-1,0
0
10
20
30
40
50
60
70
80
Temperature (°C)
TR in RNAse buffer
TR dephosp in RNAse buffer
TR-P in RNAse buffer

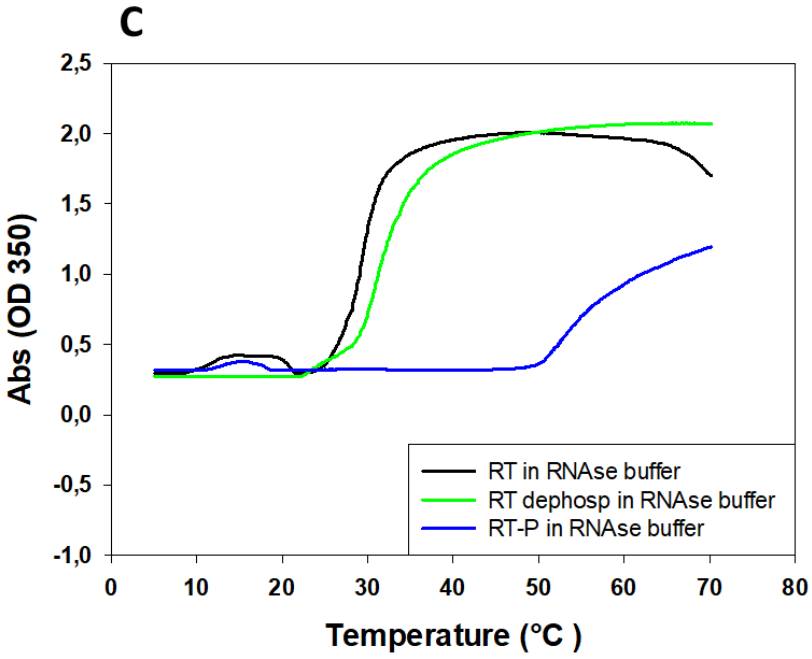
C
Abs (OD 350)
2,5
2,0
1,5
1,0
0,5
0,0
-0,5
-1,0
0
10
20
30
40
50
60
70
80
Temperature (°C)
RT in RNAse buffer
RT dephosp in RNAse buffer
RT-P in RNAse buffer

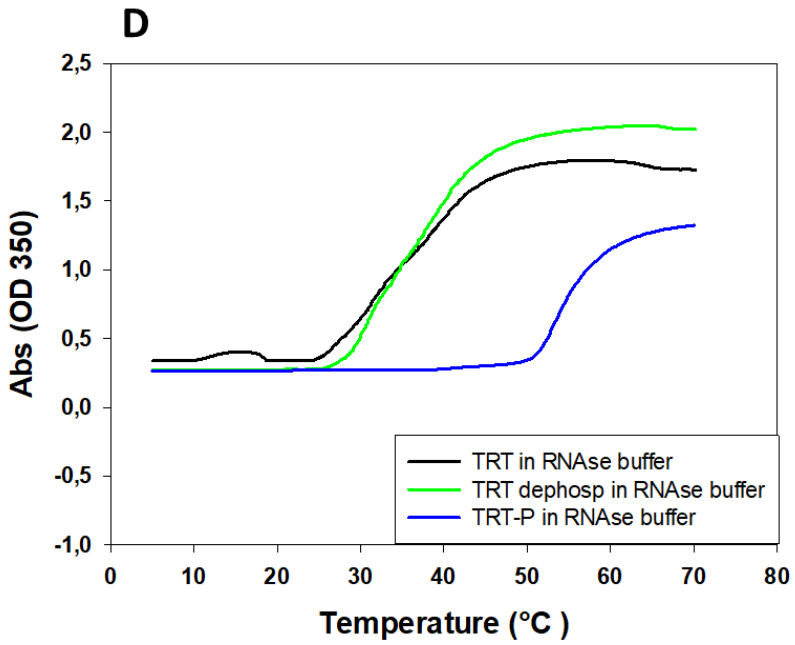

Figure 6. Turbidity analysis of TI (A), TR (B), RT (C), TRT (D) dissolved in RNase buffer at 0,5 mg/mL carrying out thermal ramp at 1 °C/min for the range between 5 and 70 °C. Black lines show the turbidity behavior of the smart-ELRs before phosphorylation; blue lines show the turbidity behavior of the smart-ELRs after phosphorylation; light green lines show the turbidity behavior of the smart-ELRs after de-phosphorylation. For all the measurements the turbidity was recorded at a wavelength of 350 nm.

In all the cases, the temperature of 37 °C has comprised in the ΔT_t occurred by the (de-)phosphorylation. Indeed, the smart-ELRs in the native and de-phosphorylated state are aggregated, whereas the smart-ELRs in the phosphorylated state are dissolved. Finally, in all the curves obtained by turbidity measurements, it can be observed a small shoulder for the smart-ELRs around 15 °C, which, always showed values less than 0,5 OD.

3.2. Dynamic Light Scattering

The temperature-dependent self-assembly of smart-ELR into supramolecular structures was investigated by DLS to determine their size and polydispersity. As it has been reported in Material and Methods section, the DLS measurements for all the smart-ELRs was performed at 0,5 mg/mL in RNase buffer at 37 °C. The DLS analysis provided the size distributions for the different smart-ELRs (TI, TR, RT, TRT) at the native and de-

phosphorylated state (Table 2). The DLS measurements showed that smart-ELRs native and dephosphorylated formed aggregate at 37 °C. The volumes of the smart-ELR aggregates in the native form were, TI: 3076 ± 299 nm; TR: 2812 ± 318 nm; RT: 2804 ± 551 nm; TRT: 2782 ± 267 nm. The smart-ELRs in the phosphorylated state were dissolved at 37 °C; indeed, no aggregates were recorded by DLS analysis. Moreover, the volume of the smart-ELR aggregates in the de-phosphorylated form were, TI: 2852 ± 538 nm; TR: 1553 ± 417 nm; RT: 1457 ± 110 nm; TRT: 1837 ± 154 nm. In this case, only TI kept the same volume size than the smart-ELR in the native state. For TR, RT and TRT the volume size of the aggregates for the de-phosphorylated state was lower compared with the native ones. Finally, the DLS analysis showed a Polydispersity Index (PDI) less than 0,2 in all the cases.

Volume (nm) (± SD) [PDI]	Native	De-phosphorylated
TI	3076 ± 299 [0,11]	2852 ± 538 [0,07]
TR	2812 ± 318 [0,16]	1553 ± 417 [0,15]
RT	2804 ± 551 [0,16]	1457 ± 110 [0,17]
TRT	2782 ± 267 [0,19]	1837 ± 154 [0,16]

Table 2. Volume (± SD) and Polydispersity Index [PDI] from three different measurements of the different smart-ELRs at 0,5 mg/mL in RNase buffer at 37 °C.

3.3. RNase A activity analysis

As it has been described above, the RNA quantification was performed over the smart-ELRs solutions at 0,5 mg/mL in RNase buffer by the spectrophotometer analysis at 688 nm after 15 min of incubation at 37 °C in the darkness. Figure 7 shows the outcomes of the set of the smart-ELRs (TI, TR, RT, TRT). The RNase A activity of each one was evaluated in different states: The native state of ELRs (N) is represented with the grey bars; the

phosphorylated state of ELRs (P) is represented with blue bars; whereas the de-phosphorylated state of ELRs (D) is represented with green bars.

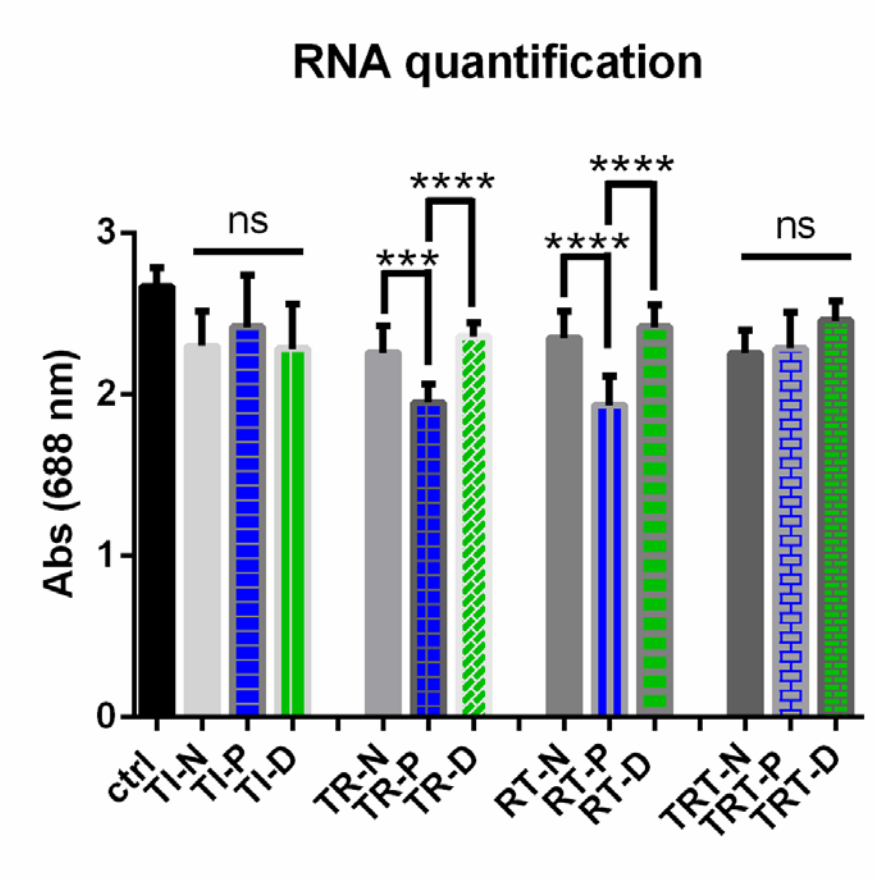

Figure 7. RNA quantification of the solutions containing the different smart-ELRs dissolved in RNase buffer at 0,5 mg/mL after 15 min of incubation in the darkness at 37 °C. Control: black bar (RNase buffer solution without any smart-ELR); grey bars: smart-ELRs in native state (TI-N, TR-N, RT-N, TRT-N); blue bars: phosphorylated smart-ELRs (TI-P, TR-P, RT-P, TRT-P); green bars: de-phosphorylated smart-ELRs (TI-D, TR-D, RT-D, TRT-D). For all the measurements, the absorbance was recorded at a wavelength of 688 nm. All experiments were carried out in triplicate and error bars show standard deviations (*P<0.05; **P<0.01; ***P<0.001; ****P<0.0001).

The comparison between the control and all the rest of the conditions showed statistical difference with all the smart-ELRs at the different state except for TI-P, RT-D and TRT-D. This may be due to the presence of the polymer, that affected by default the measurement at 688 nm. In order to make the bar charts clearer, the RNA quantification outcomes have been clustered by the smart-ELR type (TI, TR, RT, TRT) in different states. The comparison within each group of smart-ELRs has revealed that no difference in RNA quantification was recorded between the different states of TI. The same trend was

presented by TRT smart-ELR, where no difference in RNA quantification was recorded between the native, phosphorylated and de-phosphorylated state. On the other hand, the absorbance recorded for the TR-P solution after 15 min of incubation revealed a significant decrease in the amount of RNA when compared with TR-N and TR-D. Comparing the phosphorylated state (TR-P) with the de-phosphorylated state (TR-D), it was recorded a reduction in RNA amount of 17% on average. Moreover, no significant difference was recorded between TR-N and TR-D. The RT smart-ELRs presented similar values than TR. Indeed, a significant reduction (20%) in RNA amount was recorded for the RT-P compared with the RT-D. In addition, no significant difference was recorded comparing RT-N and RT-D.

4. DISCUSSION

There is a great need of new biomaterials capable to undergo a reversible change in response to small variations in solution conditions, showing a fine modulation, such as allosteric control (53). The aim of the study was to develop an enzymatic responsive smart-ELR with allosteric control of the enzymatic activity, which, allow the communication between the biological environment and the material. The allosteric control was given by the consensus sequence which, was selectively recognized by Kinase and Phosphatase enzymes for phosphorylation/de-phosphorylation. It has already been demonstrated that the enzymatic (de-)phosphorylation which, is commonly used in biology to alter structural features of proteins, can also modulate the T_t and induce gelation of other polymers kind (54-57). Indeed, the change in hydrophobicity is the key to the subsequent conformational rearrangements shows by the hydrophobic domains. The increase in polarity by phosphorylation moves the frontier of solubility to a higher temperature, as the complementary effect of de-phosphorylation moves the frontier back. Furthermore, considering that smart-biomaterials are commonly developed as enzymatic substrates rather than playing an active role in an enzymatic reaction, RNase A was chosen as a single domain protein to confer a catalytic enzyme-responsiveness. As it is reported above, the native enzyme was modified at the genetic level by adding at the amino or carboxyl end the ELR-counterpart containing (de-)phosphorylation consensus sites. Thus, it was obtained an enzymatic responsive smart-ELR with allosteric control of

RNAse A activity. Finally, three different variants of smart-ELRs were obtained by DNA recombinant techniques (TR, RT, TRT), where the position of RNase A domain change in relation to the ELR backbone sequence.

The first step towards the development of the smart-ELR with allosteric control was to verify that TI had complete responsiveness to the Kinase/Phosphatase. Mass spectrometry is an excellent method for detecting protein molecular weight and quantifying its change. Protein phosphorylation events are detected by increases in amino-acid residue mass of +80 Da, which report the addition of HPO3 (58). As shown in Table 1, the precise HPLC-HR-MS analysis for TI revealed a difference between TI before and after phosphorylation of around 800 Da in molecular weight. The incorporated consensus sequence was specifically recognized by the enzyme(s); the phosphorylation occurred completely, indeed, ten phosphate groups (which corresponds to 800 Da) were transferred above the ten consensus sequences. Also, the (de-)phosphorylation occurred completely, indeed the difference between the TI phosphorylated and TI de-phosphorylated was again of around 800 Da, demonstrating the complete reversibility of the ELR state. These results showed optimal accessibility by the enzyme(s) to the substrate, due to the adequate exposition by the hydrophilic loop flanking the consensus sequence. Furthermore, the same results were obtained for the three smart-ELRs containing the RNase A sequence (TR, RT, TRT), where the difference between the phosphorylated and the de-phosphorylated state was again around 800 Da. The presence of the RNase A domain does not prevent the recognition of the consensus sequence by the Kinase/Phosphatase enzyme(s). Moreover, the different position of the RNase A domain does not avoid the complete transferral of ten phosphate groups, meaning that the consensus sequence keeps optimal accessibility to the enzyme even when linked to the RNase A domain. Finally, the complete phosphorylation and de-phosphorylation of the smart-ELRs were accomplished in all the cases; indeed, the theoretical number of phosphate groups that can be transferred was fulfilled in all the cases, showing a 100% effectiveness of the system developed.

All the smart-ELRs before and after (de-)phosphorylation were further analyzed by turbidity (Figure 4). First, it is important to notice that, both reactions were performed at a lower temperature (20 °C) than the T_t of the ELRs, in order to guarantee the efficiency

of the reactions. Although, the turbidity analysis revealed an evident shift in T_t between the smart-ELR before and after the (de-)phosphorylation in all the cases, for TI the Δ T_t was slightly higher than for the smart-ELRs (TR, RT, TRT). This is due to the presence of RNase A domain, which, increment the size of the protein, reducing the impact of the ten phosphates groups over the T_t shift. Moreover, no difference in Δ T_t was recorded between TR, RT and TRT, demonstrating that the position of the RNase A sequence does not affect the T_t. In any case, the turbidity corroborated the reversibility of the system validated by mass spectrometry, showing the capacity of all the smart-ELRs to be driven back and forth between association (insolubility) and dissociation (solubility) by selective enzymatic activity. The smart-ELR demonstrated to be enzyme-responsive, the allosteric domains were able to switch between association and dissociation as a consequence of polarity changes caused by post-translational modification (phosphorylation). Moreover, also the effect of the saline buffers was observed; in fact, all the smart-ELRs dissolved in the phosphorylase buffer showed lower T_t compared to the kinase buffer (Figure 4). The effect of saline buffer on the T_t was highlighted by the turbidity analysis performed dissolving TI in milliQ (Figure 5A). As it has been extensively studied, an increase in saline concentration has a significant effect on the T_t (59). Due to the absence of salts, the contribution of the phosphate groups was more evident for the milliQ solution, indeed, the Δ T_t recorded in milliQ was much higher than the T_t shift recorded in saline buffer. Finally, in all the turbidity curves it can be observed a shoulder for the smart-ELRs around 15 °C. ELRs formed aggregates with a significant increase recorded at OD 350 nm, due to their conformational change and self-organization. This behavior was already reported by García-Arévalo *et al*., where a similar ELR containing Isoleucine as the guest amino acid was used (48). These low OD values indicate that neither of the ELRs forms the typical coacervate state (60), rather, the small absorbance increase suggests the formation of nanoaggregates (23, 61).

Pattaniak *et al*., have already demonstrated how the T_t of an ELR could be modulated by (de-)phosphorylation; however, they developed a system capable to be only partially phosphorylated, showing the effectiveness of 23% (54). In this work, we have developed an optimal design for the selective enzyme-responsive smart-ELR, with the ability to be completely (de-)phosphorylated, showing the effectiveness of 100%. As it is reported in

the literature, the polymer concentration has a significant effect on the altering of T_t (19). This correlation was also demonstrated for our system, where decreasing the concentration of smart-ELR it corresponded an increase in T_t (Figure 5B). In the light of this, a certain concentration was fixed in order to evaluate the modulation of the ELRs from the dissolved state (phosphorylated smart-ELR), to aggregate state (de-phosphorylated smart-ELR) and viceversa at mild conditions.

The turbidity behaviour for all the smart-ELRs dissolved at 0,5 mg/mL in RNase buffer (Figure 6) demonstrated that 37 °C was a temperature in which, smart-ELRs in the native and de-phosphorylated state are aggregated, and smart-ELRs in the phosphorylated state are dissolved. Moreover, the ΔT_t recorded in RNase buffer is much higher than the one recorded in Kinase or Phosphatase buffer. As it has been explained above, this difference depends on the concentration of the polymer and on the saline buffer of the solution. Moreover, the T_t shift of the smart-ELRs appeared slightly different comparing TR and RT with TRT; indeed, the lower concentration of polymers highlighted the small difference in self-assembly behavior. Finally, all the smart-ELRs containing RNase A domain showed a less sharply curved due to higher MW, especially for the phosphorylated state, which also showed higher T_t.

The formation of aggregates was further corroborated by DLS analysis. These measurements showed that smart-ELRs in the native and dephosphorylated state formed aggregate at 37 °C, whereas all the smart-ELRs in the phosphorylated state were dissolved, indeed no aggregates were recorded. Furthermore, the DLS analysis revealed a decrease in volume aggregates between the native TR, RT and TRT and the de-phosphorylated ones; this unexpected result can be due to some sort of reorganization after the (de-)phosphorylation reactions between the RNase A sequence and the ELR backbone, since it appeared only for TR, RT and TRT and not for TI (Table 2). A possible explanation for the unexpected smaller aggregates after the (de-)phosphorylation could be that there would be some ionic rearrangements between the ELRs backbone and the RNase domain during the phosphorylation reaction; this new charges interaction favours a tighter aggregation when the de-phosphorylation occurred. Finally, the outcomes showed above demonstrated that all the smart-ELRs assemblies were responsive to the enzymatic activities. Upon the addition of PKA, the multiple-charged ATP molecules were hydrolyzed

into ADP molecules and phosphate groups were transferred to the serine residues. The supra-amphiphilic self-assembled aggregates underwent disassembly upon addition of PKA. On the other hand, upon the addition of CIP, the phosphate groups were removed from the serine residue, causing the supra-amphiphilic self-assembled aggregates. As shown above, the system was completely reversible (Figure 2).

The allosteric control of the RNase A activity was analyzed monitoring the RNA quantification of the solutions in mild conditions. These results revealed a different behaviour of the smart-ELRs. TI does not contain the RNase A domain; indeed, it has shown no RNase A activity. Either the phosphorylated TI (TI-P) or de-phosphorylated TI (TI-D) does not have any impact over the RNA quantification, meaning that the state of the polymer does not have any cleavage activity over the RNA in the solution. On the other hand, the three variants of smart-ELR containing the RNase domain (TR, RT and TRT) showed a different RNase A activity comparing the phosphorylated state with the de-phosphorylated state. Both TR-P and RT-P exhibited a significant reduction in RNA quantification, showing a gained catalytic activity due to the selective phosphorylation. The conformation changes caused by the phosphorylation distorted the overall 3D structure of the hybrid ELR-enzyme altering its efficiency. The complete phosphorylation allowed to the TR-P and RT-P to be in its dissolved state, where the RNase A domain resulted to be free to active. The reduction in RNA amount of 17% in the case of TR and 20% in the case of RT demonstrated the capacity of our system to switch from an inactive state (de-phosphorylated) to an active state (phosphorylated) by a selective enzymatic activity performed by Kinase/Phosphatase. Contrary, TRT exhibited no significant difference between the dissolved state (TRT-P) and aggregate state (TRT-D). In this case, the RNase A catalytic site remained inactive even when the state of the smart-ELR was modulated by Kinase/Phosphatase. This phenomenon could be due to a sort of steric hindrance, where the accessibility of the RNA molecule to the catalytic site was blocked by the flanked ELR backbone, or perhaps because of the catalytic site of RNase A is stretched by the ELR backbone altering the performance of the catalytic site (Figure 8). It is well known that, when enzymatic domains are incorporated into polymer assemblies, the accessibility of the substrate to the enzyme becomes susceptible to several factors, such as the affinity and the permeability of the assemblies to the enzymes, and other

factors that can affect the kinetics of the enzyme-responsive behaviour (62-65). In this study, the accessibility of the substrate (RNA) to the catalytic site of RNase A is selectively regulated by the phosphorylation-responsive behavior. Therefore, we have demonstrated that the sequence design of the biomaterial has a crucial influence on the allosteric regulation of the enzymatic activity.

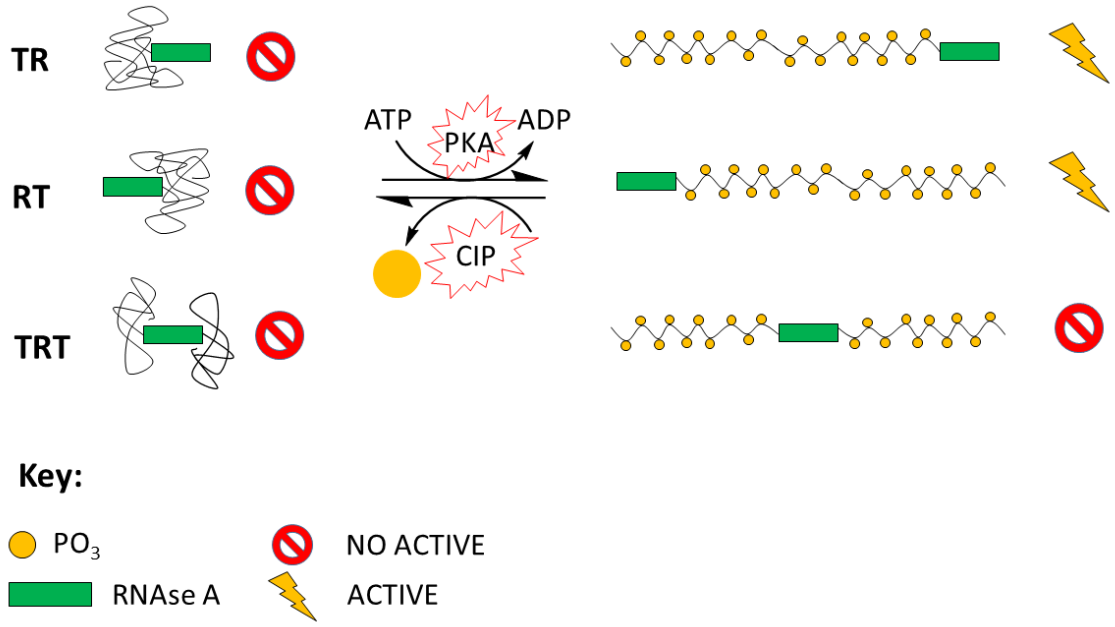

Figure 8. Schematic illustration of TR, RT and TRT allosteric control over the RNase A activity.

5. CONCLUSIONS

In this study, we have developed a smart biomaterial based on Elastin-like Recombinamers with allosteric control of RNase A activity. We have obtained an optimal design for the Kinase/Phosphatase-responsive behaviour, whereby, the 100% of phosphorylation of the smart-ELR was responsible to move the frontier of solubility. This system has demonstrated to be completely reversible, moving back and forth between association (insolubility) and dissociation (solubility) by (de-)phosphorylation. The allosteric regulation of the RNAse A activity was successfully demonstrated; the RNase A catalytic activity depended by the assembled state of the biomaterial, which, is selectively regulated by the phosphorylation-responsive sites in the assemblies. Moreover, the

design principles of phosphatase-involved self-assembling systems can stimulate the development of other smart self-assembling systems responding to other important enzymes. These designs are interesting by themselves, considering that their varying and tailored molecular architectures mean that they can be used in several areas such as thin films, hydrogels, micelles, nanofibers, microstructural surfaces. Finally, the allosteric control demonstrated for the RNase A activity represents an initial proof-of-concept for a new class of responsive macromolecules, which, can be involved in the modulation of intracellular signalling activity.

References

1. Barker, S.L., et al., Control of flow direction in microfluidic devices with polyelectrolyte multilayers. Anal Chem, 2000. 72(24): p. 5925-9.

2. Kikuchi, A. and T. Okano, Pulsatile drug release control using hydrogels. Adv Drug Deliv Rev, 2002. 54(1): p. 53-77.

3. Cunliffe, D., et al., Thermoresponsive Surface-Grafted Poly(N−isopropylacrylamide) Copolymers: Effect of Phase Transitions on Protein and Bacterial Attachment. Langmuir, 2003. 19(7): p. 2888-2899.

4. Hoffmann, J., et al., Photopatterning of thermally sensitive hydrogels useful for microactuators. Sensors and Actuators A: Physical, 1999. 77(2): p. 139-144.

5. Furth, M.E., A. Atala, and M.E. Van Dyke, Smart biomaterials design for tissue engineering and regenerative medicine. Biomaterials, 2007. 28(34): p. 5068-5073.

6. Banerjee, S., G. Chaurasia, and A. Ghosh, Smart polymers: Around the cosmos. Vol. 3. 2010. 135-141.

7. Galaev, I.Y. and B. Mattiasson, 'Smart' polymers and what they could do in biotechnology and medicine. Trends in Biotechnology, 1999. 17(8): p. 335-340.

8. Ulijn, R.V., Enzyme-responsive materials: a new class of smart biomaterials. Journal of Materials Chemistry, 2006. 16(23): p. 2217-2225.

9. Deforest, C.A., E.A. Sims, and K.S. Anseth, Peptide-Functionalized Click Hydrogels with Independently Tunable Mechanics and Chemical Functionality for 3D Cell Culture. Chemistry of materials: a publication of the American Chemical Society, 2010. 22(16): p. 4783-4790.

10. Fouladi, F., K.J. Steffen, and S. Mallik, Enzyme-Responsive Liposomes for the Delivery of Anticancer Drugs. Bioconjugate Chemistry, 2017. 28(4): p. 857-868.

11. Overstreet, D.J., H.D. Dhruv, and B.L. Vernon, Bioresponsive Copolymers of Poly(N-isopropylacrylamide) with Enzyme-Dependent Lower Critical Solution Temperatures. Biomacromolecules, 2010. 11(5): p. 1154-1159.

12. Kim, D., et al., "Bio-switch Chip" Based on Nanostructured Conducting Polymer and Entrapped Enzyme. ACS Applied Materials & Interfaces, 2016. 8(34): p. 21933-21938.

13. Yang, X., et al., Controllable Switching of Enzyme Activity by Poly(N-isopropylacrylamide)-Based Microgels Through Mineralization of Calcium Carbonate in High Pressure CO2. CLEAN – Soil, Air, Water, 2016. 44(2): p. 189-194.

14. Randolph, L.M., M.-P. Chien, and N.C. Gianneschi, Biological stimuli and biomolecules in the assembly and manipulation of nanoscale polymeric particles. Chemical Science, 2012. 3(5): p. 1363-1380.

15. Hu, J., G. Zhang, and S. Liu, Enzyme-responsive polymeric assemblies, nanoparticles and hydrogels. Chemical Society Reviews, 2012. 41(18): p. 5933-5949.

16. Wang, C., et al., An Enzyme-Responsive Polymeric Superamphiphile. Angewandte Chemie, 2010. 122(46): p. 8794-8797.

17. Koga, H., et al., Fluorescent Nanoparticles Consisting of Lipopeptides and Fluorescein-Modified Polyanions for Monitoring of Protein Kinase Activity. Bioconjugate Chemistry, 2011. 22(8): p. 1526-1534.

18. Costa, S., H. Azevedo, and R.L. Reis, Enzyme Immobilization in Biodegradable Polymers for Biomedical Applications. 2005.

19. Urry, D.W., Molecular Machines: How Motion and Other Functions of Living Organisms Can Result from Reversible Chemical Changes. Angewandte Chemie International Edition in English, 1993. 32(6): p. 819-841.

20. Urry, D.W., Free energy transduction in polypeptides and proteins based on inverse temperature transitions. Prog Biophys Mol Biol, 1992. 57(1): p. 23-57.

21. Li, B., et al., Hydrophobic hydration is an important source of elasticity in elastin-based biopolymers. J Am Chem Soc, 2001. 123(48): p. 11991-8.

22. Urry, D.W., Physical Chemistry of Biological Free Energy Transduction As Demonstrated by Elastic Protein-Based Polymers. The Journal of Physical Chemistry B, 1997. 101(51): p. 11007-11028.

23. Dreher, M.R., et al., Temperature Triggered Self-Assembly of Polypeptides into Multivalent Spherical Micelles. Journal of the American Chemical Society, 2008. 130(2): p. 687-694.

24. Meyer, D.E. and A. Chilkoti, Quantification of the effects of chain length and concentration on the thermal behavior of elastin-like polypeptides. Biomacromolecules, 2004. 5(3): p. 846-51.

25. Pastuszka, M.K., et al., A tunable and reversible platform for the intracellular formation of genetically engineered protein microdomains. Biomacromolecules, 2012. 13(11): p. 3439-3444.

26. Lee, T.A.T., et al., Thermo-Reversible Self-Assembly of Nanoparticles Derived from Elastin-Mimetic Polypeptides. Advanced Materials, 2000. 12(15): p. 1105-1110.

27. Sallach, R.E., et al., Micelle density regulated by a reversible switch of protein secondary structure. J Am Chem Soc, 2006. 128(36): p. 12014-9.

28. Roberts, S., M. Dzuricky, and A. Chilkoti, Elastin-like polypeptides as models of intrinsically disordered proteins. FEBS Letters, 2015. 589(19, Part A): p. 2477-2486.

29. Hearst, S.M., et al., The design and delivery of a PKA inhibitory polypeptide to treat SCA1. J Neurochem, 2014. 131(1): p. 101-14.

30. Alvarez-Rodríguez, R., et al., Gold Tailored Photosensitive Elastin-like Polymer: Synthesis of Temperature, pH and UV-vis Sensitive Probes. Vol. 31. 2010. 568-73.

31. Herrero-Vanrell, R., et al., Self-assembled particles of an elastin-like polymer as vehicles for controlled drug release. Journal of Controlled Release, 2005. 102(1): p. 113-122.

32. Nawroth, J.F., et al., Maleimide-Functionalized Poly(2-Oxazoline)s and Their Conjugation to Elastin-Like Polypeptides. Macromolecular Bioscience, 2016. 16(3): p. 322-333.

33. Kinikoglu, B., et al., A smart bilayer scaffold of elastin-like recombinamer and collagen for soft tissue engineering. Journal of Materials Science: Materials in Medicine, 2011. 22(6): p. 1541-1554.

34. Cipriani, F., et al., Bicyclic RGD peptides with high integrin alpha_vbeta₃ and alpha₅beta₁ affinity promote cell adhesion on elastin-like recombinamers. Biomed Mater, 2019.

35. Bandiera, A., Transglutaminase-catalyzed preparation of human elastin-like polypeptide-based three-dimensional matrices for cell encapsulation. Enzyme and Microbial Technology, 2011. 49(4): p. 347-352.

36. Li, C. and G. Zhang, The fusions of elastin-like polypeptides and xylanase self-assembled into insoluble active xylanase particles. J Biotechnol, 2014. 177: p. 60-6.

37. Dhandhukia, J., et al., Switchable elastin-like polypeptides that respond to chemical inducers of dimerization. Biomacromolecules, 2013. 14(4): p. 976-985.

38. Du, K., et al., Enhancement of the solubility and stability of d-amino acid oxidase by fusion to an elastin like polypeptide. Journal of Biotechnology, 2015. 212: p. 50-55.

39. Gao, Q., et al., Genetically-modified R-ω-transaminase: purification and self-assembly facilitating interaction with substrate droplets. Biotechnology letters., 2016. 38(3): p. 489-494.

40. Breslow, R. and W.H. Chapman, On the mechanism of action of ribonuclease A: relevance of enzymatic studies with a p-nitrophenylphosphate ester and a thiophosphate ester. Proceedings of the National Academy of Sciences of the United States of America, 1996. 93(19): p. 10018-10021.

41. T. Raines, R., Ribonuclease A: from Model System to Cancer Chemotherapeutic. 1999.

42. Udgaonkar, J.B. and R.L. Baldwin, NMR evidence for an early framework intermediate on the folding pathway of ribonuclease A. Nature, 1988. 335(6192): p. 694-9.

43. Cook, K.H., F.X. Schmid, and R.L. Baldwin, Role of proline isomerization in folding of ribonuclease A at low temperatures. Proc Natl Acad Sci U S A, 1979. 76(12): p. 6157-61.

44. Rodríguez-Cabello, J.C., et al., Synthesis of Genetically Engineered Protein Polymers (Recombinamers) as an Example of Advanced Self-Assembled Smart Materials, in Nanotechnology in Regenerative Medicine: Methods and Protocols, M. Navarro and J.A. Planell, Editors. 2012, Humana Press: Totowa, NJ. p. 17-38.

45. Shabb, J.B., Physiological substrates of cAMP-dependent protein kinase. Chem Rev, 2001. 101(8): p. 2381-411.

46. Reguera, J., et al., Nanopore Formation by Self-Assembly of the Model Genetically Engineered Elastin-like Polymer [(VPGVG)2(VPGEG)(VPGVG)2]15. Journal of the American Chemical Society, 2004. 126(41): p. 13212-13213.

47. Girotti, A., et al., Influence of the Molecular Weight on the Inverse Temperature Transition of a Model Genetically Engineered Elastin-like pH-Responsive Polymer. Macromolecules, 2004. 37(9): p. 3396-3400.

48. García-Arévalo, C., et al., Immunomodulatory Nanoparticles from Elastin-Like Recombinamers: Single-Molecules for Tuberculosis Vaccine Development. Molecular Pharmaceutics, 2013. 10(2): p. 586-597.

49. Costa, R.R., et al., Layer-by-Layer Assembly of Chitosan and Recombinant Biopolymers into Biomimetic Coatings with Multiple Stimuli-Responsive Properties. Small, 2011. 7(18): p. 2640-2649.

50. Greiner-Stoeffele, T., M. Grunow, and U. Hahn, A general ribonuclease assay using methylene blue. Anal Biochem, 1996. 240(1): p. 24-8.

51. E. Meyer, D. and A. Chilkoti, Purification of Recombinant Proteins by Fusion with Thermally Responsive Polypeptides. Vol. 17. 1999. 1112-5.

52. Miao, M., et al., Elastin Binding Protein and FKBP65 Modulate in Vitro Self-Assembly of Human Tropoelastin. Biochemistry, 2013. 52(44): p. 7731-7741.

53. Bontempo, D., et al., One-step synthesis of low polydispersity, biotinylated poly(N-isopropylacrylamide) by ATRP. Chemical Communications, 2005(37): p. 4702-4704.

54. Pattanaik, A., D.C. Gowda, and D.W. Urry, Phosphorylation and dephosphorylation modulation of an inverse temperature transition. Biochemical and Biophysical Research Communications, 1991. 178(2): p. 539-545.

55. Yang, Z. and B. Xu, A simple visual assay based on small molecule hydrogels for detecting inhibitors of enzymes. Chem Commun (Camb), 2004(21): p. 2424-5.

56. Yang, Z., et al., Enzymatic Formation of Supramolecular Hydrogels. Advanced Materials, 2004. 16(16): p. 1440-1444.

57. Winkler, S., D. Wilson, and D.L. Kaplan, Controlling β-Sheet Assembly in Genetically Engineered Silk by Enzymatic Phosphorylation/Dephosphorylation. Biochemistry, 2000. 39(41): p. 12739-12746.

58. Witze, E.S., et al., Mapping protein post-translational modifications with mass spectrometry. Nat Methods, 2007. 4(10): p. 798-806.

59. Reguera, J., et al., Effect of NaCl on the exothermic and endothermic components of the inverse temperature transition of a model elastin-like polymer. Biomacromolecules, 2007. 8(2): p. 354-8.

60. Meyer, D.E. and A. Chilkoti, Genetically Encoded Synthesis of Protein-Based Polymers with Precisely Specified Molecular Weight and Sequence by Recursive Directional Ligation: Examples from the Elastin-like Polypeptide System. Biomacromolecules, 2002. 3(2): p. 357-367.

61. Martín, L., et al., Temperature-Triggered Self-Assembly of Elastin-Like Block Co-Recombinamers: The Controlled Formation of Micelles and Vesicles in an Aqueous Medium. Biomacromolecules, 2012. 13(2): p. 293-298.

62. Samarajeewa, S., et al., Degradability of poly(lactic acid)-containing nanoparticles: enzymatic access through a cross-linked shell barrier. J Am Chem Soc, 2012. 134(2): p. 1235-42.

63. Habraken, G.J.M., et al., Selective enzymatic degradation of self-assembled particles from amphiphilic block copolymers obtained by the combination of N-carboxyanhydride and nitroxide-mediated polymerization. Biomacromolecules, 2011. 12(10): p. 3761 - 3769.

64. Xu, Y., et al., Complex micelles with a responsive shell for controlling of enzymatic degradation. Polymer, 2012. 53(16): p. 3559-3565.

65. Ding, Y., Y. Kang, and X. Zhang, Enzyme-responsive polymer assemblies constructed through covalent synthesis and supramolecular strategy. Chemical Communications, 2015. 51(6): p. 996-1003.

SUPPORTING INFORMATION

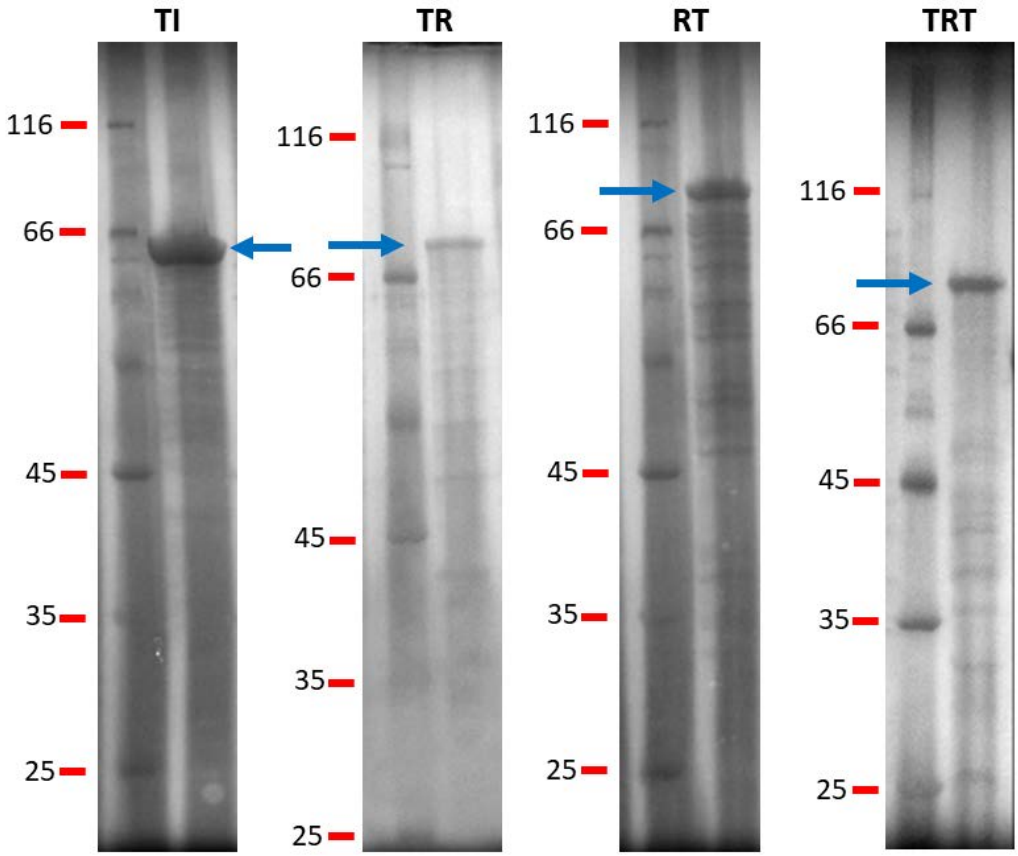

Figure S1. Purity assessment by SDS-PAGE for TI, TR, RT and TRT.

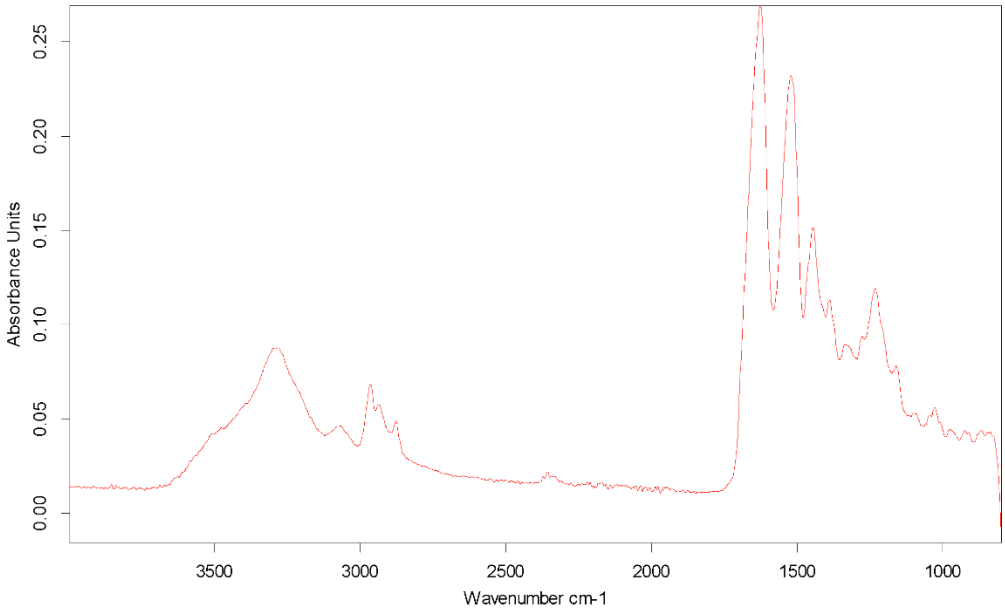

Figure S2. FTIR of TI.

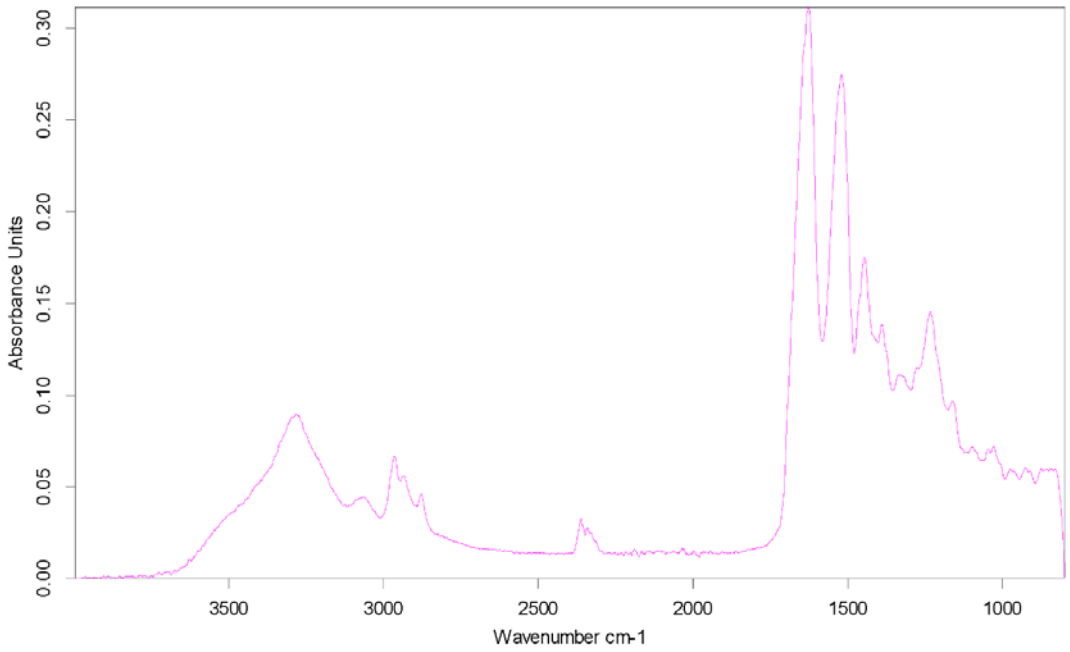

Figure S3. FTIR of TR.

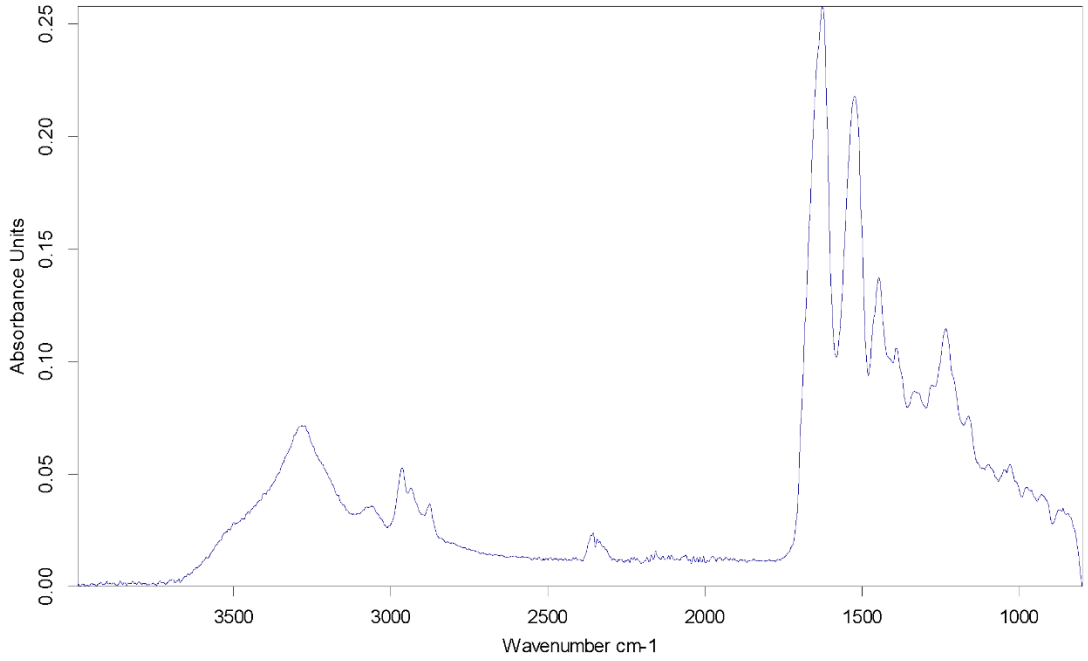

Figure S4. FTIR of RT.

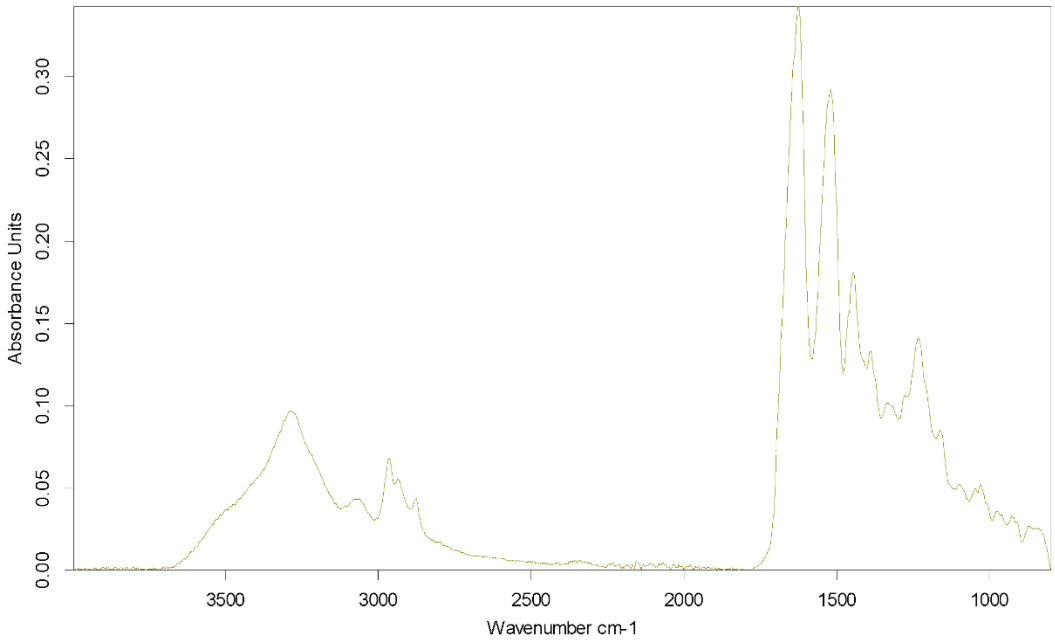

Figure S5. FTIR of TRT.

Amino acid	Theoretical	Experimental
ASP+ASN	30	30.35
GLU+GLN	11	10.89
SER	11	9.37
HIS	-	-
GLY	210	210.88
THR	-	-
ARG	30	27.86
ALA	20	19.73
TYR	-	-
CYS	-	-
VAL	130	127.13
MET	1	1
TRP	-	-
PHE	10	9.37
ILE	110	112.76

LEU	12	12.68
LYS	-	-
PRO	121	124.99

Figure S6. Comparison between the theoretical number of each amino acid and the experimental values for TI.

		TR	**RT**	**TRT**
Amino acid	**Theoretical**	**Experimental**	**Experimental**	**Experimental**
ASP+ASN	45	44.33	42.10	46.95
GLU+GLN	23	19.5	18.10	21.37
SER	26	18.26	17.87	20.24
HIS	4	2.85	3.19	3.56
GLY	213	233.17	238.69	222.38
THR	10	4.53	5.71	7.22
ARG	34	35.15	33.07	34.6
ALA	32	33.91	28.96	33.1
TYR	6	3.73	3.91	5.03
CYS	8	8.12	8.32	7.84
VAL	150	144.27	151.31	143.5
MET	5	3.8	3.21	4.86
TRP	-	-	-	-
PHE	13	11.83	11.69	12.3
ILE	113	122.58	125.04	117.13
LEU	14	18.87	13.26	16.75
LYS	9	8.96	10.72	10.3
PRO	125	123.95	124.85	125.68

Figure S7. Comparison between the theoretical number of each amino acid and the experimental values for TR, RT, TRT.

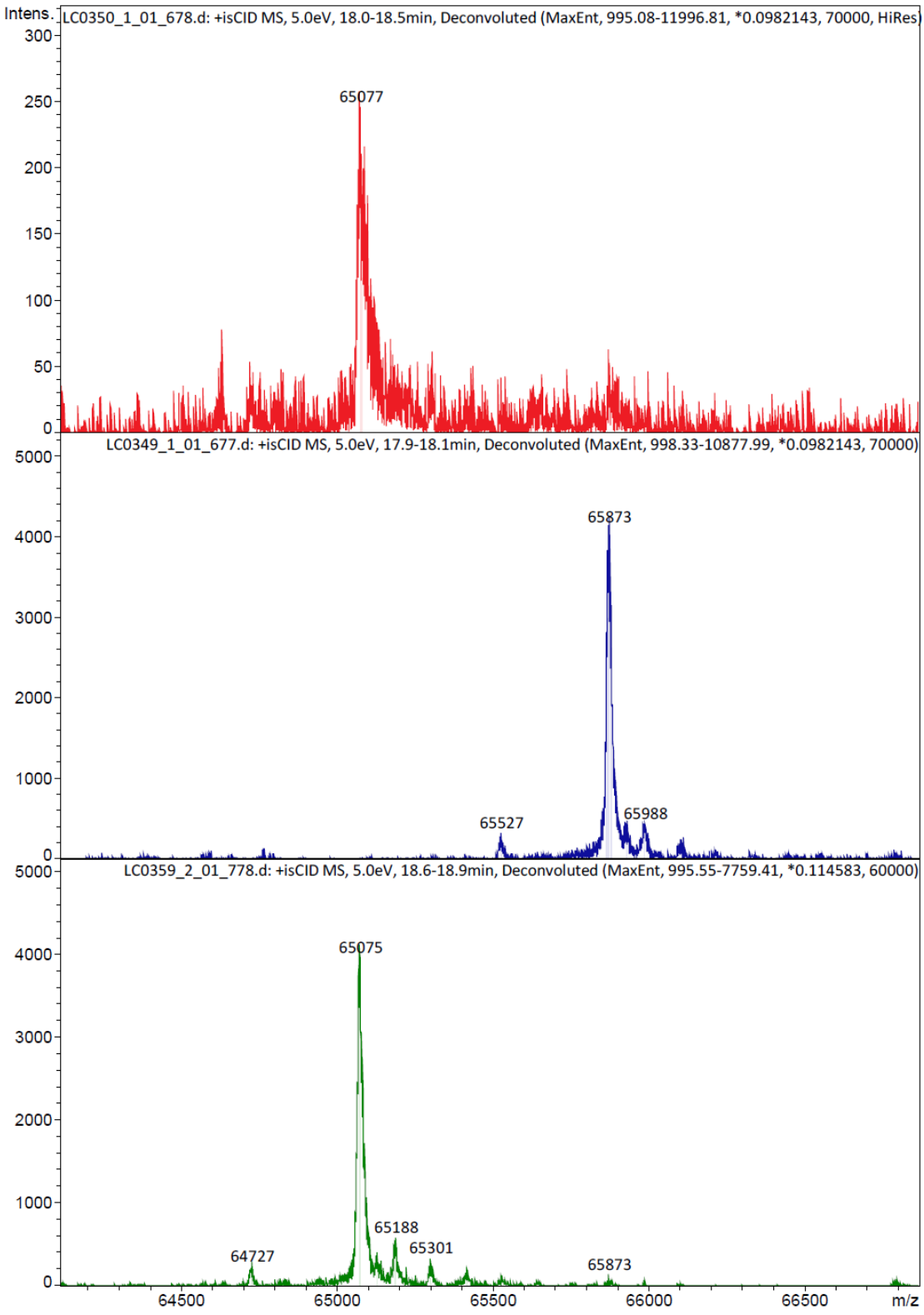

Figure S8. HPLC-HR-MS Spectra for TI-N (red spectra), TI-P (blue spectra) and TI-D (green spectra).

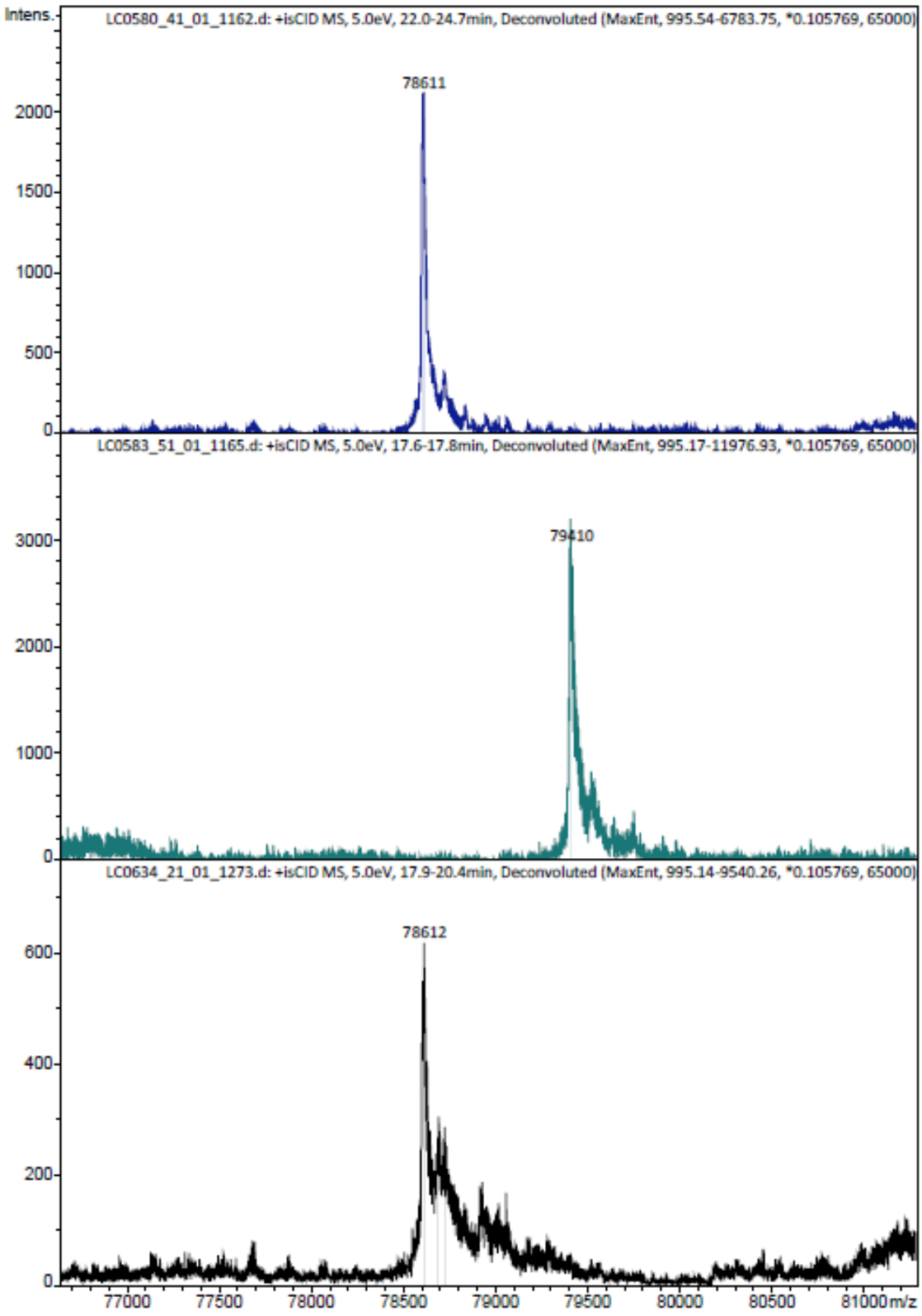

Figure S9. HPLC-HR-MS Spectra for TR-N (blue spectra), TR-P (light green spectra) and TR-D (black spectra).

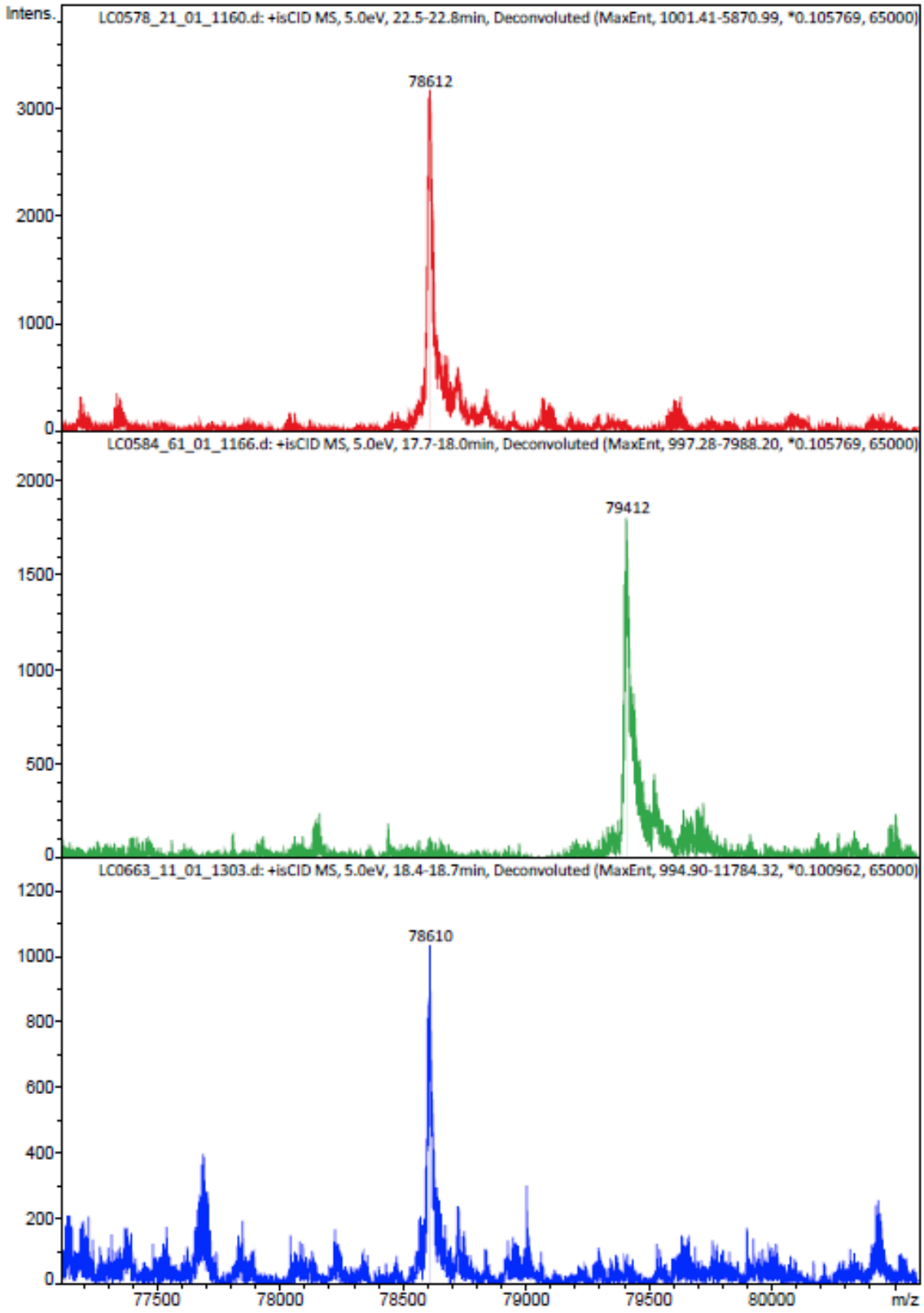

Figure S10. HPLC-HR-MS Spectra for RT-N (red spectra), RT-P (green spectra) and RT-D (blue spectra).

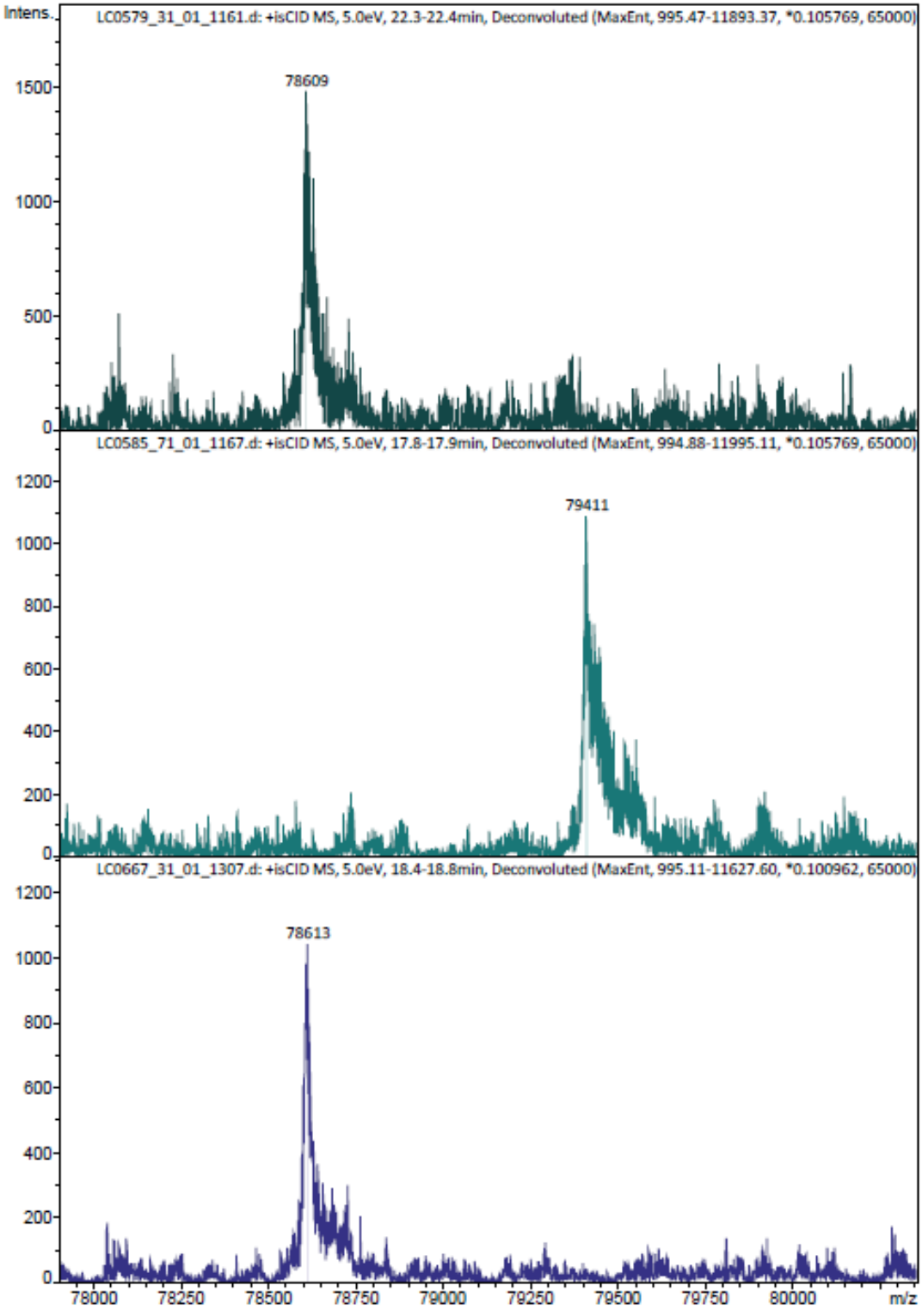

Figure S11. HPLC-HR-MS Spectra for TRT-N (dark green spectra), TR-P (light green spectra) and TR-D (purple spectra).

CONCLUSIONS AND FUTURE DIRECTIONS

Genetic engineering, bioproduction and characterization of ELRs

In this Thesis, it has been shown the development of several ELRs, each one containing bioactive sequences for tailored biomedical application. The hyphosesis to generate several ELRs comprising diverse combinations of bioactive domains was demonstrated. In terms of cell adhesion, RGD and REDV bioactive sequences have been included in the ELRs composition. For hydrogel-forming ELRs the amino acid sequences GAGAGS hexapeptide found in *Bombyx mori* silk fibroin was included in the ELR sequence giving stability to the hydrogel. Moreover, in the case of ELRs-based hydrogel for osteochondral repair an elastase target domain was also included in order to permit the replacement of the scaffold for the regenerated tissue. Furthermore, it was developed a series of ELRs containing the consensus sequence sensible for the kinase/phosphorylase in combination with the RNase A catalytic domain for allosteric domain's regulation. Characterization techniques such as SDS-PAGE and MALDI-TOF confirmed the theoretical MW of the ELRs. Moreover, the T_t was assessed through DSC for all the ELRs; confirming that it was below the physiological temperature for the ELRs forming hydrogels when injected *in vivo*. ^{1}H-NMR and HPLC for amino acid analysis assessed the purity of each batch of the different ELRs, while the FTIR analysis showed good agreement of the theoretical composition of the ELR with the experimental functional groups analyzed. Finally, the analysis of endotoxins ensured the purity of the ELRs for *in vivo* application.

Development of ELRs-based hydrogel with different gelation mechanisms for osteochondral repair

An important part of this Thesis focusses on the development of bioactive hydrogel for Tissue Engineering (TE) application. We hypothesized that the gelation mechanism had a crucial influence for the generation of a 3D hydrogel embedded with cells for osteochondral repair. Different ELRs-based hydrogels for osteochondral repair having two

different gelation mechanisms of hydrogels have been produced, either by chemical (covalent bonds) or by physical cross-linking. In both cases, injectable hydrogels were obtained. In the case of the chemically cross-linked hydrogel, the ELRs concentration selected demonstrated adequate mechanical properties for the osteochondral application. In the case of physically cross-linked hydrogels, the pre-annealing treatment applied to the Silk Elastin co-Recombinamer has shown to improve the mechanical properties of the hydrogel, guarantying fast gelation and the presence of a fibrillary structure directly after injection of the hydrogel. For both scenarios, SEM analysis showed a homogeneous porous environment with an interconnected structure. Although the ELR-based hydrogels developed in this Thesis had different gelation mechanisms, in both cases, the rheological study demonstrated how the concentration of the hydrogel could modulate the mechanical properties. For instance, according to the ELRs composition and its MW, the chemically cross-linked hydrogel allows the gelation of the hydrogel at a lower concentration than the physically cross-linked hydrogel; this thereby allows the cells embedded in the hydrogel matrix to have more space available, and also to play with a higher amount of cells for the formation of the 3D matrix. On the other hand, the physically cross-linked hydrogel does not contain covalent bonds and considering the slower process of gelation, this could provide a better environment for cells embedding.

In conclusion, both gelation mechanisms demonstrated immediate gelation, conferring the benefit of being an injectable scaffold. Moreover, both systems offer tuneable features, such as the possibility to choose between a range of hydrogel's concentration and cell's density, which give the advantage of making the therapy as much tailored as possible. For instance, moving forward in the field of Tissue Engineering for osteochondral repair, it could be formed a scaffold which comprises both proposed hydrogels; it could be designed a double layer hydrogel containing a chemically cross-linked hydrogel for the bone area, whereas a physically cross-linked hydrogel could support the regeneration of cartilage layer.

In vitro, *ex vivo* and *in vivo* evaluation of ELRs-based hydrogel for osteochondral repair

The ELRs-based hydrogels containing different bioactive sequences were tested for the osteochondral application. The physically cross-linked hydrogel containing the bioactive sequence RGD which supports cell adhesion via integrins was embedded with chondrocytes. This biomaterial has demonstrated the capacity to form a high cells density 3D hydrogel and to be delivered into the area of interest. The biocompatibility was proved by *in vitro* study; the addition of the silk allows to make hydrogels with a lower concentration, leading to larger pores, which is most likely responsible for better cell spreading, and proliferation. The regeneration capacities for cartilage repair were evaluated using an *ex vivo* culture platform. After four weeks of culturing, the hydrogel embedded with chondrocytes exhibited remarkable advantages; such as the *de novo* ECM formation, the absence of fibro-cartilage and the production of hyaline cartilage. On the other hand, the chemically cross-linked hydrogel was designed in order to contain the listed bioactive sequences: RGD and REDV to support cell adhesion via integrins and improve the selectivity for endothelial cells, and VGVAPG which provides proteolytic sensitivity to the biomaterial. This ELRs-based hydrogel was further embedded with MSCs and the biocompatibility was proved by an *in vitro* study, whereas the regeneration properties were evaluated by an *in vivo* study. Femoral bone defects were created in New Zealand rabbits, which were subsequently filled with the hydrogel embedded with MSCs and the hydrogel itself; then, after four months the samples were extracted and the regeneration was assessed by different methods. This ELR-hydrogel has been demonstrated to have an adequate composition; indeed it has shown a right ratio of bioactive sequences exhibiting a good balance between the degradation rate and adhesion behaviour, allowing for the colonization of chondrocytes with optimal secretion of extracellular matrix-collagen type II. Finally, it was demonstrated that the specific composition of this hydrogel allowed a faster bone regeneration when embedded with rMSCs compared to the injection of the hydrogel alone. On the other hand, the comparison of the regeneration between the hydrogel embedded with MSCs and the hydrogel itself has shown an excellent cartilage repair without the need for cellular

implantation. We demonstrated that the gelation mechanism has a crucial influence for the generation of a successful scaffold for osteochondral repair, especially when embedded with cells.

In conclusion, the outcomes collected using the different hydrogel's compositions with or without the cellular contribution open up other possibilities in design and combination of hydrogels, perhaps creating a scaffold composed by different layers, each one having its own composition, gelation mechanism, and cellular contribution.

Development of a new ELR-peptides hybrid biomaterial

The hypothesis that the strategy of copper-free click chemistry allows the incorporation of non-canonical amino acids and the formation of cyclized peptides on ELRs was demonstrated. A new hybrid material comprising the recombinant technique of ELRs and the strategy of the synthesis of bicyclic peptides was developed. Indeed, ELRs were covalently functionalized with each three high-affinity and selectivity $\alpha_v\beta_3$- and $\alpha_5\beta_1$-binding bicyclic RGD peptides and with various integrin-binding benchmark peptides. The covalent functionalization was validated by MALDI-TOF analysis, guarantees flexibility and minimal steric hindrance for interactions with cellular integrins. Moreover, the objective to explore the potentiality of the new hybrid biomaterial for biomedical application was achieved; indeed, after the adsorbtion of the ELR-Peptides over tissue culture plate surface (TCPS), the adhesion capacity of HUVECs was evaluated. The *in vitro* studies of ELRs have shown that covalent RGD-functionalization of ELRs via copper-free click reaction is more efficient for inducing integrin-mediated cell adhesion and proliferation than the recombinant synthesis of ELRs comprising RGD as part of their backbone. The *in vitro* studies of ELRs functionalized with high-affinity integrin $\alpha_v\beta_3$- and $\alpha_5\beta_1$-binding RGD bicycles represent an interesting alternative to promote fast cell adhesion on 2D biomaterial surfaces compared with well-known linear or monocyclic RGD peptides.

In conclusion, a new system based on two diametrically opposed strategies was developed, demonstrating that combining approaches could be a new manner to explore new frontiers. In this case, we believe that ELRs functionalized with integrin-selective

RGD-bicycles have a great potential to evaluate cell-adhesion behavior and tailor high integrin peptides for specific biomedical applications.

A new class of smart-ELRs with allosteric domain

As a final stage of this journey, in this Thesis we have explored a new class of ELRs. A smart biomaterial based on ELRs with allosteric control of RNase A activity was developed. Firstly, the consensus sequence phosphorylation site was introduced and regularly distributed (ten times) along the ELR sequence. The HPLC-HR-MS analysis demonstrated the ability to fully phosphorylate/de-phosphorylate the ELRs, and the reversibility of this system. Furthermore, the turbidity analysis demonstrated an evident shift in Temperature transition (T_t) value due to the transfer/removal of the phosphate groups. Secondly, taking advantage of the recombinant technique, the Ribonuclease A catalytic domain (RNase A) was fused to the smart-ELR at the genetic level. According to the position of RNase A relative to the ELR backbone, three variants of the smart-ELR were produced and all of them demonstrated the capacity to fully phosphorylated/de-phosphorylated. The DLS and turbidity analysis performed at 37 °C, at the mild condition for a selected concentration, showed that the system was completely reversible, moving back and forth between association (insolubility) and dissociation (solubility) by (de-)phosphorylation. Finally, the RNase A catalytic activity showed dependency by the state of the biomaterial. Indeed, the RNase A activity was selectively enhanced by the phosphorylation of the ELR consensus sequences. The allosteric regulation of the RNase A activity was successfully demonstrated, showing that the design of the sequence has a central role in the activity of the selected enzyme. However, a next step would be to find a finer methodology to assess the allosteric regulation of the RNase A activity.

In conclusion, the allosteric control demonstrated for the RNase A activity represents an initial proof-of-concept for a new class of responsive macromolecules, the design principles of phosphatase-involved self-assembling systems can stimulate the development of other smart self-assembling systems responding to other important enzymes.

Final remarks

Along this journey towards the discovery of the evolution of ELRs, we have strived to explore the potential of ELRs towards the development of tailored solutions for Biomedical applications. Across the fulfilment of the objectives of this Thesis, we came out with new outstanding biomaterials capable to overcome some limitations of the existing ones. However, this is not an ending point; it is rather an ongoing process on which we humbly gave our small contribution to scientific discovery. The leitmotiv of this Thesis has been described as a sort of journey towards the evolution of Biomaterial science. Along with the PhD program, we have learned how important is to address the complex problems from different point of views. The final take-home message is about the importance of keeping an open mindset considering all the pieces that compose the whole picture. We strongly believe that collaboration and cooperation are essentials to do “good science”; because it is only combining diverse strengths and skills that we are able to break the wall between us and the new discoveries.

ADDITIONAL

Publications

2019

- L. Poocza, **F. Cipriani**, M. Alonso Rodrigo, J.C. Rodríguez-Cabello. Hydrophobic cholesteryl moieties trigger substrate cell-membrane interaction of elastin-mimetic protein coatings in vitro. *ACS Omega* (2019). doi.org/10.1021/acsomega.9b00548.
- **F. Cipriani**, B. Ariño Palao, I. González de Torre, A. Vega Castrillo, H. José Aguado Hernández, M. Alonso Rodrigo, A. J Àlvarez Barcia, V. García, Monica Lopez Peña, J.C. Rodríguez-Cabello. An elastin-like recombinamer-based bioactive hydrogel embedded with mesenchymal stromal cells as an injectable scaffold for osteochondral repair. *Regenerative Biomaterials* (2019). doi.org/10.1093/rb/rbz023.
- **F. Cipriani**, D. Bernhagen, C. García-Arévalo, I. González de Torre, P. Timmerman, J.C. Rodríguez-Cabello. Bicyclic RGD peptides with high integrin $\alpha_v\beta_3$ and $\alpha_5\beta_1$ affinity promote cell adhesion on elastin-like recombinamers. *Biomedical Materials* (2019). doi: 10.1088/1748-605X/aafd83.

2018

- **F. Cipriani**, M. Krüger, I. González de Torre, L. Quintanilla Sierra, M. Alonso Rodrigo, L. Kock, J.C. Rodríguez-Cabello. Cartilage Regeneration in Preannealed Silk Elastin-Like Co-Recombinamers Injectable Hydrogel Embedded with Mature Chondrocytes in an Ex Vivo Culture Platform. *Biomacromolecules* (2018). doi: 10.1021/acs.biomac.8b01211.
- J.C. Rodríguez-Cabello, I. G. de Torre, **F. Cipriani**, L. Poocza. Elastin-like materials for tissue regeneration and repair. *Peptides and Proteins as Biomaterials for Tissue Regeneration and Repair* (2018). doi: 10.1016/B978-0-08-100803-4.00012-7.

2017

- J.C. Rodríguez-Cabello, A. Ibáñez-Fonseca, **F. Cipriani**, L. Poocza, I. González de Torre, M. Alonso. Elastin-like Polymers: Properties, Synthesis and Applications. *Encyclopedia of Polymer Science and Technology* (2017). doi: 10.1002/0471440264.pst656.

Conferences

2019

Tissue Engineering and Regenerative Medicine International Society (TERMIS)- EU Congress 2019. Rhodes (Greece)

ORAL COMMUNICATION:

- Dual enzyme-responsive smart-ELRs for switchable catalytic activity.

2018

WORLD TERMIS Congress 2018. Kyoto (Japan)

ORAL COMMUNICATION(S):

- Specific Detection of Proteases using novel-protein substrates for Zymographic Methods.
- Hydrophobic cholesteryl moieties trigger substrate cell-membrane interaction of elastin-mimetic protein coatings *in vitro.*

POSTER COMMUNICATION:

- Silk Elastin-like co-Recombinamers bioactive hydrogel embedded with mature chondrocytes as injectable scaffolds for cartilage regeneration in an *ex vivo* culture platform.

Kárman Conference – Materials for Life. Bensberg (Germany)

POSTER COMMUNICATION:

- Silk Elastin-Like Co-Recombinamers bioactive hydrogel for osteochondral repair in an *ex vivo* culture platform.

International Workshop on Advanced Materials for Healthcare Applications. Reykjavik (Iceland).

POSTER COMMUNICATION:

- A new class of SMART Elastin-Like Recombinamer with enzyme responsiveness.

2017

6th China-Europe Symposium on Biomaterials in Regenerative Medicine. Porto (Portugal).

ORAL COMMUNICATION:

- Elastin-Like Recombinamer bioactive hydrogel embedded with MSCs as injectable scaffolds for osteochondral repair.

POSTER COMMUNICATION:

- Functional Hybrids of elastin-like recombinamers and polyisocyanates.

TERMIS-EU Congress 2017. Davos (Switzerland)

POSTER COMMUNICATION:

- Osteochondral tissue regeneration with biofunctional hydrogel scaffolds based on MSCs embedded in an Elastin-Like Recombinamers matrix.

European Society for Biomaterials (ESB) Congress 2017. Athens (Greece).

ORAL COMMUNICATION:

- Elastin-Like Recombinamer with ATP responsiveness.

POSTER COMMUNICATION:

- Elastin-like Recombinamers and Polyisocyanates: A Functional Hybrid System for Tissue Engineering

Future Investigators of Regenerative Medicine (FIRM) Congress. Girona (Spain).

ORAL & POSTER COMMUNICATION:

- Elastin-Like Recombinamers bioactive hydrogel in tissue engineering for osteochondral repair.

Advanced Materials for Biomedical Applications (AMBA) Congress. Ghent (Belgium).

POSTER COMMUNICATION:

- A new class of SMART Elastin-Like Recombinamer with enzyme responsiveness.

International Symposium on Bioinspired macromolecular systems (ISBMS) Congress. Aveiro (Spain).

FLASH TALK & POSTER COMMUNICATION:

- "Dual" SMART Elastin-Like Recombinamer.

2016

BIOGEL Conference. Ringberg Castle (Germany).

ORAL COMMUNICATION:

- Elastin-like Recombinamers (ELRs): From Bioinspired Motifs to Biomedical Application.

POSTER COMMUNICATION:

- Self-assembled injectable ECM hydrogels from Elastin-like Co-Recombinamers biomaterials.

Courses and certifications

- **Time and Project Management.** Bpmsat (Spain).
- **Statistical Validation and Experimental Design.** Biostatech (Spain).
- **Leadership and coaching techniques.** University of Valladolid (Spain).
- **Research ethics and integrity**. Organized by BIOGEL project.
- **Mechanical properties of the biomaterials.** Radboud University. Nijmegen (the Netherlands).
- **Biomimetic hydrogels.** Organized by BIOGEL project.

- **Skills you really need when you apply for a job.** Organized by BIOGEL project.
- **The Route to Academia: How to fail successfully.** Organized by BIOGEL project.
- **Hydrogel Imaging.** Austrian Institute of Technology (AIT). (Wien) Austria.
- ***In vitro, ex vivo, and in vivo models***. LifeTec Group. (Eindhoven) the Netherlands.
- **Synthesis of Biomaterials**. University of Thessaloniki. Thessaloniki (Greece).
- **Critical thinking for public discourse.** University of Amsterdam (The Netherlands).
- **Certification "In vivo experimentation for the design and realization of animal trials**". University of Salamanca (Spain).
- **The Whole Scientist.** Jackson Laboratory. Bar Harbor (USA).

Marie Curie Fellowship for Early Stage Research Training

Attendance of the listed progress meetings with scientific communication:

- Network Meeting at TPNBT, 14th December, 2015. Valladolid (Spain).
- Network Meeting at Radboud University, 22th June, 2016. Nijmegen (the Netherlands).
- Network Meeting at University of Valladolid, 12th December, 2016. Valladolid (Spain).
- Network Meeting organized by the Centre for Research & Technology Hellas (CERTH), 14th June, 2017. Poros (Greece).
- Network Meeting at Austrian Institute of Technology (AIT), 30th January, 2018. (Wien) Austria.
- Network Meeting at DWI-Leibniz Institute for Interactive Materials, 25th July, 2018. (Aachen) Germany.
- Network Meeting at DWI-Leibniz Institute for Interactive Materials, 14th December, 2018. Aachen (Germany).

Awards

Chair-Elect TERMIS Student and Young Investigator Section- Europe (SYIS-EU).

Organization of SYIS activities at TERMIS congresses. TERMIS-SYIS provides a platform for the "next generation" of scientists and engineers in the field of tissue engineering and regenerative medicine to interact.

Best Social Outreach at FIRM conference 2017 (Girona, Spain).

SYIS-TERMIS Debate Competition Winner at TERMIS-EU Congress 2017 (Davos, Switzerland).

In concordance with the TERMIS 2017 theme on ‘Personalised Therapies for Regenerative Medicine’, the topic of the debate: “Will 3D-Printing or Decellularised organs rescue the donor-based organ scarcity for transplantation?”

Teaching

Supervision of the scientific training of the student Sandra Ramos at the University of Valladolid (Spain). The Workshop title: "POLÍMEROS RECOMBINANTES TIPO ELASTINA PARA APLICACIONES APLICACIONES BIOMÉDICAS".